Development of Thermoplastic Elastomers with Improved Elastic Properties Based on Semicrystalline Block Copolymers

Dissertation

Zur Erlangung des akademischen Grades eines
Doktors der Naturwissenschaften (Dr. rer. nat.)
im Fach Chemie der Fakultät für Biologie, Chemie und Geowissenschaften
der Universität Bayreuth

vorgelegt von

Holger Schmalz

geboren in Kronach

Bayreuth, 2003

Die vorliegende Arbeit wurde am Lehrstuhl für Makromolekulare Chemie II der Universität Bayreuth in der Arbeitsgruppe von PD Dr. V. Abetz im Zeitraum von März 1999 bis Juli 2002 durchgeführt.

Prüfungsausschuß:

PD Dr. V. Abetz (Erstgutachter)
Prof. Dr. G. Krausch (Zweitgutachter)
Prof. Dr. H.-W. Schmidt (Vorsitzender)
Prof. Dr. H. G. Alt
Prof. Dr. K. Seifert

Promotionsgesuch eingereicht am: 31.07.2002
Tag des Rigorosums: 16.12.2002

Vollständiger Abdruck der von der Fakultät für Biologie, Chemie und Geowissenschaften der Universität Bayreuth genehmigten Dissertation zur Erlangung des Grades eines Doktors der Naturwissenschaften (Dr. rer. nat.).

Danksagung

Mein besonderer Dank gilt PD Dr. V. Abetz für die interessante Themenstellung und die freundliche Arbeitsatmosphäre. Insbesondere möchte ich mich für sein Engagement während der einjährigen Übergangszeit bedanken, ohne die der Arbeitskreis die schlimme Zeit nach dem Tod von Prof. Dr. R. Stadler nicht so gut überstanden hätte. Ich möchte mich an dieser Stelle besonders für die gute Zusammenarbeit bedanken, die auch über fachliche Aspekte weit hinausging. Besonderer Dank gilt Prof. Dr. R. Stadler für die Initiierung des DSM-Projektes. Ich hoffe, daß ich in meiner Dissertation die Bearbeitung des DSM-Projektes in seinem Sinne fortgeführt habe. Bei Prof. Dr. A. H. E. Müller möchte ich mich für die vorbehaltlose Aufnahme in seinen Arbeitskreis und seine Unterstützung bedanken. Prof. Dr. G. Krausch (PC II) danke ich für seinen wichtigen Beitrag zum Macromolecules-Paper und seine Unterstützung bei den SFM Untersuchungen. Prof. Dr. A. J. Müller (Caracas) gilt mein besonderer Dank für die Hilfe bei den Selbstnukleierungsmessungen und die vielen hilfreichen Diskussionen, die wesentlich zu den Publikationen über semikristalline Dreiblockcopolymere beigetragen haben.

Sehr herzlich bedanke ich mich bei Alexander Böker, Rainer Erhardt, Michael Lanzendörfer, Cornelia Lauble, Katja Loos und Gerd Mannebach, die nicht nur stets Zeit für anregende Gespräche fanden, sondern auch für ihre Hilfe, die weit über die chemischen Belange hinausreichte. Besonders möchte ich mich bei Anette Krökel, dem „guten Geist“ unseres Labors, für die vielen praktischen Ratschläge bedanken und dafür, daß sie unser Labor so gut in Schuß gehalten hat.

Rainer Erhardt und Gerd Mannebach gebührt besonderer Dank für die ausgezeichnete Einführung in die „Anionik“ und ihre Unterstützung bei synthetischen Problemen. Für die gute Einweisung in das Computernetzwerk und seine Tücken danke ich Stefan Degen. Weiterhin möchte ich mich bedanken bei Kerstin Matussek und Stefan Stangler für ihre Unterstützung bei den Rheologiemessungen, Alexander Böker und Astrid Göpfert für die Durchführung zahlreicher GPC-Messungen, Mabel Graf und Gerd Mannebach für die Betreuung des NMR Gerätes, PD Dr. V. Abetz und Stefan Stangler für die Unterstützung bei den röntgenographischen Untersuchungen sowie Michael Lanzendörfer für die MALDI-ToF-Messungen und den Aufbau und die Betreuung der NIR-Sonde. An dieser Stelle möchte ich

mich besonders bei Michael Lanzendörfer für die Zusammenarbeit bei den kinetischen Untersuchungen zur Ethylenoxid Polymerisation bedanken, die uns sehr oft „Kopfzerbrechen“ bereitet hat. Großer Dank gilt auch Katja Loos und Karl-Heinz Bücher (Perkin Elmer), die stets Zeit zur Beseitigung von kleineren und größeren Problemen mit unseren DSC Geräten gefunden haben. Clarissa Abetz danke ich für die Durchführung der SEM-Messungen und Astrid Göpfert für die Durchführung der TEM-Untersuchungen und ihrer schier unerschöpflichen Geduld bei der Präparation von widerspenstigen Proben. Insbesondere möchte ich mich bei Alexander Böker für das Anlernen am SFM Gerät und bei Armin Knoll für die Hilfe bei den Hot-Stage-Messungen bedanken.

Gaby Rösner-Oliver gebührt besonderer Dank für ihre Unterstützung im Kampf mit der Bürokratie und die vielen hilfreichen „Kleinigkeiten“.

Bei allen Mitgliedern des Arbeitskreises - seien sie auch nicht explizit namentlich genannt - bedanke ich mich für die angenehme Atmosphäre und die stetige Hilfsbereitschaft.

Ronald Lange (DSM) möchte ich ganz besonders für die gute Zusammenarbeit in unserem DSM-Projekt danken, die weit über rein fachliche Bereiche hinausging. Weiterhin möchte ich mich bedanken bei Viola van Guldener und Wouter Gabriëlse für die Festkörper-NMR Untersuchungen, Jos van Elburg für die Hilfe bei den Mechanikmessungen, Angelika Schmidt und Maria Soliman für hilfreiche Diskussionen und DSM-Research für die finanzielle Unterstützung.

An dieser Stelle möchte ich mich ganz herzlich bei meinen Eltern und meiner Freundin für die große Unterstützung während meines Studiums bedanken. Es ist nicht zuletzt auch ihr Verdienst, der zum Gelingen dieser Arbeit beigetragen hat.

Table of Contents

Glossary of Symbols

α	Degree of crystallinity
A	Ampere
Å	Angstrom
bp	Boiling point
cm	Centimeter
χ	Florry-Huggins interaction parameter
°	Degree
°C	Degree Celsius
d	Diameter
E	Young's modulus
E'	Dynamic tensile storage modulus
E''	Dynamic tensile loss modulus
ε	Elongation
ε_B	Elongtion at break
ε_{plast}	Plastic deformation
g	Gramm
G	Gibbs free energy (free enthalpy)
G'	Dynamic shear storage modulus
G''	Dynamic shear loss modulus
h	Hour
H	Enthalpy
ΔH_m^0	Standard heat of fusion
Hz	Hertz
J	Joule
K	Kelvin
l	Liter
λ	Wave length
min	Minute
ml	Milliliter
μm	Micrometer
mm	Millimeter
mmol	Millimol
M_n	Number averaged molecular weight
μs	Microsecond
ms	Millisecond
M_w	Weight averaged molecular weight

mW	Milliwatt
M_w/M_n	Polydispersity
N	Number of monomer units
nm	Nanometer
Pa	Pascal
p. a.	Pro analysis
PB	Polybutadiene
PBT	Poly(butylene terephthalate)
PCL	Poly(ε-caprolactone)
PE	Polyethylene
PEB	Poly(ethylene-*stat*-butylene)
PEO	Poly(ethylene oxide)
PEP	Poly(ethylene-*alt*-propylene)
PI	Polyisoprene
P_n	Degree of polymerization
ppm	Parts per million
PS	Polystyrene
PTMO	Poly(tetramethylene oxide)
q	Scattering vector
dQ/dt	Heat flow
rad/s	Frequency in radiant per second
s	Second
S	Entropy
σ_B	Stress at break
tanδ	Loss tangent
τ_1	Contact time in cross-polarization experiments
τ_2	Aquisition time in NMR experiments
θ	Scattering angle
T_1	Spin-lattice relaxation time
T_c	Crystallization temperature
T_g	Glass transition temperature
T_m	Melting temperature
T_{ODT}	Order-disorder transition temperature
T_s	Self-nucleation temperature
V	Volt
V_e	Elution volume
Vol	Volume
wt-%	Weight percent

1 Introduction

1.1 Thermoplastic Elastomers[1]

Thermoplastic elastomers (TPEs) constitute a commercially relevant and fundamentally interesting class of polymeric materials. They combine the properties of irreversibly crosslinked elastomers, such as impact resistance and low-temperature flexibility, with the characteristics of thermoplastic materials, e. g. the ease of processing. In general, TPEs are phase-separated systems consisting of a hard phase, providing physical crosslinks, and a soft phase, contributing to the elastomeric properties. The hard phase is characterized by a high glass transition temperature (T_g) or a high melting point for semicrystalline systems, whereas the soft phase usually exhibits a low T_g. In many cases the phases are chemically linked by block or graft copolymerization. In other cases, a fine dispersion of the hard polymer within a matrix of the elastomer by blending also results in TPE-like behavior. Because of the covalent linkage(s) between the chemically dissimilar segments, the rigid domains can form physical crosslink sites, resulting in a three-dimensional network. Consequently, TPEs exhibit mechanical properties that are, in many ways, comparable to those of a vulcanized (covalently crosslinked) rubber, with the exception that the network and hence the properties of the TPEs are thermally reversible. This feature makes TPEs ideally suited for high-throughput thermoplastic processes, such as melt extrusion and injection molding. Mainly three classes of commercial TPEs can be distinguished: polystyrene-elastomer block copolymers, multiblock copolymers, and hard polymer-elastomer composites.

The first class includes mainly polystyrene-*block*-polybutadiene-*block*-polystyrene (PS-*b*-PB-*b*-PS), polystyrene-*block*-polyisoprene-*block*-polystyrene (PS-*b*-PI-*b*-PS), and their hydrogenated analogues polystyrene-*block*-poly(ethylene-*stat*-butylene)-*block*-polystyrene (PS-*b*-PEB-*b*-PS) and polystyrene-*block*-poly(ethylene-*alt*-propylene)-*block*-polystyrene (PS-*b*-PEP-*b*-PS) triblock copolymers. Because of the incompatibility between the hard and soft component microphase separation occurs, whereby the polystyrene minority phase forms dispersed spheres or cylinders in a rubbery matrix of the middle block. For commercial applications they are usually compounded with other polymers, oils, resins, fillers, etc..

TPEs based on multiblock copolymers comprise an alternating structure of hard and soft segments within the polymer chain. The hard segments usually consist of a

semicrystalline polymer like polyurethane, polyester, polyamide, or polyethylene, providing a good solvent resistance. Systems with a glassy hard phase are, for example, multiblock copolymers based on poly(ether imide) hard segments and polysiloxane soft segments. In multiblock copolymers with polyurethane, polyester, and polyamide hard segments frequently short chain polyethers are used as a soft component. In some cases polyesters (poly(ε-caprolactone)) are incorporated. The polymers having polyester soft segments are tougher and show a higher resistance to oils, solvents, and thermal degradation. Analogues with polyether soft segments exhibit better hydrolytic stability and an increased flexibility at low temperatures. The soft phase in multiblock copolymers with polyethylene hard segments consists of ethylene-α-olefin copolymers. They are thermally stable but less resistant against swelling by oils and organic solvents. In addition, these systems are very flexible at low temperatures but their upper service temperature is rather low due to the comparatively low melting point of polyethylene.

The last class, the hard polymer-elastomer composites, also consists of a semicrystalline polymer as the hard phase, e. g. polypropylene or a propylene copolymer. For the soft phase often ethylene-propylene random copolymers (EPR) or a similar material with a small amount of out-of-chain unsaturation (EPDM) is used. In addition, there are also systems based on butyl-, nitril-, and natural rubber elastomers.

The motivation of this work is the improvement of elastic properties of two commercially important TPEs, namely PBT-based copoly(ether ester)s and TPEs based on triblock copolymers. The elasticity of copoly(ether ester)s with PBT hard segments and low molecular weight polyether soft segments is limited due to the continuous PBT hard segment structure present in these systems, which is irreversibly disrupted upon elongation. The used strategy for improving the elastic properties implies a transformation of the continuous PBT hard phase into a disperse PBT hard phase by taking advantage of microphase separation within the soft component. This is realized by incorporation of ABA triblock copolymer soft segments with nonpolar middle blocks (Chapter 1.4). In the field of TPEs based on triblock copolymers, suppression of loop formation is the key for improved resilience. Using crystallization as a strong driving force for microphase separation, different ABC triblock copolymers with one or two semicrystalline end blocks have been investigated with respect to their morphology, thermal properties, and elasticity (Chapter 1.5).

In the following two Chapters, a brief description of the essentials of microphase separation and crystallization in block copolymers will be given.

1.2 Microphase Separation in Block Copolymers

Blending of two polymers A and B is often used to create systems with unique properties, reflecting a combination of properties of the corresponding blend components.[2] However, due to thermodynamic reasons most blends of polymers turn out to be macrophase separated. Prerequisite for the miscibility of two polymers is a decrease in the free enthalpy of mixing ($\Delta G_m < 0$), which is defined as follows:[3]

$$\Delta G_m = \Delta H_m - T\Delta S_m \qquad \textbf{Equation 1.1}$$

The energetic interactions between the blend components is described by the enthalpy of mixing ΔH_m, which can be expressed according to Flory[4] and Huggins[5,6], as:

$$\Delta H_m = R\ T\ \chi_{AB}\phi_A\phi_B \qquad \textbf{Equation 1.2}$$

R = universal gas constant
T = temperature
ϕ_i = volume fraction of component i

whereby the Flory-Huggins parameter χ_{AB} can be written as:

$$\chi_{AB} = \frac{Z}{k_B T}\left[\varepsilon_{AB} - \frac{1}{2}\left(\varepsilon_{AA} + \varepsilon_{BB}\right)\right] \qquad \textbf{Equation 1.3}$$

Z = number of nearest segments in other chains
k_b = Boltzman constant
ε_{AB} = interaction energy between segments A and B

The entropy of mixing ΔS_m is given by Equation 1.4.

$$\Delta S_m = -R\left(\frac{\phi_A}{N_A}\ln\phi_A + \frac{\phi_B}{N_B}\ln\phi_B\right) \qquad \textbf{Equation 1.4}$$

N_i = degree of polymerization for component i

The mixing entropy ΔS_m gives a negative contribution to the free enthalpy of mixing ΔG_m, since $\phi_i \leq 1$ and therefore $\ln\phi_i < 0$. However, especially for long-chain molecules (high degree of polymerization N_i) the entropic contribution decreases and even slight repulsive

interactions between the segments ($\Delta H_m > 0$) can result in a positive value for ΔG_m, i. e. macrophase separation occurs.

The macrophase separation in polymer blends does not only depend on thermodynamics, but also to a large extent on the processing conditions, e. g. kinetic parameters like melt viscosity or mixing time. Furthermore, an initially homogeneous blend can show macrophase separation after a change in temperature via spinodal decomposition or a nucleation and growth mechanism.[7]

Macrophase separation can be avoided by using compatibilizers, which self-assemble at the interface between the incompatible blend components, resulting in fine disperse phase-separated blends. For this purpose block copolymers composed of at least two different blocks, whereby one block is compatible with one of the blend components, and the other block is compatible with the other blend component, are ideal systems.[1,8,9] Due to the chemical link between the different blocks, macrophase separation is no longer possible and the block copolymers undergo microphase separation within length scales of 10 – 100 nm. There are basically two competing factors involved in the microphase-separation of block copolymers. On one hand the system tends to minimize the enthalpic unfavorable interface between the incompatible blocks, on the other hand the conformational entropy tends to a random coil conformation of the blocks resulting in a weakening of the segregation between the blocks. As a result, a morphology with a larger interface between blocks than the minimal interface is formed. Thus, the formed morphology within block copolymers is determined by the interplay of these enthalpic and entropic contributions.

Chemically well-defined diblock copolymers self-assemble into regular crystal-like lattices when microphase separation occurs. The different thermodynamically stable microphases for AB diblock copolymers are presented in Figure 1.1.[10] The equilibrium morphologies are depicted from left to right with increasing volume fraction ϕ_A ($\phi_B = 1 - \phi_A$) of the minority component. If A is getting the majority component ($\phi_A > \phi_B$) a inverse sequence of the morphologies is observed starting from the lamellar microphase.

Whereas the spherical, cylindrical, and lamellar microphases have been known for a long time, the double gyroid phase was discovered independently by two groups in the 1990s.[11,12] Other identified morphologies, such as OBDD (ordered biscontinuous double diamond) or hexagonally perforated lamellae (HPL), are considered as metastable phases.[13,14]

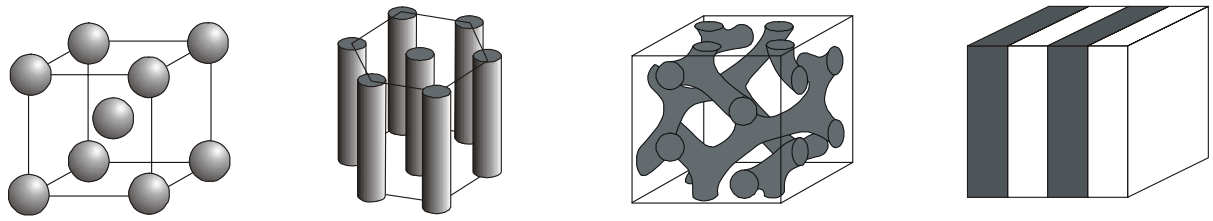

Figure 1.1: Microphase-separated morphologies of diblock copolymers. From left to right: spheres on a body-centered cubic (bcc) lattice, hexagonally packed cylinders, double gyroid, lamellae.

As mentioned above, the interplay of enthalpic and entropic contributions to the free enthalpy of mixing determines the microphase separation. As every chain segment contributes to the enthalpy of mixing, the incompatibility of the two blocks is not only proportional to χ but also to the number of segments N ($N = N_A + N_B$). Therefore, the product χN is used to express the incompatibility between two different blocks. For $\chi N << 10$ the entropic contributions overwhelm the enthalpic term, resulting in the observation of a disordered isotropic phase. Microphase separation in symmetric diblock copolymers starts at a theoretically determined critical value of $\chi N \cong 10.5$.[15] Two different limiting situations are discussed for microphase separated block copolymers, the weak-segregation limit (WSL) and the strong-segregation limit (SSL).

The WSL approach ("mean field" theory) for the description of the order-disorder transition, i. e. the transition from a microphase separated block copolymer melt to the disordered state, was developed by Leibler[15], de Gennes[16], and Erukhimovich[17]. In the WSL ($10 < \chi N < 15$) a broad smeared interface separates neighboring microdomains, i. e. there is a smooth transition of the composition across the domain boundary. For symmetric diblock copolymers a second-order transition between lamellar and disordered phase was predicted. At other compositions a first-order transition between the disordered state and a body-centered cubic phase of spherical domains formed by the minority component was predicted, which changes into hexagonally packed cylinders and finally into lamellae upon further increasing χN. Within WSL the long period scales with $L \propto N^{1/2}$, the chain conformations correspond to a Gaußian statistics. However, in Leibler's approach fluctuation effects, which become important for finite degrees of polymerization, are not included. Fredrickson and Helfand[18] expanded the theory of Leibler[15] by incorporation of compositional fluctuations into the "mean field" theory, also taking into account the degree of polymerization of the diblock copolymer. Figure 1.2 shows a comparison of phase diagrams calculated for diblock

copolymers using the approach of Leibler and Fredrickson and Helfand. In contrast to the approach of Leibler, a direct transition from the disordered state to lamellae or hexagonally packed cylinders in asymmetric diblock copolymers was found for a finite degree of polymerization. Moreover, a first-order transition between lamellar and disordered state was predicted for symmetric diblock copolymers.

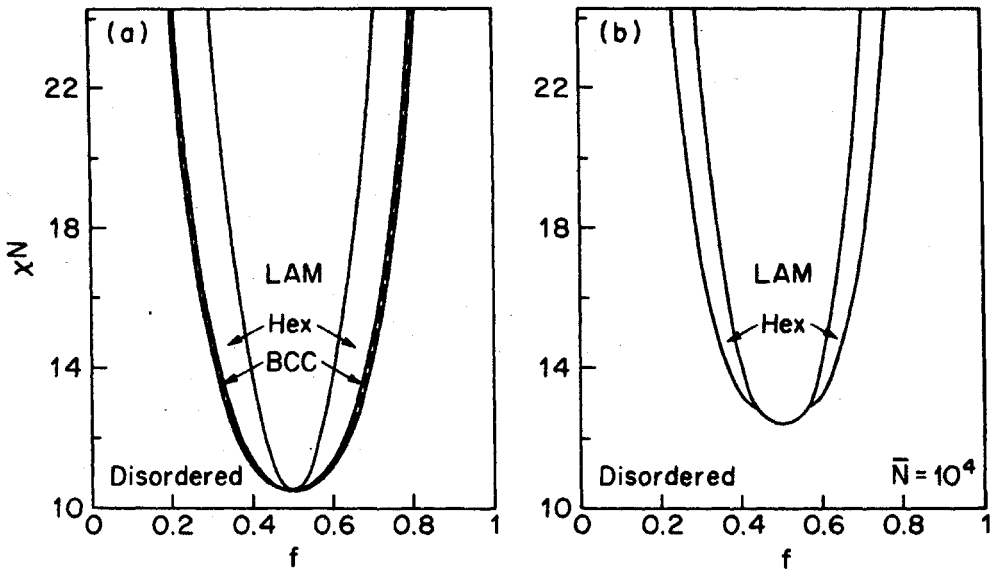

Figure 1.2: Phase diagram of a diblock copolymer according to Leibler's theory (left) and including fluctuation corrections according to Fredrickson and Helfand (right). LAM = lamellar microphase; Hex = hexagonal microphase; BCC = body-centered cubic microphase.[19]

The strong-segregation limit (SSL) accounts for values of $\chi N >> 10$, and has been first investigated theoretically by Meier[20], Helfand and coworkers[21-23], and Semenov[24]. Diblock copolymers belonging to the SSL regime show a high incompatibility of the two blocks, which is reflected by a large value for χ. As a consequence, even for low degrees of polymerization microphase-separation occurs, and a sharp interface separating the domains and therefore an abrupt change of the composition across the domain boundary is observed. Within SSL the long period scales with $L \propto N^{2/3}$. However, this theory does not extend to the WSL. Therefore, calculations on phase diagrams are limited to $\chi N > 100$, which is a rough limit for SSL.

Matsen and Bates cover the bridge between the WSL and SSL by using the self-consistent field theory (SCFT).[25] This allows the calculation of the phase diagram of diblock

copolymers starting from the disordered state, going through the WSL and ending in the SSL (Figure 1.3). This phase diagram includes also the double gyroid morphology besides lamellar, cylindrical, and spherical morphologies. Their calculations revealed that the double gyroid morphology is only stable for $\chi N < 60$.

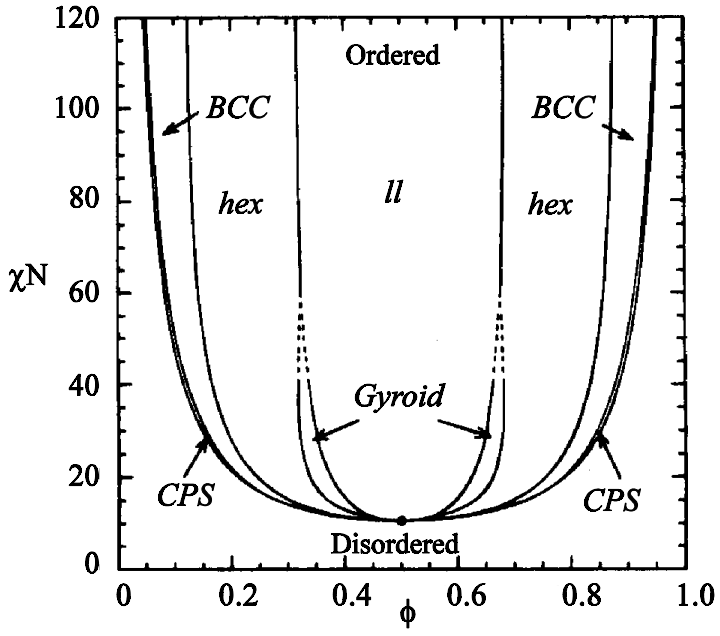

Figure 1.3: Phase diagram of a diblock copolymer following from SCFT assuming similar segment lengths of both blocks. ll = lamellae; hex = hexagonally packed cylinders; BCC = spheres arranged on a body-centered cubic lattice; CPS = spheres arranged on a face centered cubic lattice; ϕ_A = volume fraction of component A in the diblock copolymer.[26]

In addition, binary block copolymers with different topologies have been studied. For symmetric ABA triblock copolymers in the WSL a critical value of $\chi N = 18$[27] was determined for microphase-separation, and this value was confirmed in works on ABA triblock copolymers exhibiting arbitrary ratios between the two end blocks.[28,29] Studies on multiblock copolymers by SCFT also revealed higher critical values for χN.[30] For A_nB_n heteroarm star copolymers a symmetrical phase diagram with a critical value of $\chi N = 10.5$ was obtained.[28] Investigations on $(AB)_n$ starblock copolymers by SCFT, including systems with asymmetric segment lengths, revealed a lower critical value for χN compared to that of AB diblock copolymers.[31] Heteroarm star copolymers with different numbers of arms A_nB_m ($m \neq n$) have also been described theoretically.[31-34]

While the phase behavior of amorphous binary block copolymers, especially diblock copolymers, has been investigated intensively for a long time and most of the fundamental problems seem to be explored, ternary triblock copolymers, especially linear and star terpolymers have been addressed to a much lower extent.[35] In contrast to the morphology of AB diblock copolymers which is mainly determined by one interaction parameter, χ_{AB}, and one independent composition variable, ϕ_A, the morphology of ternary triblock copolymers is determined by three interaction parameters χ_{AB}, χ_{BC}, χ_{AC}, and two independent composition variables ϕ_A, ϕ_B. Moreover, there are theoretically three different block sequences possible, ABC, BAC, and ACB. As a result of the large number of independent variables, it is not surprising that ternary triblock copolymers show a huge variety of morphologies. As an example, the different morphologies in polystyrene-*block*-polybutadiene-*block*-poly(methyl methacrylate) (SBM) triblock copolymers discovered by Stadler and co-workers are summarized in Figure 1.4.[36-41]

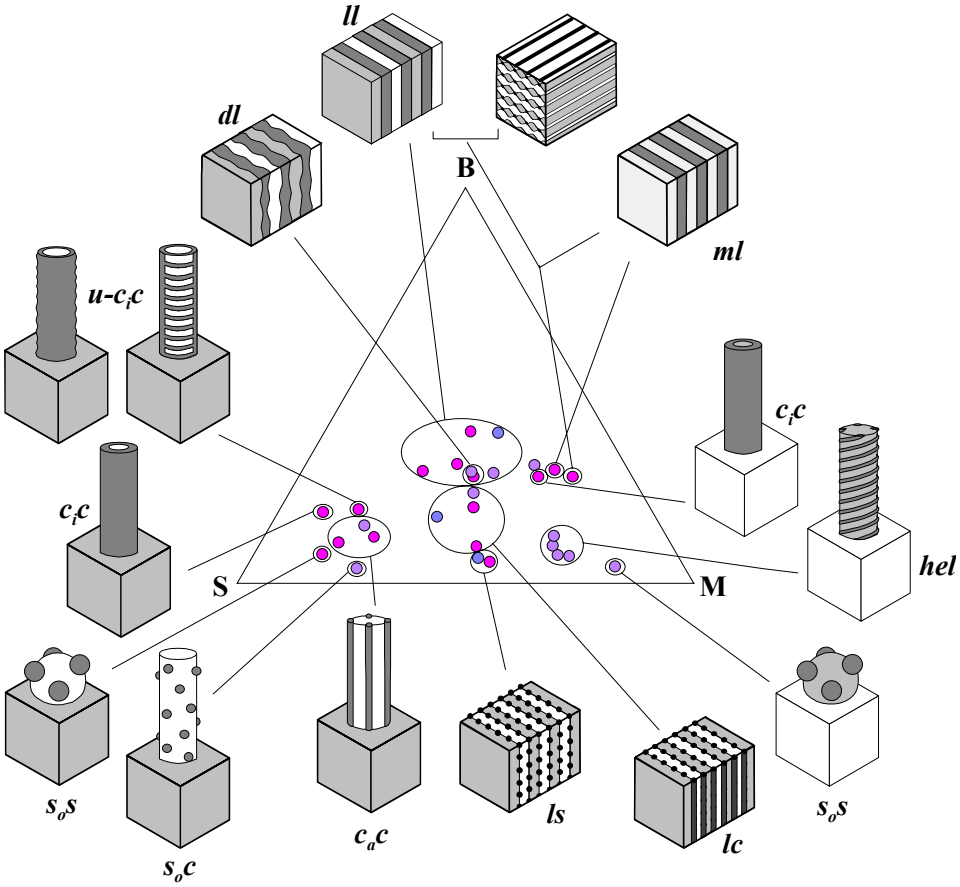

Figure 1.4: Microphase-separated morphologies for polystyrene-*block*-polybutadiene-*block*-poly(methyl methacrylate) (SBM) triblock copolymers (the displayed color shades correspond to the OsO_4 staining in the TEM micrograph).[10]

A theoretical description of the phase behavior of ABC triblock copolymers is difficult due to the large number of relevant parameters involved in the structure formation. Usually theoretical models for diblock copolymers are used and extended to ABC triblock copolymers.

The first theoretical description was given by Spontak et al., however this model is restricted to lamellar morphologies.[42] In a later work the theory of Semenov for diblock copolymers (SSL) was used, considering the end blocks and their interfaces to the middle block as diblock chains.[43] They derived that the long period within the ABC triblock copolymers scales with $L \propto N^{2/3}$. The same scaling law was found by Mogi et al., also applying the Semenov theory, and has been proven by small angle X-ray scattering on lamellar polyisoprene-*block*-polystyrene-*block*-poly(2-vinyl pyridine) (ISP) triblock copolymers.[44]

Ohta and Nakazawa describe a approach, also based on diblock copolymer models within the SSL, for the description of morphologies in symmetrical ($\phi_A = \phi_C$) ABC triblock copolymers with a matrix forming center block.[45] The calculated phase diagram for ISP triblock copolymers is qualitatively equivalent to the experimentally found structures by Matsushita and coworkers.[46-48] However, the interaction parameter between the chemically different segments, χ, is not included in the model and it fails in the description of more complex structures.

While first only the interaction parameters of directly linked blocks are taken into account,[49] later theories also focused on the interaction between the non-linked blocks. Based on the values for the three different interaction parameters in triblock copolymers, χ_{AB}, χ_{BC}, and χ_{AC} Wang et al. calculated phase diagrams which are successful in explaining some of the more complex morphologies.[50] In spite of this, they predicted for some morphologies a composition, which was significantly different from the experimental data.[51]

Stadler´s group extended the theory of Semenov to describe the phase behavior of symmetric[52] and asymmetric[39] ABC triblock copolymers. The calculations include the volume fraction of the middle block ϕ_B, as well as the interfacial tensions γ_{AB}, γ_{BC} and γ_{AC} between the different blocks ($\gamma \propto \chi^{1/2}$) as relevant parameters for structure formation. Using this approach, the experimentally discovered morphologies of linear SBM triblock copolymers were explained in terms of a minimization of interfacial energy. In these systems, the incompatibility between the two end blocks and the middle block is higher than the incompatibility of the two end blocks (χ_{AB}, $\chi_{BC} > \chi_{AC}$). As a consequence, a morphology is

preferred, where the unfavorable interactions between the end blocks and the middle block are as small as possible in order to minimize the total interfacial energy. This in turn implies, that especially for small values of ϕ_B, a large interphase between A- and C- blocks is favored. As an example, for symmetric SBM triblock copolymers the following morphologies were found with decreasing volume fraction of the middle block: ll- (lamellar), lc- (PB cylinders on a lamellar PS/PMMA interphase), and ls-morphology (PB spheres on a lamellar PS/PMMA interphase).

Besides the described models for ABC triblock copolymers in the strong-segregation limit, there are also theoretical calculations by Erukhimovich et al.[53] as well as Werner and Fredrickson[54] based on the "mean-field" approach of Leibler (WSL). Using this method order-disorder transition temperatures can be calculated for different compositions and incompatibilities.

1.3 Crystallization in Block Copolymers

The structure formation in amorphous-semicrystalline block copolymers is determined by the interplay of microphase separation in the melt and crystallization of the crystallizable block. The formed morphology strongly depends on the sequence of the two relevant physical events, i. e. if crystallization occurs from an already microphase-separated melt or from a homogeneous melt.

The kinetic nucleation theory of Hoffman and co-workers was initially developed for homopolymers. The extension of this theory to the crystallization of block copolymers was introduced by Richardson et al..[55]

In its original form, the Lauritzen-Hoffman theory provides expressions for the linear growth rate (Γ), i. e. the rate at which spherulites or axialites grow, as a function of the degree of supercooling ($T_m^0 - T_c$), with the equilibrium melting temperature T_m^0 and the crystallization temperature T_c.[56] In this model it is assumed that the crystal lamellae at the growth front grow at the same rate as the macroscopic linear growth rate (Figure 1.5). Secondary or tertiary nucleation controls the growth together with the short-range diffusion of the crystallizing units. There are also modification of this original theory in the literature, but these do not change the essential features.[57-61]

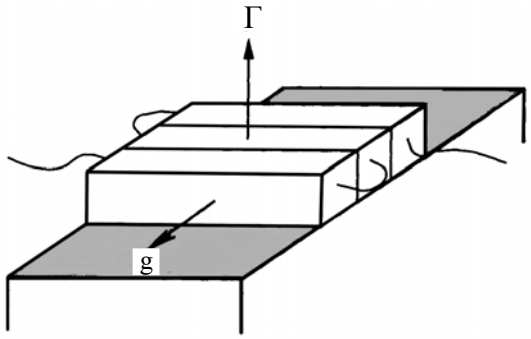

Figure 1.5: Growth of a lamellar crystal according to the Lauritzen-Hoffmann theory. The lateral growth rate is denoted g and the linear growth rate Γ.[62]

Three regimes of growth are predicted. In regime I, for small supercoolings, lateral growth of crystallites occurs with stems in a monolayer on the substrate, whereby the monolayers are added one by one according to the linear growth rate. The lateral growth rate (g) is significantly higher than the rate of formation of secondary nuclei. As a consequence, the surface of the formed crystals is smooth. For higher supercoolings regime II is reached

and the crystal growth is determined by multiple nucleation. As the multiple nucleation is no longer restricted within a monolayer, the secondary nucleation rate is faster compared to regime I. In addition, because of the multiple nucleation on the already existing monolayers the crystallite surface exhibits an increasing roughness. Finally, in regime III, growth occurs by prolific multiple nucleation.

The growth rate in the three regimes, at a given crystallization temperature T_c, can be written as:[56,63]

$$\Gamma_i = \Gamma_{0,i} \exp\left(-\frac{U^*}{R(T_c - T_\infty)}\right)\exp\left(-\frac{2jb\sigma\sigma_L}{\Delta G k T_c}\right) \qquad \textbf{Equation 1.5}$$

Here U* is an activation energy, and T_∞ reflects the temperature at which diffusion is stopped. The parameter j depends on the growing regime, and equals to 2 in regime I and III, whereas j = 1 in regime II. The monolayer thickness contributes as b, the specific free energy of the surface is denoted σ, and σ_L is the lateral surface free energy. ΔG corresponds to the specific change in free energy upon crystallization, and R and k are the universal gas constant and the Boltzmann constant, respectively. $\Gamma_{0,i}$ is a temperature dependent pre-factor, which is specific for the three regimes.

The approach of Hoffman and Lauritzen encountered in spite of its success also criticism, especially by Point[64] and Sadler[65]. Sadler constructed an alternative model which works for rough growth faces, introducing a reversible detachment and attachment of short-chain sequences as elementary steps. Calculations revealed that the growth face exhibits many configurations, of which only a minority allows the face to progress. As a consequence, the rate of growth is controlled by high entropic activation barriers. However, the different models have one common feature, as they assume that the lamellar crystallites grow directly into the entangled melt.

More recently Strobl et al. introduced a new approach based on earlier works and on own investigations, proposing that crystallization proceeds via a transition of mesomorphic and granular crystalline layers to lamellar crystallites.[66-68] A sketch of the proposed mechanism is given in Figure 1.6.

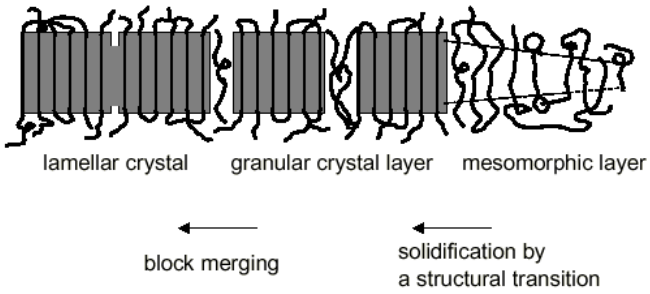

Figure 1.6: Sketch of the route proposed for the formation of polymer crystallites.[68]

The process starts with the attachment of straightened chain segments with a certain minimum length from the isotropic melt onto the lateral growth face of a layer with a mesomorphic inner structure. The stretching is not perfect, i. e. the chains, although basically helical, include many conformational defects. There exists a minimum thickness for the mesomorphic layer in order to be stable in the surrounding melt. Subsequently, each part of the mesomorphic layer thickens with time, implying a continuous rearrangement of the chain sequences in the zone composed of folds and loops near to the layer surface. When a critical thickness of the mesomorphic layer is reached, the layer solidifies by a structural transition. The resulting structure can be described as a "granular crystal layer", consisting of crystal blocks in a planar assembly. Finally, the crystal blocks merge together, which goes along with an improvement of their inner perfection. The resulting homogeneous lamellar crystallite exhibits the same thickness as the constituent blocks. The merging process provides a stabilization, however, the degree of stabilization might not be uniform through the sample. As a result, some regions in the sample may even remain in the granular crystal state.

The orientation of crystalline stems with respect to the lamellar interface in block copolymers is a subject of ongoing interest and controversy. The two possible orientations of crystalline stems within a semicrystalline block copolymer are depicted schematically in Figure 1.7. The orientation of crystalline stems has been investigated intensively for polyethylene and poly(ethylene oxide) containing diblock copolymers and was found to depend in a very sensitive fashion on the sample preparation technique. In contrast to homopolymers, where the crystalline stems are arranged perpendicular with respect to the lamellar interphase, parallel chain orientation has been observed for block copolymers crystallizing from a microphase-separated melt. However, it is not clear if the parallel folding is the most stable one, or whether perpendicular orientation can also occur for crystallization from homogeneous melts or solutions.

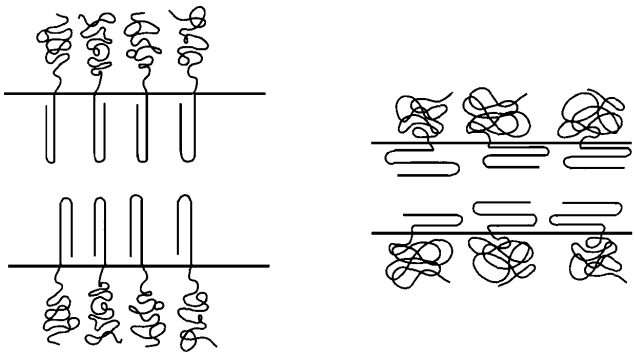

Figure 1.7: Schematic depiction of perpendicular and parallel chain folding of the crystalline chains with respect to the domain interphase in semicrystalline block copolymers.[62]

Investigations by Douzinas and Cohen on oriented polyethylene-*block*-poly(ethyl ethylene) (PE-*b*-PEE) diblock copolymers, exhibiting a microphase-separated melt, revealed that the PE chains are oriented parallel to the lamellar interphase.[69] This is in agreement with results obtained by Séguéla and Prud'homme.[70] There have been also investigations on lamellar polyethylene-*block*-poly(ethylene-*alt*-propylene) (PE-*b*-PEP) diblock copolymers which were oriented using a channel die.[71] It turned out that the lamellae orient perpendicular to the plane of shear when the diblock copolymers were oriented above the melting temperature of PE, whereas a parallel orientation was found when compression occurred below the melting temperature. However, in both cases the crystalline PE chains were oriented parallel to the lamellar interphase. In contrast to these results, Rangarajan et al. observed for PE-*b*-PEP diblock copolymers (12 – 56 wt-% PE) a perpendicular orientation of the crystalline PE stems.[72] In this case the samples were not oriented and crystallization occurred from a homogeneous melt.

Investigations on oriented PE-*b*-PEE, PE-*b*-PEP, and polyethylene-*block*-poly(vinyl cyclohexane) (PE-*b*-PVCH) diblock copolymers have been performed by Hamley et al.[73,74] In symmetric PE-*b*-PVCH diblock copolymers crystallization of PE is confined within a lamellar morphology with glassy PVCH lamellae, as the glass transition of PVCH is higher than the crystallization temperature of PE. A parallel orientation of the crystalline PE stems with regard to the lamellar interphase was observed both for diblock copolymers with a rubbery or a glassy amorphous block.

In contrast to the preferential parallel orientation of crystalline stems with respect to the domain interphase in PE containing diblock copolymers, investigations on poly(ethylene oxide) based diblock copolymers revealed a perpendicular folding of the crystalline PEO

chains. In this context, the reader is referred to representative works on poly(ethylene oxide)-*block*-poly(butylene oxide) (PEO-*b*-PBO)[75,76] and polyisoprene-*block*-poly(ethylene oxide) (PI-*b*-PEO)[77] diblock copolymers.

In semicrystalline-amorphous diblock copolymers basically two different situations can occur depending on the segregation strength between the chemically different blocks. Crystallization can be either confined in lamellar, cylindrical or spherical microdomains for strongly segregated systems, or crystallization predominates the structure formation for weakly segregated or homogeneous systems. The final microphase and crystalline morphology is determined by three competing physical events: the microphase-separation in the melt (order-disorder transition temperature T_{ODT}), the crystallization temperature T_c of the crystallizable component, and the vitrification (glass transition temperature T_g) of the amorphous block. In general three different situations can be distinguished (a more detailed description including citations of various contributions can be found in chapter 3.2.1 and ref.[78]). In systems exhibiting a homogeneous melt ($T_{ODT} < T_c > T_g$), microphase-separation is driven by crystallization. This results in a lamellar morphology where crystalline lamellae are sandwiched by the amorphous block layers, regardless of the composition. In weakly segregated systems ($T_{ODT} > T_c > T_g$), often referred to as "soft confinement", crystallization frequently occurs with little morphological constraint enabling a "breakout" from the ordered melt structure. Consequently, any preexisting morphology in the molten state is overwritten by crystallization, resulting in a lamellar structure. However, confined crystallization within spherical or cylindrical microdomains is possible in strongly segregated systems and/or for highly entangled amorphous blocks. A strictly confined crystallization within microdomains is observed for strongly segregated diblock copolymers with a glassy amorphous block ($T_{ODT} > T_g > T_c$, hard confinement). As a result, the initially formed melt structure is preserved upon crystallization.

Crystallization within block copolymer microdomains is not only affected by the strength of confinement. Furthermore, the structure of the microdomain, i. e. continuous (gyroid, lamellae) or dispersed (cylinders, spheres), and even the size of the microdomain exhibit a significant influence. For example, Chen et al. observed for blends of a polybutadiene-*block*-poly(ethylene oxide) (PB-*b*-PEO) diblock copolymer with PB a decrease in crystallization temperature for the PEO block with decreasing PEO domain size (PEO content).[79] Similar results were obtained for other block copolymers, exhibiting confined crystallization within isolated spherical or cylindrical microdomains.[80-84] In addition, confined crystallization is often connected with a substantial decrease in crystallinity compared to the

corresponding semicrystalline homopolymers due to spatial restrictions.[82,84-91] Crystallization can even be suppressed if the crystallizable block is confined into spheres or cylinders.[90-92] Studies on the crystallization kinetics revealed a strong dependence on the confinement active during crystallization. Unusual first-order crystallization kinetics with an Avrami exponent of n = 1 have been observed for strongly confined crystallization within spherical or cylindrical microdomains.[93-95] This observation has been related to a homogeneous nucleation mechanism. However, in some special cases even lower Avrami exponents have been detected.[80,90]

The crystallization in polymers is usually induced by heterogeneous nucleation, homogeneous nucleation or self-nucleation. In crystallizable homopolymers crystallization in the bulk state commonly occurs on heterogeneous nuclei (catalyst debris, impurities, and other types of heterogeneities of unknown nature) at relatively low supercoolings (10 - 15 °C).[96] Homogeneous nucleation includes the formation of a crystal-like embryo induced by density fluctuations in the melt, which occurs at comparatively high supercoolings (50 - 70 °C). The nucleation on remaining crystal fragments in the melt, which reflect crystallographically "ideal" nuclei, is referred to as self-nucleation. Within block copolymers the type of nucleation strongly depends on the type of microdomain. Crystallization in large or continuous domains is mostly induced by heterogeneous nucleation, since the probability that a heterogeneity is located within the crystallizable domain is sufficiently high. However, if the crystallizable block is confined into small isolated microdomains (spheres, cylinders) crystallization proceeds in a fractionated manner, i. e. several crystallization exotherms are observed, or crystallization can only be induced by homogeneous nucleation.[79-84,90,97-101] Microdomains that contain the heterogeneities usually active at low supercoolings in the bulk homopolymer will crystallize at an identical temperature compared to that of the bulk polymer. However, if less efficient heterogeneities are present in the microdomain, a larger supercooling is necessary in order to induce crystallization. Those microdomains that do not contain any heterogeneity will only be able to nucleate homogeneously, in the case that the interphase does not affect the nucleation process. Especially, in block copolymers where the crystallizable component is confined into small isolated microdomains the number density of isolated microdomains is significantly higher than the average number of available heterogeneities.[83] At least 10^{15} isolated microdomains/cm^3 could be present, while for instance a bulk PEO homopolymer contains less than 10^6 heterogeneities/cm^3. As a result, the probability of a heterogeneity to be situated in an isolated microdomain is vanishing small, thus favoring homogeneous nucleation.

Besides the vast number of publications concerning the crystallization within semicrystalline-amorphous diblock copolymers, there have been only few contributions on ABC triblock copolymers with crystallizable components. Among them are reports by Stadler et al. and other groups on polystyrene-*block*-polybutadiene-*block*-poly(ε-caprolactone) (PS-*b*-PB-*b*-PCL) triblock copolymers and their hydrogenated analogues (PS-*b*-PE-*b*-PCL) in which a complex interplay between microphase-separation and crystallization has been found.[100-108] In addition, there are also reports on PS-*b*-PI-*b*-PEO[109-112], PS-*b*-PEP-*b*-PE[113], poly(α-methyl styrene)-*block*-polyisobutylene-*block*-polypivalolactone (PmS-*b*-PIB-*b*-PVL)[114] and PS-*b*-PEO-*b*-PCL[82] triblock copolymers.

1.4 PBT-Based Copoly(ether ester)s

Copoly(ether ester)s are multiblock copolymers consisting of polyester hard segments and low molecular weight polyether soft segments. The crystalline hard segments typically consist of poly(butylene terephthalate) (PBT) or poly(ethylene terephthalate) (PET), sometimes also poly(butylene isophthalate) (PBI) is used.[115] The soft segment comprises different hydroxy telechelic polyethers, like poly(ethylene oxide) (PEO), poly(propylene oxide) (PPO), poly(tetramethylene oxide) (PTMO), and poly(ethylene oxide)-*block*-poly(propylene oxide)-*block*-poly(ethylene oxide) (PEO-*b*-PPO-*b*-PEO) triblock copolymers.[116] Copoly(ether ester)s were discovered independently in the 1950s by Imperial Chemical Industries and Du Pont by the incorporation of PEO into PET.[117,118] The synthesis of PBT based copoly(ether ester)s has been studied intensively by Hoeschele and co-workers (Du Pont).[116,119,120] In analogy to the preparation of PBT[121,122], the synthesis is accomplished by a 2 step melt polycondensation of a mixture of dimethyl terephthalate, 1,4-butandiol, and a low molecular weight polyether in the presence of a suitable catalyst (Scheme 1.1).

In the first step transesterification between dimethyl terephthalate and the diol components occurs at ca. 200 °C under formation of a prepolymer. Usually an excess of 1,4-butandiol is used to accelerate the formation of the pre-polymer. The released methanol from the transesterification reaction is removed by distillation. Polycondensation proceeds in the second step under release of 1,4-butandiol. Here the temperature is increased to ca. 250 °C and vacuum is applied in order to distill of surplus 1,4-butandiol. The degree of polymerization strongly depends on the complete removal of the formed 1,4-butandiol during the second step, since the polycondensation reflects an equilibrium reaction. Usually tetrabutyl orthotitanate is used as catalyst. More recent investigations show that mixtures of tetrabutyl orthotitanate with lanthanide- and hafnium-acetylacetonate catalysts exhibit a higher activity compared to pure tetrabutyl orthotitanate.[123,124] In addition, the polymerization time can be significantly reduced using this novel catalyst system.

1. Step (transesterification)

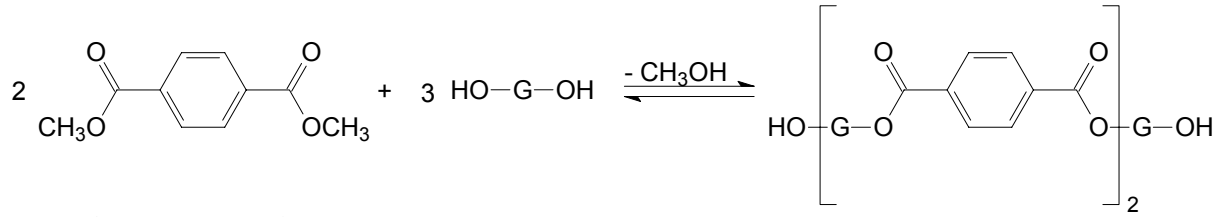

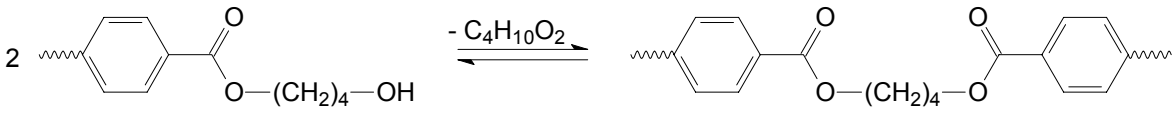

2. Step (polycondensation)

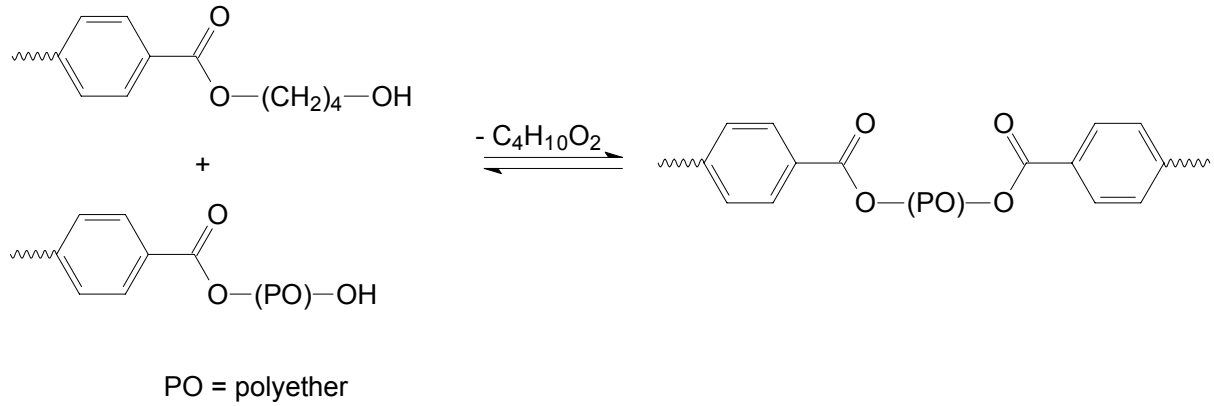

Scheme 1.1: Preparation of copoly(ether ester)s by a 2 step melt polycondensation.

Copoly(ether ester)s are multiblock copolymers with alternating hard and soft segments along the polymer chain (Figure 1.8). In these materials the soft polyether chains act as network chains, while the polyester hard segments form crystalline domains acting as physical (thermoreversible) crosslinks. The high melting point of the polyester hard segment (PBT, T_m = 220 °C) in combination with the low glass transition temperature of the polyether soft segment (T_g ca. –60 °C) results in a rubber like behavior over a wide temperature range.

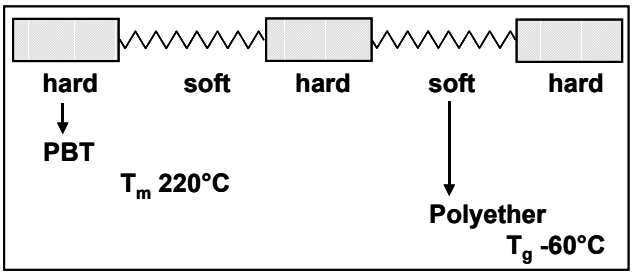

Figure 1.8: Schematic representation of the multiblock structure of copoly(ether ester)s.

Commercially important are copoly(ether ester)s based on PBT hard segments. The two main commercial grades are Hytrel® (Du Pont) and Arnitel® (DSM). The mechanical properties can be adjusted by variation of the amount and block length of hard and soft segments, which in turn creates a wide range of properties. PBT based copoly(ether ester)s show good tear, fatigue, high abrasion and solvent resistance as well as very good low- and high-temperature properties. Thus, these materials are used in applications where severe requirements are demanded towards stiffness and strength at high and low temperatures. For Arnitel grades the main market segments are: automotive (constant velocity joints, air bag covers), hose and tube (hydraulic tubing, cover jackets for fire hoses), wire and cable (fiber optic applications, steel cable sheaths, retractable coil cords for telephones), and film (breathable films for sportswear, shoes, rainwear, etc.).

The morphology of PBT-PTMO based copoly(ether ester)s has been studied intensively.[116,119,125-129] It is generally assumed that the structure can be described by a two-phase model consisting of a crystalline PBT hard phase and a mixed PBT-PTMO soft phase, both being co-continuous (Figure 1.9).[119,125,128,129] Because of the miscibility of PBT and PTMO segments in the melt structure formation upon cooling is induced by crystallization, resulting in the formation of the characteristic two-phase structure consisting of interconnected PBT crystallites embedded in an amorphous matrix of mixed PBT and PTMO segments.[126,130] However, more recent studies utilizing solid-state NMR[131] and thermomechanical analysis[132] demonstrate that the amorphous phase is not homogeneous, but consists of a PTMO-rich phase and a PBT/PTMO mixed phase.

The structure of the crystalline polyester hard segment phase strongly depends on the crystallization conditions. Different structures have been reported: next to lamellar[128,133-135], spherulitic[125,127,136,137], dendritic[125,136], and even shish kebab structures[125].

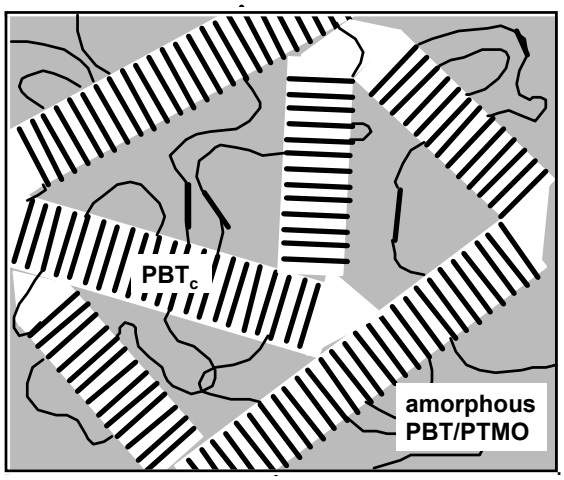

Figure 1.9: Schematic representation of the two-phase structure of PBT-PTMO-based copoly(ether ester)s (PBT_c corresponds to crystalline PBT domains).[128]

The presence of a co-continuous PBT hard phase in PBT-PTMO based copoly(ether ester)s causes a significant plastic deformation and hence minor elastic properties of these materials especially upon relatively large elongations.[138] Orientation studies revealed that upon elongation, the soft segments orient parallel to the direction of the applied stress[139], whereas the crystalline hard segments orient transverse to the stress direction for small strain values. Upon higher elongations the crystalline PBT segments orient parallel to the direction of stress, which is connected with an irreversible disruption of the continuous crystalline hard segment phase.[140] This in turn results in the observed high plastic deformations especially at high strains. Finally, after complete reorientation of the crystalline PBT phase the stress is submitted through the continuous soft segment phase, until it breaks.

The general idea is that the elasticity of copoly(ether ester)s can be improved by changing the continuous PBT hard phase to a dispersed phase (Figure 1.10). This can be achieved by increasing the incompatibility of the hard and soft segments, as was demonstrated in thermoplastic polyurethanes[141,142], and in strongly phase separated copoly(ether ester aramides)[143].

In this work (cooperation with DSM Research, Geleen) the incorporation of hydroxy telechelic hydrogenated polybutadiene soft segments (HO-PEB-OH, KRATON® liquid Polymer HPVM-2203 (Shell)) into PBT based copoly(ether ester)s in order to improve the elasticity of common PBT-PTMO based systems has been investigated. The high incompatibility of the nonpolar PEB segments should result in an extreme phase separation between the PEB and the PBT segments in the melt, and thus in a dispersed PBT hard phase, even for high PBT contents. However, the incorporation of polyolefinic soft segments into

copoly(ether ester)s is limited due to macrophase-separation during the melt polycondensation process. This was shown for poly(butylene terephthalate)-*block*-polyisobutylene segmented block copolymers with polyisobutylene soft segments.[144,145] Due to the high incompatibility of polyisobutylene with the polar reactants dimethyl terephthalate and 1,4-butandiol phase-separation occurs during the melt polycondensation, resulting in a very poor incorporation of the soft segment. The macrophase-separation can be reduced to some extent by using high boiling solvents like *m*-cresol and 1,2,4-trichlorobezene, which are good solvents for PBT and polyisobutylene. The solvent is removed together with surplus 1,4-butandiol in the polycondensation step by applying vacuum during polymerization. Nevertheless, incorporation of polyisobutylene is incomplete, which in turn results in poor mechanical properties.

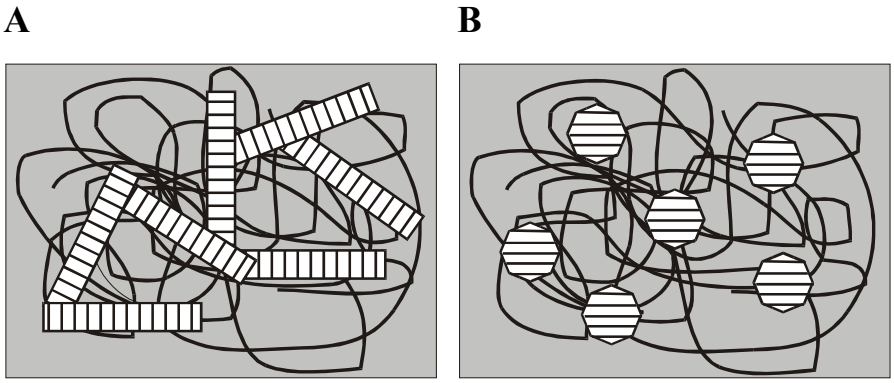

Figure 1.10: Schematic representation of a continuous (A) and a dispersed (B) crystalline hard phase.

The approach used in this work to avoid macrophase-separation implies the chain extension of HO-PEB-OH (M_n = 3600 g/mol) with ethylene oxide by means of anionic ring-opening polymerization to yield the corresponding PEO-*b*-PEB-*b*-PEO triblock copolymers. The polar PEO blocks are expected to act as compatibilizer between the nonpolar PEB block and the polar PBT segments, thus resulting in a homogeneous reaction mixture during melt polycondensation. Several PEO-*b*-PEB-*b*-PEO triblock copolymers with varying PEO block length have been synthesized and successfully incorporated into PBT-based copoly(ether ester)s.[146] Copoly(ether ester)s with PBT contents below 45 wt-% and PEO-*b*-PEB-*b*-PEO triblock copolymers exhibiting a PEO block length < 1400 g/mol show a clear melt during melt polycondensation. This demonstrates, that the PEO blocks efficiently act as compatibilizer between the nonpolar PEB blocks and the polar PBT segments. The

comparatively high molecular weight of the PEO-*b*-PEB-*b*-PEO soft segments (M_n = 5300 – 8600 g/mol) results in an increased average PBT hard segment length, compared to the case of conventional PBT-PTMO-based copoly(ether ester)s with an average M_n of the PTMO soft segment between 1000 and 2000 g/mol, assuming similar PBT contents. This in turn results in a comparatively higher melting point of the PBT hard segments (T_m = 190 – 220 °C) in PEO-*b*-PEB-*b*-PEO based copoly(ether ester)s.

Dynamic shear experiments in combination with small-angle X-ray scattering (SAXS) reveal that crystallization of the PBT hard segments occurs from a microphase-separated melt.[147] This in turn results in the formation of a dispersed PBT hard phase, as is demonstrated by transmission electron microscopy (TEM) and scanning force microscopy (SFM). As an example the TEM micrograph of PBT30-1380 is shown in Figure 1.11. Because of the used staining technique (RuO_4), the crystalline PBT domains remain unstained and appear as bright regions, which are clearly dispersed within the matrix of the PEO-*b*-PEB-*b*-PEO soft segment.

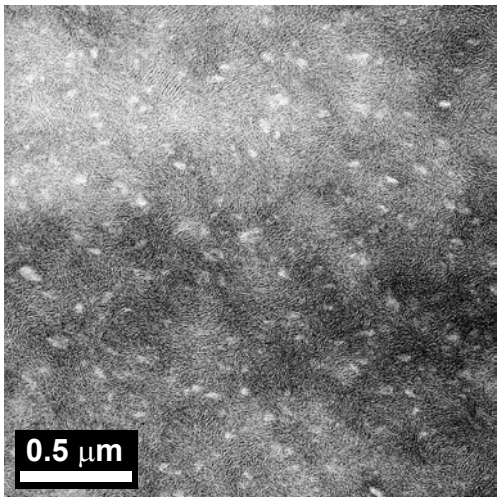

Figure 1.11: TEM micrograph of PBT30-1380 (30 wt-% PBT. M_n(PEO) = 1380 g/mol) stained with RuO_4 vapor, showing dispersed crystalline PBT domains.

The microphase structure has been investigated in more detail applying differential scanning calorimetry (DSC) and dynamic mechanical analysis (DMA).[147] The results indicate a pronounced microphase separation in the soft segment phase, exhibiting a pure microphase separated PEB phase. This is reflected by the observation of a glass transition temperature at ca. –60 °C, which is independent of composition. In addition, glass transition temperatures attributable to a mixed amorphous PEO/PBT phase and a pure amorphous PBT phase are visible. Besides the melting temperature of the PBT hard segments a low temperature melting

endotherm is observed for the PEO blocks, indicating the presence of a PEO rich phase, enabling crystallization of PEO. Thus, from the combination of results obtained by DSC and DMA a structure model can be proposed as depicted in Figure 1.12. The copoly(ether ester)s with PEO-*b*-PEB-*b*-PEO triblock copolymer soft segments consist of a crystalline PBT phase and an amorphous phase, which can be divided into a pure PEB phase, a PEO-rich phase besides a mixed PEO/PBT phase, and a pure amorphous PBT phase. However, the existence of a pure amorphous PBT phase and a mixed amorphous PEO/PBT phase cannot be proven from the performed DMA experiments. To provide more evidence for the proposed different phases, the PEB containing copoly(ether ester)s have been studied in more detail at DSM Research using solid-state NMR.

Figure 1.12: Schematic representation of the proposed structure of copoly(ether ester)s with PEO-*b*-PEB-*b*-PEO soft segments.

Solid-state NMR is a powerful tool to study the microphase structure of polymers.[148] NMR relaxation experiments are of special interest, since relaxation times are highly sensitive towards differences in chain mobility, and thus provide information about morphological changes. A combination of ^{13}C inversion recovery cross-polarization measurements (IRCP), proton-$T_{1\rho}$ relaxation experiments, and investigations on PEB based copoly(ether ester)s with selectively deuterated PBT segments using ^{2}H-solid-state echo and inversion recovery-T_1 techniques has been applied to confirm the structure model proposed from DSC and DMA investigations.[149]

The IRCP experiment distinguishes between carbons with high and low mobility. This enables the study of the molecular mobility of the hard and soft segments within PEB-based copoly(ether ester)s. The experiment is composed of two contiguous parts. The first part is a classical cross-polarization step, during which magnetization is transferred from protons to carbons for a contact time τ_1 in order to enhance the ^{13}C signal. In the subsequent step (τ_2) the carbon magnetization is inverted. The rate of this inversion is determined by the cross-polarization dynamics. The cross-polarization rate depends on the strength of the magnetic dipole-dipole coupling between ^{13}C and ^{1}H spins, which in turn is affected by molecular motions. For rigid segments showing slow motions, the cross-polarization is relatively fast. On the contrary, in the case of fast motions the cross-polarization is a relatively slow process.

Therefore, it can be expected that the magnetization of the crystalline PBT hard segments inverts faster than that of the PEO and PEB segments in the soft phase (Figure 1.13).

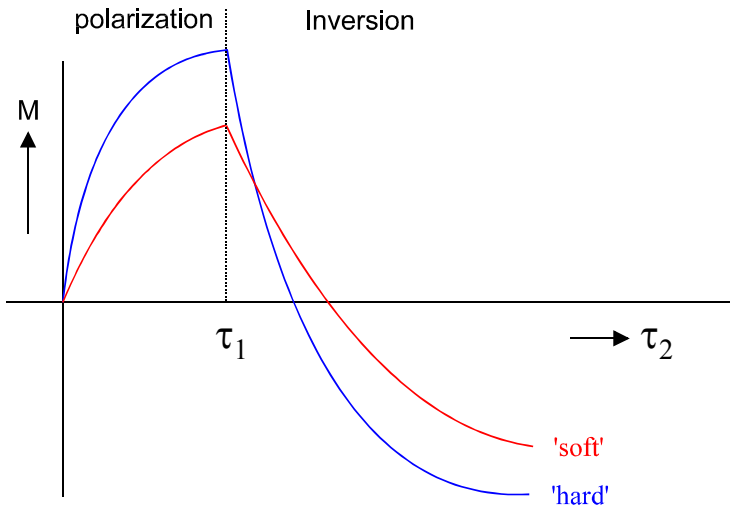

Figure 1.13: Magnetization build-up and decay during an IRCP experiment.

As an example, the results from IRCP investigations will be described for the PEO segments in the following.[149] The IRCP measurements show that the PEO resonance is actually composed of two parts, exhibiting different inversion times. This is contributed to PEO segments showing different mobility. The resonance that inverts faster is attributed to an amorphous PEO-rich phase exhibiting a higher mobility. The resonance with a higher inversion time corresponds to a mixed amorphous PEO/PBT phase, reflecting a restricted mobility due to partial mixing with the more rigid PBT segments (T_g ca. 50 °C).

In summary, the IRCP results indicate that the amorphous phase is composed of a highly mobile PEO-rich phase, a PEO/PBT mixed phase, and a pure PEB phase. This assignment is in agreement with the DSC and DMA results and has been further underlined by ^{1}H-$\tau_{1\rho}$ relaxation experiments and ^{2}H-solid-state echo measurements on copoly(ether ester)s with selectively deuterated PBT segments.[149] However, from these experiments it is not possible to prove the existence of a pure amorphous PBT phase, as was concluded from the observation of a glass transition temperature at ca. 50 °C.[147] Therefore, additional inversion-recovery solid state deuterium NMR investigations on deuterated PBT and copoly(ether ester)s with selectively deuterated PBT segments have been performed, and confirm the presence of a pure amorphous PBT phase in PEB-based copoly(ether ester)s with relatively high PBT contents.

Morphological investigations show that the nonpolar PEB segments in copoly(ether ester)s with PEO-*b*-PEB-*b*-PEO triblock copolymer soft segments induce a pronounced microphase-separation within the soft segment phase. This results in the formation of a dispersed PBT hard segment. This in turn is expected to improve the elasticity of these materials compared to the case of conventional PBT-PTMO-based copoly(ether ester)s exhibiting a continuous PBT hard phase. Mechanical testing reveals a significantly improved elastic recovery for the copoly(ether ester)s based on PEO-*b*-PEB-*b*-PEO soft segments.[147] As an example, the stress-strain traces obtained for a PEB-based copoly(ether ester) with 20 wt-% PBT (PBT20-1000) and a PTMO-based copoly(ether ester) (PBT1000/50) are compared in Figure 1.14. It can be clearly deduced, that the elastic recovery is significantly improved by changing the continuous PBT hard phase in PBT1000/50 to a dispersed hard phase in PBT20-1000.

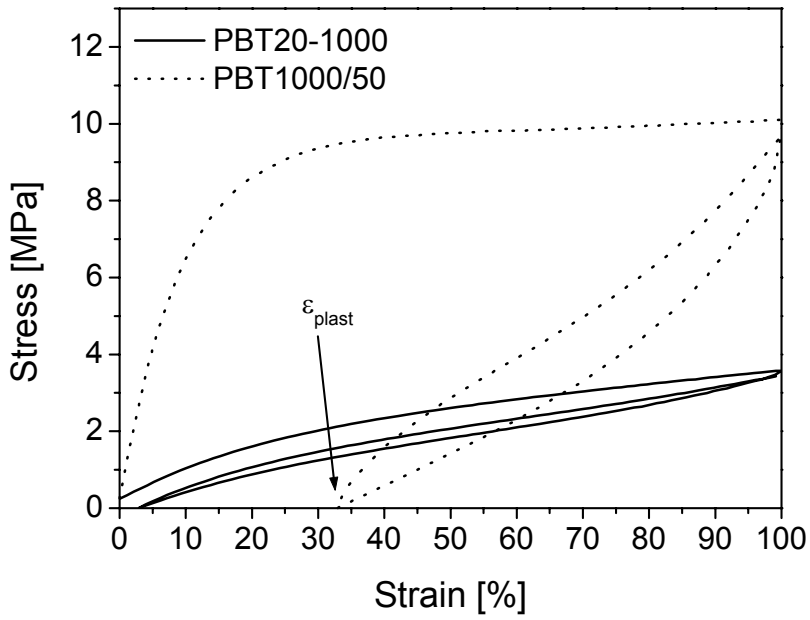

Figure 1.14: Comparison of hysteresis measurements for PBT20-1000 (20 wt-% PBT, M_n(PEO) = 1000 g/mol) and PBT1000/50 (50 wt-% PBT, M_n(PTMO) = 1000 g/mol), a PBT-PTMO-based copoly(ether ester) exhibiting a continuous PBT hard phase.

1.5 ABA and ABC Triblock Copolymers

The discovery of TPEs based on PS-*b*-PB-*b*-PS and PS-*b*-PI-*b*-PS triblock copolymers was initiated by the development of alkyllithium initiators for the anionic living polymerization of isoprene in nonpolar solvents, which yields polyisoprene with a high cis-1,4 content.[150] The synthesis of PS and PB containing block copolymers using alkyllithium initiators was first described in 1957[151], however, at this time these polymers were not recognized as TPEs. At that time intensive studies on the melt rheology of polybutadienes[152] and polyisoprenes[153] have been performed. Both show Newtonian behavior, which in turn gives severe problems in their commercial manufacture and subsequent storage, as they behave like very viscous liquids. To solve this problem, investigations on ABA block copolymers with short polystyrene end blocks were made at Shell chemical research. It turned out that these materials showed non-Newtonian behavior, i. e. their melt viscosities tended toward infinity as the shear rate approached zero. In addition, tensile testing revealed properties similar to those of conventional vulcanizates, i. e. high tensile strength, high elongation at break, and rapid and almost complete recovery after elongation.[154,155] These unique mechanical properties have been attributed to a two-phase structure, arising from the incompatibility of the polymer blocks ("domain theory").[156] The PS minority phase forms dispersed domains (spheres or cylinders), acting as thermoreversible crosslinks, embedded in the matrix of the PB or PI soft blocks.

The mechanical properties of PS-*b*-PI-*b*-PS and PS-*b*-PB-*b*-PS triblock copolymers are mainly determined by the ratio of the PS hard phase to the PB or PI soft phase.[1] An increasing PS content results in an increased tensile modulus, whereby the tensile strength remains nearly unchanged in the case of PS-*b*-PI-*b*-PS triblock copolymers. However, there is a limiting value for the PS content arising from partial miscibility of the hard and soft segments, if the PS content is getting too low. This leads to a substantial weakening of the network strength, resulting in poor mechanical properties, i. e. low tensile strength and low elongation at break. Systems with relative high PS contents ($\geq$ 40 wt-%) show a initial yield point. This can be attributed to the fact that at these high PS contents the PS domains are no longer isolated but show some interconnections. Successive break up of interconnected PS domains upon elongation results in the observed yielding behavior, and in a poor elastic recovery. In addition, the tensile modulus depends on the glass transition temperature of the hard domains. Investigations on ABA triblock copolymers with poly(α-methyl styrene)

(PmS) hard domains (T_g ca. 165 °C) show a significantly increased tensile modulus compared to that of systems with PS hard domains (T_g ca. 105 °C) exhibiting a comparable composition.[157] There have been also investigations on poly(α-methyl styrene)-*block*-poly(dimethyl siloxane)-*block*-poly(α-methyl styrene) (PmS-*b*-PDMS-*b*-PmS) triblock copolymers, which are of special interest due to the thermal stability of the PDMS blocks.[158] However, mechanical testing shows a significantly lower tensile strength compared to that of PS-*b*-PI-*b*-PS triblock copolymers. This was attributed to the low interphase adhesion in the PDMS-based triblock copolymers.

In ABA triblock copolymers the middle block chains can form loops or bridges (Figure 1.15 A). In the loop both ends of the middle block chain are attached to the same A microdomain, whereas in the bridge the two end blocks reside on different A microdomains. The bridges contribute to the elastic properties of the material, whereas the loops in general do not but decrease the elastic modulus.

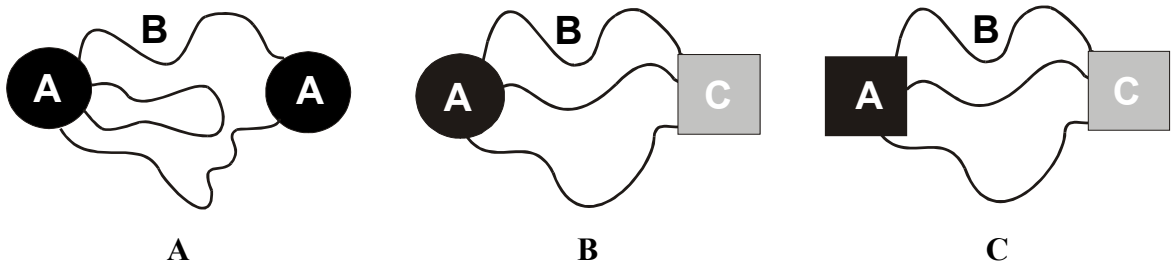

Figure 1.15: Schematic representation of the middle block chains in triblock copolymers. (A) amorphous ABA triblock copolymers: loops and bridges; ABC triblock copolymers with one (B) or two (C) semicrystalline end blocks: only bridges.

There have been several investigations on the loops to bridges population ratio in ordered ABA triblock copolymers.[159-164] Based on theoretical calculations, Matsen and co-workers[160,161] found a bridge fraction of $\phi_{bridge} \cong 0.4$, whereas Jones et al.[162] assumed a value of $\phi_{bridge} \cong 0.63$. Experimental investigations on the loops to bridges ratio in symmetrical PS-*b*-PI-*b*-PS triblock copolymers were performed by Watanabe[163] and Karatasos et al.[164] using dielectric relaxation spectroscopy. For compression-molded samples they found a bridge fraction of $\phi_{bridge} \cong 0.4$. Based on Monte Carlo computer simulations using the Cooperative Motion Algorithm (CMA) they determined an equilibrium bridge fraction of $\phi_{bridge} \cong 0.5 - 0.37$, depending on the molecular weight. In general, the population of bridges decreases with increasing molecular weight of the ABA triblock copolymer.

In terms of improving the elastic properties of common ABA-type thermoplastic elastomers it would be favorable to increase the fraction of bridges, since loops do not contribute to the elastic properties. ABC triblock copolymers offer a way to build thermoplastic elastomers without any loops, if the A- and C-blocks are immiscible (Figure 1.15B, C). Since the immiscibility is a function of the product $N_{AC}\chi_{AC}$, either strongly incompatible components or a high degree of polymerization is necessary (N_{AC} is the degree of polymerization of the A- and C-block and χ_{AC} is the segmental interaction parameter between the two species).[165] However, a high incompatibility and/or a high molecular weight are disadvantageous in view of processing, as they result in a comparatively high melt viscosity. For polystyrene-*block*-polybutadiene-*block*-poly(methyl methacrylate) (PS-*b*-PB-*b*-PMMA) triblock copolymers it was shown that a sufficient microphase separation between the minority components PS and PMMA can only be achieved with a relatively high molecular weight.[41,166]

One way to achieve high immiscibility at low molecular weights is the use of semicrystalline block copolymers, since crystallization is a strong driving force for microphase-separation. Investigations on polyethylene-*block*-poly(ethylene-*alt*-propylene) (PE-*b*-PEP) diblock copolymers revealed that even for low molecular weights a microphase-separated structure is obtained due to crystallization induced microphase-separation.[71,72,167] Furthermore, the segmental interaction parameter between PE and PEP segments shows a comparatively low value of $\chi = 0.007$[168] at 120 °C resulting in a homogeneous melt in a wide composition range, which in turn is advantageous in view of processing.

Semicrystalline ABA type thermoplastic elastomers with polyethylene end blocks have already been investigated with respect to their morphology and mechanical properties.[70,169-175] Morton and co-workers compared polyethylene-*block*-polyisoprene-*block*-polyethylene (PE-*b*-PI-*b*-PE) and polyethylene-*block*-poly(ethylene-*stat*-butylene)-*block*-polyethylene (PE-*b*-PEB-*b*-PE) triblock copolymers with polystyrene-based TPEs.[171,173-175] The PE-based ABA triblock copolymers show better solvent resistance and exhibit a homogeneous melt in the case of the PE-*b*-PEB-*b*-PE systems. Triblock copolymers with a PE content ≤ 30 wt-% show an elastomeric behavior with low plastic sets after elongation, whereas systems with a higher PE content exhibit more plastic properties. Compared to ABA triblock copolymers with glassy PS domains, the plastic deformations even for the systems with 30 wt-% PE are higher especially at high strains. This was attributed to a weaker resistance of the crystalline PE domains against distortion compared to the case of glassy PS

domains. The Young's modulus increases with increasing PE content, whereby the tensile strength mainly depends on the molecular weight of the PE block. However, the identical end blocks also result in loop formation as it is the case for polystyrene-based TPEs, thus limiting the elastic properties.

In this thesis the morphology, thermal properties, and elasticity of ABC triblock copolymers with one (Figure 1.15 B) or two (Figure 1.15 C) semicrystalline end blocks are investigated. The influence of confinement on the morphology, crystallization behavior, and self-nucleation properties is examined for PE-*b*-PEP-*b*-PEO triblock copolymers exhibiting two different semicrystalline end blocks. The mechanical properties of PS-*b*-PEP-*b*-PE triblock copolymers with one semicrystalline end block are compared to the corresponding amorphous PS-*b*-PEP-*b*-PS triblock copolymers with comparable block contents. The nomenclature of the triblock copolymers is $A_xB_yC_z^M$, with the subscripts x, y, and z denoting the weight fraction of the corresponding block (in %), and M being the number averaged overall molecular weight (in kg/mol).

1.5.1 PB-*b*-PI-*b*-PEO and PE-*b*-PEP-*b*-PEO Triblock Copolymers

The PE-*b*-PEP-*b*-PEO triblock copolymers have been synthesized by homogeneous catalytic hydrogenation of the corresponding poly(1,4-butadiene)-*block*-poly(1,4-isoprene)-*block*-poly(ethylene oxide) (PB-*b*-PI-*b*-PEO) triblock copolymers, the latter being synthesized by sequential anionic polymerization.[78,176,177] The anionic polymerization has been performed in benzene using *sec*-BuLi as initiator in order to achieve a high degree of 1,4-addition for the PB block, which in turn is a prerequisite to obtain the corresponding "pseudo polyethylene" structure after hydrogenation. Usually polymerization of ethylene oxide in the presence of lithium counterions is not possible due to the formation of strong lithium alkoxide aggregates.[178,179] However, polymerization of ethylene oxide can be achieved by using the strong phosphazene base *t*-BuP_4, as has been recently shown by Möller and co-workers.[180-182] In this case the phosphazene base *t*-BuP_4 forms a strong complex with Li^+, resulting in a break up of the strong lithium alkoxide aggregates, and thus enabling the polymerization of ethylene oxide. Using this method, a one-pot synthesis of PB-*b*-PI-*b*-PEO triblock copolymers is possible using *sec*-BuLi as initiator. In addition, the phosphazene base *t*-BuP_4 was successfully applied by other groups in the synthesis of PEO containing block copolymers

using organolithium initiators.[180,183-185] In contrast to the kinetic results given in the literature[181,182], we find an unexpected induction period involved in the synthesis of the PEO blocks. Kinetic investigations, applying online FT-NIR spectroscopy, of ethylene oxide homopolymerization with organolithium initiators reveals that the induction period depends on reaction temperature, amount of added phosphazene base *t*-BuP_4, type of organolithium initiator, and the sequence of reactant addition (Chapter 3.4).[186,187] An induction period is also present in the synthesis of PS-*b*-PEO diblock copolymers, and has been additionally proven by MALDI-ToF mass spectroscopy on samples taken during the polymerization of the PEO block in a low molecular weight PS-*b*-PEO diblock copolymer (Chapter 3.4). The induction period decreases with increasing reaction temperature and amount of added phosphazene base. This points to an association-dissociation pre-equilibrium, which might be responsible for the observed induction period, since the phosphazene base *t*-BuP_4 has first to break up the strong lithium alkoxide aggregates in order to enable ethylene oxide polymerization. However, experiments using an altered sequence of reactant addition and sequential ethylene oxide addition reveals that dissociation of the strong lithium alkoxide aggregates by complexation of Li^+ with *t*-BuP_4 is not the only factor which contributes to the observed induction period. Chain length effects arising from the complexation properties of PEO and/or a contribution of ethylene oxide itself in the formation of the active center might also be responsible for the induction period.

Thermal analysis utilizing differential scanning calorimetry (DSC) reveals a strong influence of the confinement active during crystallization on the crystallization and self-nucleation behavior of the PEO and PE blocks within PE-*b*-PEP-*b*-PEO triblock copolymers.[78,177] Applying the self-nucleation technique developed by Fillon et al.,[188] more detailed information on the crystallization behavior of the two crystalline end blocks and the influence of confinements can be obtained. Self-nucleation consists of the partial melting of an initial crystalline "standard" state of the polymer at a given self-nucleation temperature (T_s). Upon subsequent cooling recrystallization takes place, using as nuclei the crystallographically "ideal" nuclei which are produced during partial melting, i. e. self-nuclei or crystal fragments of the same polymer under considerations. In a crystallizable homopolymer usually three different domains of self-nucleation can be defined. In domain I, or complete melting domain, crystallization always takes place at the same temperature. Domain II (self-nucleation domain) represents a T_s range, where the concentration of remaining crystal fragments varies dramatically with T_s. Small variations in T_s result in

significant shifts of the crystallization peak to higher temperatures. In domain III_{SA} (SA stands for self-nucleation and annealing) incomplete melting takes place, which is directly linked to the occurrence of considerable annealing of the remaining crystalline material. However, for block copolymers the situation might be different, especially for systems where the crystallizable block is confined into small isolated microdomains. It has been observed, that domain II vanishes completely in polystyrene-*block*-polybutadiene-*block*-poly(ε-caprolactone) (PS-*b*-PB-*b*-PCL) and PS-*b*-PE-*b*-PCL triblock copolymers exhibiting low PE and PCL contents.[83,189,190] This results directly from the confinement of the crystallizable blocks within small isolated microdomains.

Because of the strong incompatibility of the polar PEO segments with respect to the other block components, the crystallization of PEO is confined into isolated microdomains in PB-*b*-PI-*b*-PEO and PE-*b*-PEP-*b*-PEO triblock copolymers. The morphology of the synthesized PE-*b*-PEP-*b*-PEO triblock copolymers has been investigated using transmission electron microscopy (TEM) and scanning force microscopy (SFM).[78,177] As an example the TEM micrograph of $E_{11}EP_{71}EO_{18}$[123], obtained by catalytic homogeneous hydrogenation of the corresponding precursor $B_{11}I_{70}EO_{19}$[120] using Wilkinson catalyst, is shown in Figure 1.16.

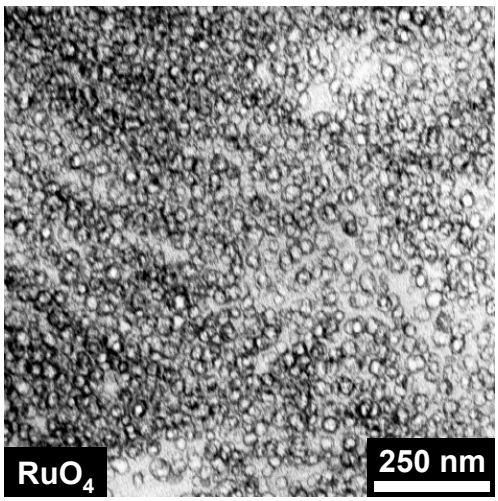

Figure 1.16: TEM micrograph of $E_{11}EP_{71}EO_{18}$[123] stained with RuO_4.

The use of RuO_4 results in a preferential staining of the amorphous PEP and PEO segments. Thus, the crystalline PEO domains (thin sections were cut at –130 °C) appear bright and exhibit a distorted spherical structure, which clearly shows the confinement of the PEO blocks within isolated PEO domains. The crystalline PE domains, which are expected to be located in between the amorphous PEP phase, cannot be visualized using RuO_4 staining. As a result of confinement, large supercoolings are necessary to induce crystallization of PEO in PB-*b*-PI-*b*-PEO and PE-*b*-PEP-*b*-PEO triblock copolymers with PEO contents < 30 wt-% and < 20 wt-%, respectively. The observed crystallization temperatures of -20 to -25 °C are significantly lower compared to the crystallization temperature observed in PEO homopolymer (T_c ca. 40 °C).[83] This is a direct result from the huge number density of PEO microdomains (≈ 10^{16} spheres/cm^3 or ≈ 10^{14} cylinders/cm^3 assuming a spherical or cylindrical PEO microdomain)[78] compared to the number density of heterogeneous nuclei usually present in PEO homopolymer (≈ 10^5 nuclei/cm^3, for a spherulite radius of 100 μm)[79]. Consequently, crystallization of PEO cannot proceed via heterogeneous nucleation. The observed large supercoolings necessary for crystallization of PEO within isolated microdomains might arise from weakly nucleating heterogeneities within the PEO phase, surface nucleation of the interphase, or homogeneous nucleation. The absence of domain II (self nucleation domain) in self-nucleation experiments[191] combined with the fact that the crystallization temperatures observed for homogeneous nucleation in PEO containing block copolymers (T_c ≈ -40 °C)[82] are significantly lower compared to the detected values (T_c ca. –20 °C) point to a nucleation of the interphase. This absence of domain II is a direct result of the confined PEO crystallization within isolated microdomains. To induce self-nucleation of the confined PEO segments a high concentration of self-seeding nuclei is necessary. Therefore, T_s has to be lowered well into domain III_{SA}, where already annealing takes place, in order to provide a sufficiently high concentration of self-seeds. In addition, a strong influence of Wilkinson catalyst ($(Ph_3P)_3Rh(I)Cl$) residues in the non-purified triblock copolymers, arising from the hydrogenation reaction, has been observed. In PE-*b*-PEP-*b*-PEO triblock copolymers (PEO content < 20 wt-%) the crystallization temperature of the strongly confined PEO blocks exhibits a shift to higher temperatures (T_c ca. 20 °C), which can be attributed to a nucleating property of the Wilkinson catalyst residues. This is also connected to a change in the self-nucleation behavior, since in the non-purified triblock copolymers all three self-nucleation domains are visible.[191] Increasing the PEO content to approximately 40 wt-% in $B_{19}I_{39}EO_{42}$[135] and $E_{19}EP_{40}EO_{41}$[138] results in a fractionated crystallization, whereby the main PEO fraction crystallizes at temperatures comparable to those observed in PEO

homopolymers ($T_c \approx 20/40$ °C, double exotherm), thus resembling a heterogeneous nucleation mechanism. Because of the increasing PEO content, most PEO blocks are no longer confined into small isolated PEO microdomains, as is revealed by the lamellar and cylindrical PEO microdomains observed in $B_{19}I_{39}EO_{42}$[135] and $E_{19}EP_{40}EO_{41}$[138], respectively.[78] However, a minor PEO fraction still crystallizes at comparatively low temperatures ($T_c \approx$ -20 °C). This might be attributed to the fact, that still small isolated PEO microdomains are present in the system, as the samples were not subjected to annealing prior to the DSC investigations, i. e. the morphologies are not perfectly ordered. Self-nucleation experiments reveal that for the PEO fraction crystallizing in the high temperature exotherm all three self-nucleation domains can be detected. In contrast, the PEO fraction crystallizing in the low temperature exotherm exhibits a similar behavior compared to the PEO blocks in PE-*b*-PEB-*b*-PEO with PEO contents < 20 wt-%, i. e. domain II vanishes.

For the PE blocks the situation is different. Due to the low segmental interaction parameter between PEP and PE segments of $\chi = 0.007$[168] at 120 °C crystallization of PE is expected to occur from a homogeneous mixture of PE and PEP segments. This in turn should result in a continuous crystalline PE domain, consisting of interconnected PE crystallites. Figure 1.17 shows the TEM micrograph of $E_{19}EP_{40}EO_{41}$[138], which was obtained by hydrogenation of the corresponding $B_{19}I_{39}EO_{42}$[135] precursor with *p*-toluenesulfonyl hydrazide.

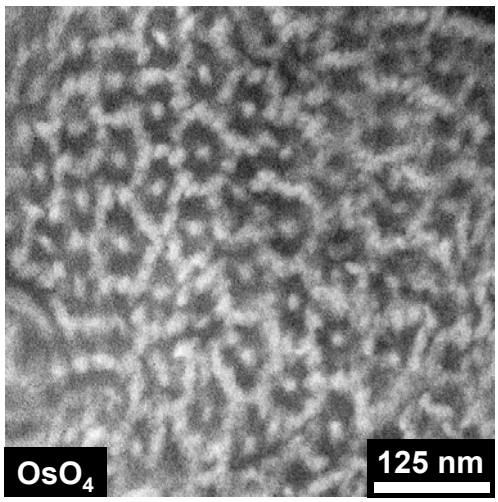

Figure 1.17: TEM micrograph of $E_{19}EP_{40}EO_{41}$[138]. The triblock copolymer contains 30% residual double bonds within the PEP block, which were selectively stained with OsO_4.

Because of the used hydrogenation method, the PEP block contains ca. 30% residual olefinic double bonds, which can be selectively stained using OsO_4. As a consequence, the crystalline PE and PEO domains appear bright (Figure 1.17). The PE block forms a hexagonal array of interconnected PE crystallites, surrounding the crystalline PEO cylinders, both embedded in a matrix of the selectively stained PEP block. This phase assignment has been derived by comparison of TEM images showing different projections with respect to the PEO cylinder long axis in combination with TEM investigations of the completely hydrogenated $E_{19}EP_{40}EO_{41}$[138] triblock copolymer.[78] The hexagonal array of PE crystallites show strong distortions, but interconnections between several PE crystallites are still clearly visible.

In conclusion, crystallization of PE is not confined into small isolated microdomains, since it occurs from a homogeneous mixture of PEP and PE segments in the melt, resulting in the formation of a continuous crystalline PE phase. In addition, a continuous crystalline PE phase is also observed in SFM investigations on thin films, prepared from toluene solutions.[78] However, in this case the formation of a continuous PE phase is found to be partially induced by gelation of the polymer solution upon film preparation. The lack of confinement is directly reflected in the crystallization behavior of the PE blocks within PE-*b*-PEP-*b*-PEO triblock copolymers. Triblock copolymers with ca. 20 wt-% PE exhibit crystallization temperatures at about 65 to 72 °C[78] reflecting a heterogeneous nucleation mechanism, since the observed values are very close to the crystallization temperature of ca. 73 °C[83] detected in a hydrogenated polybutadiene of similar branching content. In addition, regardless of the low PE content in the investigated PE-*b*-PEP-*b*-PEO triblock copolymers (10 - 25 wt-%) all three self-nucleation domains can be located for the PE blocks.[191]

Mechanical testing reveals poor mechanical properties for the PE-*b*-PEP-*b*-PEO triblock copolymers, exhibiting elongations at break below 100%. This might be attributed to the hindered crystallization of PEO in systems with PEO contents below 20 wt-% (T_c ca. -20 °C). However, cooling of the sample to –30 °C over night in order to induce PEO crystallization results only in an increased Young's modulus and shows no improvement with respect to the elongation at break. Also $E_{19}EP_{40}EO_{41}$[138] shows a comparatively low elongation at break, despite the fact that here PEO crystallization can take place well above room temperature. In addition, the continuous crystalline PE phase, observed by TEM and SFM investigations, might also contribute to the poor mechanical properties, as it is expected to be easily disrupted upon elongation. From these results, it might be concluded that two different crystalline end blocks, here PE and PEO, are not favorable with respect to good mechanical properties, i. e. high elongation at break, and low plastic deformation.

One problem encountered in PE-*b*-PEP-*b*-PEO triblock copolymers is the hindered crystallization of the strongly confined PEO blocks for PEO contents below 20 wt-%. As a result, large supercoolings (T_c ca. –20 °C) are necessary in order to induce PEO crystallization. It is well known that PEO homopolymers can form well-defined complexes with low molecular weight components like *p*-nitrophenol (PNP) and resorcinol (RES), resulting in an increase of both melting and crystallization temperatures.[192-195] Investigations on PEO/PNP complexes with a molar ratio of ethylene oxide (EO) units to PNP units of 3/2 (M_n(PEO) ca. 6000 g/mol) showed that these complexes can be isothermally crystallized at temperatures well above room temperature and exhibit a melting temperature range of 75 – 95 °C, depending on the crystallization temperatures employed.[195] To check the applicability of these molecular complexes for increasing the melting and crystallization temperature of the PEO block within PE-*b*-PEP-*b*-PEO triblock copolymers, a complex between the PEO end block in $E_{24}EP_{57}EO_{19}$[69] and PNP (molar ratio EO/PNP = 3/2) has been prepared from toluene solution.[196] DSC investigations show that upon cooling at 10 °C/min only the PE blocks are able to crystallize, whereas no crystallization exotherm attributable to the PEO-block/PNP complex can be detected. Upon subsequent heating at about 20 °C a cold crystallization exotherm is observed for the PEO-block/PNP complex. The melting transition of the PEO-block/PNP complex shows a shift of approximately 30 °C to higher temperatures compared to that of the neat PEO block within the copolymers, as is extracted from self-nucleation experiments. In addition, an increased capability for self-nucleation of the PEO block is produced by the complexation with PNP. In contrast to the PEO block in the neat triblock copolymer, where domain II vanishes completely[191], all three self-nucleation domains are clearly observed for the PEO-block within the $E_{24}EP_{57}EO_{19}$[69]/PNP complex.[196] Similar results are obtained by complexation of the same PE-*b*-PEP-*b*-PEO triblock copolymer with resorcinol.

1.5.2 PS-*b*-PI-*b*-P(S/B) and PS-*b*-PEP-*b*-P(S/E) Triblock Copolymers

PS-*b*-PEP-*b*-P(S/E) triblock copolymers have been synthesized by homogeneous catalytic hydrogenation of the corresponding precursor PS-*b*-PI-*b*-P(S/B) triblock copolymers using Wilkinson catalyst ($(Ph_3P)_3Rh(I)Cl$).[176,197] The synthesis of PS-*b*-PI-*b*-PS and PS-*b*-PI-*b*-PB triblock copolymers has been accomplished by sequential anionic polymerization in benzene using *sec*-BuLi as initiator. The combination of two laboratory autoclaves allows the synthesis of two ABC triblock copolymers, having identical A- and B-blocks, here PS and PI, respectively. The solution of the living PS-*b*-PI precursor has been divided into two parts. Subsequent addition of equivalent amounts of styrene to one part of the living PS-*b*-PI precursor, and butadiene to the second part results in the formation of the corresponding PS-*b*-PI-*b*-PS and PS-*b*-PI-*b*-PB triblock copolymers with identical block content. Polymerization of butadiene and isoprene in benzene, using *sec*-BuLi as initiator, results in a high degree of 1,4-addition, which especially for butadiene is indispensable to get a semicrystalline PE block after hydrogenation. Comparable compositions of the hydrogenated PS-*b*-PEP-*b*-PS and PS-*b*-PEP-*b*-PE triblock copolymers are important for the comparison of mechanical properties, since differences in composition might also result in different mechanical properties.

Thermal analysis of PS-*b*-PEP-*b*-PE triblock copolymers utilizing DSC and dynamic mechanical analysis (DMA) reveals a glass transition for the PS block and a melting endotherm for the PE block, even for small end block contents (< 20 wt-%), reflecting a strong microphase-separation. In the case of the PE block, microphase-separation is induced by crystallization, since PEP and PE segments are miscible in the melt due to their low segmental interaction parameter of $\chi = 0.007$ at 120 °C.[168] Thus, PS-*b*-PEP-*b*-PE triblock copolymers exhibit a two-phase melt rather than a three-phase melt compared to amorphous ABC triblock copolymers with strongly incompatible block components. This in turn is advantageous in view of processing, since a two-phase melt exhibits a lower melt viscosity compared to a three-phase melt, assuming comparable molecular weights.

The morphology of the synthesized PS-*b*-PEP-*b*-P(S/E) triblock copolymers has been investigated using scanning electron microscopy (SEM), transmission electron microscopy (TEM), and scanning force microscopy (SFM), both on solution-cast samples and compression molded samples.[176,197,198] Because of problems involved in the staining of PS-*b*-PEP-*b*-PE triblock copolymers, the crystalline PE domains cannot be visualized using conventional electron microscopy techniques. This problem can be solved using SFM. The

large differences in stiffness between amorphous and crystalline domains makes SFM the ideal tool for investigating semicrystalline-amorphous block copolymers, without the need of special sample preparation. Investigations on compression-molded samples are of special interest, since samples for tensile testing are prepared in an identical manner. As an example, the SFM phase contrast image obtained from a thin film of $S_{14}EP_{64}E_{22}^{122}$, cast from toluene solution, is depicted in Figure 1.18A.

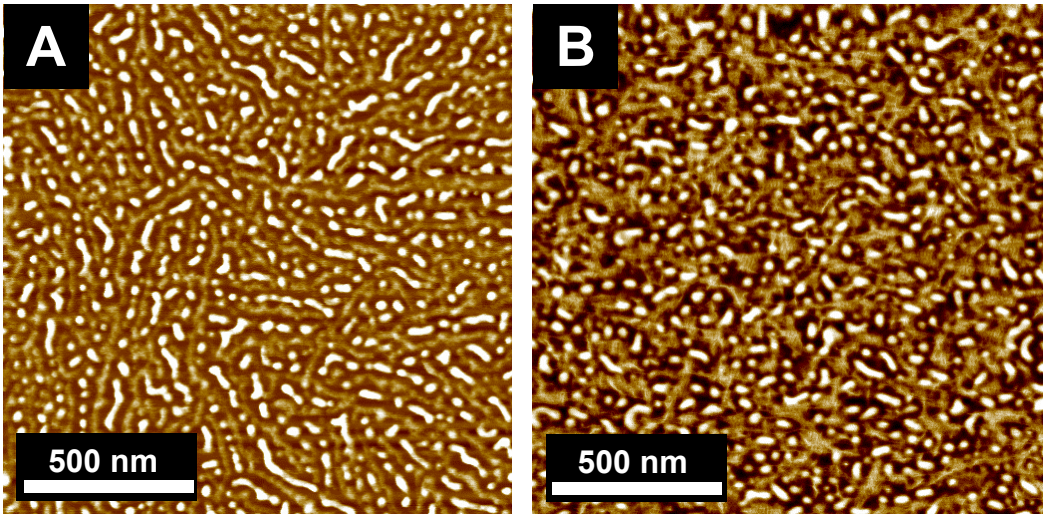

Figure 1.18: SFM phase contrast images: (A) thin film of $S_{14}EP_{64}E_{22}^{122}$ prepared by spin-coating from a 5 mg/ml solution in toluene (z range = 50°); (B) $S_{13}EP_{57}E_{30}^{112}$ prepared by compression-molding, measurement was performed on a smooth cut surface (z range = 15°).

From the phase contrast image three different phases can be distinguished. The bright appearing (high phase shift) dot- and worm-like structures correspond to PS cylinders, which are located in between less bright appearing PE crystallites (elongated domains with rough boundaries), viewed edge on. The PE crystallites are strongly interconnected and form a network of crystalline PE lamellae. The third phase, appearing dark in the phase contrast image, corresponds to the PEP blocks, as the amorphous PEP is expected to show a low phase shift due to its low glass transition temperature. This phase assignment has been proven by selective swelling of PS domains with toluene vapor in combination with SEM investigations.[197] Furthermore, the cylindrical PS domains are obviously distorted. As during film preparation the PE crystallizes before solidification of the PS cylinders (the PE blocks exhibit a low solubility in toluene), the latter have to cope with the confined geometry given by the network of interconnected PE crystallites, resulting in the observed distortion of the PS domains.

Figure 1.18B shows the SFM phase contrast image of $S_{13}EP_{57}E_{30}$[112], prepared by compression-molding. Again three different phases can be distinguished, as in the case of the solution-cast film of $S_{14}EP_{64}E_{22}$[122] (Figure 1.18A). Thus, the bright appearing dot- and worm-like structures can be attributed to PS cylinders in a matrix of the darker appearing PEP block. The third, less bright appearing phase, corresponds to crystalline PE domains. Compared to the solution cast film of $S_{14}EP_{64}E_{22}$[122] (Figure 1.18A) the PE crystallites in the compression molded $S_{13}EP_{57}E_{30}$[112] (Figure 1.18B) are significantly smaller in length, despite the higher PE content, and exhibit a more distorted structure. In contrast to the film preparation from solution, the PS solidifies first upon cooling from the melt due to its higher glass transition temperature of ca. 100 °C compared to the crystallization temperature of the PE block of ca. 60 °C.[197,198] As a result of the already existing glassy PS domains, the PE blocks have to cope with the confined geometry given by the PS cylinders upon crystallization.

To check the assumption that a suppressed loop formation in PS-*b*-PEP-*b*-PE triblock copolymers leads to an improved elastic recovery compared to PS-*b*-PEP-*b*-PS triblock copolymers, hysteresis measurements have been performed.[176,197,198] Figure 1.19 shows a comparison of plastic deformations (ε_{plast}) for various PS-*b*-PEP-*b*-PS and PS-*b*-PEP-*b*-PE triblock copolymers with comparable block contents. For elongations < 300% the PS-*b*-PEP-*b*-PE triblock copolymers reveal significantly smaller plastic sets compared to those of the corresponding PS-*b*-PEP-*b*-PS triblock copolymers. This might result from the suppressed loop formation in PS-*b*-PEP-*b*-PE triblock copolymers due to the strong incompatibility of the end blocks. However, it has to be taken into account that the morphologies of the PS-*b*-PEP-*b*-PS and PS-*b*-PEP-*b*-PE triblock copolymers are not identical. For higher strains the situation is reversed and the PS-*b*-PEP-*b*-PS triblock copolymers exhibit better elastic properties. Obviously, the glassy PS domains show a stronger resistance against distortion compared to crystalline PE domains, especially at high strains.

Comparison of PS-*b*-PEP-*b*-PE triblock copolymers with identical PS content but varying PE content reveals an improved elastic recovery for the triblock copolymers with lower PE content. The same accounts for the PS content if triblock copolymers with the same PE content but varying PS content are investigated.[198]

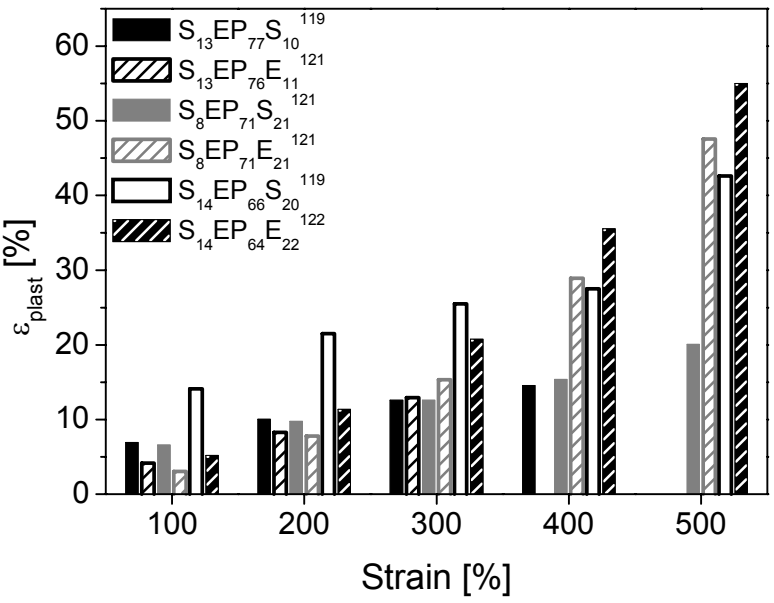

Figure 1.19: Comparison of plastic deformations (ε_{plast}) obtained from hysteresis measurements on PS-*b*-PEP-*b*-PS and PS-*b*-PEP-*b*-PE triblock copolymers with comparable block contents.

In conclusion, mechanical testing shows that PS-*b*-PEP-*b*-PE triblock copolymers exhibit a significantly improved elastic recovery compared to PS-*b*-PEP-*b*-PS triblock copolymers for small elongations. This proves the idea that a suppression of loops in ABA triblock copolymers by switching to ABC triblock copolymers with one semicrystalline end block results in improved elastic properties. However, especially for high strains the PS-*b*-PEP-*b*-PS triblock copolymers exhibit superior elastic recovery. This might be attributed to a weaker resistance of crystalline PE domains against distortion, compared to glassy PS domains.

1.6 References

(1) Holden, G.; Legge, N., R.; Quirk, R. P.; Schroeder, H., E., Eds. *Thermoplastic Elastomers*, 2nd ed.; Hanser: New York, 1996.

(2) Utracki, L. A. *Polymer Alloys and Blends*; Hanser: Munich, 1989.

(3) Wedler, G. *Lehrbuch der Physikalischen Chemie*; VCH: Weinheim, 1987.

(4) Flory, P. J. *J. Chem. Phys.* **1942**, 51.

(5) Huggins, M. *J. Phys. Chem.* **1942**, *46*, 151.

(6) Huggins, M. *J. Am. Chem. Soc.* **1942**, *64*, 1712.

(7) Binder, K. *Adv. Polym. Sci.* **1994**, *112*, 181.

(8) Auschra, C.; Stadler, R.; Voigt-Martin, I. *Polymer* **1993**, *34*, 2094.

(9) Auschra, C.; Stadler, R. *Macromolecules* **1993**, *26*, 6364.

(10) Abetz, V.; Goldacker, T. *Macromol. Rapid Commun.* **2000**, *21*, 16.

(11) Hajduk, D. A.; Harper, P. E.; Gruner, S. M.; Honeker, C. C.; Kim, G.; Thomas, E. L.; Fetters, L. J. *Macromolecules* **1993**, *27*, 4063.

(12) Schulz, M. F.; Bates, F. S.; Almdal, K.; Mortensen, K.; Hajduk, D. A. *Phys. Rev. Lett.* **1994**, *77*, 3153.

(13) Hajduk, D. A.; Harper, P. E.; Gruner, S. M.; Honeker, C. C.; Thomas, E. L.; Fetters, L. J. *Macromolecules* **1995**, *28*, 2570.

(14) Vigild, M. E.; Almdal, K.; Mortensen, K.; Hamley, I. W.; Fairclough, J. P. A.; Ryan, A. J. *Macromolecules* **1998**, *31*, 5702.

(15) Leibler, L. *Macromolecules* **1980**, *13*, 1602.

(16) De Gennes, P. G. *Faraday Disc. Chem. Soc.* **1979**, *68*, 96.

(17) Erukhimovich, I. *Polym. Sci. USSR* **1982**, *24*, 2223.

(18) Fredrickson, G. H.; Helfand, E. *J. Chem. Phys.* **1987**, *87*, 697.

(19) Bates, F. S.; Rosedale, J. H.; Fredrickson, G. H. *J. Chem. Phys.* **1990**, *92*, 6255.

(20) Meier, D. J. *J. Polym. Sci., Polym. Lett. Ed.* **1969**, *26*, 81.

(21) Helfand, E.; Sapse, A. M. *J. Chem. Phys.* **1975**, *62*, 1327.

(22) Helfand, E.; Wassermann, Z. R. *Macromolecules* **1976**, *9*, 879.

(23) Helfand, E.; Wassermann, Z. R. *Macromolecules* **1978**, *11*, 960.

(24) Semenov, A. N. *Sov. Phys. JETP* **1985**, *61*, 733.

(25) Matsen, M. W.; Bates, F. S. *J. Chem. Phys.* **1997**, *106*, 2436.

(26) Matsen, M. W.; Bates, F. S. *Macromolecules* **1996**, *13*, 1091.

(27) Mayes, A. M.; Olvera de la Cruz, M. *J. Chem. Phys.* **1989**, *91*, 7228.

(28) Dobrynin, A. V.; Erukhimovich, I. *Vysokomol. Soedin.* **1990**, *32B*, 663.

(29) Dobrynin, A. V.; Erukhimovich, I. *Macromolecules* **1993**, *26*, 276.

(30) Matsen, M. W.; Schick, M. *Macromolecules* **1994**, *27*, 7157.

(31) Matsen, M. W.; Schick, M. *Macromolecules* **1994**, *27*, 6761.

(32) Erukhimovich, I. *Polym. Sci. USSR* **1982**, *24*, 2232.

(33) Olvera de la Cruz, M.; Sanchez, I. C. *Macromolecules* **1986**, *19*, 2501.

(34) Grayer, V.; Dormidontova, E. E.; Hadziioannou, G.; Tsitsilianis, C. *Macromolecules* **2000**, *33*, 6330.

(35) Bates, F. S.; Fredrickson, G. H. *Physics Today* **1999**, *52*, 32.

(36) Breiner, U.; Krappe, U.; Stadler, R. *Macromol. Rapid Commun.* **1996**, *17*, 567.

(37) Breiner, U.; Krappe, U.; Thomas, E. L.; Stadler, R. *Macromolecules* **1998**, *31*, 135.

(38) Krappe, U.; Stadler, R.; Voigt-Martin, I. *Macromolecules* **1995**, *28*, 4458.

(39) Breiner, U.; Krappe, U.; Abetz, V.; Stadler, R. *Macromol. Chem. Phys.* **1997**, *198*, 1051.

(40) Breiner, U.; Krappe, U.; Jakob, T.; Abetz, V.; Stadler, R. *Polym. Bull.* **1998**, *40*, 219.

(41) Brinkmann, S.; Stadler, R.; Thomas, E. L. *Macromolecules* **1998**, *31*, 6566.

(42) Spontak, R. J.; Zielinski, J. M. *Macromolecules* **1992**, *25*, 663.

(43) Spontak, R. J.; Kane, L. *Macromolecules* **1994**, *27*, 1267.

(44) Mogi, Y.; Mori, K.; Kotsuji, H.; Matsushita, Y.; Noda, I.; Han, C. C. *Macromolecules* **1993**, *26*, 5169.

(45) Nakazawa, H.; Ohta, T. *Macromolecules* **1993**, *26*, 5503.

(46) Mogi, Y.; Kotsuji, H.; Kaneko, Y.; Mori, K.; Matsushita, Y.; Noda, I. *Macromolecules* **1992**, *25*, 5408.

(47) Mogi, Y.; Mori, K.; Matsushita, Y.; Noda, I. *Macromolecules* **1992**, *25*, 5412.

(48) Matsushita, Y.; Tamura, M.; Noda, I. *Macromolecules* **1994**, *27*, 3680.

(49) Lyatskaya, Y. V.; Birshtein, T. M. *Polymer* **1995**, *36*, 975.

(50) Zheng, W.; Wang, Z. G. *Macromolecules* **1995**, *28*, 7215.

(51) Auschra, C.; Stadler, R. *Macromolecules* **1993**, *26*, 2171.

(52) Stadler, R.; Auschra, C.; Beckmann, J.; Krappe, U.; Voigt-Martin, I.; Leibler, L. *Macromolecules* **1995**, *28*, 3080.

(53) Erukhimovich, I.; Abetz, V.; Stadler, R. *Macromolecules* **1997**, *30*, 7435.

(54) Werner, A.; Fredrickson, G. H. *J. Polym. Sci., Part B: Polym. Phys.* **1997**, *35*, 849.

(55) Richardson, P. H.; Richards, R. W.; Blundell, D. J.; MacDonald, W. A.; Mills, P. *Polymer* **1995**, *36*, 3059.

(56) Lauritzen, E. A.; Hoffman, J. D. *Journal of Research of the National Bureau of Standards* **1960**, *64A*, 73.

(57) Hoffman, J. D. *Polymer* **1983**, *24*, 3.

(58) Hoffman, J. D.; Davis, G. T.; Lauritzen, J. I. In *Treatise on Solide State Chemistry*; Hannay, N. B., Ed.; Plenum: New York, 1976; Vol. 3.

(59) Hoffman, J. D.; Guttman, C. M.; DiMarzio, E. A. *Disc. Faraday Soc.* **1979**, *68*, 177.

(60) Hoffman, J. D.; Miller, R. L. *Macromolecules* **1988**, *21*, 3038.

(61) Hoffman, J. D.; Miller, R. L. *Macromolecules* **1989**, *22*, 3502.

(62) Hamley, I. W. *The Physics of Block Copolymers*; Oxford University Press: Oxford, 1998.

(63) Gedde, U. W. *Polymer Physics*; Chapman and Hall: London, 1995.

(64) Point, J. J.; Dosiére, M. *Polymer* **1989**, *30*, 2292.

(65) Sadler, D. M. *Nature* **1987**, *326*, 174.

(66) Heck, B.; Hugel, T.; Iijima, M.; Sadiku, E.; Strobl, G. *New J. Phys.* **1999**, *1*, 17.1.

(67) Heck, B.; Hugel, T.; Iijima, M.; Strobl, G. *Polymer* **2000**, *41*, 8839.

(68) Strobl, G. *Eur. Phys. J. E* **2000**, *3*, 165.

(69) Douzinas, K. C.; Cohen, R. E. *Macromolecules* **1992**, *25*, 5030.

(70) Séguéla, R.; Prud'homme, J. *Polymer* **1989**, *30*, 1446.

(71) Kofinas, P.; Cohen, R. E. *Macromolecules* **1994**, *27*, 3002.

(72) Rangarajan, P.; Register, R. A.; Fetters, L. J. *Macromolecules* **1993**, *26*, 4640.

(73) Hamley, I. W.; Fairclough, J. P. A.; Ryan, A. J.; Bates, F. S.; Towns-Andrews, E. *Polymer* **1996**, *37*, 4425.

(74) Hamley, I. W.; Patrick, J.; Fairclough, A.; Terrill, N. J.; Ryan, A. J.; Lipic, P. M.; Bates, F. S.; Towns-Andrews, E. *Macromolecules* **1996**, *29*, 8835.

(75) Ryan, A. J.; Fairclough, J. P. A.; Hamley, I. W.; Mai, S.-M.; Booth, C. *Macromolecules* **1997**, *30*, 1723.

(76) Mai, S. M.; Fairclough, J. P. A.; Viras, K.; Gorry, P. A.; Hamley, I. W.; Ryan, A. J.; Booth, C. *Macromolecules* **1997**, *30*, 8392.

(77) Hirata, H.; Ijitsu, T.; Soen, T.; Hashimoto, T.; Kawai, H. *Polymer* **1975**, *16*, 249.

(78) Schmalz, H.; Knoll, A.; Müller, A. J.; Abetz, V. *Macromolecules* **2002**, *35*, 10004.

(79) Chen, H.-L.; Hsiao, S.-C.; Lin, T.-L.; Yamauchi, K.; Hasegawa, H.; Hashimoto, T. *Macromolecules* **2001**, *34*, 671.

(80) Lotz, B.; Kovacs, A. J. *Polym. Prep. (Am. Chem. Soc., Div. Polym. Chem.)* **1969**, *10*, 820.

(81) Robitaille, C.; Prud'homme, J. *Macromolecules* **1983**, *16*, 665.

(82) Arnal, M. L.; Balsamo, V.; López-Carrasquero, F.; Contreras, J.; Carrillo, M.; Schmalz, H.; Abetz, V.; Laredo, E.; Müller, A. J. *Macromolecules* **2001**, *34*, 7973.

(83) Müller, A. J.; Balsamo, V.; Arnal, M. L.; Jakob, T.; Schmalz, H.; Abetz, V. *Macromolecules* **2002**, *35*, 3048.

(84) Nojima, S.; Toei, M.; Hara, S.; Tanimoto, S.; Sasaki, S. *Polymer* **2002**, *43*, 4087.

(85) Rohadi, A.; Endo, R.; Tanimoto, S.; Sasaki, S.; Nojima, S. *Polym. Int.* **2000**, *32*, 602.

(86) Rohadi, A.; Tanimoto, S.; Sasaki, S.; Nojima, S. *Polym. J.* **2000**, *32*, 859.

(87) Floudas, G.; Tsitsilianis, C. *Macromolecules* **1997**, *30*, 4381.

(88) Zhu, L.; Mimnaugh, B. R.; Ge, Q.; Quirk, R. P.; Cheng, S. Z. D.; Thomas, E. L.; Lotz, B.; Hsiao, B. S.; Yeh, F.; Liu, L. *Polymer* **2001**, *42*, 9121.

(89) Zhu, L.; Cheng, S. Z. D.; Huang, P.; Ge, Q.; Quirk, R. P.; Thomas, E. L.; Lotz, B.; Hsiao, B. S.; Yeh, F.; Liu, L. *Adv. Mater.* **2002**, *14*, 31.

(90) Shiomi, T.; Tsukada, H.; Takeshita, H.; Takenaka, K.; Tezuka, Y. *Polymer* **2001**, *42*, 4997.

(91) Liu, L.-Z.; Yeh, F.; Chu, B. *Macromolecules* **1996**, *29*, 5336.

(92) Nojima, S.; Tanaka, H.; Rohadi, A.; Sasaki, S. *Polymer* **1998**, *39*, 1727.

(93) Loo, Y.-L.; Register, R. A. *Phys. Rev. Lett.* **2000**, *84*, 4120.

(94) Loo, Y.-L.; Register, R. A.; Ryan, A. J. *Macromolecules* **2002**, *35*, 2365.

(95) Loo, Y.-L.; Register, R. A.; Ryan, A. J.; Dee, G. T. *Macromolecules* **2001**, *34*, 8968.

(96) Cormia, R. L.; Price, F. P.; Turnbull, D. *J. Chem. Phys.* **1962**, *37*, 1333.

(97) Reiter, G.; Castelein, G.; Sommer, J.-U.; Röttele, A.; Thurn-Albrecht, T. *Phys. Rev. Lett.* **2001**, *87*, 226101.

(98) O'Malley, J. J. *J. Polym. Sci., Part C: Polym. Symp.* **1977**, *60*, 151.

(99) O'Malley, J. J.; Crystal, R.; Erhardt, P. F. *Polym. Prep. (Am. Chem. Soc., Div. Polym. Chem.)* **1969**, *10*, 796.

(100) Balsamo, V.; von Gyldenfeldt, F.; Stadler, R. *Macromol. Chem. Phys.* **1996**, *197*, 3317.

(101) Balsamo, V.; Müller, A. J.; von Gyldenfeldt, F.; Stadler, R. *Macromol. Chem. Phys.* **1998**, *199*, 1063.

(102) Balsamo, V.; Stadler, R. *Macromol. Symp.* **1997**, *117*, 153.

(103) Balsamo, V.; Stadler, R. *Macromolecules* **1999**, *32*, 3994.

(104) Balsamo, V.; von Gyldenfeldt, F.; Stadler, R. *Macromolecules* **1999**, *32*, 1226.

(105) Balsamo, V.; Paolini, Y.; Ronca, G.; Müller, A. J. *Macromol. Chem. Phys.* **2000**, *201*, 2711.

(106) Balsamo, V.; Collins, S.; Hamley, I. W. *Polymer* **2002**, *43*, 4207.

(107) Buzdugan, E.; Ghioca, P.; Stribeck, N.; Beckman, E. J.; Serban, S. *Macromol. Mater. Eng.* **2001**, *286*, 497.

(108) Kim, G.; Han, C. C.; Libera, M.; Jackson, C. L. *Macromolecules* **2001**, *34*, 7336.

(109) Koetsier, D. W.; Bantjes, A.; Feijen, J.; Lyman, D. J. *J. Polym. Sci., Part A: Polym. Chem.* **1978**, *16*, 511.

(110) Benson, R. S.; Wu, Q.; Ray, A. R.; Lyman, D. J. *J. Polym. Sci., Part A: Polym. Chem.* **1985**, *23*, 399.

(111) Mitov, Z. G.; Velichkova, R. S. *Eur. Polym. J.* **1992**, *28*, 771.

(112) Bailey, T. S.; Pham, H. D.; Bates, F. S. *Macromolecules* **2001**, *34*, 6994.

(113) Park, C.; De Rosa, C.; Fetters, L. J.; Thomas, E. L. *Macromolecules* **2000**, *33*, 7931.

(114) Kwon, Y.; Kim, M. S.; Faust, R. *Polym. Prep. (Am. Chem. Soc., Div. Polym. Chem.)* **2001**, *42*, 483.

(115) Philips, R. A.; Cooper, S. L. *J. Polym. Sci., Part B: Polym. Phys.* **1996**, *34*, 737.

(116) Hoeschele, G. K. *Chimia* **1974**, *28*, 544.

(117) Coleman, D.; Imperial Chemical Industries Ltd., Brit. P. 682 866, 1949.

(118) Snyder, M. D.; Du Pont, U. S. P. 2 744 087, 1951.

(119) Hoeschele, G. K.; Witsiepe, W. K. *Angew. Makromol. Chem.* **1973**, *29/30*, 267.

(120) Hoeschele, G. K. *Angew Makromol. Chem.* **1977**, *58/59*, 299.

(121) Greber, G.; Gruber, H., Eds. *Methoden Org. Chem.*, 4th ed.; Houben-Weyl, 1987; Vol. 20, pp 1405.

(122) Pilati, F. Polyesters. In *Comprehensive Polymer Science*; Allen, G., Ed.; Pergamon Press: Oxford, 1989; Vol. 5, pp 275.

(123) Banach, T. E.; Berti, C.; Colonna, M.; Fiorini, M.; Marianucci, E.; Messori, M.; Pilati, F.; Toselli, M. *Polymer* **2001**, *42*, 7511.

(124) Banach, T. E.; Colonna, M. *Polymer* **2001**, *42*, 7517.

(125) Zhu, L.-L.; Wegner, G. *Macromol. Chem.* **1981**, *182*, 3625.

(126) Veenstra, H.; Hoogvliet, R. M.; Norder, B.; Boer, A. P. *J. Polym. Sci., Part B: Polym. Phys.* **1998**, *36*, 1795.

(127) Seymour, R. W.; Overton, J. R.; Corley, L. S. *Macromolecules* **1975**, *8*, 331.

(128) Cella, R. J. *J. Polym. Sci., Part C: Polym. Symp.* **1973**, *42*, 727.

(129) Adams, R. K.; Hoeschele, G. K.; Witsiepe, W. K. Thermoplastic Polyether Ester Elastomers. In *Thermoplastic Elastomers*; Holden, G.; Legge, N. R.; Quirk, R.; Schroeder, H. E., Eds.; Hanser: Munich, 1996; pp 191.

(130) Soliman, M.; Dijkstra, K.; Borggreve, R. J. M.; Wedler, W.; Winter, H. H. In *Makromolekulares Kolloquium, Book of Abstracts*: Freiburg, **1998**.

(131) Gabriëlse, W.; Soliman, M.; Dijkstra, K. *Macromolecules* **2001**, *34*, 1685.

(132) Pesetskii, S. S.; Jurkowski, B.; Olkhov, Y. A.; Olkhova, O. M.; Storozhuk, I. P.; Mozheiko, U. M. *Eur. Polym. J.* **2001**, *37*, 2187.

(133) Buck, W. H.; Cella, R. J.; Gladding, E. K.; Wolfe, J. R. *J. Polym. Sci., Part C: Polym. Symp.* **1974**, *48*, 77.

(134) Bandara, U.; Droscher, M. *Colloid Polym. Sci.* **1983**, *261*, 26.

(135) Briber, R. M.; Thomas, E. L. *Polymer* **1985**, *26*, 8.

(136) Zhu, L.-L.; Wegner, G. *Makromol. Chem.* **1981**, *182*, 3639.

(137) Lilaonitkul, A.; Cooper, S. L. *Rubber Chem. Technol.* **1977**, *50*, 1.

(138) Wolfe, R. J. *Rubber Chem. Technol.* **1977**, *50*, 688.

(139) Schmidt, A.; Veeman, W. S.; Litvinov, V. M.; Gabriëlse, W. *Macromolecules* **1998**, *31*, 1652.

(140) Lilaonitkul, A.; West, J.; Cooper, S. L. *J. Macromol. Sci., Phys.* **1976**, *4*, 563.

(141) Bonart, R. *J. Macromol. Sci., Phys.* **1968**, *B2*, 115.

(142) Dieterich, D. Polyurethane. In *Kunststoff Handbuch*; Becker, G. W.; Braun, D., Eds.; Hanser: Munich, 1983.

(143) Niesten, M. C. E. J.; Bosch, H.; Gaymans, R. J. *J. Appl. Polym. Sci.* **2001**, *81*, 1605.

(144) Deák, G.; Kennedy, J. P. *Macromol. Rep.* **1996**, *A33 (Suppls. 7&8)*, 439.

(145) Walch, E.; Gaymans, R. J. *Polymer* **1994**, *35*, 636.

(146) Schmalz, H.; Abetz, V.; Lange, R.; Soliman, M. *Macromolecules* **2001**, *34*, 795.

(147) Schmalz, H.; van Guldener, V.; Gabriëlse, W.; Lange, R.; Abetz, V. *Macromolecules* **2002**, *35*, 5491.

(148) Komoroski, R. A. *High Resolution NMR Spectroscopy of Synthetic Polymers in Bulk*; VCH: Weinheim, 1986.

(149) Gabriëlse, W.; van Guldener, V.; Schmalz, H.; Abetz, V.; Lange, R. *Macromolecules* **2002**, *35*, 6946.

(150) Foreman, L. E. In *Polymer Chemistry of Synthetic Elastomers, Part II*; Kennedy, J. P.; Tornquist, E., Eds.; John Wiley & Sons: New York, 1969; pp 497.

(151) Porter, L. M.; U. S. Patent 3,149,182, 1964 (filed 1957).

(152) Gruver, J. T.; Kraus, G. *J. Polym. Sci., Part A: Polym. Chem.* **1964**, *2*, 797.

(153) Holden, G. *J. Appl. Polym. Sci.* **1965**, *9*, 2911.

(154) Holden, G.; Bishop, E. T.; Legge, N. R. In *Proceedings of the International Rubber Conference*; MacLaren and Sons: London, **1968**; pp 287.

(155) Holden, G.; Bishop, E. T.; Legge, N. R. *J. Polym. Sci., Part C: Polym. Symp.* **1969**, *26*, 37.

(156) Holden, G.; Milkovich, R.; U. S. Patent 3,265,765, 1964 (filed January 1962).

(157) Morton, M. In *Encyclopedia of Polymer Science and Technology*; John Wiley & Sons: New York, 1971; Vol. 15, pp 508.

(158) Morton, M.; Kesten, Y.; Fetters, L. J. *Appl. Polym. Symp.* **1975**, *26*, 113.

(159) Zhulina, E.; Halperin, A. *Macromolecules* **1992**, *25*, 5730.

(160) Matsen, M. W. *J. Chem. Phys.* **1995**, *102*, 3884.

(161) Matsen, M. W.; Schick, M. *Macromolecules* **1994**, *27*, 187.

(162) Jones, R. L.; Kane, L.; Spontak, R. *J. Chem. Eng. Sci.* **1996**, *51*, 1365.

(163) Watanabe, H. *Macromolecules* **1995**, *28*, 5006.

(164) Karatasos, K.; Anastasiadis, S. H.; Pakula, T.; Watanabe, H. *Macromolecules* **2000**, *33*, 523.

(165) Abetz, V.; Stadler, R.; Leibler, L. *Polym. Bull.* **1996**, *37*, 135.

(166) Brinkmann-Rengel, S.; Abetz, V.; Stadler, R.; Thomas, E. L. *Kautschuk Gummi Kunststoffe* **1999**, *52*, 806.

(167) Rangarajan, P.; Register, R. A.; Adamson, D. H.; Fetters, L. J.; Bras, W.; Naylor, S.; Ryan, A. J. *Macromolecules* **1995**, *28*, 1422.

(168) Bates, F. S.; Schultz, M. F.; Rosedale, J. H. *Macromolecules* **1992**, *25*, 5547.

(169) Falk, J. C.; Schlott, R. J. *Macromolecules* **1971**, *4*, 152.

(170) Falk, J. C.; Schlott, R. J. *Angew. Makromol. Chem.* **1972**, *21*, 17.

(171) Morton, M.; Lee, N.-C.; Terrill, E. R. *Polym. Prep. (Am. Chem. Soc., Div. Polym. Chem.)* **1981**, *22*, 136.

(172) Mohajer, Y.; Wilkes, G. L.; Wang, I. C.; McGrath, J. E. *Polymer* **1982**, *23*, 1523.

(173) Morton, M.; Lee, N.-C.; Terrill, E. R. Elastomeric Polydiene ABA Triblock Copolymers with Crystalline End Blocks. In *ACS Symposia Series, Elastomers and Rubber Elasticity*: Washington, 1982; Vol. 193, pp 101.

(174) Morton, M. *Rubber Chem. Technol.* **1983**, *56*, 1096.

(175) Quirk, R. P.; Morton, M. Anionic Triblock Copolymers. In *Thermoplastic Elastomers: A Comprehensive Review*, 2nd ed.; Holden, G.; Legge, N. R.; Quirk, R. P.; Schroeder, H. E., Eds.; Hanser: Munich, 1996; pp 71.

(176) Schmalz, H.; Böker, A.; Lange, R.; Abetz, V. *Polym. Mater. Sci. Eng.* **2001**, *85*, 478.

(177) Schmalz, H.; Knoll, A.; Müller, A. J.; Abetz, V. *Polym. Prep. (Am. Chem. Soc., Div. Polym. Chem.)* **2002**, *43*, 371.

(178) Wesdemiotis, C.; Arnould, M. A.; Lee, Y.; Quirk, R. P. *Polym. Prep. (Am. Chem. Soc., Div. Polym. Chem.)* **2000**, *41*, 629.

(179) Hsieh, H. L., Quirk, R. P. *Anionic Polymerization - Principles and Practical Applications*; Marcel Dekker: New York, 1996.

(180) Eßwein, B.; Möller, M. *Angew. Chem., Int. Ed. Engl.* **1996**, *108*, 703.

(181) Eßwein, B.; Molenberg, A.; Möller, M. *Macromol. Symp.* **1996**, *107*, 331.

(182) Eßwein, B. PhD Thesis, Ulm, 1998.

(183) Förster, S.; Krämer, E. *Macromolecules* **1999**, *32*, 2783.

(184) Zhu, L.; Cheng, S. Z. D.; Calhoun, B. H.; Ge, Q.; Quirk, R. P.; Thomas, E. L.; Hsiao, B. S.; Yeh, F.; Lotz, B. *Polymer* **2001**, *42*, 5829.

(185) Floudas, G.; Vazaiou, B.; Schipper, F.; Ulrich, R.; Wiesner, U.; Iatrou, H.; Hadjichristidis, N. *Macromolecules* **2001**, *34*, 2947.

(186) Lanzendörfer, M.; Schmalz, H.; Abetz, V.; Müller, A. H. E. *Polym. Prep. (Am. Chem. Soc., Div. Polym. Chem.)* **2001**, *42*, 329.

(187) Lanzendörfer, M. G.; Schmalz, H.; Abetz, V.; Müller, A. H. E. Application of FT-NIR Spectroscopy for Monitoring the Kinetics of Living Polymerizations. In *In-Situ Spectroscopy of Monomer and Polymer Synthesis*; Puskas, J. E.; Storey, R., Eds.; Kluwer Academic/Plenum: New York/Dordrecht, 2002, pp 67. Schmalz, H.; Lanzendörfer, M. G.; Abetz, V.; Müller, A. H. E. *Macromol. Chem. Phys.* **2003**, submitted.

(188) Fillon, B.; Wittmann, J. C.; Lotz, B.; Thierry, A. *J. Polym. Sci., Part B: Polym. Phys.* **1993**, *31*, 1383.

(189) Balsamo, V.; Müller, A. J. In *ANTEC Conference Proceedings*: New York, **1999**; Vol. 3, pp 3756.

(190) Balsamo, B.; Paolini, Y.; Ronca, G.; Müller, A. J. *Macromol. Chem. Phys.* **2000**, *201*, 2711.

(191) Schmalz, H.; Müller, A. J.; Abetz, V. *Macromol. Chem. Phys.* **2003**, accepted.

(192) Harris, D. J.; Bonagamba, T. J.; Hong, M.; Schmidt-Rohr, K. *Macromolecules* **2000**, *33*, 3375.

(193) Paternostre, L.; Damman, P.; Dosiere, M. *Macromolecules* **1997**, *30*, 3946.

(194) Damman, P.; Point, J. J. *Macromolecules* **1993**, *26*, 1722.

(195) Dosiere, M. *J. Macromol. Sci., Phys.* **1996**, *35*, 303.

(196) Schmalz, H.; Abetz, V.; Müller, A. J. *Macromol. Symp.* **2002**, *183*, 179.

(197) Schmalz, H.; Böker, A.; Lange, R.; Krausch, G.; Abetz, V. *Macromolecules* **2001**, *34*, 8720.

(198) Schmalz, H.; Abetz, V.; Lange, R. *Composites Sci. Technol.* **2003**, accepted.

2 Experimental Part

2.1 Materials

The used chemicals and the purification of solvents and monomers for anionic polymerization can be found in the experimental sections of the corresponding publications (Chapter 3). The used materials and purification procedures for the synthesis of copoly(ether ester)s with PEO-*b*-PEB-*b*-PEO triblock copolymer soft segments are given in Chapter 3.1. Information about purification of solvents and monomers for the anionic synthesis of PB-*b*-PI-*b*-PEO and PS-*b*-PI-*b*-P(S/B) triblock copolymers are described in Chapter 3.2 and Chapter 3.3, respectively.

2.2 Synthesis of Copoly(ether ester)s

2.2.1 Synthesis of PEO-*b*-PEB-*b*-PEO Triblock Copolymers

The synthesis of poly(ethylene oxide)-*block*-poly(ethylene-*stat*-butylene)-*block*-poly(ethylene oxide) (PEO-*b*-PEB-*b*-PEO) triblock copolymers was accomplished by anionic ring opening polymerization of ethylene oxide in tetrahydrofuran using HO-PEB-OH (M_n = 3600 g/mol; KRATON Liquid polymer HPVM-2203, Shell) as macroinitiator. The HO-PEB-OH precursor was purified prior to reaction by freeze drying in benzene for 3 to 4 times, followed by drying in vacuum (10^{-4} – 10^{-5} mbar) at 60 °C for 2 - 3 d. Polymerizations were carried out in an upscaling plant equipped with thermostated laboratory autoclaves (BÜCHI, 1 – 3L) under inert atmosphere (Figure 2.3). First a ca. 0.04 M solution of the HO-PEB-OH precursor in dry tetrahydrofuran was prepared by condensation of tetrahydrofuran, which was purified in advance over *sec*-BuLi, onto HO-PEB-OH using a vacuum line. This solution was transferred into the polymerization reactor via syringe or a glass ampoule. Reactivation of the terminal hydroxy groups of HO-PEB-OH for anionic ring opening polymerization of ethylene oxide was accomplished by titration with a 0.5 M solution of potassium naphthalide at 35 °C in tetrahydrofuran to yield the corresponding bifunctional macroinitiator KO-PEB-OK (Scheme 2.1). The intensive green color of potassium naphthalide allows a very precise end-point determination which is indispensable in order to avoid the formation of homo-PEO

during ethylene oxide polymerization initiated by excess potassium naphthalide. The titration was stopped after the slight green color of excess potassium naphthalide remains for at least 45 min. After addition of ethylene oxide at 0 °C the polymerization was carried out at 55 °C for 3 – 4 d. The reaction temperature has to be kept above 50 °C, as polymerization at lower temperatures results in triblock copolymers with a bimodal molecular weight distribution. After complete conversion the reaction was terminated with degassed mixture of acetic acid and methanol (5 : 1 by vol.). Purification of the triblock copolymers was accomplished by extraction with water, followed by precipitation in petrol ether (bp 40 - 60 °C, M_n(PEO) > 1400 g/mol) or acetone at –30 °C (M_n(PEO) < 1400 g/mol).

Due to the strong association of potassium alkoxides the concentration of active centers had to be kept below $1 \cdot 10^{-2}$ M in order to avoid gelation of the reaction mixture. The gelation of higher concentrated solutions can be avoided by using cryptands like C222 which effectively complex the potassium cation. However, the use of cryptands resulted in no significant improvement of the molecular weight distribution of the triblock copolymers.

The used potassium naphthalide solutions were prepared by reaction of potassium with naphthalene in tetrahydrofuran at room temperature under a dry nitrogen atmosphere. The solutions can be stored in a freezer for several weeks without significant decomposition. Concentrations were determined by titration. For this purpose 1 ml of the potassium naphthalide solution was hydrolyzed in a mixture of 10 ml distilled water and 20 ml tetrahydrofuran. Titration was carried out with a 0.1 N aqueous HCl solution against phenolphthalein.

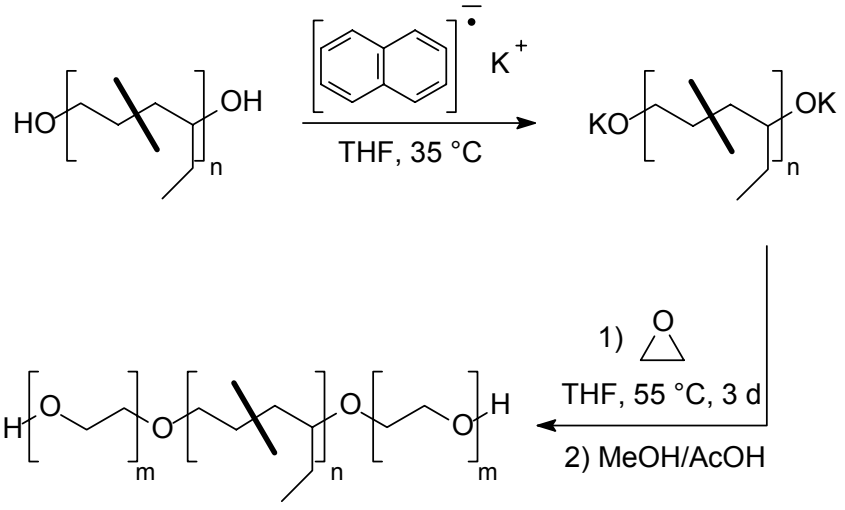

Scheme 2.1: Synthesis of PEO-*b*-PEB-*b*-PEO triblock copolymers by chain extension of HO-PEB-OH with ethylene oxide.

2.2.2 Melt Polycondensation

Melt polycondensation was performed in a home-built apparatus, the used setup is illustrated schematically in Figure 2.1. In order to ensure an optimal heat transfer from the aluminum block to the reactor, the hole is filled with a low melting alloy (Woods metal). The stirrer (glass or metal) is constructed in a way that the distance between the leaves of the stirrer and the reactor wall is as small as possible in order to ensure an effective mixing of the highly viscous melt. Using this setup polymerizations in a 5 - 20 g scale are possible.

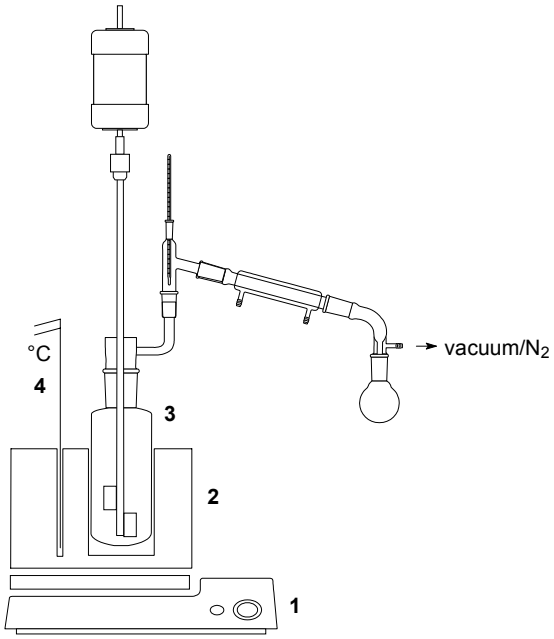

Figure 2.1: Schematic setup for melt polycondensation. 1) heating plate; 2) aluminum block, hole filled with Woods alloy for improved heat transfer; 3) glass reactor for polymerizations in 5 - 20 g scale; 4) electronic thermometer.

The synthesis of copoly(ether ester)s was accomplished using a common two step melt polycondensation procedure (Scheme 2.2). In the first step (transesterification) a mixture of PEO-*b*-PEB-*b*-PEO triblock copolymer, dimethyl terephthalate, 1,4-butandiol (50% molar excess with regard to the methyl ester units), a phenolic antioxidant, and tetrabutyl orthotitanate (1.42 mmol/kg polymer) as a solution in 1,4-butandiol was heated under nitrogen for 1 h to 190, 210, and 220 °C, respectively, in order to distill off the methanol. The catalyst solution in 1,4-butandiol was prepared directly before addition to the reaction mixture under an inert nitrogen atmosphere. In the subsequent polycondensation step the temperature was raised stepwise to 230 °C for 1h and 250 °C for 1.5 h, and vacuum (2 - $5 \cdot 10^{-2}$ mbar) was

applied after reaching 230 °C in order to remove excess 1,4-butandiol. As the viscosity of the reaction mixture increases rapidly after vacuum is applied, the melt was first stirred at 230 °C for 15 – 30 min under nitrogen to obtain a better mixing. For the synthesis of copoly(ether ester)s with selectively deuterated PBT segments 2,2,3,3,-d_4-butandiol was used.

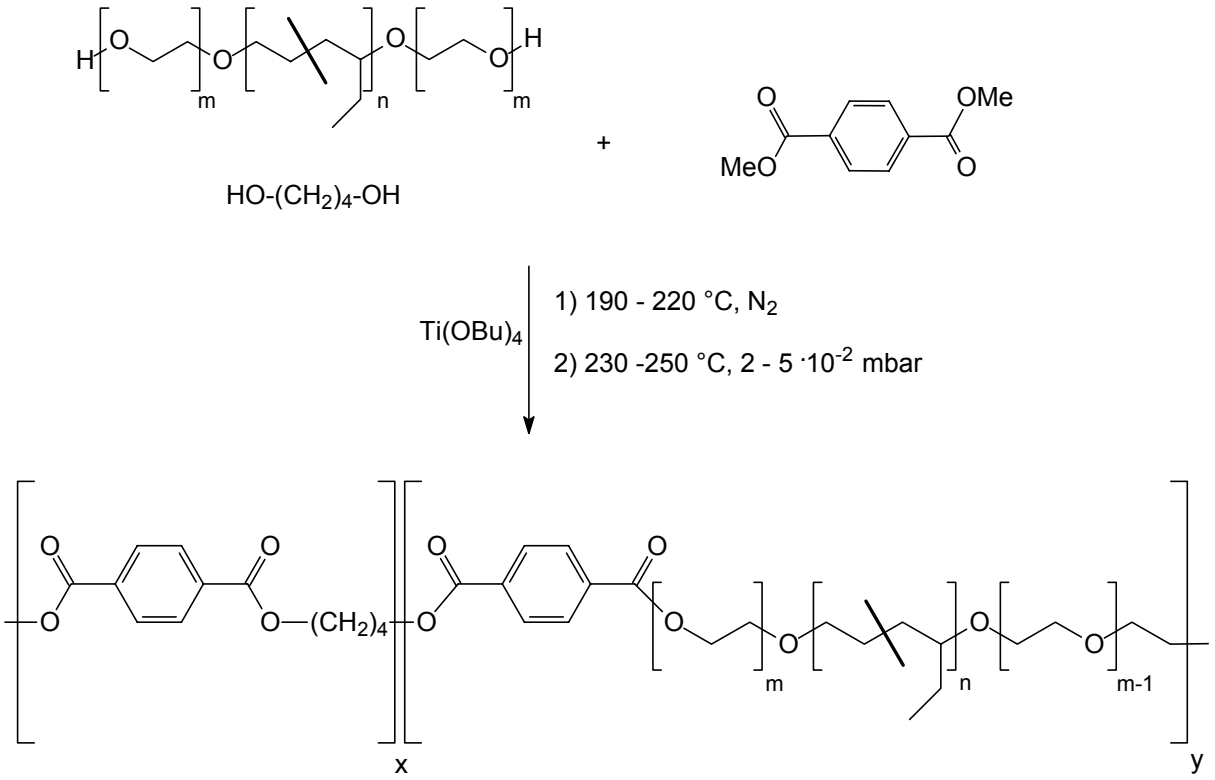

Scheme 2.2: Synthesis of copoly(ether ester)s via a 2 step melt polycondensation procedure.

2.3 Synthesis of ABA and ABC Triblock Copolymers

2.3.1 PB-*b*-PI-*b*-PEO Triblock Copolymers

Poly(1,4-butadiene)-*block*-poly(1,4-isoprene)-*block*-poly(ethylene oxide) (PB-*b*-PI-*b*-PEO) triblock copolymers were synthesized by sequential anionic polymerization in benzene using *sec*-BuLi as initiator (Scheme 2.3). One day prior to the reaction dry benzene (ca. 500 ml) was transferred into the polymerization reactor and additionally purified by titration with *sec*-BuLi. For this purpose a few drops of degassed styrene were added to benzene at room temperature followed by drop-wise addition of *sec*-BuLi until the pale yellow color of styryl

anions appears. Usually the color disappears after stirring at room temperature over night, indicating that the styryl anions have reacted with residual impurities.

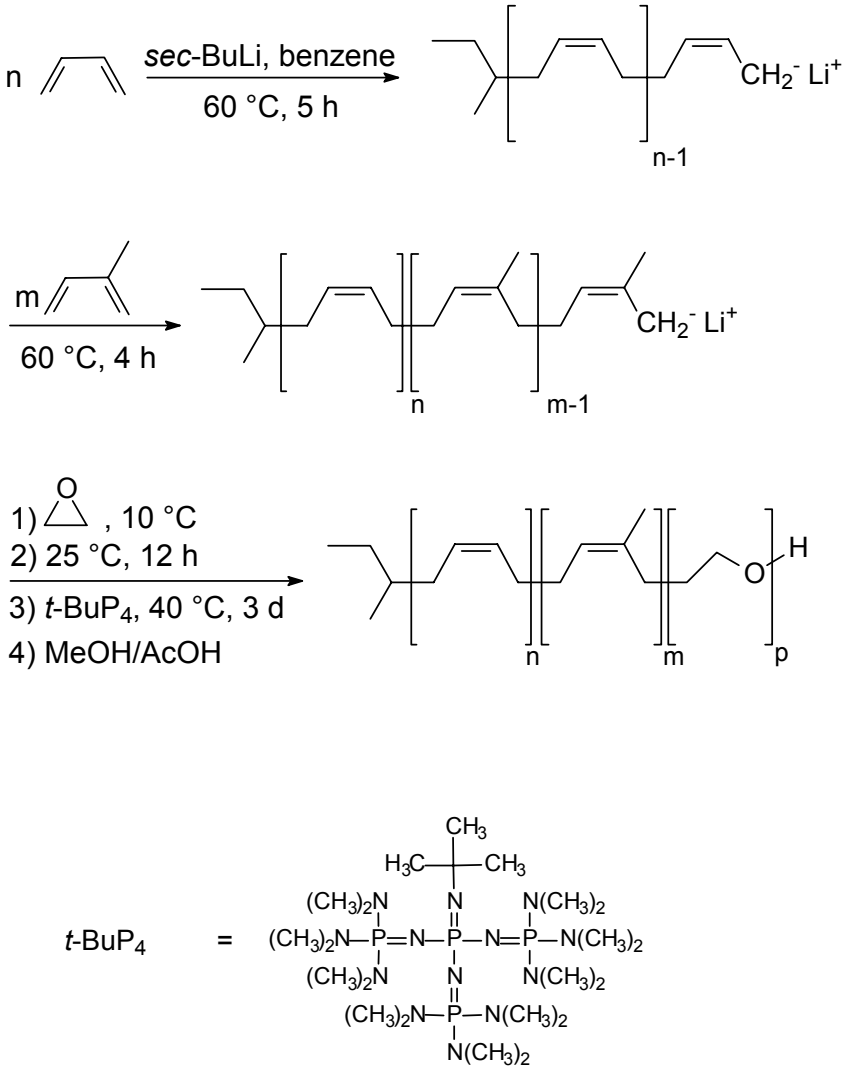

Scheme 2.3: Synthesis of PB-*b*-PI-*b*-PEO triblock copolymers by sequential anionic polymerization using the phosphazene base *t*-BuP_4 for ethylene oxide polymerization with Li^+ counterions.

After injection of the calculated amount of *sec*-BuLi into the reactor the required amount of butadiene was added, which has been condensed in advance from the butadiene purification reactor into a pre-cooled burette (-20 °C, Chapter 2.4.11: Figure 2.3). Subsequently the reaction temperature was increased to 60 °C and butadiene was allowed to polymerize for 5 h. After that time the reaction mixture was cooled to 25 °C and a small amount of the reaction mixture was isolated and precipitated into degassed methanol in order to extract the polybutadiene precursor. Then the second monomer, isoprene, was added and allowed to react for 4 h at 60 °C. The polymerization of butadiene and isoprene at 60 °C in

benzene results in a high degree of 1,4-addition, which especially for butadiene is indispensable to get the corresponding "pseudo polyethylene" structure after hydrogenation. After complete conversion of isoprene the reaction mixture was cooled to 10 °C followed by the addition of ethylene oxide. After stirring for 1 h at 10 °C the temperature was increased to 25 °C followed by stirring over night. Under these conditions only one ethylene oxide unit adds to the living PB-*b*-PI precursor due to the strong aggregation of the formed lithium alkoxides. To initiate the polymerization of ethylene oxide the phosphazene base *t*-BuP_4 was added, which results in a break-up of lithium alkoxide aggregates due to complexation of the Li^+ counterion ([*sec*-BuLi] : [*t*-BuP_4] = 1 : 1).[1-6] Subsequently, polymerization of ethylene oxide was performed at 40 °C for 3 d followed by termination with a degassed mixture of acetic acid and methanol (5 : 1 by vol.). Due to their amphiphilic character the PB-*b*-PI-*b*-PEO triblock copolymers were isolated by precipitation in cold methanol (ca. –10 - 0 °C). The molecular weight of the final triblock copolymer was calculated using the molecular weight of the PB precursor, obtained by SEC, and the molar ratio of the three segments obtained by ^{1}H-NMR.

2.3.2 PS-*b*-PI-*b*-P(S/B) Triblock Copolymers

The synthesis of polystyrene-*block*-poly(1,4-isoprene)-*block*-polystyrene (PS-*b*-PI-*b*-PS) and polystyrene-*block*-poly(1,4-isoprene)-*block*-poly(1,4-butadiene) (PS-*b*-PI-*b*-PB) was accomplished in an identical manner compared to the preparation of PB-*b*-PI-*b*-PEO triblock copolymers (chapter 2.3.1). In a typical procedure 1.5 L benzene were added to the polymerization reactor and purified by titration with *sec*-BuLi. After injection of the calculated amount of *sec*-BuLi, styrene was added and allowed to react for 4 h at 40 °C. Afterwards the reaction mixture was cooled to 25 °C and a small amount of the reaction mixture was isolated and precipitated in degassed methanol to extract the PS precursor. Subsequently, isoprene was added and the yellow color of living polystyryl anions disappeared, since living polyisoprenyl anions are nearly colorless. Then the reaction temperature was increased to 60 °C and isoprene was allowed to polymerize for 4 h. The successful blocking reaction can be monitored during the reaction by an increase in temperature of ca. 5 °C at the early stage of isoprene polymerization. After complete conversion the reaction mixture was cooled to 25 °C. Subsequently, the solution of the living PS-*b*-PI precursor was divided into two equal parts by using two interconnected laboratory autoclaves.

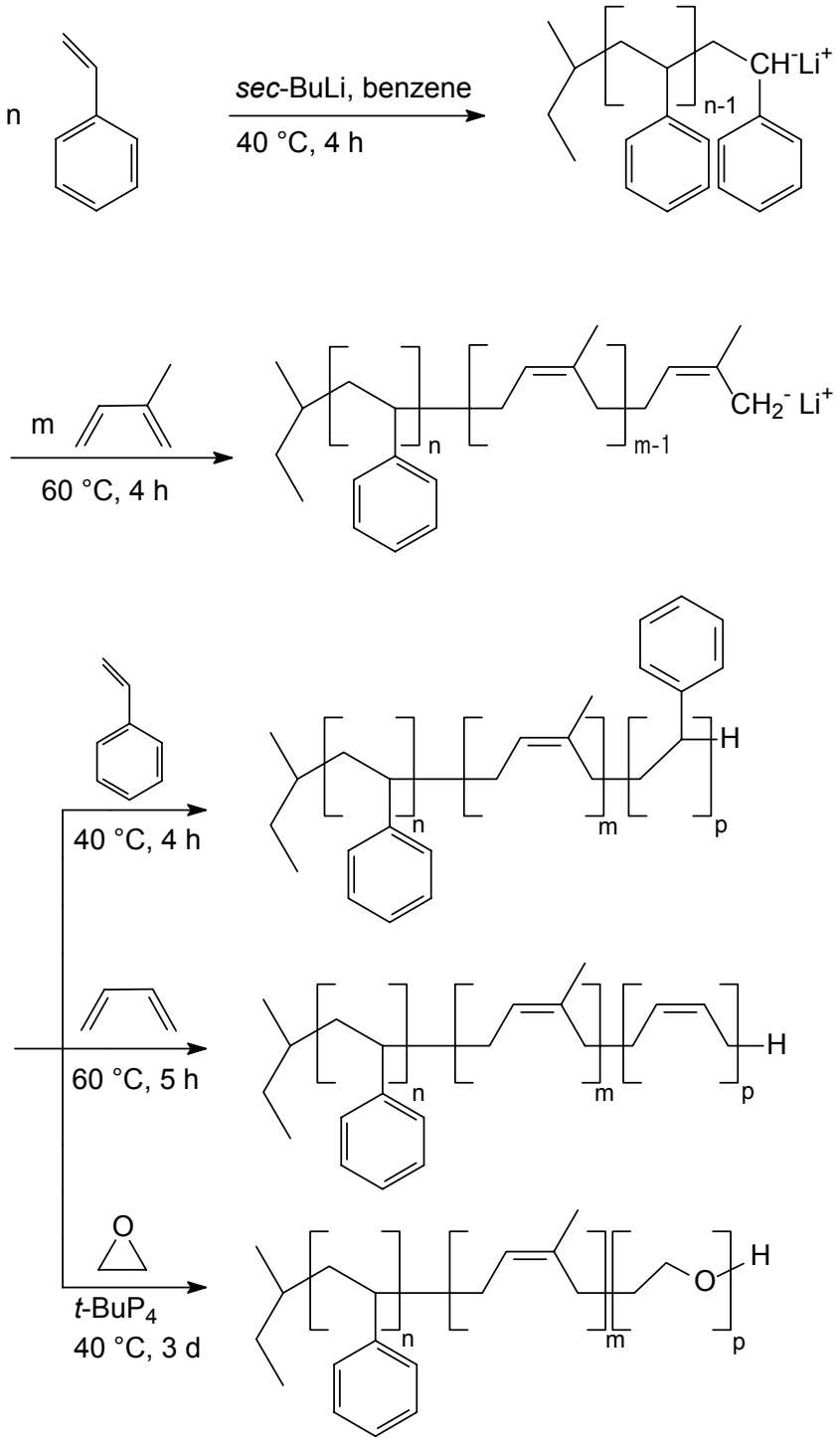

Scheme 2.4: Synthesis of PS-*b*-PI-*b*-PS and PS-*b*-PI-*b*-PB triblock copolymers with identical PS and PI blocks by combination of two laboratory autoclaves, and synthesis of PS-*b*-PI-*b*-PEO triblock copolymers.

Applying this procedure allows the synthesis of two different ABC triblock copolymers with identical A and B blocks, here PS and PI, respectively. Consequently, styrene was added to one part of the solution of the living PS-*b*-PI precursor and allowed to

react for 4 h at 40 °C to yield the corresponding PS-*b*-PI-*b*-PS triblock copolymer. Butadiene was added to the second part of the living PS-*b*-PI precursor and polymerization was accomplished at 60 °C for 5 h. In both cases, polymerizations were terminated with degassed methanol and the corresponding PS-*b*-PI-*b*-PS and PS-*b*-PI-*b*-PB triblock copolymers were isolated by precipitation in methanol.

For the sake of completeness also the synthesis of polystyrene-*block*-poly(1,4-isoprene)-*block*-poly(ethylene oxide) (PS-*b*-PI-*b*-PEO) triblock copolymers will be described, even though this system was not further investigated in this thesis. The preparation of the living PS-*b*-PI diblock copolymer precursor was identical to the synthesis of PS-*b*-PI-*b*-P(S/B) triblock copolymers. Subsequently, the reaction mixture was cooled to 10 °C and ethylene oxide was added followed by stirring at 10 °C for 1 h and at 25 °C overnight. This resulted in an endcapping of the living PS-*b*-PI precursor with one ethylene oxide unit, in agreement to the synthesis of PB-*b*-PI-*b*-PEO triblock copolymers. Then the polymerization of ethylene oxide was initiated by addition of the phosphazene base *t*-BuP_4 using a ratio of [*sec*-BuLi] : [*t*-BuP_4] = 1: 1. After polymerization of ethylene oxide at 40 °C for 3 d the reaction was terminated with a degassed mixture of acetic acid and methanol (5 : 1 by vol.). The corresponding PS-*b*-PI-*b*-PEO triblock copolymer was isolated by precipitation in cold isopropanol (ca. -10 - 0 °C).

2.3.3 Hydrogenation

Homogeneous catalytic hydrogenation of PB-*b*-PI-*b*-PEO and PS-*b*-PI-*b*-P(S/B) triblock copolymers was performed using the Wilkinson catalyst ($(Ph_3P)_3Rh(I)Cl$) to yield the corresponding polyethylene-*block*-poly(ethylene-*alt*-propylene)-*block*-poly(ethylene oxide) (PE-*b*-PEP-*b*-PEO) and polystyrene-*block*-poly(ethylene-*alt*-propylene)-*block*-poly(styrene/ethylene) (PS-*b*-PEP-*b*-P(S/E) triblock copolymers.[7] As an example, the hydrogenation of PB-*b*-PI-*b*-PEO triblock copolymers is depicted in Scheme 2.5. In a typical procedure 10 - 15 g of the triblock copolymer along with a small amount of stabilizer (2,6-di-*t*-butyl-4-methylphenol) were dissolved in dry toluene (p. a., Merck) and degassed for at least 30 min with dry nitrogen. Subsequently, Wilkinson catalyst (1 mol-% with respect to the number of double bonds) was added to the solution in a slight stream of nitrogen. This solution was transferred into a steel autoclave, which was previously rinsed with nitrogen for several times followed by hydrogen in order to remove traces of oxygen. The hydrogenation was carried out at 100 °C and 90 bar hydrogen pressure for 3 – 4 d. Shorter reaction times resulted in an

incomplete hydrogenation of PI block. After complete hydrogenation the triblock copolymers were isolated from the solution by precipitation in isopropanol. For the PE-*b*-PEP-*b*-PEO triblock copolymers cold acetone (-10 – 0 °C) was used, due to the amphiphilic character of these triblock copolymers. As a result of the highly polar PEO blocks, which tend to bind Wilkinson catalyst, precipitation is not efficient to remove residual catalyst completely. Therefore, the PE-*b*-PEP-*b*-PEO triblock copolymers were subjected to a further purification step by refluxing a solution of the polymer in toluene with a small amount of concentrated HCl for a short time followed by precipitation in cold acetone. The success of the purification can be followed by the disappearance of the brown color, which arises from residual catalyst.

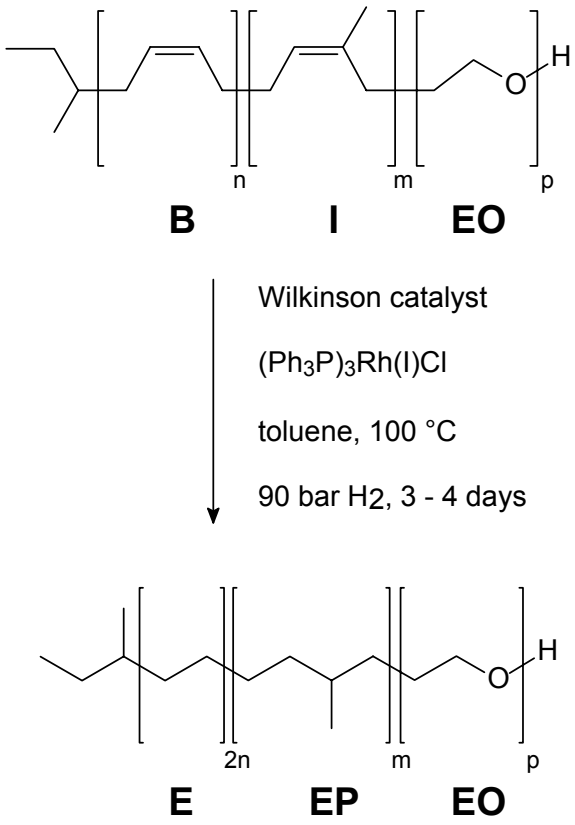

Scheme 2.5: Preparation of PE-*b*-PEP-*b*-PEO triblock copolymers by homogeneous catalytic hydrogenation of PB-*b*-PI-*b*-PEO triblock copolymers using Wilkinson catalyst.

Alternatively, PB-*b*-PI-*b*-PEO triblock copolymers were hydrogenated with diimide, generated in situ by thermolysis of *p*-toluenesulfonyl hydrazide (Scheme 2.6).[8] During the reaction diimide can react with olefinic double bonds of butadiene and isoprene segments under addition of hydrogen (six-center cyclic transition state[9]) or decompose under

disproportionation into hydrazine and nitrogen. The rate constants decrease in the following order: hydrogenation of butadiene segments (k_B), disproportionation (k_d), and hydrogenation of isoprene segments (k_I). The comparatively low rate constant for the hydrogenation of isoprene segments can be attributed to sterical hindrance arising from the methyl group of isoprene. As a result, the PB blocks get completely hydrogenated, whereas the PI blocks exhibit a degree of hydrogenation of only ca. 70%. To avoid side reactions arising from *p*-toluenesulfonic acid (thermolysis product of *p*-toluenesulfonyl hydrazide), which can attack olefinic sites resulting in addition of *p*-tolylsulfone functionality or chain degradation, tri-*n*-propylamine is added to the reaction mixture.

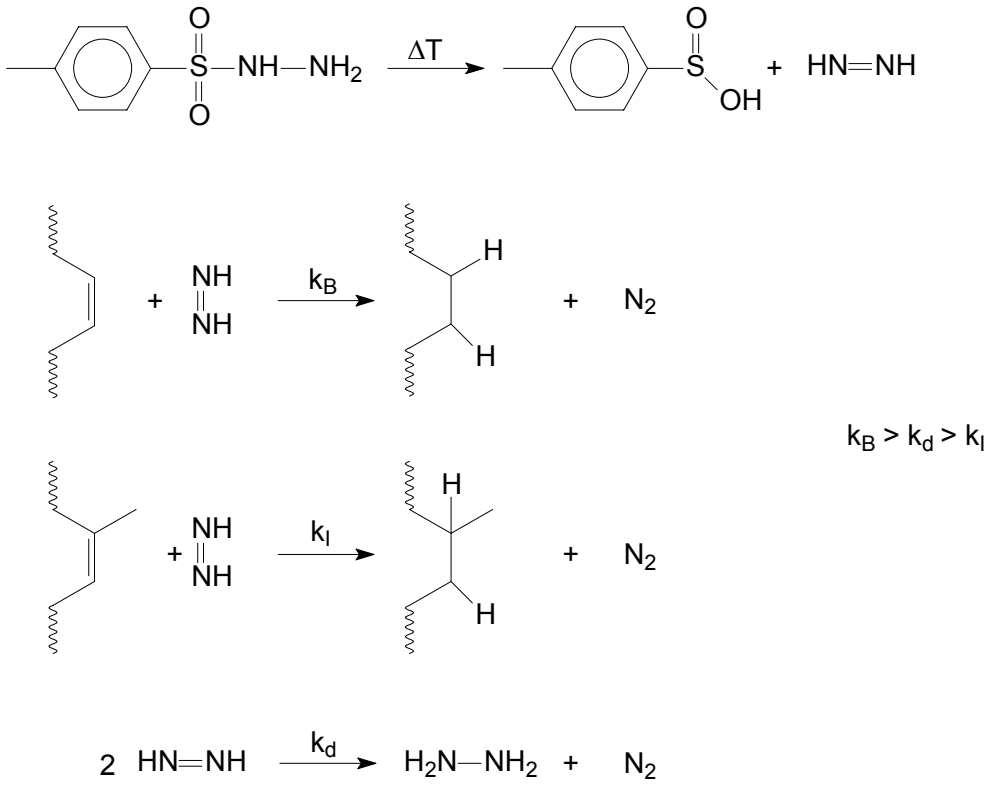

Scheme 2.6: Hydrogenation with diimide, prepared in situ by thermolysis of *p*-toluenesulfonyl hydrazide.

In a typical reaction 10 g of the PB-*b*-PI-*b*-PEO triblock copolymer, *p*-toluenesulfonyl hydrazide (TSH, 4-fold excess with respect to the number of double bonds), tri-*n*-propylamine (equimolar with regard to the amount of TSH), and a small amount of stabilizer (2,6-di-*t*-butyl-4-methylphenol) were dissolved in 500 ml o-xylene (purified over potassium) under nitrogen. Hydrogenation was carried out by refluxing the solution under a slight stream of

nitrogen for 6 h. The hydrogenated triblock copolymer was isolated by precipitation in cold acetone (-10 – 0 °C). In order to remove residual *p*-toluenesulfonic acid, a solution of the triblock copolymer in toluene was filtered over basic aluminum oxide followed by precipitation into cold acetone.

2.4 Equipment

2.4.1 NMR Spectroscopy

For ^{1}H-NMR measurements in solution a Bruker AC 250 spectrometer (250 MHz for ^{1}H) was used. PB-*b*-PI-*b*-PEO and PS-*b*-PI-*b*-P(S/B) triblock copolymers were measured in $CDCl_3$ at room temperature. Measurements on hydrogenated triblock copolymers were performed in d_8-toluene at 40 °C in order to avoid gelation of the solution. For calibration tetramethylsilane (TMS) was added as internal standard to the corresponding solvent. Usually solutions of 15 - 20 mg triblock copolymer in 0.8 ml of the corresponding deuterated solvent were used.

^{13}C solid-state NMR investigations of copoly(ether ester)s were carried out at DSM Research on a Varian Inova 400 (400 MHz for ^{1}H) and on a Varian Unity 200 (200 MHz for ^{1}H) spectrometer using the 7 mm Jacobsen style VT CP-MAS probe. The ^{13}C cross-polarization magic angle spinning (CP-MAS) and ^{13}C inversion recovery cross-polarization (IRCP) experiments were performed on the Inova 400, while the ^{1}H-$T_{1\rho}$ experiments were performed on the Unity 200. Adamantane was used as an external chemical shift reference (38.3 ppm for the methylene resonance relative to TMS). All experiments were performed under magic angle spinning conditions. Solid-state ^{2}H spectra were recorded on a Varian Inova 400 (400 MHz for ^{1}H) using a wideline probe. More detailed informations about the used puse sequences are given in Chapter 3.1.3. All samples were compression molded into plates at 240 °C.

2.4.2 Differential Scanning Calorimetry (DSC)

For thermal analysis a Perkin Elmer DSC 7 with a CCA 7 liquid nitrogen cooling device was used. For all measurements a two point calibration with chloroform (or decane) and indium was applied. Measurements on copoly(ether ester)s and PEO-*b*-PEB-*b*-PEO triblock copolymers were performed at heating rates of 20, 30 and 40 °C/min. Given transition temperatures correspond to an extrapolated heating rate of 0 °C/min, unless otherwise specified. Measurements on PB-*b*-PI-*b*-PEO, PS-*b*-PI-*b*-P(S/B) and the corresponding hydrogenated triblock copolymers were carried out at a scanning rate of 10 °C/min. Degrees of crystallinity were calculated assuming a heat of fusion of ΔH_m^0 = 196.6 J/g[10] for PEO, ΔH_m^0 = 145.3 J/g[11] for PBT, and ΔH_m^0 = 276.98 J/g[12] for PE. All displayed heating traces correspond to the second heating run in order to exclude effects resulting from any previous thermal history of the samples.

A detailed description of the performed self-nucleation experiments can be found in Chapter 3.2.2.

2.4.3 Size Exclusion Chromatography (SEC)

SEC experiments were performed on a Waters instrument calibrated with narrowly distributed polystyrene standards at 30 °C. Four PSS-SDV columns (5µm, Polymer Standards Service, Mainz) with a porosity range from 10^2 to 10^5 Å were used together with a differential refractometer and a UV-detector at 254 nm. Measurements were performed in THF with a flow rate of 1 ml/min using toluene as internal standard. Molecular weights of the PB precursors were calculated from the apparent values obtained by SEC using given K and α values for PS and PB resulting in the equation $M_n(PB) = 0.696\ M_n(PS)^{0.985}$ (Mark-Houwink-Sakurada relation).[12] Molecular weight determination of PEO homopolymers was accomplished using a calibration with narrowly distributed PEO standards.

2.4.4 Dynamic Mechanical Analysis (DMA)

For the determination of glass transition temperatures a Rheometrics DMTA IV operated in the rectangular torsion/compression mode at a heating rate of 2 °C/min and a constant frequency of 10 rad/s was used. Compression molded samples with dimensions of $6 \cdot 15 \cdot 0.5$ mm^3 were used. Dynamic shear experiments were performed with an Advanced Rheometric Expansion System (ARES, Rheometrics) in the plate-plate configuration. For measurements on copoly(ether ester)s a plate diameter of 25 mm and a gap of 1.5 mm were used. Temperature dependent measurements of G' and G" were performed at a scanning rate of 1 °C/min at a constant frequency of 1 rad/s. PEO-*b*-PEB-*b*-PEO triblock copolymers were measured using 50 mm plates with a gap of 1 mm at a scanning rate of 1 °C/min at a constant frequency of 0.5 rad. Order disorder transitions were detected by a sharp drop of G' and G'' upon heating. Given order disorder transition temperatures correspond to the cross-over of G' and G", *i. e.* G' = G". It was made sure that all experiments were done in the linear viscoelastic regime.

2.4.5 Mechanical Testing

Mechanical testing of copoly(ether ester)s was carried out at DSM Research on a Zwick 1455 tensile testing machine equipped with optical extensometers and a 200 N load cell. Hysteresis measurements were performed at a testing speed of 100 mm/min with a preload of 1 N without applying a holding time between the cycles in order to reduce relaxation phenomena. Young´s modulus was determined at the same rate for small elongations (0 – 4%). Cyclic measurements were performed for 100 and 500% strain and were repeated for 3 times, respectively. Samples were pressed into plates by compression molding between PTFE sheets at 240 °C for 5 min followed by cooling to room temperature (ca. –20 °C/min). All samples were allowed to acclimatize at room temperature (23 °C) under a relative air humidity of 50% for one day.

Experiments on PS-*b*-PI-*b*-PS, PS-*b*-PEP-*b*-P(S/E) and PE-*b*-PEP-*b*-PEO triblock copolymers were carried out using an Instron 5565 (100 N load cell) and a Zwick (equipped with optical extensometers, 200 N load cell) tensile testing machine. Young´s modulus was determined at a testing speed of 0.2 mm/min at small elongations (0 – 0.5%), or at 20 mm/min for strains between 0 – 4%, depending on the experiment. Elongations at break were

measured at 20 mm/min. Hysteresis measurements were performed at a testing speed of 20 mm/min for elongations to 100, 200, 300, 400 and 500% followed by extension to break. No holding time between the cycles was applied. Preparation was accomplished by compression molding into plates at 140 – 150 °C followed by cooling to room temperature (≈ -1.5 °C/min).

For all experiments test specimens according to ISO 37:1994 were used. It was made sure that the cutting of test specimens from the compression molded plates always occurred in the same direction in order to exclude any effects resulting from different orientations within the test samples.

2.4.6 Transmission Electron Microscopy (TEM)

TEM investigations were performed using a Zeiss CEM 902 electron microscope operated at 80 kV in the bright field mode. Thin sections (thickness ca. 50 Å) were cut from sample films at - 130 °C using a Reichert-Jung Ultracut E microtome equipped with a diamond knife. The thin sections were placed on gold grids.

Films of copoly(ether ester)s with PEO-*b*-PEB-*b*-PEO soft segments (around 1 mm thick) were prepared by compression molding at 240 °C for 5 min followed by cooling to room temperature (ca. –20 °C/min). Staining was achieved by exposure of the sections to RuO_4 vapor for 45 min. Since RuO_4 preferentially stains the amorphous PBT and PEO segments, the crystalline PBT domains and amorphous PEB domains appear bright.

Films of ABC triblock copolymers (around 0.5 mm thick) were prepared by solvent casting from a 2 - 3 wt-% solution in $CHCl_3$, or toluene. The solvent was allowed to slowly evaporate over a period of 2 weeks followed by drying under vacuum for 1 day. Film casting of hydrogenated triblock copolymers was performed from toluene solutions at 70 °C in order to avoid gelation upon solvent evaporation. In addition, compression molded samples, which were used for mechanical testing, were also taken for morphological investigations. Selective staining of PI domains was achieved by exposure of the sections to OsO_4 vapor for 60 s, while the thin sections of hydrogenated triblock copolymers were exposed to RuO_4 vapor for 45 min to selectively stain the PS domains.

For OsO_4 staining a grid was placed in a small sealed flask and exposed to OsO_4 vapor (from a OsO_4 grain) in vacuum (20 mbar) for 60 s. RuO_4 staining was carried out in a desiccator. The RuO_4 vapor was generated by the reaction of 10 mg ruthenium(III)chloride hydrate with 1.5 ml of a 5 wt-% aqueous solution of sodium hypochlorite. After exposure of

the samples to RuO_4 vapor for 30 – 45 min the solution was disposed of by adding a large excess of a saturated aqueous sodium disulfite ($Na_2S_2O_5$) solution.

2.4.7 Scanning Electron Microscopy (SEM)

SEM images were taken on a LEO 1530 Gemini instrument equipped with a field emission cathode and an In-Lens detector (scintillation detector) possessing a lateral resolution of approximately 2 nm. Measurements were performed at a working distance of 3 mm using an acceleration voltage of 1 kV. Thin films of PS-*b*-PEP-*b*-PE triblock copolymers were prepared by dip coating onto a polished silicon wafer from a 1 mg/ml solution of the triblock copolymer in toluene. The films were stained with RuO_4 vapor for 45 min prior to SEM imaging in order to visualize the PS domains.

2.4.8 Scanning Force Microscopy (SFM)

Scanning force microscopy images were taken on a Digital Instruments Dimension 3100 microscope operated in Tapping Mode™ (free amplitude of the cantilever: 20 nm; set point ratio: 0.95). Standard silicon nitride cantilevers were used and exchanged regularly in order to avoid contamination. Polished silicon wafers were used and purified prior to use with a stream of CO_2 crystals ("snow jet"). For temperature dependent measurements a D3/D5 SPC01 hot stage from Digital Instruments was used.

Measurements on copoly(ether ester)s were performed on compression molded films prepared on polished silicon wafers using polytetrafluoroethylene (PTFE) cover sheets. The samples were first heated to 250 °C for 3 min under nitrogen followed by cooling at a constant rate of 5 °C/min to room temperature.

Thin films of PE-*b*-PEP-*b*-PEO and PS-*b*-PEP-*b*-PE triblock copolymers were prepared by dip- or spin coating (2000 rpm, 1 min) from toluene solutions. Detailed information about the used concentrations can be found in the corresponding publications (Chapter 3.2.1, 3.3.1, and 3.3.2). Selective swelling of the PS-microdomains in PS-*b*-PEP-*b*-PE triblock copolymer thin films was accomplished by exposing a vacuum dried film to toluene vapor for 1 min. In addition, measurements were performed on compression molded samples of PS-*b*-PEP-*b*-PE triblock copolymers, which were prepared similar to the samples

used for mechanical testing. SFM imaging was carried out on smooth cut surfaces obtained by cutting with a diamond knife at -130 °C using a Reichert-Jung Ultracut E microtome.

2.4.9 X-Ray Scattering

2.4.9.1 Small Angle X-ray Scattering (SAXS)

SAXS was performed on a Bruker-AXS Nanostar equipped with a Histar-Detector and crossed Goebel mirrors. As a radiation source a sealed Cu-tube was used generating a wavelength of 0.1542 nm. Temperature dependent measurements were conducted using a Paar Physica TCU50 temperature control unit.

2.4.9.2 Wide Angle X-ray Diffraction (WAXD)

WAXD patterns were taken from a Bruker-AXS D8 Advance diffractometer equipped with a scintillation counter and a Goebel mirror using CuK_α radiation at room temperature.

2.4.10 Matrix Assisted Laser Desorption Ionization Time of Flight Mass Spectrometry (MALDI-ToF MS)

MALDI-Tof MS was performed on a Bruker Reflex III with a UV laser operating at 337 nm and an accelerating voltage of 20 kV. 2,5-Dihydroxybenzoic acid (DHB) was used as matrix for the PEO homopolymers together with lithium trifluoromethanesulfonate as cationizing agent. 1,8,9-trihydroxyanthracene (dithranol) and silver triflate as cationizing agent was used in the case of the low molecular weight PS-*block*-PEO diblock copolymers. Samples were dissolved in THF (10 mg/mL) and mixed with matrix (20 mg/mL in THF) and salt (10 mg/mL in THF) at a mixing ratio of 10 : 2 – 1 : 1 (v/v, matrix : analyte : salt). 1 μL of this mixture was spotted onto the target and allowed to dry. 200 – 500 laser shots were accumulated for a spectrum. All samples were measured after complete drying without removing the phosphazene base to keep the composition unchanged without loss of low molecular weight fractions.

2.4.11 Online Fourier-Transform Near Infrared (FT-NIR) Fiber-Optic Spectroscopy

Online FT-NIR monitoring was accomplished using an all glass low temperature immersion transmission probe (HELLMA) with an optical path length of 10 mm, which was connected to the FT-IR by 2 m fiber-optical cables. This probe can be used at reaction temperatures in between -180 to +200 °C. For the polymerizations a laboratory autoclave (Büchi, 1 L) equipped with a stirrer was used. The probe was fed through a port in the stainless steel top plate of the reactor and immersed into the reaction mixture (Figure 2.2).

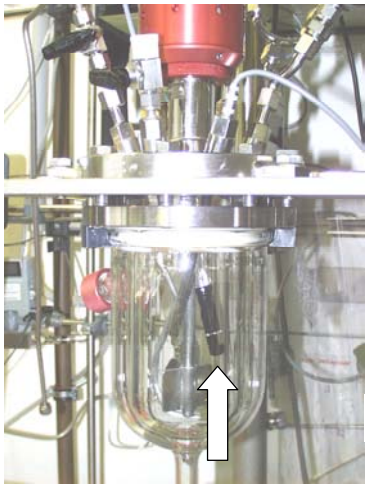

Figure 2.2: 1 L Büchi reactor equipped with a low temperature immersion NIR probe (HELMA).

The whole setup together with the solvent distillation is a completely closed system that can be evacuated and held under dry inert atmosphere (Figure 2.3). NIR spectra were recorded with a Nicolet Magna 560 FT-IR optical bench equipped with a white light source and a PbS detector. Data collection and processing was performed with Nicolet's OMNIC Series software. Each spectrum was obtained by accumulating 32 scans with a resolution of 4 cm^{-1}. The total collection time per spectrum was about 22 s.

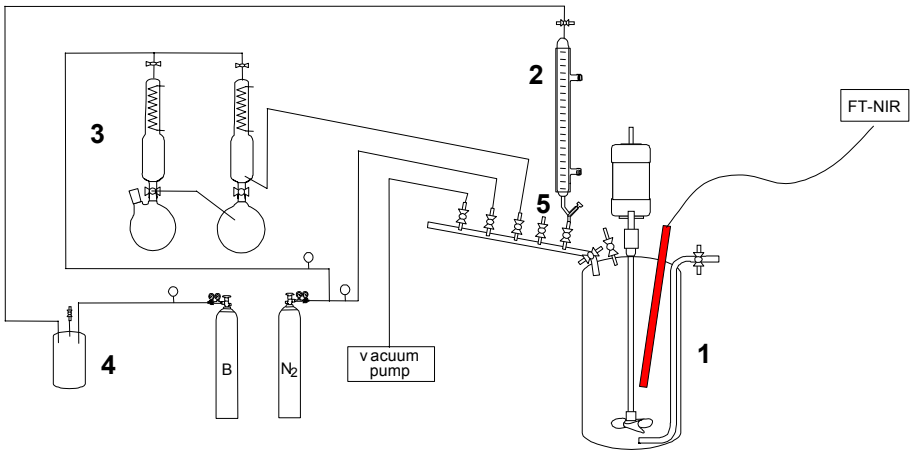

Figure 2.3: Setup of upscaling reactor and fiber optic equipment for online measurement. 1, autoclave with NIR fiber-optic probe; 2, burette for condensation of gaseous monomers (e. g. butadiene, isobutylene); 3, solvent distillation setup; 4, reactor for purification of butadiene; 5, connector for monomer ampoules, e. g. ethylene oxide.

Kinetic investigations on ethylene oxide homopolymerizations were performed using the first overtone C-H stretching of EO at 6070 cm^{-1} for conversion determination. In addition, peak heights were used instead of peak areas for evaluation, since they usually gave less noise.

Conversions, X_p, were calculated using the following equation:

$$X_p = \frac{A_0 - A_t}{A_0 - A_\infty}$$

where A_t is the relative absorbance at time t, A_0 = initial absorbance, and A_∞ = absorbance at full conversion. The apparent rate constants of propagation were extracted from the linear regime in the corresponding first-order time-conversion plots ($-\ln(1-X_p)$ versus t), by the slope of the linear fit at values of $-\ln(1-X_p)$ between 1 and 2. Induction times were calculated from the linear fit, i. e. reflect the point of intersection of the linear fit line with the time axis.

2.5 References

(1) Zhu, L.; Cheng, S. Z. D.; Calhoun, B. H.; Ge, Q.; Quirk, R. P.; Thomas, E. L.; Hsiao, B. S.; Yeh, F.; Lotz, B. *Polymer* **2001**, *42*, 5829.

(2) Förster, S.; Krämer, E. *Macromolecules* **1999**, *32*, 2783.

(3) Floudas, G.; Vazaiou, B.; Schipper, F.; Ulrich, R.; Wiesner, U.; Iatrou, H.; Hadjichristidis, N. *Macromolecules* **2001**, *34*, 2947.

(4) Eßwein, B.; Möller, M. *Angew. Chem.* **1996**, *108*, 703.

(5) Eßwein, B.; Molenberg, A.; Möller, M. *Macromol. Symp.* **1996**, *107*, 331.

(6) Eßwein, B.; Steidl, N. M.; Möller, M. *Macromol. Rapid Commun.* **1996**, *17*, 143.

(7) Balsamo, V. PhD thesis, Mainz, 1996.

(8) Hahn, S. F. *J. Polym. Sci., Part A: Polym. Chem.* **1992**, *30*, 397.

(9) Carey, F. A.; Sundberg, R. J. Organische Chemie: ein weiterführendes Lehrbuch. VCH: Weinheim, 1995.

(10) Wunderlich, B. Macromolecular Physics. Academic Press: New York, 1980; Vol. 3.

(11) Van Krevelen, D. W. *Properties of Polymers*, 2nd ed.; Elsevier: Oxford, 1976.

(12) Brandrup, J.; Immergut, E. H. *Polymer Handbook*, 3rd ed.; Wiley: New York, 1989.

3 Publications

3.1 PBT-Based Copoly(ether ester)s

3.1.1 New Thermoplastic Elastomers by Incorporation of Nonpolar Soft Segments in PBT-Based Copolyesters

Holger Schmalz[a], Volker Abetz[a*], Ronald Lange[b*], Maria Soliman[b]

a) Makromolekulare Chemie II, Universität Bayreuth, 95440 Bayreuth, Germany
b) DSM Research, 6160 MD Geleen, The Netherlands

in Memoriam Prof. Dr. Reimund Stadler

ABSTRACT: The incorporation of hydroxy functionalized hydrogenated polybutadienes (HO-PEB-OH, KRATON® liquid polymer) into PBT based copolyesters by a conventional 2 step melt polycondensation procedure is described. The usually occuring macrophase separation with non-polar soft segments is avoided by chain extension of HO-PEB-OH with ethylene oxide to yield the corresponding hydroxy terminated PEO-PEB-PEO triblock copolymers. Several PEO-PEB-PEO triblock copolymers with different PEO block lengths have been synthesized by means of anionic synthesis and incorporated into PBT based copolyesters with varying PBT content. We show that the chain extension of HO-PEB-OH with ethylene oxide compatibilizes the non-polar KRATON® with the polar reactants 1,4-butanediol and dimethyl terephthalate during melt polycondensation, leading to a complete incorporation of the triblock copolymer into the copolyester. Morphological studies using SFM as well as mechanical testing show that the morphology is strongly influenced by the soft segment leading to dispersed PBT crystallites in a matrix of the soft phase. Thermal characterization of the synthesized copolyesters by DSC exhibits a low glass transition temperature and a high PBT melting point even at high soft segment contents, making these materials suitable for low and high temperature range applications.

Introduction

Thermoplastic elastomers combine the properties of crosslinked elastomers, such as impact-resistance and low-temperature flexibility, with the ease of processing of thermoplastic materials (extrusion, injection molding, etc.). In general thermoplastic elastomers consist of a hard phase which provides a physical crosslinking and a soft phase providing elastic properties even at low temperatures.

Intensive studies have been done on copolyether-esters based on polybutylene terephthalate (PBT) hard segments and low molecular weight polyether soft segments like poly(ethylene oxide) (PEO), poly(tetramethylene oxide) (PTMO) or poly(ethylene oxide)-*block*-poly(propylene oxide)-*block*-poly(ethylene oxide) (PEO-PPO-PEO) triblock copolymers.[1-4] These materials are suitable for applications in a wide temperature range due to a high PBT melting point and a low glass transition temperature of the soft phase. However, polyether soft segments tend to oxidative degradation and hydrolysis at elevated temperatures which makes the use of stabilizers necessary. In order to overcome these problems saturated dimerized fatty acids were used as alternative soft segments.[5-8] The commercially available dimerized fatty acids are usually synthesized by dimerization of unsaturated C_{18} fatty acids which yields a mixture of branched C_{36} dimerized fatty acids with molecular weights of approximately 560 g/mol, but there were also higher molecular C_{44} and C_{70} dimerized fatty acids used as alternative soft segments. The properties concerning thermo-oxidative stability were improved while the overall properties were not significantly changed.

In order to enhance the mechanical properties of copolyesters in terms of elasticity it would be preferable to have a stronger phase separation between hard and soft phase and in addition a more "rubber-like" soft segment like polyolefins with low entanglement molecular weight. Not much work has been published concerning the incorporation of polyolefinic soft segments in PBT based copolyesters. Walch et al. describes the synthesis of poly(butylene terephthalate)-*block*-polyisobutylene segmented block copolymers by using α,ω-anhydride functionalized polyisobutylenes with molecular weights up to 3000 g/mol.[9] Due to the high incompatibility of polyisobutylene with the polar reactants dimethyl terephthalate and 1,4-butanediol phase separation occurs during the melt polycondensation process, resulting in a very poor incorporation of the soft segment. This problem was solved by using high boiling solvents like *m*-cresol and 1,2,4-trichlorobenzene, which are good solvents for PBT and polyisobutylene. The solvent was then removed together with surplus 1,4-butanediol in the polycondensation step by applying vacuum during polymerization. Nevertheless, there is

some macrophase separation in the second step of the polycondensation when most of the solvent is evaporated. This macrophase separation is responsible for the relatively high amount of extractable polyisobutylene for copolyesters with high soft segment content. Kennedy et al. describes a similar solvent based approach for the synthesis of poly(butylene terephthalate)-*block*-polyisobutylene using hydroxy telechelic polyisobutylenes with molecular weights up to 10,000 g/mol.[10] In both contributions only little information is given with regard to the mechanical properties of these systems. Mechanical testing results in poor mechanical properties probably due to incomplete incorporation of the non-polar polyisobutylene and inhomogeneities in the material arising from insufficient stirring during synthesis.

So far it has not been possible to incorporate polyolefinic soft segments by conventional melt polycondensation processes due to the above mentioned macrophase separation. The macrophase separation can be avoided by using co-solvents during the synthesis. However, this is not acceptable for processing and environmental reasons. An alternative way of preventing the macrophase separation during melt polycondensation could be an anionic chain extension of KRATON® (HO-PEB-OH) with ethylene oxide. This results in the corresponding poly(ethylene oxide)-*block*-poly(ethylene-*stat*-butylene)-*block*-poly(ethylene oxide) triblock copolymers where the PEO blocks should compatibilize the non-polar KRATON® with the polar reactants dimethyl terephthalate and 1,4-butanediol during melt polycondensation. This leads to a homogeneous reaction mixture which is necessary to obtain high molecular weight copolyesters with good mechanical properties. Here, we present a new method for the synthesis of polyesters with polyolefinic soft segments based on hydroxy telechelic hydrogenated polybutadienes (HO-PEB-OH, KRATON® liquid polymer HPVM-2203) by a conventional melt polycondensation procedure without using any co-solvents.

Experimental

Materials. Tetrahydrofuran (Merck) was purified by successive distillation over CaH_2 and potassium. Ethylene oxide (Linde) was condensed onto CaH_2 and stirred at 0 °C for 3 h before being transferred into glass ampules. KRATON® liquid polymer HPVM-2203 (Shell) was purified by freeze drying with benzene for at least 3 times followed by drying under high vacuum at 60 °C for 2 d. Naphthalene (Bayer) was purified by sublimation and stored under nitrogen until use. Potassium naphthalide solutions were synthesized by reaction of naphthalene with potassium in THF under nitrogen. The green colour of potassium naphthalide appeared immediately and the reaction mixture was allowed to stir over night at room temperature before use. The solutions had a typical concentration of 0.5 mol/l and could be stored in a freezer for several weeks.

Dimethyl terephthalate (Fluka), 1,4-butanediol (Fluka) and tetrabutyl orthotitanate (Fluka) were used without further purification.

Synthesis of PEO-PEB-PEO Triblock Copolymers. The synthesis of PEO-PEB-PEO triblock copolymers was accomplished by anionic ring opening polymerization of ethylene oxide in THF using HO-PEB-OH (KRATON® liquid polymer HPVM-2203) with a molecular weight of 3600 g/mol as starting material. The terminal hydroxy groups of HO-PEB-OH were first deprotonated by titration with a 0.5 M solution of potassium naphthalide at 35 °C to yield the corresponding bifunctional macroinitiator KO-PEB-OK.[11,12,13] The titration was stopped after the slight green colour of excess potassium naphthalide remains for at least 45 min. After addition of ethylene oxide at 0 °C the polymerization was carried out at 55 °C for 3 to 4 d. The reaction was terminated with acetic acid/methanol (5:1 by vol.) and the products were precipitated in petrol ether (bp. 40 – 60 °C, M_n(PEO) > 1400 g/mol) or acetone at - 30 °C (M_n(PEO) < 1400 g/mol).

Synthesis of Copolyesters. The synthesis of copolyesters based on PEO-PEB-PEO soft segments was accomplished by using common 2 step melt polycondensation procedures.[3] The reaction was carried out in a cylindrical flask with nitrogen inlet, mechanical stirrer and distillation bridge. In the first step a mixture of PEO-PEB-PEO triblock copolymer, dimethyl terephthalate, 1,4-butanediol (50% molar excess with regard to the methylester units), a phenolic antioxidant and tetrabutyl orthotitanate (1.42 mmol/kg polymer) as a solution in 1,4-butanediol was heated for 1 hour to 190 °C, 200 °C and 210 °C, respectively, under nitrogen

in order to distil off the methanol. Then the temperature was raised stepwise to 230 and 250 °C and vacuum (0.05 – 0.1 mbar) was applied for 2.5 h after reaching 230 °C.

Measurements. Size exclusion chromatography (SEC) experiments were performed on a Waters instrument calibrated with polystyrene standards at 30 °C. Four PSS-SDV columns (5 μm, Polymer Standards Service, Mainz) with a porosity range from 10^2 to 10^5 Å were used together with a differential refractometer and a UV-detector. Measurements on the PEO-PEB-PEO triblock copolymers were performed in THF with a flow rate of 1 ml/min using toluene as internal standard. For thermal analysis a Perkin Elmer DSC 7 with a CCA 7 liquid nitrogen cooling device was used. For all measurements a two point calibration with chloroform and indium was applied. All experiments were performed at heating rates of 20, 30 and 40 K/min. Given transition temperatures correspond to an extrapolated heating rate of 0 K/min, heat of fusions refer to a heating rate of 20 K/min unless otherwise specified. The displayed heat flow traces correspond to a heating rate of 20 K/min (second heating run). Mechanical testing was performed on an Instron 5565 tensile testing machine at room temperature. The Young´s modulus was determined at a testing speed of 0.2 mm/min at small elongations (up to 3 - 4%), elongations at break were measured at 20 mm/min. For ^{1}H-NMR measurements a Bruker AC 250 spectrometer was used. For small angle X-ray scattering (SAXS) a Bruker AXS-Nanostar with sealed tube (Cu), crossed Göbel mirrors, 2-dimensional Hi-Star detector and temperature controlling unit was used. The SFM image was taken from melt pressed films using Teflon plates on a Digital Instruments Nanoscope IIIa operated in Tapping Mode™.

Results and Discussion

The preparation of PEO-PEB-PEO triblock copolymers involves in the first step the transfer of the starting material HO-PEB-OH (M_n = 3600 g/mol, OH-functionality = 1.9) to the corresponding bifunctional macroinitiator KO-PEB-OK for the anionic ring opening polymerization of ethylene oxide.

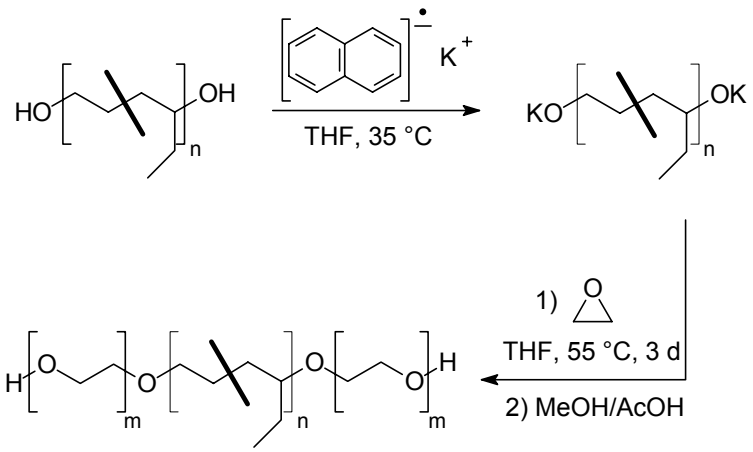

Scheme 1. Synthesis of poly(ethylene oxide)-*block*-poly(ethylene-*stat*-butylene)-*block*-poly(ethylene oxide) triblock copolymers.

This was accomplished by titration of a HO-PEB-OH solution in dry tetrahydrofuran with potassium naphthalide solution under nitrogen. The intensive green colour of potassium naphthalide allows a very precise end-point determination which is indispensable in order to avoid the formation of homo-PEO during ethylene oxide polymerization initiated by excess potassium naphthalide. The titration was carried out at 35 °C due to precipitation of associates at lower temperatures when approaching the end-point of titration. Ethylene oxide polymerization was performed at 55 °C in tetrahydrofuran for 3 to 4 d to give the corresponding hydroxy terminated PEO-PEB-PEO triblock copolymers (Scheme 1). Due to the strong association of potassium alkoxides the concentration of active centres had to be kept low ($< 1 \cdot 10^{-2}$ mol/l) in order to avoid precipitation of associates. The use of cryptands like C222 to suppress association is not necessary in this case and furthermore do not effect the molecular weight distribution.

Different $PEO_xPEB_yPEO_x^m$ triblock copolymers (the subscripts x and y give the weight percentage of the corresponding block, and the superscript m is the molar mass of the triblock copolymer in kilograms per mole) with PEO block lengths between 800 and 4600 g/mol have been synthesized and characterized by ^{1}H-NMR spectroscopy and SEC (Table 1, Figure 1).

Table 1. Molecular Weights and Polydispersities of PEO-PEB-PEO Triblock Copolymers

sample	$M_{n,SEC}$[a] [g/mol]	$M_{n,NMR}$ [g/mol]	$M_n(PEO)_{NMR}$ [g/mol]	M_w/M_n
HO-PEB-OH	7990	3600[b]	-	1.09
PEO_{36}-PEB_{28}-$PEO_{36}^{12.8}$	16420	12800	4600	1.13
PEO_{29}-PEB_{42}-$PEO_{29}^{8.6}$	13820	8620	2510	1.08
PEO_{27}-PEB_{46}-$PEO_{27}^{8.0}$	13190	7980	2190	1.08
PEO_{25}-PEB_{50}-$PEO_{25}^{7.1}$	11930	7060	1730	1.09
PEO_{22}-PEB_{56}-$PEO_{22}^{6.4}$	11580	6360	1380	1.08
PEO_{18}-PEB_{64}-$PEO_{18}^{5.6}$	10080	5600	1000	1.11
PEO_{16}-PEB_{68}-$PEO_{16}^{5.2}$	9570	5240	820	1.12

[a] Determined by SEC in THF, calibrated against polystyrene standards.
[b] Determined by end group analysis.

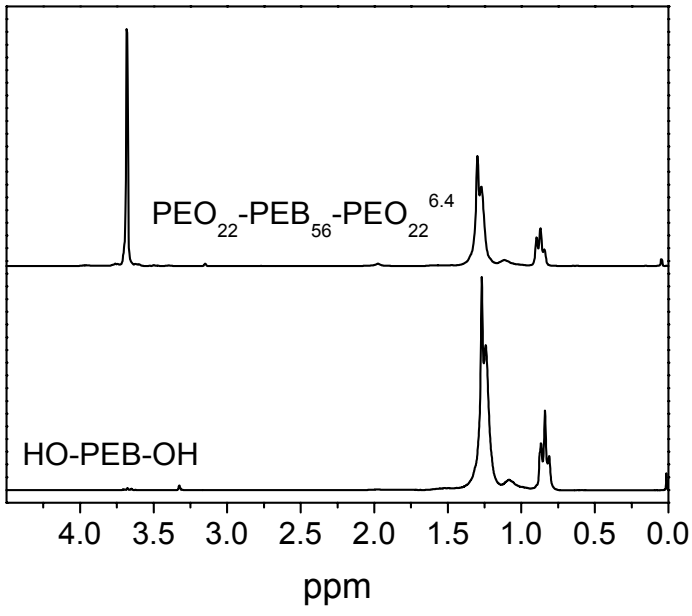

Figure 1. 250 MHz ^{1}H-NMR spectra of the starting material HO-PEB-OH and the triblock copolymer PEO_{22}-PEB_{56}-$PEO_{22}^{6.4}$ in $CDCl_3$.

Size exclusion chromatography measurements in tetrahydrofuran show that the chain extension of HO-PEB-OH with ethylene oxide yields narrowly distributed triblock copolymers ($1.08 < M_w/M_n < 1.13$) without residual starting material and homo-PEO impurities (Figure 2). The SEC-trace of the triblock copolymer exhibits a small tailing at the lower molecular weight side which can also be seen for HO-PEB-OH. This can be attributed to monofunctional or not functionalized components in HO-PEB-OH which exhibits an OH-functionality of only 1.9.

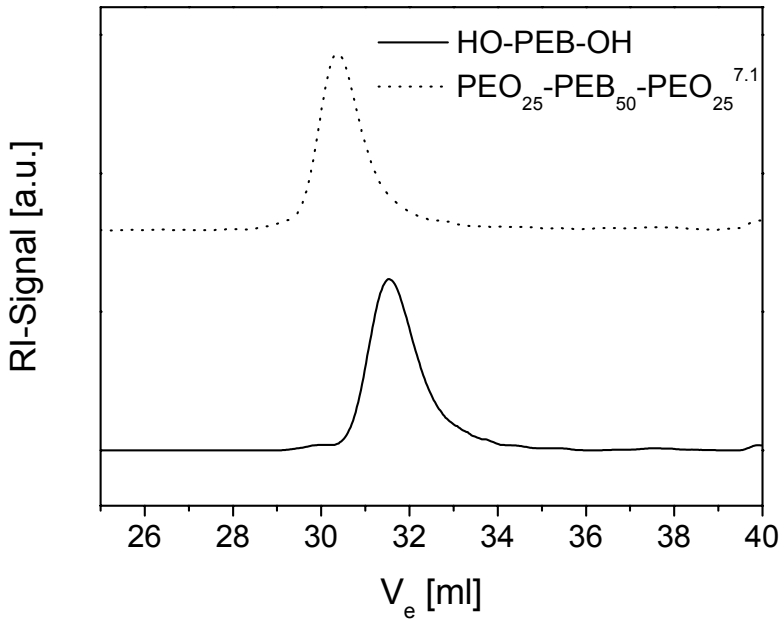

Figure 2. SEC-traces of HO-PEB-OH and the triblock copolymer PEO_{25}-PEB_{50}-PEO_{25}[7.1] using THF as eluent and toluene as internal standard.

The results of thermal analysis on the PEO-PEB-PEO triblock copolymers are listed in Table 2. All triblock copolymers show one glass transition temperature at - 61 to - 66 °C corresponding to the PEB middle block and amorphous poly(ethylene oxide). A differentiation between T_G(PEB) and T_G(PEO) is not possible probably due to overlapping transition temperatures resulting in a broad glass transition region. The degree of crystallinity for poly(ethylene oxide) is nearly constant for M_n(PEO) ≥ 1380 g/mol ($\alpha \sim 75\%$) and decreases for smaller PEO block lengths. The degree of crystallinity was calculated assuming a heat of fusion for PEO of $\Delta H_m^0 = 196.6$ J/g.[14]

Table 2. DSC Data of PEO-PEB-PEO Triblock Copolymers[a]

sample	M_n(PEO) [g/mol]	T_m [°C]	T_c[b] [°C]	α (PEO) [%]	T_G [°C]
PEO_{36}-PEB_{28}-PEO_{36} $^{12.8}$	4600	53.7	18.3	78.0	-61.9
PEO_{29}-PEB_{42}-PEO_{29} $^{8.6}$	2510	44.3	6.3	75.2	-63.8
PEO_{27}-PEB_{46}-PEO_{27} $^{8.0}$	2190	39.7	9.9	73.3	-66.1
PEO_{25}-PEB_{50}-PEO_{25} $^{7.1}$	1730	38.3	5.4	73.8	-64.3
PEO_{22}-PEB_{56}-PEO_{22} $^{6.4}$	1380	35.9	2.5	74.3	-62.2
PEO_{18}-PEB_{64}-PEO_{18} $^{5.6}$	1000	29.8	-28.3	60.3	-60.9
PEO_{16}-PEB_{68}-PEO_{16} $^{5.2}$	820	24.4	-31.2	60.1	-61.2

[a] T_m = melting point, T_c = crystallization temperature, α = degree of crystallinity, T_G = glass transition temperature.
[b] Measured at a cooling rate of 40 K/min.

The investigated triblock copolymers exhibit a strong dependence between the melting point of crystallizable PEO blocks and the average degree of polymerization P_n(PEO). Figure 3 shows a plot of $1/T_m$(PEO) versus $1/P_n$(PEO) demonstrating the linear dependence of $1/T_m$ on $1/P_n$ for the synthesized triblock copolymers.

The synthesis of copolyesters with PEO-PEB-PEO soft segments was accomplished by using a conventional 2 step melt polycondensation procedure using tetrabutyl orthotitanate as catalyst. For materials with good elastic properties it is crucial that the soft segment, providing the elastic properties, forms the matrix and the crystalline PBT domains are dispersed within the matrix. Therefore we focused on the investigation of copolyesters with soft segment contents ≥ 50 wt-%. Several copolyesters with PBT contents between 10 - 50 wt-% and different PEO-PEB-PEO soft segments (varying M_n(PEO)) have been synthesized (Table 3). Copolyesters with PBT contents > 45 wt-% and molecular weights of the soft segments ≥ 7000 g/mol (M_n(PEO) ≥ 1700 g/mol) exhibit a turbid melt during melt polycondensation indicating a phase separation in the melt. This might be due to the high content of polar monomers in the reaction mixture and the high molecular weight of the soft segment. All other copolyesters show a clear melt during the synthesis, i.e. the reaction mixture is homogeneous and no macrophase separation occurs.

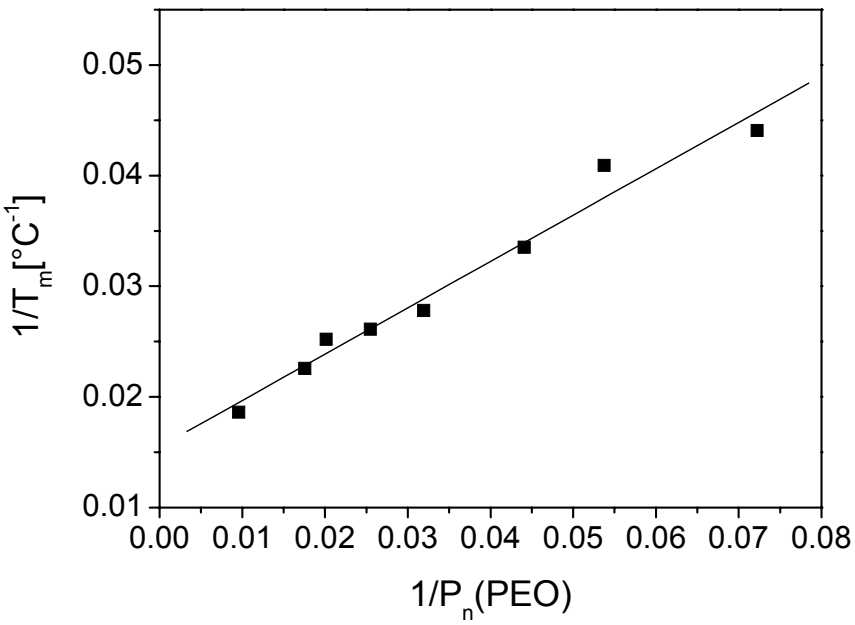

Figure 3. Dependence of $1/T_m$(PEO) on $1/P_n$(PEO) for the synthesized PEO-PEB-PEO triblock copolymers.

The incorporation of the PEO-PEB-PEO triblock copolymer into the polyester can be confirmed by successive soxhlet extraction of the copolyesters with chloroform and tetrahydrofuran. For PBT50-2190 soxhlet extraction yields only 4 wt-% THF-soluble extract confirming the almost complete incorporation of the soft segment, even for systems exhibiting turbid melts during melt polycondensation. In addition SEC analysis of the extract, compared with the used soft segment, show that the extract contains only negligible amounts of pure triblock copolymer, i.e. most of the soluble components contain soft segment with short PBT blocks. From these measurements it can be concluded that chain extension of HO-PEB-OH with ethylene oxide is a very useful method to incorporate non-polar soft segments into polyesters without using any co-solvents in the first step of the melt polycondensation.

Table 3. Data of Synthesized Copolyesters

sample	w (PBT) [%]	M_n(PEO) [g/mol]	x_{HS}[a]	l_{HS}[b]	melt	code
1	50	4600	0.983	58.3	turbid	PBT50-4600
2	50	2510	0.975	40.1	turbid	PBT50-2510
3	50	2190	0.973	37.2	turbid	PBT50-2190
4	50	1730	0.970	33.0	turbid	PBT50-1730
5	40	2510	0.963	27.1	slightly turbid	PBT40-2510
6	40	2190	0.960	25.1	slightly turbid	PBT40-2190
7	40	1730	0.955	22.4	slightly turbid	PBT40-1730
8	40	1380	0.951	20.2	clear	PBT40-1380
9	30	1380	0.925	13.4	clear	PBT30-1380
10	20	1380	0.878	8.2	clear	PBT20-1380
11	45	1000	0.954	21.8	clear	PBT45-1000
12	40	1000	0.944	17.9	clear	PBT40-1000
13	35	1000	0.932	14.7	clear	PBT35-1000
14	30	1000	0.916	11.9	clear	PBT30-1000
15	25	1000	0.894	9.5	clear	PBT25-1000
16	20	1000	0.864	7.4	clear	PBT20-1000
17	10	1000	0.739	3.8	clear	PBT10-1000
18	40	820	0.941	16.9	clear	PBT40-820
19	30	820	0.911	11.2	clear	PBT30-820

[a] Mole fraction of hard segment (PBT).
[b] Average segment length of the hard segment calculated according to $l_{HS}=1/(1-x_{HS})$.

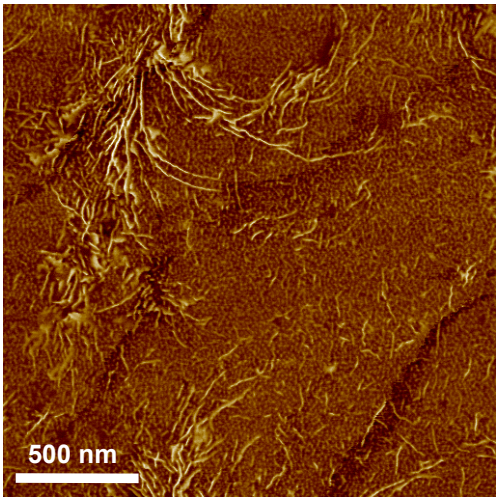

Figure 4. SFM phase contrast image of a melt pressed film of PBT20-1000 onto a glass wafer; z = 40°.

Characterization of the copolyesters by SFM shows the typical TPE morphology with well phase separated hard and soft phases as depicted in Figure 4. The bright longish domains correspond to PBT crystallites which exhibit a higher phase contrast compared to the more softer soft segment phase. The PBT crystallites are dispersed within a matrix of the soft segment and exhibit a broad crystallite size distribution. The darker regions, representing the soft segment phase, show a microstructure arising from the microphase separation of the incorporated PEO-PEB-PEO triblock copolymer.

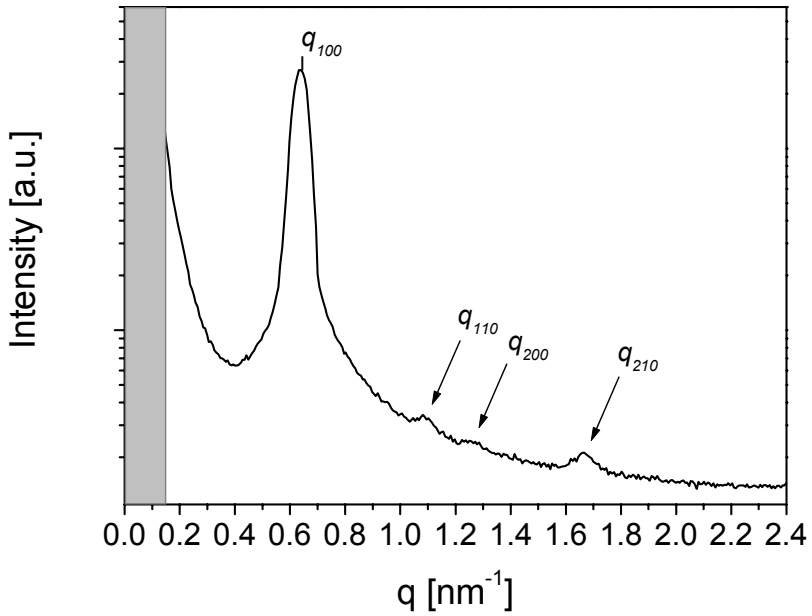

Figure 5. Semilogarithmic SAXS profile for the triblock copolymer PEO_{18}-PEB_{64}-PEO_{18}[5.6] at 80 °C (scattering vector $q = 4\pi/\lambda \sin\Theta$ with 2Θ being the scattering angle and $\lambda = 0.1542$ nm).

Taking into account that the PEO blocks in PBT20-1000 are molten at room temperature, the structure of the incorporated triblock copolymer PEO_{18}-PEB_{64}-PEO_{18}[5.6] was investigated by small angle X-ray scattering. The semilogarithmic SAXS profile at 80 °C (molten PEO blocks) exhibits reflex positions at a ratio of $1 : \sqrt{3} : 2 : \sqrt{7}$ which are typical for hexagonally packed cylinders (Figure 5). In conclusion, the microstructure of the soft segment phase in PBT20-1000 might be attributed to a distorted cylindrical structure with the bright spots referring to PEO cylinders. As SAXS is a very useful method for investigating the morphology of the PEO-PEB-PEO soft segments, we also performed measurements on the synthesized copolyesters. Unfortunately, the experiments do not give sufficient information for structure elucidation.

Table 4. DSC Data of Copolyesters[a]

	T_m(PEO) [°C]	T_c(PEO) [°C]	T_{rc}(PEO) [°C]	α (PEO) [%]	T_m(PBT) [°C]	T_{c1} (PBT)[b] [°C]	T_{c2} (PBT)[b] [°C]	T_{c3} (PBT)[b] [°C]	α (PBT) [%]	T_G [°C]
PBT40-2510	23.8	-14.9	-	16.5	210.2	-	90.5	33.1	21.5	-65.7
PBT40-2190	25.7	-16.7	-	14.3	215.7	-	92.7	41.0	18.7	-59.1
PBT40-1730	12.5	-37.4	-	12.4	208.8	-	85.6	37.3	17.5	-65.5
PBT40-1380	7.0	-49.2	-46.3	8.1	207.7	-	78.3	46.5	15.8	-66.1
PBT30-1380	3.8	-	-47.6	7.9	202.5	-	74.7	53.3	24.0	-66.5
PBT20-1380	13.5	-42.3	-40.6	9.6	184.0	-	-	51.8	21.9	-60.3
PBT45-1000	6.1	-	-35.2	3.7	217.5	-	93.3	58.3	27.3	-57.6
PBT40-1000	3.4	-	-36.0	3.7	211.4	-	89.9	52.6	21.8	-58.2
PBT35-1000	4.2	-46.4	-35.2	3.9	213.5	-	89.9	54.3	23.3	-58.0
PBT30-1000	4.9	-45.7	-32.9	4.0	212.1	126.3	85.9	58.3	27.8	-58.1
PBT25-1000	10.8	-46.7	-41.9	9.8	214.9	136.3	83.6	60.6	31.1	-59.1
PBT20-1000	5.5	-46.7	-38.5	8.3	190.0	-	-	60.6	27.0	-59.8
PBT10-1000	8.5	-	-31.5	6.3	-	-	-	-	-	-59.5
PBT40-820	-	-	-	-	213.8	-	81.4	-	24.4	-59.9
PBT30-820	-	-	-	-	212.4	-	81.7	44.9	16.0	-59.7

[a] T_m = melting temperature, T_c = crystallization temperature, T_{rc} = recrystallization temperature, α = degree of crystallinity and T_G = glass transition temperature.

[b] Crystallization temperatures refer to a cooling rate of 20 K/min for PBTx-1000 and 40 K/min for all other samples.

The DSC data of some representative copolyesters are given in Table 4. The degree of crystallinity for PBT was calculated using a heat of fusion of ΔH_m^0 = 145.3 J/g.[15] The detected glass transition temperatures are only slightly shifted compared to the glass transition temperatures of the pure triblock copolymers and are almost independent on composition, indicating a pronounced microphase separation in the soft phase. A glass transition temperature of pure amorphous PBT cannot be seen in the heat flow traces, probably due to partial mixing of amorphous PBT and PEO, although a glass transition temperature of a mixed amorphous PBT/PEO-phase is also not detectable.

Usually the copolyesters exhibit a melting endotherm corresponding to crystalline PEO and PBT (Table 4, Figure 6). Only for systems with very short PEO blocks like PBT40-820 and PBT30-820 no melt transition for PEO is observed; i.e. in these systems the poly(ethylene oxide) blocks are not able to form crystalline domains. The melting points and degrees of crystallinity of PEO blocks in copolyesters are shifted to lower values compared to the pure soft segment (Tables 2 and 4). Upon cooling the PBT segments crystallize and predefine the morphology. The crystallization of PEO which appears at much lower temperatures is influenced by the existing morphology leading to smaller and less perfect crystallites. This shift in the PEO melting endotherm and degree of crystallinity also confirms the incorporation of the triblock copolymer soft segment into the polyester.

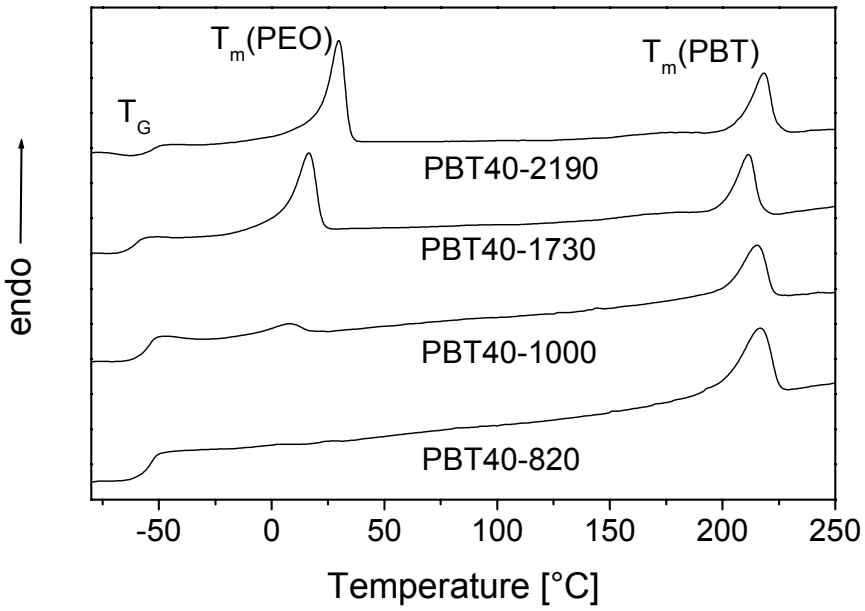

Figure 6. Thermal properties of copolyesters in dependence of the incorporated soft segment.

Figure 7 shows some copolyesters with PEO_{18}-PEB_{64}-PEO_{18}[5,6] soft segments and varying PBT content. As the melting point of the hard segment in copolyesters strongly depends on its average segment length $l_{HS} = 1/(1-x_{HS})$, where x_{HS} = mole fraction of PBT hard segment, the PBT melting point decreases with increasing soft segment content.[16] In addition, a broadening of the PBT melting endotherm can be observed with decreasing PBT content indicating a broadening of the crystallite size distribution. The latter was also detected by SFM investigations (Figure 4). Especially copolyesters with high soft segment content and low molecular weight PEO segments like PBT20-1000 exhibit crystallization of the PEO segments upon heating. In these systems the PEO crystallization is hindered upon cooling which leads to recrystallization upon heating followed by melting of the formed metastable crystals. Compared to conventional copolyether-ester with low molecular weight polyether soft segments like poly(tetramethylene oxide), the PBT melting point in our systems is much higher at the same soft segment content, which can be attributed to a higher hard segment block length.[17,18] Together with the low glass transition temperature, the high PBT melting point enables the application of these copolyesters in a wide temperature range.

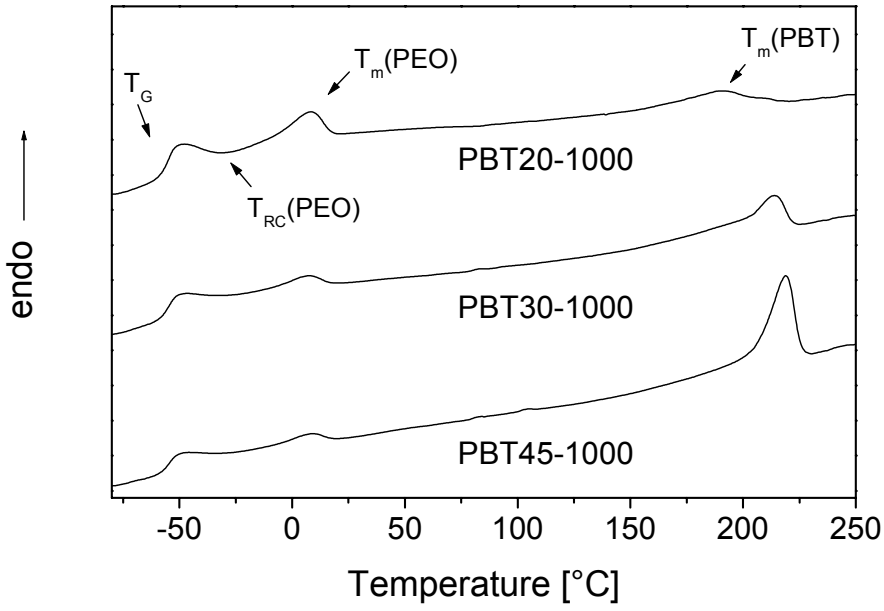

Figure 7. Thermal properties of copolyesters in dependence of the hard segment content.

Mechanical testing was performed on melt-pressed test samples with an average size of 1.0 cm × 4.8 cm (Table 5). Figure 8 shows the stress-strain traces of copolyesters with PEO_{18}-PEB_{64}-PEO_{18}[5.6] soft segments measured at room temperature.

Table 5. Mechanical Properties of Copolyesters with PEO_{18}-PEB_{64}-PEO_{18}[5.6] Soft Segments[a]

sample	E [GPa]	σ_B [MPa]	ε_B [%]
PBT40-1000	$1.27 \cdot 10^{-2}$ ($5.7 \cdot 10^{-4}$)	11.0 (1.3)	370 (99)
PBT30-1000	$1.05 \cdot 10^{-2}$ ($7.3 \cdot 10^{-4}$)	10.8 (0.4)	670 (57)
PBT20-1000	$7.02 \cdot 10^{-3}$ ($1.3 \cdot 10^{-3}$)	9.31 (0.5)	980 (55)
PBT10-1000	$3.94 \cdot 10^{-3}$ ($1.1 \cdot 10^{-4}$)	3.72 (0.3)	450 (58)
PBT40-820	$1.87 \cdot 10^{-2}$ ($3.1 \cdot 10^{-3}$)	11.4 (1.2)	400 (50)
PBT30-820	$1.31 \cdot 10^{-2}$ ($1.8 \cdot 10^{-3}$)	8.98 (0.4)	490 (37)

[a] E = Young´s modulus, σ_B = stress at break and ε_B = elongation at break; the values in parenthesis give the standard deviations (derived from at least three experiments).

The stress-strain behavior is typical for elastic materials. All samples show a lack of yielding, indicating a dispersed PBT phase within a matrix of soft segment, as also detected by SFM measurements (Figure 4). The elongation at break increases with increasing soft segment content up to ~ 1000% for PBT20-1000 (Figure 8). A further increase in the soft segment content (PBT10-1000) results in a smaller elongation at break, probably due to the low crystallinity of PBT in this sample (Table 4, T_m(PBT) not detectable).

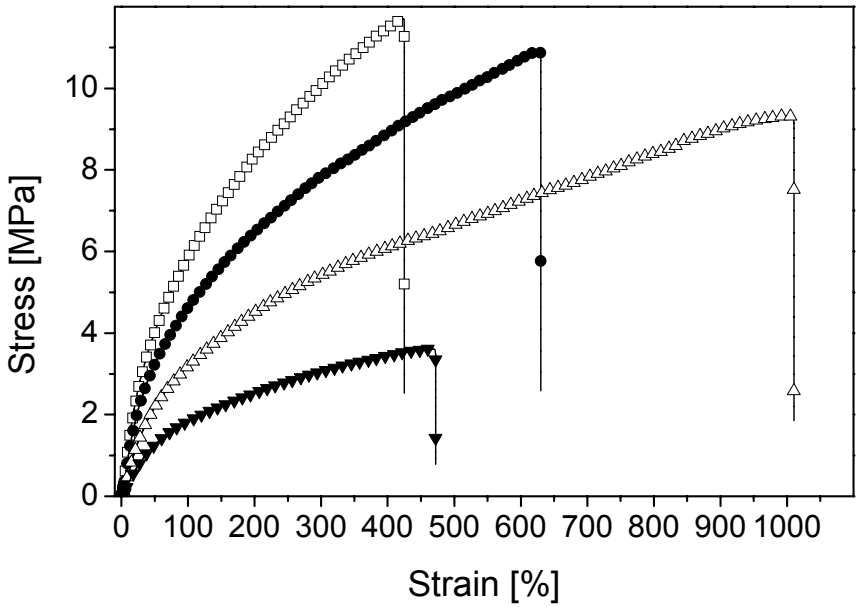

Figure 8. Stress-strain traces for copolyesters with PEO_{18}-PEB_{64}-PEO_{18}[5.6] soft segments; (□) PBT40-1000, (●) PBT30-1000, (Δ) PBT20-1000, (▼) PBT10-1000.

In the range of soft segment contents of 60 - 90% the Young´s modulus exhibits a linear decrease with increasing soft segment content whereas the stress at break decreases significantly above a soft segment content of about 80% (Figure 9).

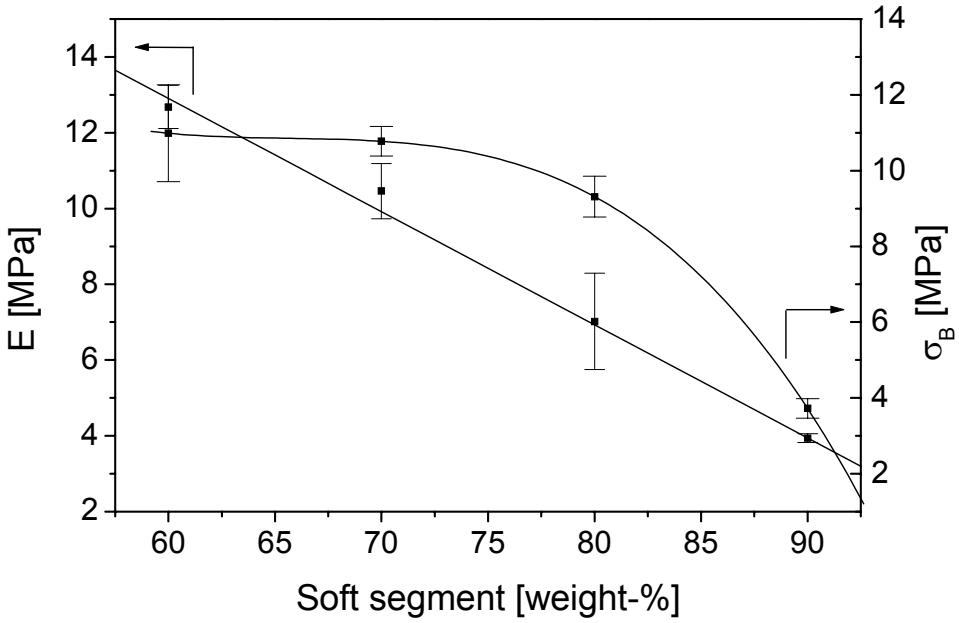

Figure 9. Young´s modulus E and stress at break σ_B in dependence of the soft segment content for copolyesters with PEO_{18}-PEB_{64}-PEO_{18}[5.6] soft segments.

Conclusion

We have shown for the first time that the incorporation of polyolefinic soft segments like HO-PEB-OH (KRATON® liquid polymer HPVM-2203) in PBT based copolyesters by a conventional 2 step melt polycondensation is possible without using any co-solvents by chain extension of the soft segment with ethylene oxide. The resulting amphiphilic PEO-PEB-PEO triblock copolymers are able to dissolve in a mixture of dimethyl terephthalate and 1,4-butanediol during melt polycondensation. This leads to a homogeneous reaction mixture and a quantitative incorporation of the soft segment. The synthesized copolyesters exhibit low glass transition temperatures combined with high PBT melting points even at high soft segment contents, making these polymers suitable for low and high temperature range applications. The mechanical properties, e.g. Young´s modulus and elongation at break, can be adjusted to product requirements by varying the soft segment content. Depending on the composition, elongations at break up to 1000% can be achieved with these materials. Further

investigations on elastic properties and morphology are in progress and will be published elsewhere.

Acknowledgment. The authors are very grateful to Reimund Stadler, who initiated this work. Also the fruitful discussions with many colleagues at the University of Bayreuth and DSM Research are acknowledged. We especially like to thank B. Goderis for the SFM measurements, K. Loos for help with DSC measurements, and S. Stangler for assistance with SAXS investigations.

References and Notes

(1) Legge, N. R.; Holden, G.; Schroeder, H. E. *Thermoplastic Elastomers, A Comprehensive Review*; Hanser: Munich, 1987.

(2) Cella, R. J. *J. Polym. Sci., Polym. Symp.* **1973**, *42*, 727.

(3) Hoeschele, G. K.; Witsiepe, W. K. *Angew. Makromol. Chem.* **1973**, *29/30*, 267.

(4) Hoeschele, G. K. *Chimia* **1974**, *28*, 544.

(5) Hoeschele, G. K. *Angew. Makromol. Chem.* **1977**, *58/59*, 299.

(6) Manuel, H. J.; Gaymans, R. J. *Polymer* **1993**, *34*, 636.

(7) Manuel, H. J.; Gaymans, R. J. *Polymer* **1993**, *34*, 4325.

(8) Fray, M. E.; Slonecki, J. *Kautsch. Gummi Kunstst.* **1996**, *49*, 692.

(9) Walch, E.; Gaymans, R. J. *Polymer* **1994**, *35*, 636.

(10) Deák, G.; Kennedy, J. P. *Macromol. Rep.* **1996**, *A33 (Suppls. 7&8)*, 439.

(11) Bayer, U.; Stadler, R. *Macromol. Chem. Phys.* **1994**, *195*, 2709.

(12) Hillmeyer, M. A.; Bates F. S. *Macromolecules* **1996**, *29*, 6994.

(13) Allgaier, J.; Poppe, A.; Willner, L.; Richter, R. *Macromolecules* **1997**, *30*, 1582.

(14) Wunderlich, B. *Macromolecular Physics*; Academic Press: New York, **1980**; Vol. 3, p 67.

(15) Van Krevelen, D. W. *Properties of Polymers*, 2nd ed.; Elsevier: Oxford, 1976, p 578.

(16) Frensdorff, H. K. *Macromolecules* **1971**, *4*, 369.

(17) Baik, D. H.; Lee, M. S.; Jeon, B. Y.; Han, M. S. *J. Korean Fiber Soc.* **1994**, *31*, 613.

(18) Cella, R. J. *Polyesters, Elastomeric*, In *Encyclopedia of Polymer Science and Technology*; Interscience Publishers: New York, Suppl. Vol. 2, 1977.

3.1.2 Morphology, Surface Structure and Elastic Properties of PBT-Based Copolyesters with PEO-*b*-PEB-*b*-PEO Triblock Copolymer Soft Segments

Holger Schmalz[a], Viola van Guldener[b], Wouter Gabriëlse[b], Ronald Lange[b,c*], and Volker Abetz[a*]

a) Makromolekulare Chemie II, Universität Bayreuth, 95440 Bayreuth, Germany
b) DSM Research, P.O. Box 18, 6160 MD Geleen, The Netherlands
c) present address: BASF Aktiengesellschaft, GKS/B1, 67056 Ludwigshafen, Germany

ABSTRACT: The elasticity of commonly known poly(butylene terephthalate)-poly(tetramethylene oxide) PBT-PTMO based copoly(ether ester)s is increased by replacement of PTMO soft segments with poly(ethylene oxide)-*block*-poly(ethylene-*stat*-butylene)-*block*-poly(ethylene oxide) (PEO-*b*-PEB-*b*-PEO) triblock copolymer soft segments containing a non-polar middle block based on hydrogenated polybutadiene (PEB). The incorporation of this strongly incompatible PEB block resulted in the aimed increased phase separation between the PBT hard blocks and the soft segment phase, leading to a dispersed PBT phase and hence to an increased elasticity. Dynamic shear experiments in combination with small-angle X-ray scattering revealed that crystallization of the PBT hard segments occurs from a microphase separated melt. The resulting dispersed PBT hard phase in these materials is shown using transmission electron microscopy (TEM) and scanning force microscopy (SFM), whereas the increased elasticity is demonstrated using mechanical characterization. Hysteresis measurements reveal that the plastic deformation after recovery from 100% strain is only 1 - 6% (depending on composition) for the new PEB containing copolyesters compared to 33% for a PBT-PTMO based copoly(ether ester). The combination of results obtained with differential scanning calorimetry (DSC) and dynamic mechanical analysis (DMA) point towards a complex morphology for the PEB containing copolyesters. Five different phases exist: a crystalline pure PBT phase, pure amorphous PEB, and PBT phases, and a PEO-rich phase besides an amorphous mixed PEO/PBT phase.

Introduction

Thermoplastic elastomers (TPE`s) combine the properties of irreversibly crosslinked elastomers with the easy processing of thermoplastic materials. This enables product designs not easily achieved for conventional rubbers. One class of TPE's are copoly(ether ester)s or TPE-E's.[1] These segmented block copolymers possess a soft elastomeric polyether segment, e.g. poly(tetramethylene oxide) (PTMO), and a polyester hard segment, e.g. poly(butylene terephthalate) (PBT). Because of their phase separated morphology, copoly(ether ester)s show unique properties such as good low temperature flexibility and excellent mechanical properties up to high temperatures as well as a good resistance towards many solvents. However, the elastic properties of copoly(ether ester)s at relatively high elongations are limited. This is due to the presence of a co-continuous PBT hard phase as was revealed by morphological and mechanical characterization. The morphology of PBT-PTMO based copoly(ether ester)s has been studied extensively.[1-7] It is generally assumed that, upon cooling from the homogeneous PBT-PTMO melt, the crystallization of PBT initiates the formation of the characteristic phase separated structure consisting of PBT crystallites embedded in an amorphous matrix.[7,8] Although the crystallization process and the structure of the crystalline phase have been studied in detail (next to lamellar[2,9-11], spherulitic[5,6,12,13], dendritic[6,13], even shish kebab[6] structures have been reported), much less attention was paid to the structure of the amorphous phase. It is thought that this amorphous phase is homogeneous, resulting in the description of the copoly(ether ester)s by a two-phase model: a crystalline PBT phase and a homogeneous amorphous PTMO/non-crystalline PBT phase, both being co-continuous.[1-3,6] However, more recent studies using solid-state NMR[14] and thermomechanical analysis[15] demonstrate that the amorphous phase is not homogeneous but consists of a PTMO-rich phase and a PBT/PTMO mixed phase.

The relatively high modulus obtained in a stress-strain experiment reflects the presence of the co-continuous PBT morphology in copoly(ether ester)s. The stress strain curves of copoly(ether ester)s can be divided into three distinct regions.[2] At low elongations a reversible elastic deformation of the co-continuous crystalline PBT matrix is obtained. At higher strains this co-continuous PBT matrix is disrupted along with orientation of the crystalline lamellae. This process is irreversible and results in the high plastic deformation hampering the elastic recovery, which is typical for these materials.[16] Finally, after crystallite orientation is completed the stress is submitted through the continuous amorphous phase, until it breaks. The general idea is that the elasticity of copoly(ether ester)s could be improved by

changing the co-continuous PBT hard phase into a dispersed phase. This can be achieved by increasing the phase separation as was demonstrated in thermoplastic polyurethanes or TPE-U's[17,18], and in strongly phase separated copoly(ether ester aramides)[19]. Incorporation of a non-polar hydrogenated polybutadiene (PEB) soft block in PBT based copoly(ether ester)s should result in an extreme phase separation and hence in an increased elasticity. Recently, we reported the successful synthesis of hydrogenated polybutadiene (PEB) containing PBT based copolyesters.[20] Macrophase separation during melt condensation was avoided by using a poly(ethylene oxide)-*block*-poly(ethylene-*stat*-butylene)-*block*-poly(ethylene oxide) (PEO-*b*-PEB-*b*-PEO) triblock copolymer. The PEO acts as a compatibilizer between the polar PBT and non-polar PEB blocks. Here, we present a detailed study dealing with the characterization of the PEO-*b*-PEB-*b*-PEO containing PBT based copolyesters. The formation of a dispersed PBT hard phase by crystallization from a microphase separated melt will be demonstrated using rheological techniques in combination with small-angle X-ray scattering (SAXS). Morphological studies using transmission electron microscopy (TEM), small-angle X-ray scattering (SAXS), differential scanning calorimetry (DSC), and dynamic mechanical analysis (DMA) as well as scanning force microscopy (SFM) for surface structure analysis will be described. The increase in elasticity will be demonstrated by mechanical characterization.

Experimental Section

Synthesis. Detailed information about the synthesis of PEO-*b*-PEB-*b*-PEO containing copolyesters can be found in a previous contribution.[20] Solid-state post-condensation of copolyesters was performed in vacuum (1 - 2 mbar) under a slight stream of nitrogen in a home-built apparatus. The copolyesters were cut into small pieces in order to enlarge the active surface, and the reaction was carried out for two days at temperatures ca. 30 °C below the melting temperature of the copolyester. The structure of the synthesized copolyesters with PEO-*b*-PEB-*b*-PEO triblock copolymer soft segments is depicted in Figure 1. In this contribution we will focus on copolyesters based on $PEO_{18}PEB_{64}PEO_{18}^{5.6}$ and $PEO_{22}PEB_{56}PEO_{22}^{6.4}$ soft segments (the subscripts give the weight percentage of the corresponding block, and the superscript is the molar mass of the triblock copolymer in kg/mol).

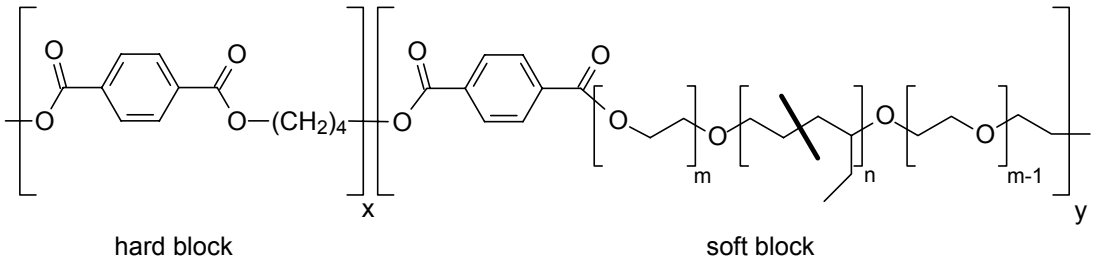

Figure 1. Structure of copolyesters with PEO-*b*-PEB-*b*-PEO soft segments.

Several copolyesters with varying hard segment content have been synthesized (Table 1). PBT1000/50, a copoly(ether ester) containing 50% (w/w) PTMO with a molecular weight of 1000 g/mol, is used as reference material for comparison of elastic properties. The nomenclature of the new materials like PBT45-1000, is as follows: 45 is the weight percentage of PBT, and 1000 refers to the molecular weight of the PEO block (in g/mol).

Table 1. Composition of Copolyesters

	w (PBT) [%]	x_{HS}[a]	l_{HS}[b]	soft segment
PBT1000/50	50	0.837	6.1	PTMO
PBT45-1000	45	0.954	21.8	$PEO_{18}PEB_{64}PEO_{18}^{5.6}$
PBT40-1000	40	0.944	17.9	$PEO_{18}PEB_{64}PEO_{18}^{5.6}$
PBT35-1000	35	0.932	14.7	$PEO_{18}PEB_{64}PEO_{18}^{5.6}$
PBT30-1000	30	0.916	11.9	$PEO_{18}PEB_{64}PEO_{18}^{5.6}$
PBT25-1000	25	0.894	9.5	$PEO_{18}PEB_{64}PEO_{18}^{5.6}$
PBT20-1000	20	0.864	7.4	$PEO_{18}PEB_{64}PEO_{18}^{5.6}$
PBT40-1380	40	0.951	20.2	$PEO_{22}PEB_{56}PEO_{22}^{6.4}$
PBT30-1380	30	0.925	13.4	$PEO_{22}PEB_{56}PEO_{22}^{6.4}$
PBT20-1380	20	0.878	8.2	$PEO_{22}PEB_{56}PEO_{22}^{6.4}$

[a] Mole fraction of hard segment (PBT).
[b] Average segment length of the hard segment calculated according to $l_{HS} = 1/(1-x_{HS})$.

Dynamic Mechanical Analysis (DMA). For the determination of glass transition temperatures, a Rheometrics DMTA IV operated in the rectangular torsion/compression mode at a heating rate of 2 K/min, and a constant frequency of 10 rad/s was used. Sample films with dimensions of 6 · 15 · 0.5 mm were used. Given glass transition temperatures correspond to a maximum in the loss modulus (E"), unless otherwise specified. Dynamic shear experiments were performed with an Advanced Rheometric Expansion System (ARES, Rheometrics) in the plate-plate configuration. For measurements on copolyesters a plate diameter of 25 mm and a gap of 1.5 mm were used. Temperature dependent measurements of G' and G" were

performed at a scanning rate of 1 K/min at a constant frequency of 1 rad/s. PEO-*b*-PEB-*b*-PEO triblock copolymers were measured using 50 mm plates with a gap of 1 mm at a scanning rate of 1 K/min at a constant frequency of 0.5 rad/s. Order-disorder transitions were detected by a sharp drop of G' and G'' upon heating. Given order-disorder transition temperatures correspond to the cross-over of G' and G", i. e. G' = G". It was made sure that all experiments were done in the linear viscoelastic regime.

Differential Scanning Calorimetry (DSC). For thermal analysis a Perkin Elmer DSC 7 with a CCA 7 liquid nitrogen cooling device was used. For all measurements a two point calibration with chloroform and indium was applied. All experiments were performed at heating rates of 20, 30 and 40 K/min. Given transition temperatures correspond to an extrapolated heating rate of 0 K/min, unless otherwise specified. Degrees of crystallinity were calculated assuming a heat of fusion of ΔH_m^0 = 196.6 J/g[21] for PEO and ΔH_m^0 = 145.3 J/g[22] for PBT.

Transmission Electron Microscopy (TEM). The bulk morphology of copolyesters was examined by bright field TEM using a Zeiss CEM 902 electron microscope operated at 80 kV in the bright field mode. Films (around 1 mm thick) were prepared by compression molding at 240 °C for 5 min followed by cooling to room temperature (ca. –20 K/min) in an identical manner compared to the preparation of test specimens for tensile testing. Thin sections were cut at -130 °C using a Reichert-Jung Ultracut E microtome equipped with a diamond knife. Staining was achieved by exposure of the sections to RuO_4 vapor for 45 min. Since the staining agent penetrates only into the amorphous regions, the crystalline PBT domains appear bright.

Scanning Force Microscopy (SFM). Scanning force microscopy images were taken on a Digital Instruments Dimension 3100 microscope operated in Tapping Mode™ (free amplitude of the cantilever: 20 nm; set point ratio: 0.95). Measurements were performed on compression-molded films prepared on polished silicon wafers using poly(tetrafluoroethylene) (PTFE) cover sheets. The samples were first heated to 250 °C for 3 min under nitrogen followed by cooling at a constant rate of 5 K/min to room temperature.

Small Angle X-ray Scattering (SAXS). SAXS was performed on a Bruker-AXS Nanostar equipped with a Histar-Detector and crossed Goebel mirrors. As a radiation source a sealed Cu-tube was used, generating a wavelength of 0.1542 nm. Temperature dependent measurements were conducted using a Paar Physica TCU50 temperature control unit.

Mechanical Testing. Mechanical testing was carried out on a Zwick 1455 tensile testing machine equipped with optical extensometers and a 200 N load cell. Hysteresis measurements were performed at a testing speed of 100 mm/min with a preload of 1 N without applying a holding time between the cycles in order to reduce relaxation phenomena. Cyclic measurements were performed for 100 and 500% strain and were repeated for 3 times. The geometry of test specimens was based on ISO 37:1994. Samples were pressed into plates by compression-molding between PTFE sheets at 240 °C for 5 min followed by cooling to room temperature (ca. –20 K/min). All samples were allowed to acclimatize at room temperature (23 °C) under a relative air humidity of 50% for 1 day.

Results and Discussion

Dynamic Shear Experiments. To investigate the structure formation in PEB containing copolyesters upon cooling from the melt, dynamic shear experiments have been performed. The pure PEO-*b*-PEB-*b*-PEO triblock copolymers were measured first as a reference. Figure 2A shows the temperature dependence of storage (G') and loss (G") modulus for the triblock copolymer $PEO_{18}PEB_{64}PEO_{18}$[5.6]. Upon heating, the crystalline PEO blocks melt at ca. 35 °C, resulting in a simultaneous drop in G' and G". In the following plateau the modulus is nearly constant up to ca. 124 °C. At this temperature a sharp drop over several decades in both G' and G" indicates the order-disorder transition (T_{ODT}), resulting in a homogeneous melt.[23-28] The triblock copolymer $PEO_{22}PEB_{56}PEO_{22}$[6.4] exhibits a similar temperature dependence of G' and G" (results not shown). Because of the increased molecular weight of the PEO blocks, the order-disorder transition shifts to 180 °C. Please note that crystallization of the PBT hard segments in the PEB containing copolyesters occurs below the observed order-disorder transition for the soft segments (Table 2). This might indicate that crystallization of PBT occurs from a microphase-separated melt consisting of pure PEB domains and mixed PBT/PEO domains. (Amorphous PBT and PEO domains are miscible in the melt).

A

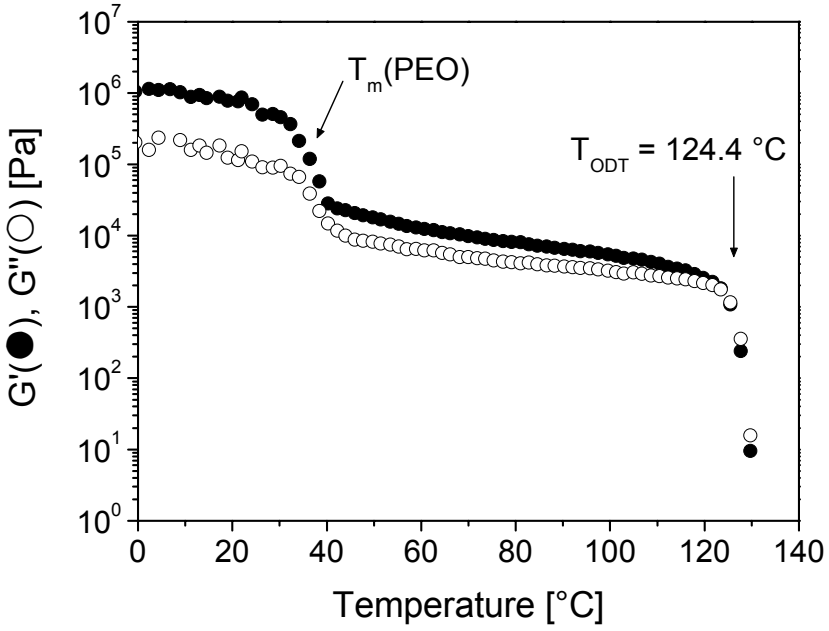

B

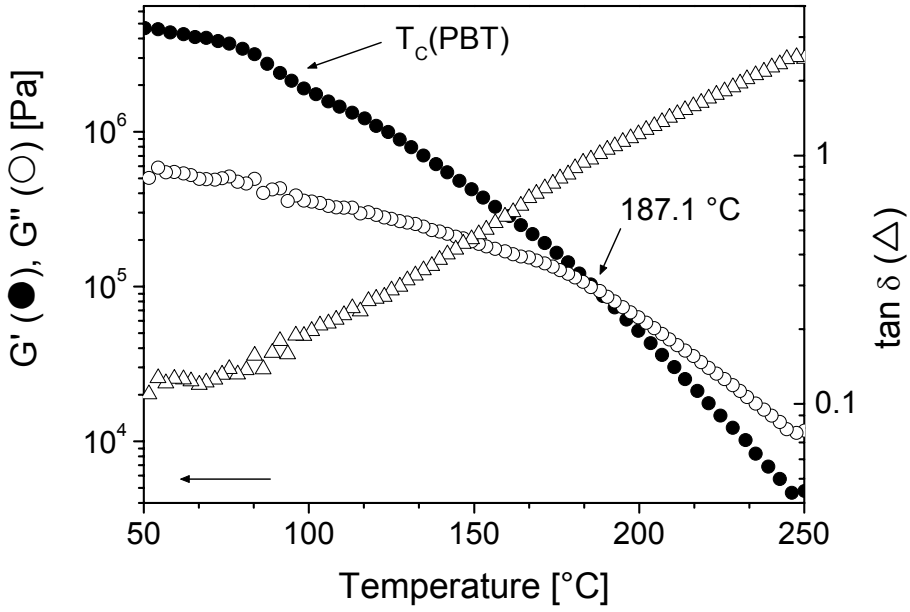

Figure 2. (A) Temperature dependence of storage (G') and loss (G'') modulus for $PEO_{18}PEB_{64}PEO_{18}$[5.6] upon heating. (B) Temperature dependence of storage (G') and loss (G'') modulus for PBT20-1000 upon cooling.

Figure 2B shows the dependence of G' and G" on temperature for PBT20-1000 upon cooling. In this case no sharp rise in G' upon cooling, which would indicate an order-disorder transition, can be detected. For high temperatures the viscous response of the melt predominates, i. e., G" > G'. Upon cooling at ca. 187 °C a crossover point can be detected, *i. e.* G' = G". Below this temperature the elastic response of the melt prevails, i. e., G' > G", indicating that either entanglements become active or the melt microphase separates, leading to a thermoreversible network. Upon further cooling the PBT hard segments start to crystallize resulting in a rise in G' at ca. 90 °C, which points to a crystallization of PBT from a microphase-separated melt. The copolyesters PBT45-1000 and PBT20-1380 show a similar temperature dependence of G' and G" upon cooling (results not shown). The crossover of G' and G" is shifted to higher temperatures compared to PBT20-1000, i. e., 205 °C for PBT45-1000 and 215 °C for PBT20-1380. This might be attributed on one hand to the increased average hard segment block length in PBT40-1000 and on the other hand to the higher molecular weight of the incorporated triblock copolymer soft segment in PBT20-1380 (Table 1), which is equivalent with a higher viscosity and an increased incompatibility between the components. The melt rheology of copoly(ether ester)s consisting of PBT hard segments and PTMO soft segments is significantly different. Veenstra et al.[7] showed that for these materials crystallization occurs from a homogeneous melt. Temperature dependent dynamic shear experiments revealed that upon cooling from the homogeneous melt a sharp rise in G' is observed, resulting from crystallization of the hard segment. Here, microphase separation is induced by crystallization of the hard segment and not by liquid-liquid demixing of incompatible chain segments. A similar behavior is observed for the copoly(ether ester) PBT1000/50 (not shown here). In conclusion, for PEO-*b*-PEB-*b*-PEO containing copolyesters crystallization of the PBT hard segments might occur from a microphase separated melt due to the fact that crystallization of PBT takes place at temperatures well below the order-disorder transition of the incorporated triblock copolymer soft segment (Table 2).

Table 2. Transition Temperatures for Copolyesters Obtained by DSC and DMA[a]

	T_G(DSC) [°C]	T_G^1(DMTA) [°C]	T_G^2(DMTA)[b] [°C]	T_G^3(DMTA) [°C]	T_m(PEO) [°C]	T_m(PBT) [°C]	T_c^1(PBT)[c] [°C]	T_c^2(PBT)[c] [°C]	T_c^3(PBT)[c] [°C]	α(PBT) [%]
PEB	-62	-52	-	-	-	-	-	-	-	-
PEO	-67/-27[22]	-	-	-	-	-	-	-	-	-
PBT	45[29]	-	-	-	-	-	-	-	-	-
PBT1000/50[d]	-64	-62	-	-	-	190	123	-	-	50
PBT45-1000	-57.6	-51.4	n.d.	47.5	6.1	217.5	-	93.3	58.3	27.3
PBT40-1000	-58.2	-50.9	-8.0	53.8	3.4	211.4	-	89.9	52.6	21.8
PBT35-1000	-58.0	-53.6	-11.0	52.1	4.2	213.5	-	89.9	54.3	23.3
PBT30-1000	-58.1	-51.3	-7.0	53.4	4.9	212.1	126.3	85.9	58.3	27.8
PBT25-1000	-59.1	-53.4	n.d.	n.d.	10.8	214.9	136.3	83.6	60.6	31.1
PBT20-1000	-59.8	-51.0	-7.0	n.d.	5.5	190.0	-	-	60.6	27.0
PBT40-1380	-66.1	-51.3	-7.0	48.5[e]	7.0	207.7	-	97.9	-	15.8
PBT30-1380	-66.5	-52.7	-10.0	42.2[e]	3.8	202.5	-	97.3	62.6	24.0
PBT20-1380	-60.3	-50.3	n.d.	n.d.	13.5	184.0	-	-	56.3	21.9

[a] T_G = glass transition temperature, T_m = melting point of corresponding block (peak maximum), T_c = crystallization temperature of corresponding block (peak maximum), and α = degree of crystallinity. Order disorder transition temperatures (T_{ODT}) of soft segments determined by dynamic shear experiments: $PEO_{18}PEB_{64}PEO_{18}$[5.6], T_{ODT} = 124.4 °C; $PEO_{22}PEB_{56}PEO_{22}$[6.4], T_{ODT} = 180.4 °C.

[b] Shoulder of main relaxation T_G^1.

[c] Crystallization temperatures correspond to a cooling rate of 20 K/min.

[d] DSC experiments were performed at a scanning rate of 10 K/min, DMA measurements correspond to a heating rate of 5 K/min at a constant frequency of 1 rad/s.

[e] Very weak, determined from maximum in tan δ.

Small Angle X-ray Scattering. To gain more insight into the melt structure of the synthesized copolyesters, SAXS investigations on the PEO-*b*-PEB-*b*-PEO triblock copolymers and the corresponding copolyesters have been performed. Measurements on the triblock copolymers have been conducted at 80 °C taking into account that the PEO blocks are molten at room temperature in the corresponding copolyesters (Table 2). The semi-logarithmic SAXS profile for $PEO_{18}PEB_{64}PEO_{18}^{5.6}$ at 80 °C (molten PEO blocks) exhibits reflex positions at ratios of 1 : $\sqrt{3}$: 2 : $\sqrt{7}$, which are typical for hexagonally packed cylinders (Figure 3A). The SAXS profile of PBT20-1000 at 30 °C (Figure 3A) shows no distinct reflexes pointing to a cylindrical structure arising from the incorporated soft segment. Only a very broad intensity distribution can be detected which may arise from an overlap of reflexes from interlamellar PBT spacings and reflexes originating from the cylindrical domains in the triblock copolymer soft segment. The corresponding measurement at 250 °C (molten PBT blocks) shows a broad reflex at q = 0.56 nm^{-1}, indicating a microphase separation in the melt. The reflex position is slightly shifted to higher spacings compared to the q_{100} reflex of the pure triblock copolymer which can be attributed to the chain extension of the PEO block with PBT units in the copolyester. Because of the lack of higher order reflexes, a structure assignment is not possible in this case.

The semilogarithmic SAXS profile of $PEO_{22}PEB_{56}PEO_{22}^{6.4}$ at 80 °C exhibits reflex positions at ratios of 1 : 2 : 3, typical for a lamellar structure (Figure 3B). The SAXS profile of PBT20-1380 at 30 °C (Figure 3B) shows a broad intensity distribution up to q ~ 0.4 nm^{-1} which might correspond to interlamellar PBT spacings. In addition, two sharp reflexes can be detected at a ratio of 1 : 2 pointing to a lamellar structure which can also be seen in TEM investigations as will be discussed later. The corresponding lamellar spacing (12.6 nm) is slightly shifted to higher values compared to that of the pure triblock copolymer (11.4 nm). The measurement at 250 °C (molten PBT blocks) reveals a microphase-separated melt with a lamellar structure corresponding to the observed reflex positions at a ratio of 1 : 2 (Figure 3B). In conclusion, the SAXS experiments confirm the results obtained from dynamic shear experiments, and it can be deduced that crystallization of PBT occurs from a microphase-separated melt.

A

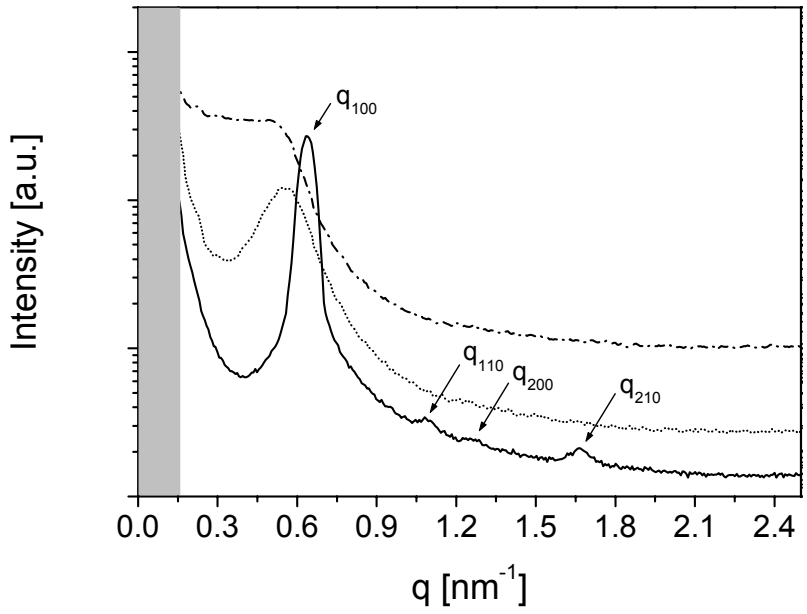

B

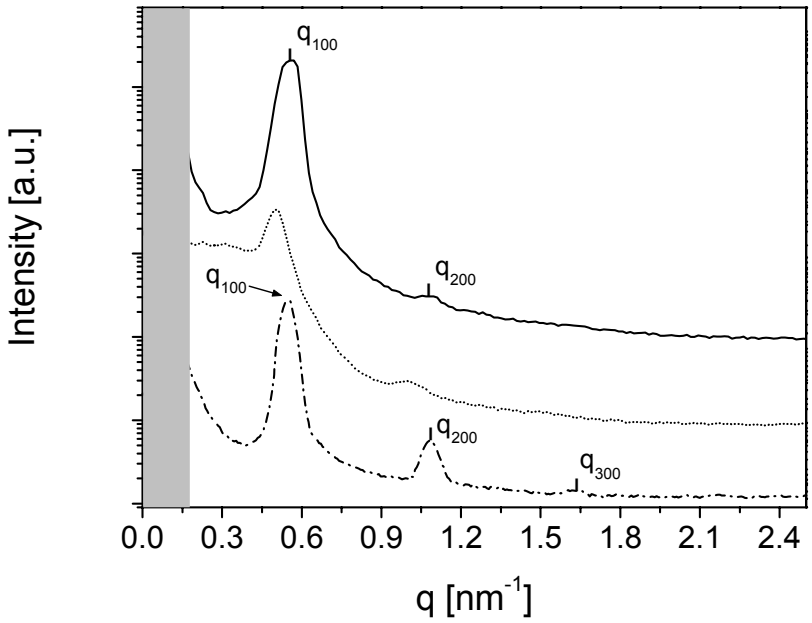

Figure 3. Semilogarithmic SAXS profiles: (A) $PEO_{18}PEB_{64}PEO_{18}$[5.6] at 80 °C (——), PBT20-1000 at 30 °C (-·-·-·-) and 250 °C (·····); (B) $PEO_{22}PEB_{56}PEO_{22}$[6.4] at 80 °C (-·-·-·-), PBT20-1380 at 30 °C (·····) and 250 °C (——); scattering vector $q = 4\pi/\lambda \sin\Theta$ with the scattering angle 2Θ and $\lambda = 0.1542$ nm.

Transmission Electron Microscopy. To investigate whether crystallization from the observed microphase-separated melt results in the formation of a dispersed PBT hard phase, TEM experiments have been performed. Figure 4 shows TEM images for several copolyesters based on $PEO_{18}PEB_{64}PEO_{18}^{5.6}$ (PBTx-1000) and $PEO_{22}PEB_{56}PEO_{22}^{6.4}$ (PBTx-1380) soft segments. As the staining agent (RuO_4) gets preferentially adsorbed by the amorphous PBT and PEO segments in the soft segment phase, the crystalline PBT and amorphous PEB domains appear as bright regions. As depicted for PBT45-1000 in Figure 4A, the spherical, bright appearing, crystalline PBT domains are dispersed within a matrix of the soft segment. However, because of the selective staining of the amorphous soft segment phase, no fine structure of the crystalline PBT domains can be observed. Comparison with PBT35-1000 (Figure 4B) shows that the number density of crystalline PBT domains decreases as expected with decreasing PBT content. A closer look to the soft segment rich regions in PBT35-1000 indicates a microstructure within the soft segment phase, which is seen as white fine structure in the amorphous phase and originates from the unstained PEB domains. From the TEM image no conclusions can be drawn about the kind of microstructure visible in the soft segment phase. Taking into account that the incorporated triblock copolymer exhibits a cylindrical structure (Figure 3A), the observed microstructure in the soft segment phase might be attributed to a kind of distorted cylindrical structure, which will be underlined in the discussion of the SFM results. Figure 4C, D shows the corresponding TEM micrographs of PBT40-1380 and PBT30-1380. The dispersed crystalline PBT domains are clearly visible. In addition, Figure 4D shows that the soft segment phase exhibits a lamellar microstructure which is in line with SAXS investigations of the incorporated triblock copolymer (Figure 3B). This lamellar microstructure is more pronounced in PBT20-1380 (Figure 4E, F) emphasizing the strong influence of the incorporated triblock copolymer on the morphology of the copolyester. Figure 4F shows the lamellar microstructure of PBT20-1380 in more detail. The bright lamellae correspond to the nonpolar PEB, which is not stained by RuO_4. The dark appearing lamellae accord with the amorphous PEO/PBT mixed phase and show some white "inclusions" which might be attributed to thin crystalline PBT lamellae (denoted as PBT_c in Figure 4F). This assumption is supported by an increase of the long spacing from 11.4 nm in the pure triblock copolymer to 12.6 nm in PBT20-1380 as derived from SAXS measurements (Figure 3B). In conclusion, TEM investigations show that the PBT hard phase in the PEO-*b*-PEB-*b*-PEO containing copolyesters is dispersed within a matrix of the soft phase.

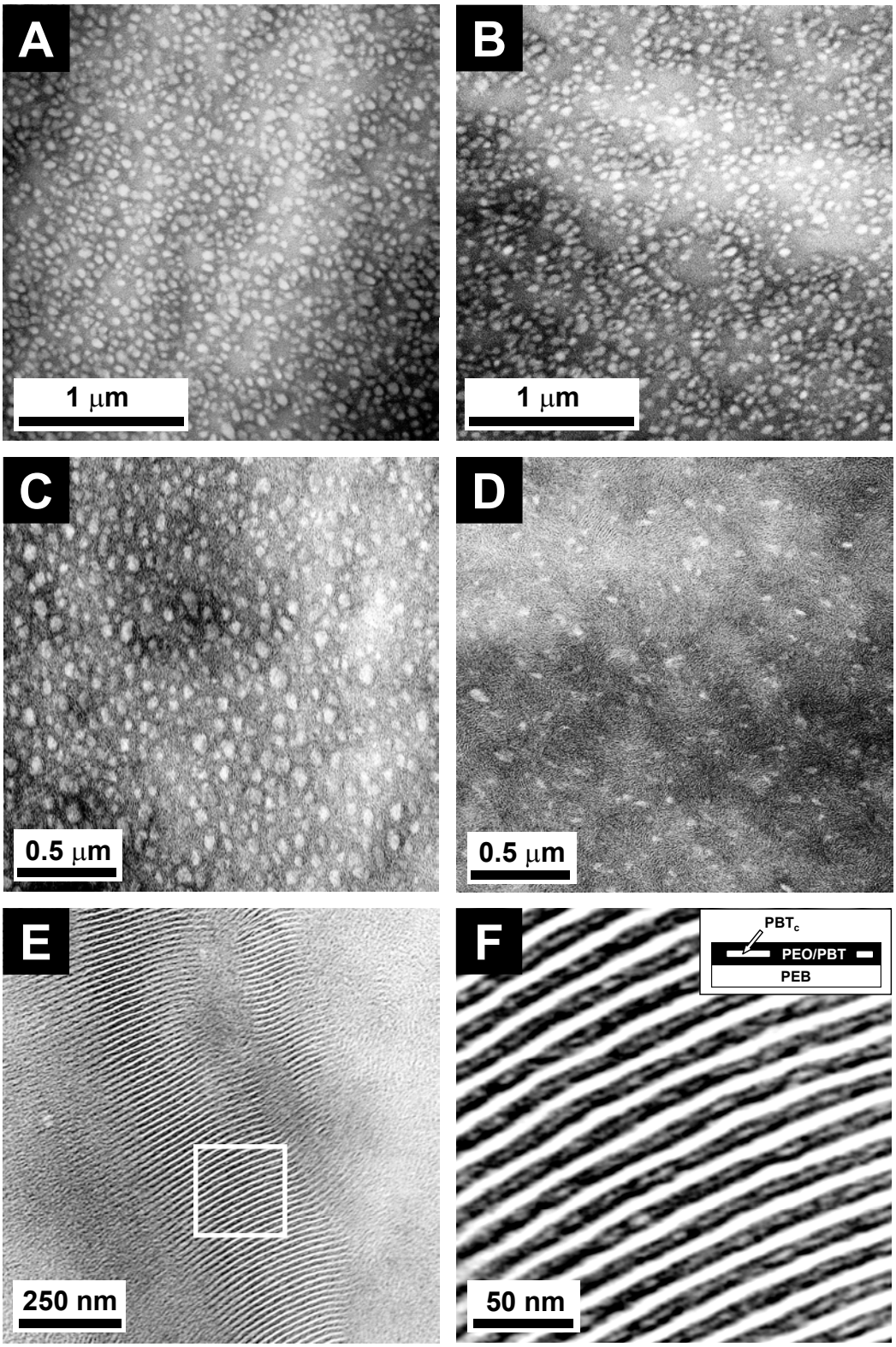

Figure 4. TEM images of PBT45-1000 (A), PBT35-1000 (B), PBT40-1380 (C), PBT30-1380 (D) and PBT20-1380 (E and F, PBT_c = crystalline PBT) stained with RuO_4 vapor.

Scanning Force Microscopy. To analyze the fine structure of the crystalline PBT domains, which appears bright using TEM analysis, scanning force microscopy (SFM) has been performed. An additional advantage of using SFM is the elimination of possible cutting effects that could be introduced by the sample preparation for TEM, especially for these soft materials. Figure 5 shows several SFM phase contrast images of copolyesters based on $PEO_{18}PEB_{64}PEO_{18}^{5.6}$ (PBTx-1000) and $PEO_{22}PEB_{56}PEO_{22}^{6.4}$ (PBTx-1380) triblock copolymer soft segments. The phase contrast images of PBT45-1000 (Figure 5A) and PBT40-1380 (Figure 5B) clearly show that the bright appearing elongated domains, which correspond to crystalline PBT lamellae (viewed edge on), are dispersed within a matrix of the soft segment. This is in agreement with the results obtained by TEM (Figure 4A, C). At this point it has to be mentioned that the SFM experiments were performed on compression molded films using PTFE cover sheets. As PTFE is a very nonpolar polymer, the also nonpolar PEB blocks have a strong tendency to accumulate at the surface in order to reduce the surface tension. The effect of PTFE on the surface structure is clearly visible in Figure 5C, showing a compression-molded film of PBT45-1000 which was again molten and crystallized without using a PTFE cover sheet. The surface almost completely consists of crystalline PBT lamellae, which agglomerate into more or less globular domains and are dispersed in a matrix of the soft segment. In addition, the lamellar fine structure of the crystalline PBT domains is visible. This structure is very similar to the bright spherical PBT domains observed in TEM investigations (Figure 4A), whereas in the TEM micrographs the lamellar fine structure is not visible. Figure 5D shows the SFM phase contrast image obtained for PBT30-1000. In analogy to PBT45-1000, the crystalline PBT lamellae (bright appearing elongated domains) are again dispersed within a matrix of the soft segment and sometimes form aggregates consisting of several lamellae. This aggregation of several crystalline lamellae might also explain the observed spherical PBT domains in the TEM investigations. As it is not possible to resolve the lamellar fine structure by TEM, the aggregates appear as bright spherical domains. A closer look to the regions rich in soft segment reveals the existence of a microstructure in the soft phase as was also concluded from TEM investigations on PBT35-1000 (Figure 4B). A more detailed insight into the microstructure of the soft segment phase is given in Figure 5E, F showing SFM phase contrast images of PBT20-1000. The bright elongated domains again correspond to crystalline PBT lamellae viewed edge on, which tend to form aggregates consisting of several lamellae.

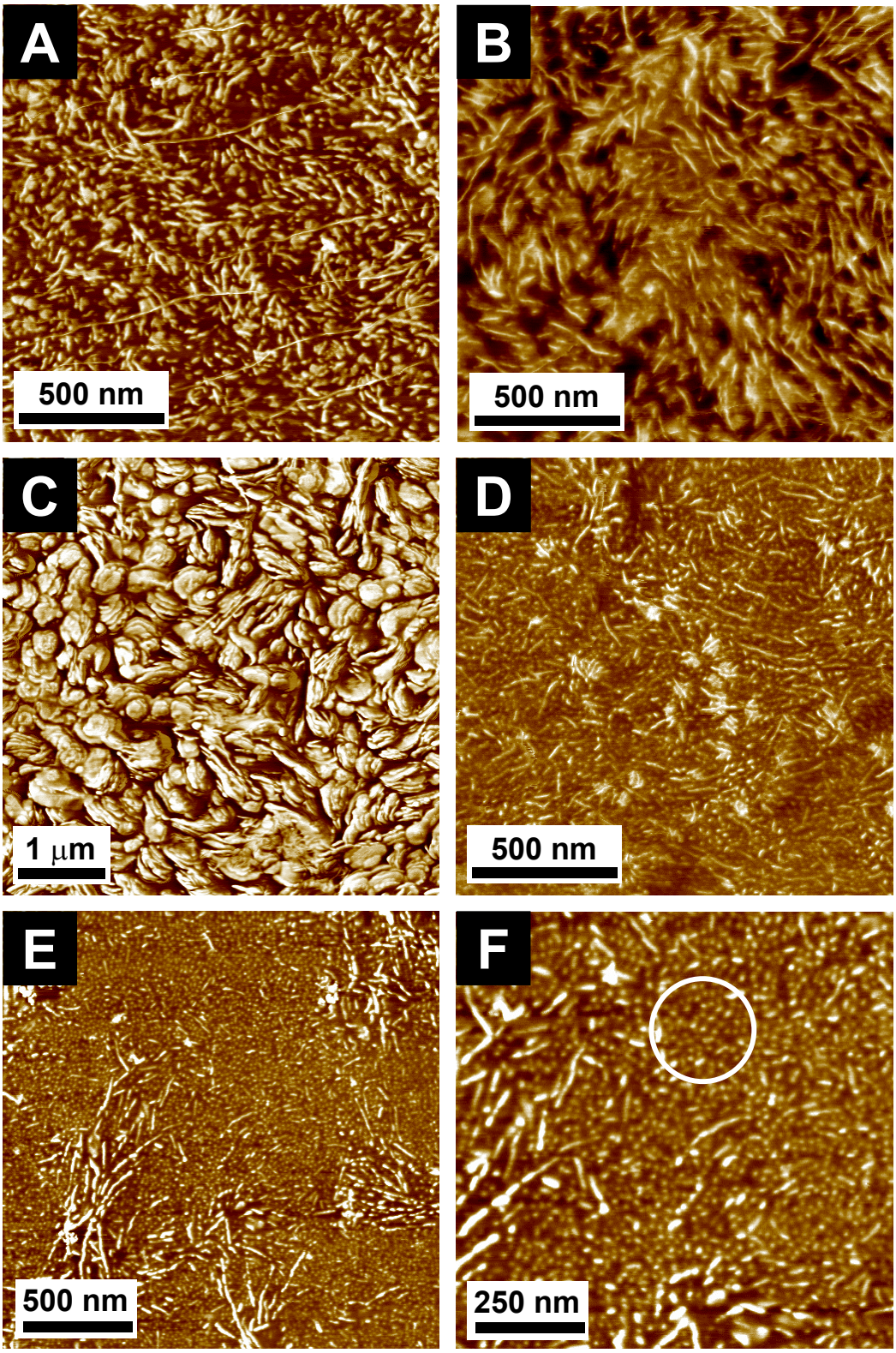

Figure 5. SFM phase contrast images of PBT45-1000 (A: z = 60°), PBT40-1380 (B: z = 50°), PBT45-1000 prepared without a PTFE cover sheet (C: z = 40°), PBT30-1000 (D: z = 30°) and PBT20-1000 (E: z = 20°; F: z = 15°, circle = soft segment phase showing PEO-cylinders (bright dots)).

A zoom into the soft segment phase as depicted in Figure 5F clearly shows a microstructure within the soft segment. Inside a dark appearing matrix (lower phase shift) bright spherical domains can be detected which might be attributed to PEO cylinders within a matrix of the PEB block (circle in Figure 5F). This is in line with the SAXS result on the pure $PEO_{18}PEB_{64}PEO_{18}^{5.6}$ triblock copolymer discussed before (Figure 3A). In summary, dynamic shear and SAXS experiments demonstrate that the morphology in these PEO-*b*-PEB-*b*-PEO containing copolyesters originates from a microphase-separated melt. This in turn results in a dispersed PBT hard phase, as observed by TEM and SFM investigations.

Differential Scanning Calorimetry and Dynamic Mechanical Analysis. To investigate the phase behavior of the different PEB containing copolyesters, DMA and DSC[20] measurements have been performed. Dynamic mechanical analysis of copolyesters with $PEO_{18}PEB_{64}PEO_{18}^{5.6}$ (PBTx-1000, Figure 6A) and $PEO_{22}PEB_{56}PEO_{22}^{6.4}$ (PBTx-1380, Figure 6B) soft segments shows for all samples a sharp glass transition temperature at approximately -60 °C. Above this temperature an extended rubber plateau is observed, which is typical for copoly(ether ester)-like elastomeric materials. At temperatures above 150 °C (Figure 6A) melting of crystalline PBT segments starts, resulting in a marked drop in the storage modulus. These observed glass transition temperatures and melting points correspond with the detected transition temperatures using DSC (Table 2). For PBTx-1000 (Figure 6A) and PBTx-1380 (Figure 6B) the storage modulus at room temperature reveals only a slight decrease with decreasing PBT content, reflecting the disperse PBT phase. A closer look to the DMA traces shows that below the melting point of PBT four separate transitions can be distinguished (Figure 6A, B, Table 2). The first glass transition temperature T_G^1 at ca. -60 °C can be attributed to the PEB phase. This glass transition temperature is independent of composition, revealing a strongly phase-separated PEB phase. The loss tangent shows that this first relaxation is not symmetric but shows a shoulder at higher temperatures. This shoulder at ca. -10 °C (T_G^2) might be attributed, in analogy to PTMO containing copoly(ether ester)s,[14] to the glass transition of a mixed amorphous PEO/PBT phase. In the temperature region between 0 and 15 °C the storage modulus E' exhibits a drop. This is more obvious for the polymers PBT20-1000 (Figure 6A) and PBT20-1380 (Figure 6B), possessing higher soft segment contents. Comparison with DSC results (Table 2) shows that this transition can be ascribed to the melting of the PEO blocks. The appearance of a PEO melting point indicates the presence of a PEO-rich phase besides the mixed amorphous PEO/PBT phase, which allows crystallization of PEO as observed by DSC.[20]

A

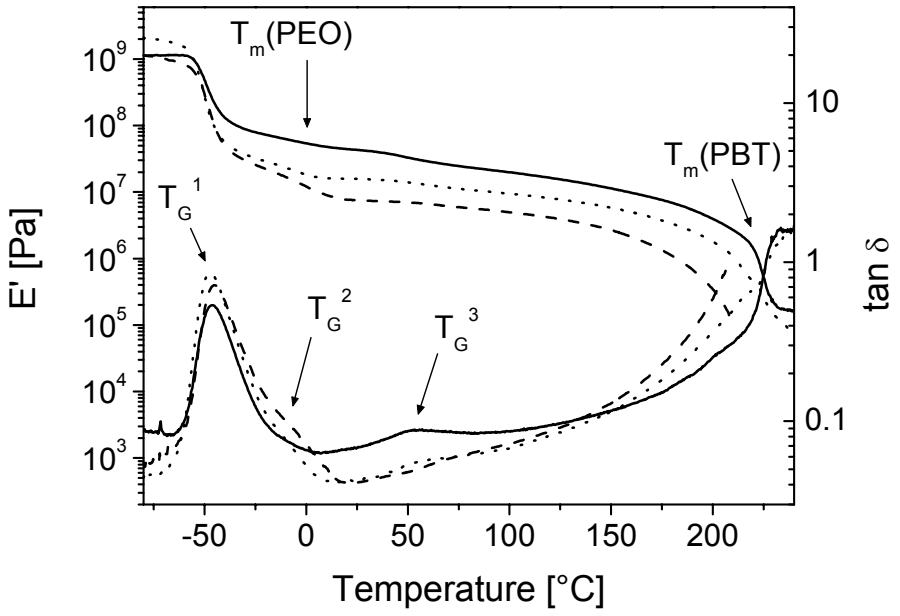

B

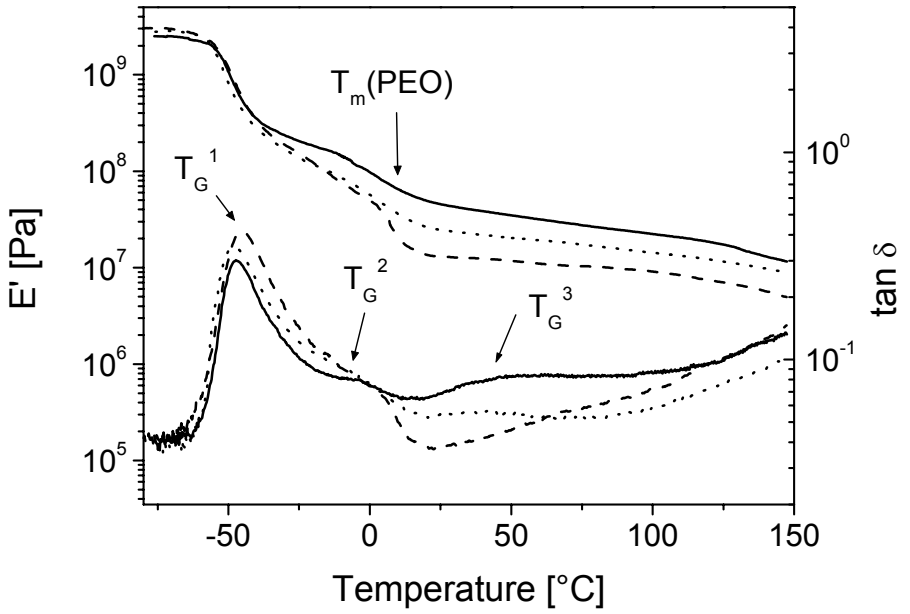

Figure 6. DMA measurements for copolyesters with (A) $PEO_{18}PEB_{64}PEO_{18}$[5.6] soft segments (PBTx-1000): PBT45-1000 (——), PBT35-1000 (·····), PBT20-1000 (------); (B) $PEO_{22}PEB_{56}PEO_{22}$[6.4] soft segments (PBTx-1380): PBT40-1380 (——), PBT30-1380 (·····), PBT20-1380 (------).

A third glass transition temperature (T_G^3) can be observed at ca. 50 °C, as indicated by a small drop in E' and a corresponding maximum in tan δ. This glass transition is more pronounced for copolyesters PBTx-1000 with a high PBT content (Figure 6A). In the samples PBTx-1380 (Figure 6B) the transition region is probably very broad. For PBT homopolymer the glass transition temperature is 45 °C.[29] Therefore, the observed third glass transition temperature T_G^3 can be attributed to a pure amorphous PBT phase. A corresponding transition in the second DSC heating traces is not detectable (Table 2). However, this transition is visible in the first heating trace or after annealing at temperatures slightly below the glass transition temperature of PBT for copolyesters with PBT contents ≥ 30 wt-% (results not shown). The results obtained by DSC and DMA experiments refine the morphology picture obtained by TEM and SFM. The following structure can be proposed. The copolyesters with PEO-*b*-PEB-*b*-PEO soft segments consist of a crystalline PBT phase and an amorphous phase, which can be divided into a pure PEB phase, a PEO-rich phase besides a mixed PEO/PBT phase, and a pure amorphous PBT phase. To provide more evidence for the existence of these proposed different phases, the PEB containing PBT-based copolyesters have been studied in more detail using solid-state NMR. These results will be presented elsewhere.[30]

Mechanical Characterization. TEM and SFM investigations show that in the PEB containing copolyesters the hard phase is dispersed within a matrix of the soft phase. Compared to the co-continuous hard phase in PBT-PTMO based copoly(ether ester)s like PBT1000/50, a dispersed hard phase should result in a better elastic recovery. To prove this assumption, hysteresis measurements have been performed on copolyesters with $PEO_{18}PEB_{64}PEO_{18}^{5.6}$ soft segments. Figure 7 shows a comparison of hysteresis measurements up to 100% strain for PBT20-1000 and PBT1000/50. The course of the traces underline the disperse and co-continuous morphology found for PBT20-1000 and PBT1000/50, respectively. At any strain value PBT20-1000 exhibits a smaller stress value compared to PBT1000/50; i. e., PBT20-1000 is a "softer" material. Comparing the obtained plastic deformations (ε_{plast}) after elongation to 100%, PBT20-1000 shows a significantly lower plastic deformation. As depicted in Table 3, all copolyesters based on $PEO_{18}PEB_{64}PEO_{18}^{5.6}$ soft segments reveal a significantly lower plastic deformation compared to that of PBT1000/50. This effect is visible not only at 100% elongation but also, and even more pronounced, at 500% elongation (Table 3).

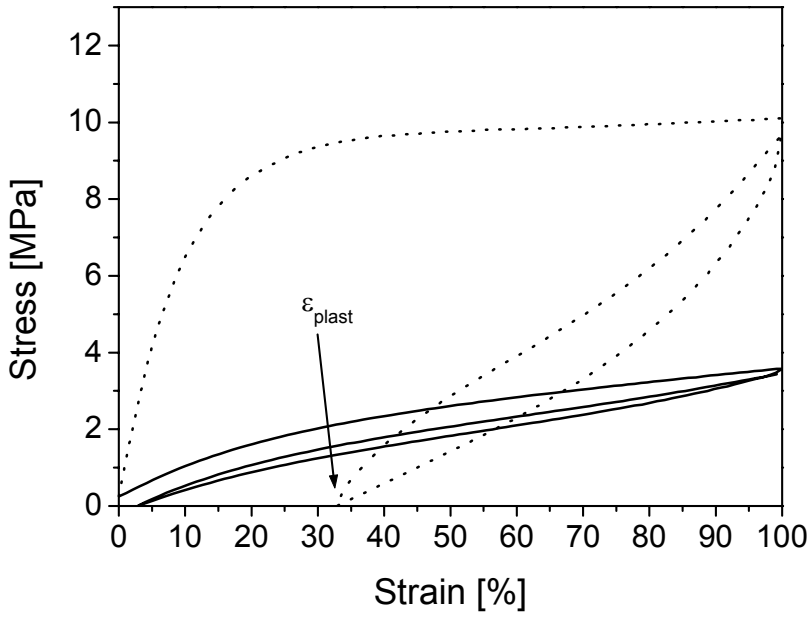

Figure 7. Comparison of hysteresis measurements up to 100% strain for PBT20-1000 (——) and PBT1000/50 (·····).

Increasing the molecular weight by solid-state postcondensation results in an additional improvement, as is demonstrated by the postcondensated samples PBT20-1000_P and PBT25-1000_P (Table 3). The significantly increased elasticity results not only from the increased amount of soft block (due to the less extreme phase separation between PBT and PTMO, incorporation of a higher amount of PTMO will result in a homogeneously mixed system) but also mainly from differences in the hard segment structure. The co-continuous hard phase in PBT1000/50 is much easier irreversibly disrupted upon elongation compared to the disperse hard phase in PEO-*b*-PEB-*b*-PEO-based copolyesters, resulting in a much higher plastic deformation.

An irreversible disruption of the hard phase in the PEB containing copolyester should result in a so-called strain softening effect. This effect is reflected by a decrease of the "second" initial modulus in the second cycle of a hysteresis test compared to the original initial modulus.[31,32] Table 3 shows a comparison of the original Young modulus ($E_{initial}$) and the "second" initial modulus in the second cycle after an elongation to 100% (E_{100}). The copolyesters based on $PEO_{18}PEB_{64}PEO_{18}$[5.6] soft segments exhibit a significantly lower decrease in the "second" initial modulus E_{100} compared to that of PBT1000/50. This supports the assumption that a dispersed PBT hard phase undergoes less irreversible disruption upon elongation compared to a co-continuous hard phase.

Table 3. Elastic Properties of Copolyesters Obtained by Cyclic Stress-Strain Measurements[a]

sample	$\varepsilon_{plast}(100)$ [%]	$\varepsilon_{plast}(500)$ [%]	$E_{initial}$ [MPa]	E_{100} [MPa]	$E_{100}/E_{initial}$ [%]
PBT1000/50	32.4 (0.2)	314 (1.0)	73.2 (2.5)	20.4 (0.3)	27.9
PBT40-1000	5.9 (0.2)	-	15.2 (1.0)	11.2 (0.4)	73.7
PBT35-1000	4.2 (0.2)	-	12.0 (0.6)	10.2 (0.2)	85.0
PBT30-1000	4.7 (0.2)	-	12.2 (0.2)	9.3 (0.2)	76.2
PBT25-1000	8.3 (0.3)	-	13.9 (1.0)	9.5 (0.5)	68.3
PBT20-1000	2.8 (0.1)	104 (0.5)	8.7 (0.1)	7.5 (0.1)	86.2
PBT25-1000_P[b]	4.6 (0.2)	-	9.3 (0.1)	8.5 (0.1)	91.4
PBT20-1000_P[b]	0.6 (0.1)	-	6.9 (0.2)	6.6 (0.2)	95.7

[a] $\varepsilon_{plast}(x)$ = remaining plastic deformation after a cyclic extension to x%; $E_{initial}$ = initial Young modulus; E_{100} = initial Young modulus for the second cyclic extension to 100% strain; values in parenthesis give the standard deviations.
[b] Samples were subjected to a solid state post-condensation.

Conclusions

We have investigated the morphology and elastic properties of several PBT based copolyesters with PEO-*b*-PEB-*b*-PEO soft segments. Dynamic shear experiments in combination with small-angle X-ray scattering show that crystallization of the PBT hard segments occurs from a microphase-separated melt. This results in a dispersed hard segment phase within a matrix of the soft phase as revealed by TEM and SFM investigations. DMA and DSC measurements show an enhanced microphase separation in the soft segment phase induced by the nonpolar PEB segments. A structure model can be proposed consisting of a crystalline PBT hard phase and an amorphous soft phase, which can be divided into a pure PEB phase, an amorphous PEO-rich phase besides a mixed PEO/PBT phase, and a pure amorphous PBT phase. Mechanical testing shows a significantly improved elastic recovery compared to the case of PBT1000/50, a copoly(ether ester) exhibiting a co-continuous hard and soft phase structure. This demonstrates that an increased phase separation, which results here in a disperse PBT hard phase, leads to significantly improved elastic properties.

Acknowledgment. The authors thank J. van Elburg (DSM) for assistance with mechanical testing, A. Böker and Prof. G. Krausch (Physikalische Chemie II) for support concerning the SFM measurements, A. Göpfert (Makromolekulare Chemie II) for TEM investigations, K. Matussek (Makromolekulare Chemie II) and M. Soliman (DSM) for help with rheological analysis, and A. Schmidt (DSM) for helpful discussions. The work was financially supported by DSM Research and in part by the Bayreuther Institut für Makromolekülforschung (BIMF) and the Deutsche Forschungsgemeinschaft (DFG) through SFB 481.

References and Notes

(1) Adams, R. K.; Hoeschele, G. K.; Witsiepe, W. K. In *Thermoplastic Elastomers*; Holden, G.; Legge, N. R.; Quirk, R.; Schroeder, H. E., Eds.; Hanser: Munich, 1996; p 191.

(2) Cella, R. J. *J. Polym. Sci., Polym. Symp.* **1973**, *42*, 727.

(3) Hoeschele, G. K.; Witsiepe, W. K. *Angew. Makromol. Chem.* **1973**, *29/30*, 267.

(4) Hoeschele, G. K. *Chimia* **1974**, *28*, 544.

(5) Seymour, R. W.; Overton, J. R.; Corley, L. S. *Macromolecules* **1975**, *8*, 331.

(6) Zhu, L.-L.; Wegner, G. *Macromol. Chem.* **1981**, *182*, 3625.

(7) Veenstra, H.; Hoogvliet, R. M.; Norder, B.; Boer, A. P. *J. Polym. Sci., Polym. Phys.* **1998**, *36*, 1795.

(8) Soliman, M.; Dijkstra, K.; Borggreve, R. J. M.; Wedler, W.; Winter, H. H. In *Makromolekulares Kolloquium Book of Abstract*, Freiburg, 1998.

(9) Buck, W. H.; Cella, R. J.; Gladding, E. K.; Wolfe, J. R. *J. Polym. Sci., Polym. Symp.* **1974**, *48*, 77.

(10) Bandara, U.; Droscher, M. *Colloid Polym. Sci.* **1983**, *261*, 26.

(11) Briber, R. M.; Thomas, E. L. *Polymer* **1985**, *26*, 8.

(12) Lilaonitkul, A.; Cooper, S. L. *Rubber Chem. Technol.* **1977**, *50*, 1.

(13) Zhu, L.-L.; Wegner, G. *Makromol. Chem.* **1981**, *182*, 3639.

(14) Gabriëlse, W.; Soliman, M.; Dijkstra, K. *Macromolecules* **2001**, *34*, 1685.

(15) Pesetskii, S. S.; Jurkowski, B.; Olkhov, Y. A.; Olkhova, O. M.; Storozhuk, I. P.; Mozheiko, U. M. *Eur. Polym. J.* **2001**, *37*, 2187.

(16) Wolfe, R. J. *Rubber Chem. Technol.* **1977**, *50*, 688.

(17) Bonart, R. *J. Macromol. Sci., Phys.* **1968**, *B2*, 115.

(18) Dieterich, D. *Polyurethane*; Hanser: Munich, 1983.

(19) Niesten, M. C. E. J.; Bosch, H.; Gaymans, R. J. *J. Appl. Polym. Sci.* **2001**, *81*, 1605.

(20) Schmalz, H.; Abetz, V.; Lange, R.; Soliman, M. *Macromolecules* **2001**, *34*, 795.

(21) Wunderlich, B. *Macromolecular Physics*; Academic Press: New York, 1980; Vol. 3.

(22) Van Krevelen, D. W. *Properties of Polymers*, 2nd ed.; Elsevier: Oxford, 1976.

(23) Rosedale, J. H.; Bates, F. S. *Macromolecules* **1990**, *23*, 2329.

(24) Gehlsen, M. D.; Almdal, K.; Bates, F. S. *Macromolecules* **1992**, *25*, 939.

(25) Riise, B. L.; Fredrickson, G. H.; Larson, R. G.; Pearson, D. S. *Macromolecules* **1995**, *28*, 7653.

(26) Floudas, G.; Hadjichristidis, N.; Iatrou, H.; Pakula, T.; Fischer, E. W. *Macromolecules* **1994**, *27*, 7735.

(27) Adams, J. L.; Graessley, W. W.; Register, R. A. *Macromolecules* **1994**, *27*, 6026.

(28) Adams, J. L.; Quiram, D. J.; Graessley, W. W.; Register, R. A.; Marchand, G. R. *Macromolecules* **1996**, *29*, 2929.

(29) Turi, E. A. *Thermal Characterization of Polymeric Materials*; Academic Press: Orlando, 1981.

(30) Gabriëlse, W.; van Guldener, V.; Schmalz, H.; Abetz, V.; Lange, R. *Macromolecules, 35*, 6946.

(31) Grady, B. P.; Cooper, S. L. In *Science and Technology of Rubber*; Mark, J. E.; Erman, B.; Eirich, F. R., Eds.; Academic Press: San Diego, 1978; Chapter 13.

(32) Niesten, M. C. E. J.; Gaymans, R. J. *J. Appl. Polym. Sci.* **2001**, *81*, 1372.

3.1.3 Morphology and Molecular Miscibility of Segmented Copoly(ether ester)s with Improved Elastic Properties as Studied by Solid-State NMR

Wouter Gabriëlse[a*], Viola van Guldener[a], Holger Schmalz[b], Volker Abetz[b], and Ronald Lange[a,c]

a) DSM Research, P.O. Box 18, 6160 MD Geleen, The Netherlands
b) Makromolekulare Chemie II, Universität Bayreuth, 95440 Bayreuth, Germany
c) present address: BASF Aktiengesellschaft, ZKS/B1, 67056 Ludwigshafen, Germany

ABSTRACT: The morphology of copoly(ether ester) elastomers, based on poly(butylene terephthalate) (PBT) hard blocks and poly(ethylene oxide)-*block*-poly(ethylene-*stat*-butylene)-*block*-poly(ethylene oxide) (PEO-*b*-PEB-*b*-PEO) soft blocks, has been investigated by various solid-state NMR methods. ^{13}C IRCP and ^{1}H-$T_{1\rho}$ NMR experiments show a heterogeneity in molecular motions for the PEO and PBT segments, indicating the presence of a PEO-rich phase and a PEO/PBT mixed phase. In contrast, for the PEB segments a homogeneous NMR relaxation behaviour is observed, indicating the presence of a separate pure PEB phase. Deuterium NMR spectra recorded of block copolymers with selectively deuterated PBT, clearly show at least 2 distinct motional environments of PBT already at room temperature: a broad peak which is assigned to PBT segments in a crystalline phase, and an extremely narrow peak which is assigned to highly mobile PBT segments embedded in an amorphous matrix (PBT/PEO mixed phase). For copoly(ether ester)s with a relatively high PBT content (45% (w/w)), ^{2}H T_1-inversion recovery experiments even reveal the presence of a 'pure' amorphous PBT phase next to the PBT/PEO mixed phase. Hysteresis experiments show that copoly(ether ester)s based on PEO-*b*-PEB-*b*-PEO soft blocks have a significantly improved elastic behavior, i.e. lower plastic set, compared to PTMO-based copoly(ether ester)s.

Introduction

One of the goals in polymer science is to gain control over the relation between the molecular structure, the morphology, and the resulting mechanical properties. This is especially true for thermoplastic elastomers or TPE's. The aim in these TPE's is to obtain a well-defined two-phase morphology in which the elastomeric properties are fully exploited with the preservation of the thermoplastic processing characteristics. In this paper the relation between the morphology and the elastic properties of one class of TPE's, *i.e.* copoly(ether ester)s or TPE-E's is described. TPE-E's consist in general of a poly(butylene terephthalate) or PBT hard phase and a poly(tetramethylene oxide) or PTMO soft phase.[1,2] Due to the partial immiscibility of the PBT and the PTMO segments a co-continuous two-phase morphology is obtained.[3-7] It was assumed that this co-continuous two-phase morphology consists of crystalline PBT and a homogeneous amorphous PBT-PTMO phase. A recent study, using amongst others various solid-state NMR techniques, demonstrated the existence of a non-homogeneous amorphous soft phase consisting of a PTMO rich and a mixed amorphous PBT-PTMO phase.[8]

It is generally accepted that the presence of a co-continuous crystalline PBT phase causes the significant plastic deformation and hence minor elastic properties of TPE-E's upon relative large elongations. Orientation studies have shown that upon deformation, the soft segments orient parallel to the stress direction,[9] whereas the hard segments initially orient transverse to the stress direction and only at higher elongations parallel to the stress direction.[10] This process of alignment of the crystalline polymer chains with the direction of stress continues up to 300% elongation, and results in irreversible disruption of the crystalline matrix. In addition, it has been shown that the degree of crystallinity is of importance for the elastic properties.[11] The general idea is that the elasticity of copoly(ether ester)s could be improved by changing the co-continuous PBT hard phase into a disperse phase. This can be achieved by increasing the phase separation as was demonstrated in thermoplastic polyurethanes or TPE-U's,[12,13] and in strongly phase separated copoly(ether ester aramides).[14] Recently, we reported the successful synthesis of hydrogenated polybutadiene (PEB) containing PBT based copolyesters.[15] Preliminary studies using TEM, SFM, DSC, DMA and melt rheology showed that the incorporation of the non-polar PEB soft block in PBT based copoly(ether ester)s resulted in an extreme phase separation.[16] To elucidate the obtained morphology in more detail, the PEB containing copolyesters have been analysed using solid-state NMR spectroscopy, which is a powerful tool to study the microphase structure of

polymers.[17] NMR relaxation experiments are of special interest, since changes in molecular mobility are accompanied by changes in NMR relaxation times. ^{13}C inversion recovery cross-polarization measurements (IRCP), and proton-$T_{1\rho}$ relaxation experiments have been performed. In addition, selectively deuterated PBT homopolymer and selectively deuterated PBT-based copoly(ether ester)s have been prepared and analysed using ^{2}H-solid-state echo and inversion recovery-T_1 techniques. Based on the results of these NMR studies a model is proposed in which the morphology of this novel type of TPE-E is related to the elastic properties of this material.

Experimental

Samples. The copoly(ether ester)s studied in this paper consist of PBT hard blocks and PEO-*b*-PEB-*b*-PEO soft blocks. The soft block is synthesized by chain extension of hydroxy-terminated hydrogenated polybutadiene by means of anionic ring opening polymerization of ethylene oxide. The synthesis of the copolymers and the molecular characterization is described in detail by Schmalz et al.[15] We investigated three types of copoly(ether ester)s varying in the amount and block length of PBT. The designation code for the samples is PBTx-y, in which x is the amount of PBT (in % (w/w)) and y is the molecular weight of PEO in the soft block (in g/mol). The composition of the samples and the average block lengths (in number of monomer units, P_n) of the hard and soft blocks are given in Table 1. The hydrogenated polybutadiene has a molecular weight of 3600 g/mol. The total molecular weight of the soft block was 5600 g/mol, which was kept constant. The PBT concentration was varied between 25 and 45% (w/w). All samples were melt-pressed into plates.

Table 1. Composition of the PEB-Based Copoly(ether ester)s

Sample	Amount of PBT [% (w/w)]	P_n (PBT)	P_n (soft block) PEO-*b*-PEB-*b*-PEO
PBT25-1000	25	10	23-64-23
PBT35-1000	35	15	23-64-23
PBT45-1000	45	22	23-64-23

Selectively labeled PBT homopolymer and selectively labeled PBT-containing copoly(ether ester)s were synthesized using 2,2,3,3-d_4-butylene glycol as the starting diol. The selectively deuterated copoly(ether ester) has the same composition as PBT45-1000.

NMR. ^{13}C solid-state NMR experiments were carried out on a Varian Inova 400 (400 MHz for ^{1}H) and on a Varian Unity 200 (200 MHz for ^{1}H) spectrometer using the 7 mm Jacobsen style VT CP-MAS probe. The ^{13}C cross-polarization magic angle spinning (CP-MAS) and ^{13}C inversion recovery cross-polarization (IRCP) experiments were performed on the Inova 400, while the ^{1}H-$T_{1\rho}$ experiments were performed on the Unity 200. The 90º-pulse width was 5 μs for protons and carbons. Adamantane was used as an external chemical shift reference (38.3 ppm for the methylene resonance relative to TMS). All experiments were performed under magic angle spinning conditions. The spinning rate was 7 kHz for experiments carried out on the 400 MHz spectrometer and 4 kHz for experiments performed on the 200 MHz spectrometer. A recycle time of 2 seconds was used in all cross-polarization experiments. The ^{13}C IRCP pulse sequence is given in Figure 1A.

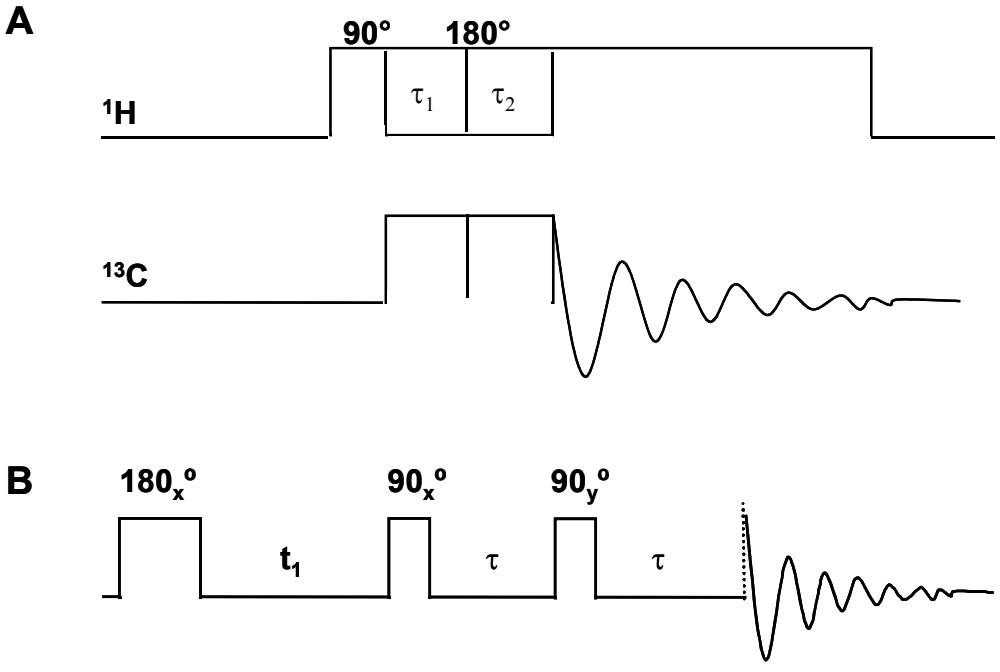

Figure 1. A) Pulse sequence of ^{13}C IRCP experiment with spin temperature inversion on the proton reservoir. B) Pulse sequence of ^{2}H-T_1 inversion-recovery quadrupole echo deuterium experiment.

The first step is a classical cross-polarization step, during which magnetization is transferred from the abundant ^{1}H spins to the dilute ^{13}C spins for a contact time τ_1. During the second part of the experiment (τ_2), the proton magnetization is inverted by applying a 180º phase shift on the proton spin locking field. The cross-polarization time τ_1 was set to a fixed value of 1 ms for the PEB containing copoly(ether ester)s. The inversion time τ_2 was varied between 0.005 and 20 ms. The $T_{1\rho}$-decay of protons was measured from the decay of carbons attached to them by using cross-polarization. By applying spectral deconvolution the integral peak intensities of the various peaks could be determined as a function of the decay time. In the ^{1}H-$T_{1\rho}$ experiments the spin lock time on protons was varied between 10 μs and 30 ms.

Solid-state ^{2}H spectra were recorded on a Varian Inova 400 (400 MHz for ^{1}H) using a wideline probe. Spectra were obtained using the standard quadrupole echo pulse sequence[18] (90_x-τ-90_y-τ). The τ-value was 20 μs, recycle delay was 2 seconds the 90° pulse width was 2.5 μs. Inversion-recovery T_1-deuterium NMR spectra were obtained by using a 180° pulse followed by a variable delay t_1 and followed by the standard quadrupole echo pulse sequence (Figure 1B). The t_1 time varied between 1 μs and 1 and the τ-value was set to 20 μs.

Results and Discussion

^{13}C CP-MAS Spectrum. Figure 2 shows the ^{13}C CP-MAS NMR spectrum of PBT45-1000 recorded at 400 MHz for ^{1}H. In addition to the spinning side bands (marked by an asterisk), nine resonances (a-i) are observed, which are assigned to structural units shown in Figure 2. The spectrum shows four PBT resonances of the carbonyl carbons at 165.1 ppm (h), the protonated aromatic carbons at 130.7 ppm (g), the non-protonated aromatic carbons at 134.7 ppm (f), and the PBT-OCH_2 groups at 65.9 ppm (a). For the soft block a resonance for the OCH_2 groups of PEO at 71.7 ppm (c) is observed. The ^{13}C NMR spectrum of the PEB block, which appears between 25 and 40 ppm, is rather complex since there are many overlapping lines originating from the sequence distribution in the soft PEB block. These lines can be resolved in a liquid state spectrum but show severe overlapping in a solid-state spectrum. The assignments of the resolved peaks to the various structural units in the PEB block are indicated in Figure 2. It is noted that the main peak of the PEB unit shows severe overlapping with the CH_2 resonance of PBT at 27 ppm (b).

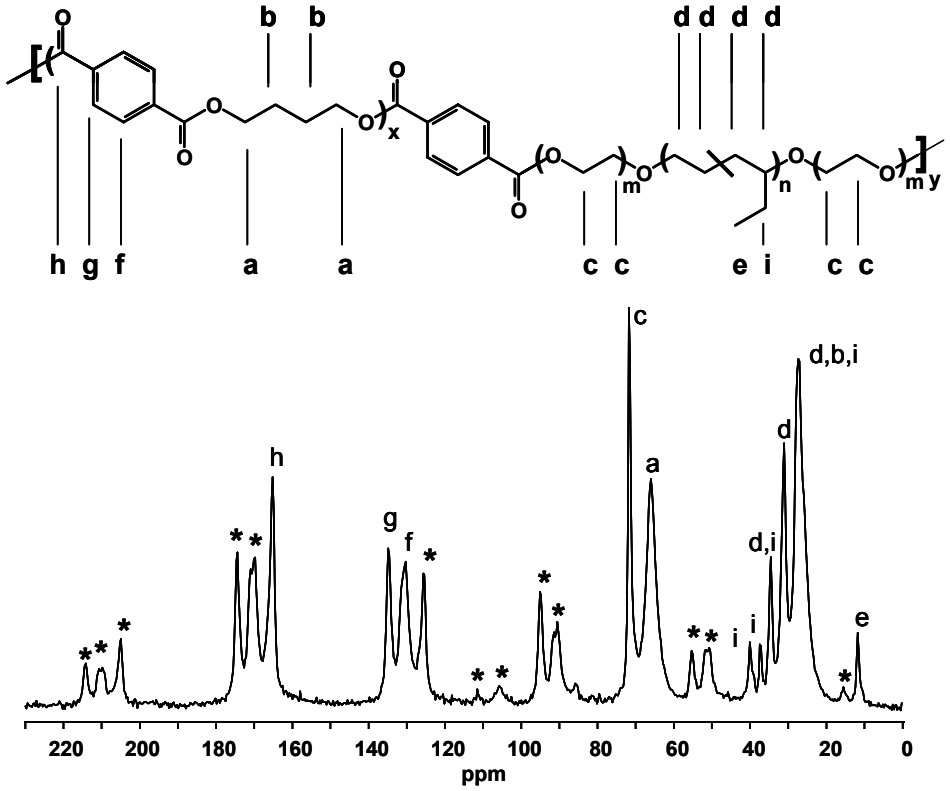

Figure 2. ^{13}C CP-MAS spectrum of PBT45-1000 at a spinning rate of 4 kHz and a contact time of 1ms, recorded at 400 MHz for ^{1}H. Peaks marked with an asterisk are spinning side bands. Note that the OCH_2 carbons of the first PEO unit directly connected to the terephthalate group belong to resonance a and not to c.

^{13}C Inversion Recovery Cross-polarization (IRCP) Experiments. To study the molecular mobility of the hard and soft segment in more detail, we applied a ^{13}C IRCP experiment.[19] The IRCP experiment is composed of two contiguous parts. The first step is a classical cross-polarization step, during which magnetization is transferred from the abundant ^{1}H spins to the dilute ^{13}C spins for a contact time τ_1. During the second part of the experiment (τ_2), the carbon magnetization is inverted. The rate of this inversion process or depolarization process is determined by the cross-polarization dynamics. The cross-polarization or depolarization rate depends on the strength of the magnetic dipole-dipole coupling between ^{13}C and ^{1}H spins, which is affected by molecular motions. In case of slow motions or low amplitude motions cross-polarization is a relatively fast process, in case of fast motions or high amplitude motions, cross-polarization is a relatively slow process. We expect therefore the magnetization of the hard block to invert faster than that of the soft block. By using this IRCP pulse sequence, one component can be selectively nulled to yield a spectrum of the other. This experiment has been successfully applied before on copoly(ether ester)s based on PBT hard blocks and PTMO soft blocks.[8] Based on this experiment it could be clearly shown

that the amorphous phase is not a homogeneous mixture of hard and soft segments, but is phase separated in a 'PTMO-rich' phase and a mixed 'PBT/PTMO' phase.

The results for sample PBT45-1000 are shown in Figure 3A and 3B for respectively the OCH_2 carbons of the PEO and PBT segment (58 – 77 ppm) and the CH and CH_2 groups of the PEB between 15 and 45 ppm. The spectra recorded at different τ_2 are presented. The spectra are fitted with Lorentzian and/or Gaussian lines. In Figure 3A we see that the OCH_2 resonances of the 'hard' PBT segment invert, as expected, faster than those of the PEO groups. Most interestingly is the inversion of the OCH_2 groups of PEO at an inversion time (τ_2) of 600 μs. Here we clearly see that the PEO-OCH_2 resonance at 71.7 ppm is actually composed of two resonances: a narrow peak (blue line), which is still positive and not yet inverted, and a broader peak (red line), which is already inverted. The broader peak is slightly shifted upfield (~0.3 ppm) with respect to the narrow line. For all samples we observe for the PEO-OCH_2 peak this splitting into 2 resonances. These two lines are almost individually observed at 400 μs (narrow line) and 800 μs (broad peak). These two lines, with different line width and cross-polarization behavior, are attributed to PEO segments with different molecular mobility. The narrow line, which inverts slow, can be assigned to PEO segments with relatively high mobility, whereas the broad line corresponds to PEO segments with more restricted mobility. These results indicate that the PEO segments do not form a completely demixed separate phase. Instead we assign the narrow peak to highly mobile PEO segments in a PEO-rich phase and the broad peak to PEO segments with more restricted mobility due to partial mixing with more rigid PBT segments. These assignments are in agreement with previous studies on similar copoly(ether ester)s.[8]

For all PEB resonances (Figure 3B) we observe almost identical cross-polarization and depolarization behavior. At 800 μs all signals are at their 'cross-over point'. This indicates that there is no heterogeneity in mobility for the PEB segment. It should be noted that the resonance at 27 ppm inverts faster, but this peak originates from the CH_2 carbons of PBT.

In summary, these results already indicate that the amorphous phase is composed of a highly mobile PEO-rich phase, a PEO/PBT mixed phase, and a pure PEB phase. These assignments are also in agreement with DMTA results[16] that are discussed in more detail in a separate contribution, in which for all samples two distinct T_g's are observed; a first T_g at -60 °C (PEB-pure phase) and a second T_g at -10 °C (PBT/PEO mixed phase). Furthermore, DSC measurements reveal the presence of a pure PEO phase[16] since in a DSC curve a clear melting peak at about 5 °C is observed.

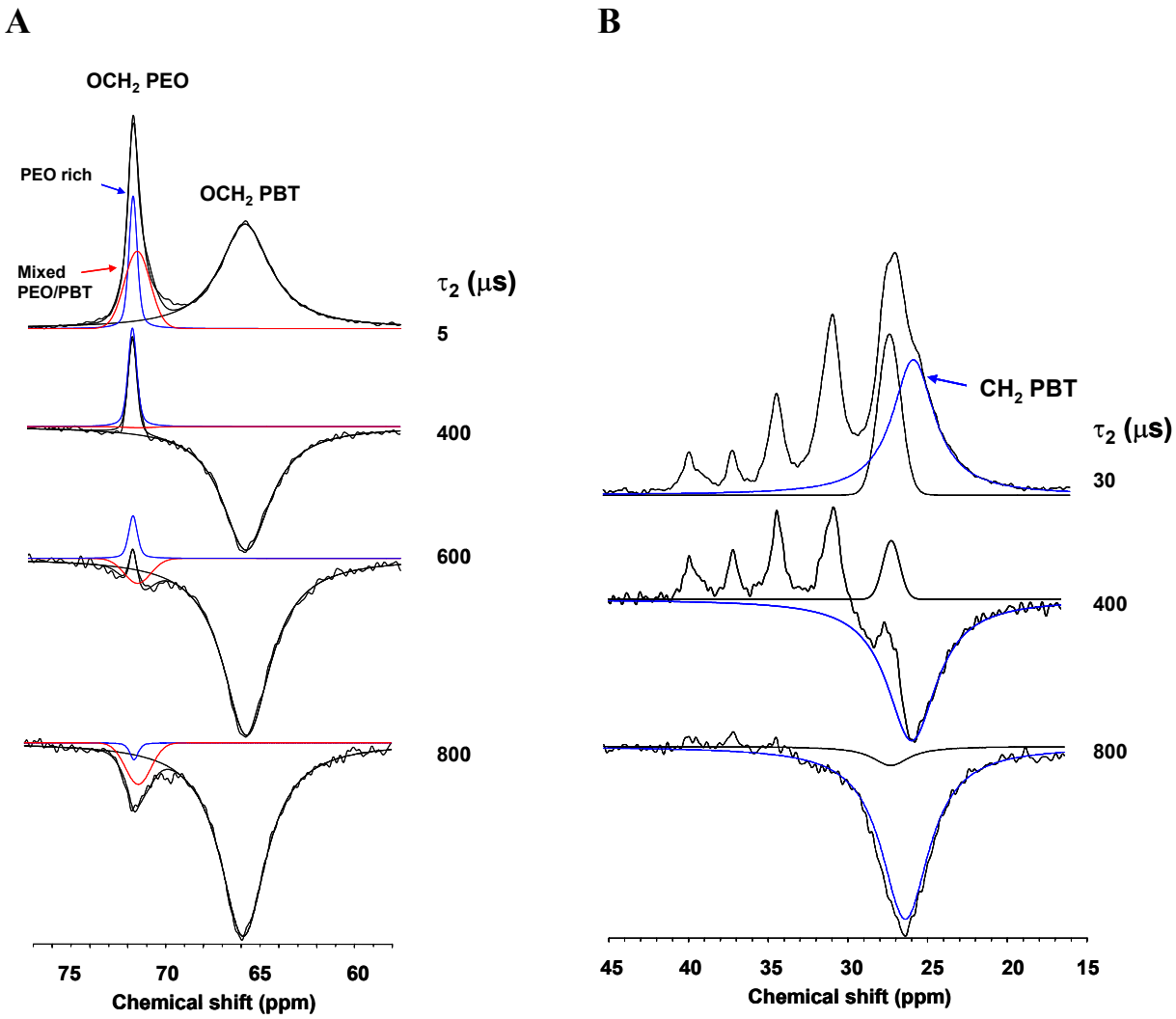

Figure 3. (A) ^{13}C IRCP spectra of PBT45-1000 showing the OCH_2 resonances of PBT and PEO. The PEO resonance is fitted with two lines, a narrow red peak and a blue broader peak. (B) ^{13}C IRCP spectra of PBT45-1000 showing the CH and CH_2 groups of the PEB soft block. Note the overlapping CH_2 resonance of PBT at 27 ppm, shown in blue. The black line is fitted to the resonances of the PEB soft block, whereas the blue line indicates the overlapping CH_2 of PBT. The rest of the fitted lines is left away for clarity.

^{1}H-$T_{1\rho}$ Experiments. The ^{13}C IRCP experiments discussed above are sensitive to local motions of individual C-H groups. Hence, the heterogeneity in cross-polarization behavior, as determined for the various groups, does not necessarily reflect different domains (phases) with different molecular mobility. Here ^{1}H-$T_{1\rho}$ experiments can provide valuable information. ^{1}H-$T_{1\rho}$ relaxation times in solids usually represent averaged values over the relaxation behavior of the ensemble of protons. This is due to the strong dipolar coupling between protons, which gives rise to spin diffusion. When domains with different molecular mobility are relatively small (< ca. 5 nm), the relaxation behavior is averaged out to give a

single value. Only for larger domains (> ca. 5 nm), a heterogeneity in the ^{1}H-$T_{1\rho}$ relaxation behavior is observed.

The ^{1}H-$T_{1\rho}$ decay curves are plotted in Figure 4 for sample PBT45-1000 at different temperatures (room temperature, 50 °C and 80 °C). The solid lines represent least squares fits of a mono- or bi-exponential decay function to the experimental data points. Only the experimental data and fits for the PEO-OCH_2 groups, the PBT-OCH_2 groups and the CH_2 and CH groups of PEB are given.

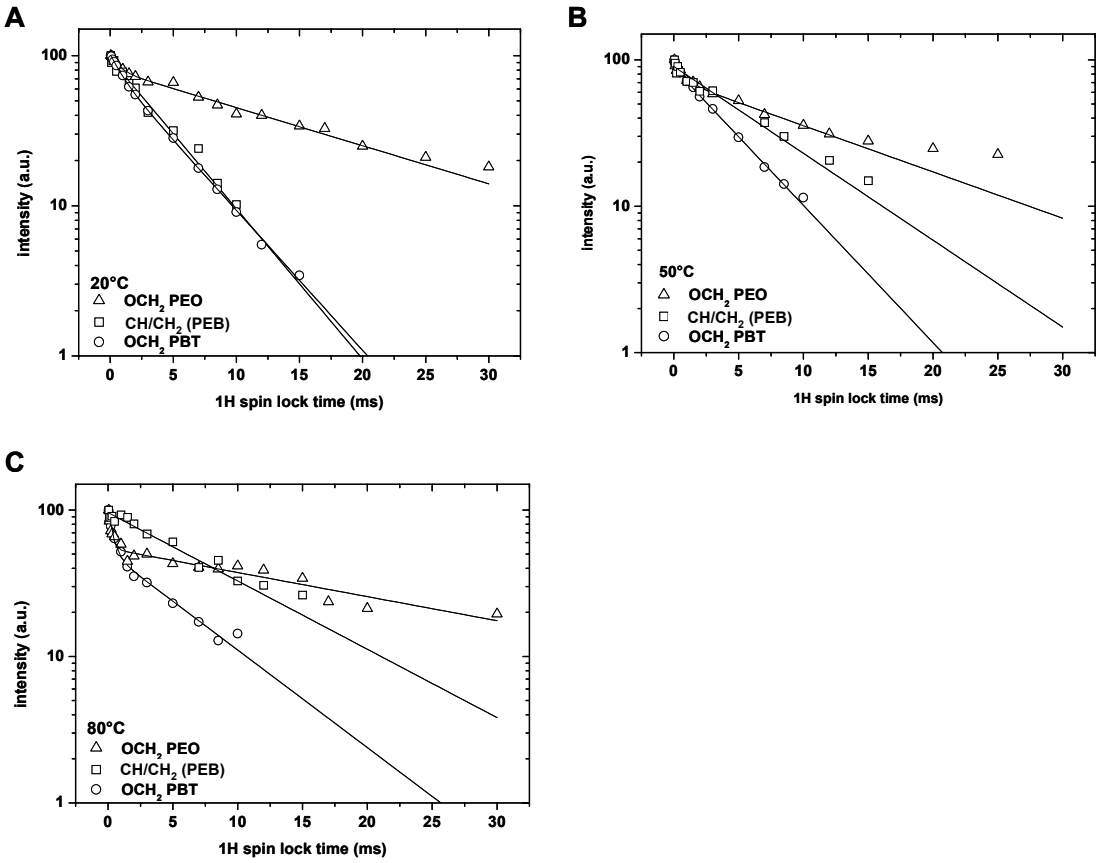

Figure 4. ^{1}H-$T_{1\rho}$ decay of the OCH_2 (PEO), OCH_2 (PBT) and CH_2 (PEB) carbons of PBT45-1000 at different temperatures: A) room temperature B) 50 °C and C) 80 °C. The solid lines represent least-squares fits of the experimental data using a bi-exponential decay function.

The relaxation time constants obtained from the fits are given in Table 2. At room temperature (Figure 4A) we observe a bi-exponential decay for the OCH_2 groups of PEO and for the OCH_2 groups of PBT and a mono-exponential decay for the CH and CH_2 groups of PEB. For PEO, the slow decaying component is assigned to the highly mobile PEO-rich phase since at higher temperatures this relaxation time increases (Table 2) which is typical for

highly mobile segments. The fast decaying component is assigned to PEO segments with the more restricted mobility, mixed with PBT. For PBT the fast relaxing component is assigned to amorphous PBT segments with a relatively high mobility, and the slow relaxing component to rigid crystalline PBT segments. Most interestingly, the relaxation time of the fast decaying component of PBT is in the same order of magnitude as the fast decaying component of PEO. Therefore the short ^{1}H-$T_{1\rho}$ relaxation times of PEO and PBT are assigned to an amorphous PEO/PBT mixed phase.

The mono-exponential relaxation behavior of the CH and CH_2 groups of PEB indicates that the PEB forms a homogeneous amorphous phase without mixing with PEO or PBT segments. Also at elevated temperatures, the relaxation behavior of the PEB phase is clearly different from the relaxation behavior of PEO and PBT.

Table 2. ^{1}H-$T_{1\rho}$ Relaxation Time Constants for PBT45-1000 Measured at 200 MHz for ^{1}H at Different Temperatures

PBT45-1000	Carbons	$T_{1\rho}(^1H)^A$ [ms]	$T_{1\rho}(^1H)^B$ [ms]	I^A [%]	I^B [%]
RT	PEO (OCH_2)	0.69 ± 0.25	17.1 ± 1.3	21 ± 3	79 ± 3
	PEB (CH and CH_2)	4.34 ± 0.26	-	-	-
	PBT (OCH_2)	1.02 ± 0.17	4.66 ± 0.14	22 ± 3	78 ± 3
T = 50 °C	PEO (OCH_2)	0.74 ± 0.38	13.74 ± 2.1	25 ± 5	75 ± 5
	PEB (CH and CH_2)	7.31 ± 0.76	-	-	-
	PBT (OCH_2)	0.33 ± 0.10	4.63 ± 0.13	14 ± 2	86 ± 2
T = 80 °C	PEO (OCH_2)	0.24 ± 0.06	26.38 ± 3.54	48 ± 6	52 ± 2
	PEB (CH and CH_2)	9.3 ± 0.8	-	-	-
	PBT (OCH_2)	0.39 ± 0.09	6.51 ± 1.0	49 ± 5	51 ± 5

Deuterium NMR Experiments. ^{2}H-NMR spectra provide detailed information about the type of molecular motions of specific groups. In fact, for PBT-PTMO block copolymers it has been reported[20] that deuterium NMR experiments showed two distinct motional environments for the hard PBT segments (at room temperature). One of the environments is identical to that observed in the PBT homopolymer, whereas the other motional environment is nearly isotropic. The isotropic motions of PBT segments are attributed to short blocks of hard segments residing in the soft segment matrix.

Figure 5 shows solid-state ^{2}H-NMR spectra of selectively labelled PBT homopolymer (Figure 5A) and a selectively labeled PBT based copoly(ether ester) (Figure 5B). For both systems the 2,3 methylene groups of the butanediol were deuterated. The spectra were recorded at temperatures between –80 °C and 120 °C.

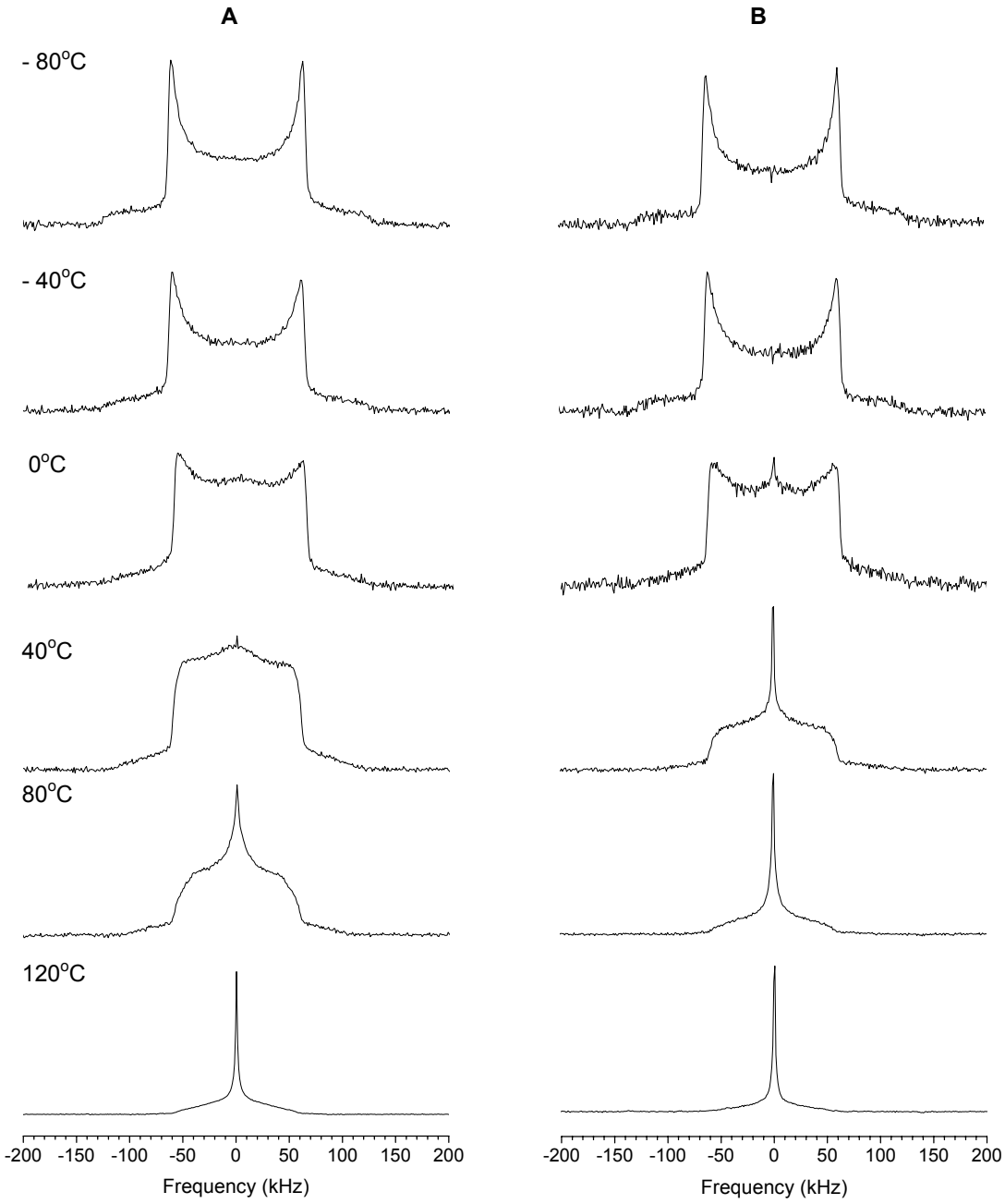

Figure 5. Temperature-dependent solid-state deuterium spectra for PBT (A) and a PEB-based copoly(ether ester) (B). The spectra are scaled arbitrarily.

At low temperatures (-80 °C) the mobility is frozen, therefore we observe for both polymers a typical Pake pattern.[16] At 40 °C a narrow peak superimposed on a broad line shape is observed for the PBT homopolymer. This narrow peak becomes more pronounced in the spectrum recorded at 80 °C. This narrow peak is assigned to amorphous PBT segments, which is in agreement with Jelinski et al.[21] For the PEB-based copoly(ether ester), a narrow peak appears already at 0 °C. In agreement with DMTA measurements,[16] in which a second T_g at -10 °C is observed, this narrow peak can be assigned to the PBT segments with a relatively high mobility, *i.e.* PBT segments that are embedded in a highly mobile soft matrix (amorphous PBT/PEO mixed phase).

It might be further discussed whether all amorphous PBT is mixed with PEO or partly resides in a separate amorphous phase. A first indication for a separate amorphous PBT phase was obtained in a DMTA curve, which showed a glass transition temperature at 50 °C. This transition was most pronounced for a sample containing 45% (w/w) hard block.[16] Indications for the presence of a pure amorphous PBT phase can be derived from ^{2}H-T_1 inversion recovery experiments. Some of the ^{2}H spectra recorded in ^{2}H-T_1 experiments are shown in Figure 6. The first spectrum (Figure 6A), which is plotted negative, resembles the spectrum of the PEB-based copoly(ether ester) recorded at 80 °C as shown in Figure 5B. At an inversion time (t_3) of 8 ms (Figure 6B) we see that the narrow peak is still negative while the broad component is nulled. At 9 ms (Figure 6C), a 'less narrow' peak becomes positive, while the narrow peak is still negative. This peak becomes more pronounced in the spectra depicted in Figures 6D-6F. Especially in spectrum 6F, the extremely narrow peak is nulled, yielding a spectrum composed of two resonances, a relatively broad peak due to crystalline PBT and a relatively narrow peak, which is assigned to amorphous PBT. In fact, this spectrum resembles (only the relative intensities are different) the spectrum of the PBT homopolymer at 80 °C (Figure 5A). Summarizing, we conclude that for samples with a relatively high PBT content (45% (w/w)), a 'pure' amorphous PBT phase exists besides the amorphous PBT/PEO mixed phase. It is stressed that this conclusion cannot be drawn from ^{2}H-NMR experiments alone, but is based on the combined results obtained from ^{2}H-NMR experiments and DMTA experiments,[16] which reveal a T_g at 50 °C, which is typical for amorphous PBT.

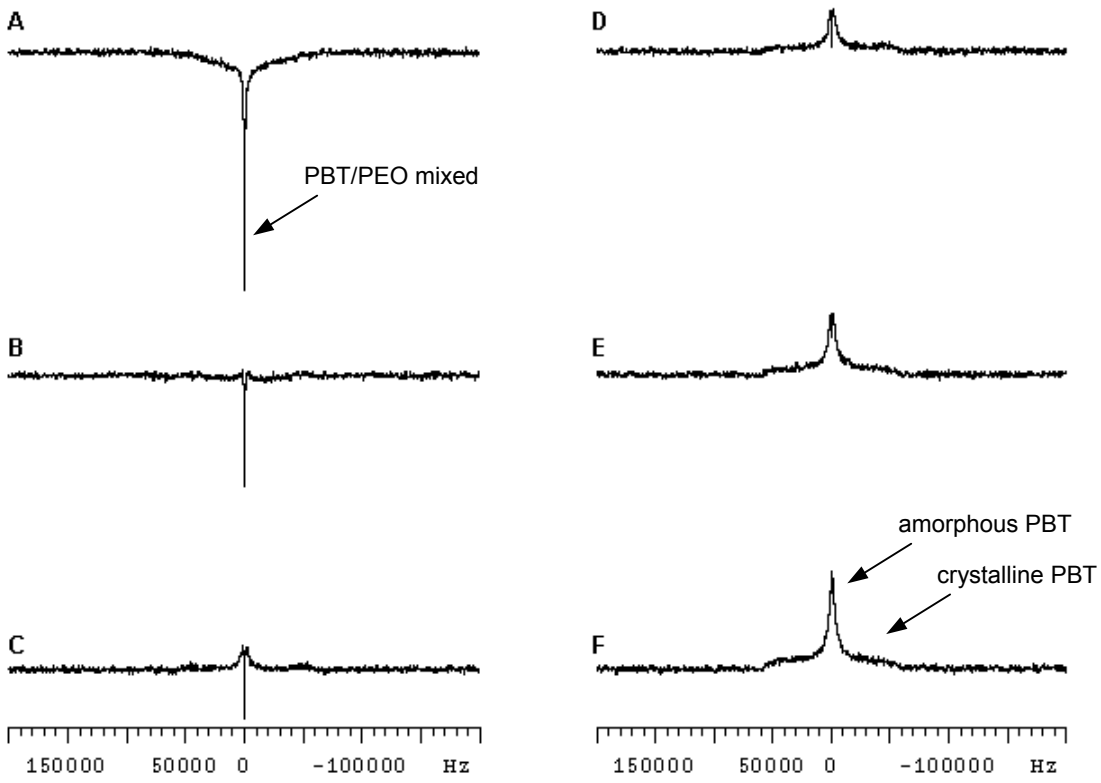

Figure 6. Inversion-recovery solid-state deuterium NMR spectra of a PEB-based copoly(ether ester) containing 45% (w/w) PBT at 80 °C. The spectra A-F are obtained with increasing inversion time (t_3): spectrum A at 6 ms, B at 8 ms, C at 9 ms, D at 10 ms, E at 11 ms, and F at 12ms.

Hysteresis Experiments. The NMR experiments described above unambiguously demonstrate that the PEB containing copoly(ether ester)s possess an increased phase separation compared to the conventionally used PTMO containing copoly(ether ester)s. To show that this increased phase separation results in an improved elasticity, hysteresis experiments are performed. Figure 7 shows a comparison of hysteresis measurements up to 100% strain for PBT20-1000 and the PTMO containing PBT1000-50 (possessing 50% PTMO with a molecular weight of 1000 $g \cdot mol^{-1}$). The curves underline the existence of the disperse and co-continuous morphology found for PBT20-1000[16] and PBT50-1000,[8] respectively. Comparing the obtained plastic deformations after elongation to 100%, which are 6 and 33% for PBT20-1000 and PBT50-1000, respectively, it is clearly demonstrated that an increased phase separation results in an improved elastic behavior. This significantly increased elastic behavior results not only from the increased amount of soft block (due to the less extreme phase separation between PBT and PTMO, incorporation of a higher amount of PTMO will prevent a phase separation and is hence not possible), but mainly from the difference in hard segment structure. The co-continuous hard phase in PBT1000-50 is much easier irreversibly

disrupted upon elongation, resulting in a much higher plastic deformation, compared to the disperse hard phase in the PEO-*b*-PEB-*b*-PEO based copoly(ether ester)s.

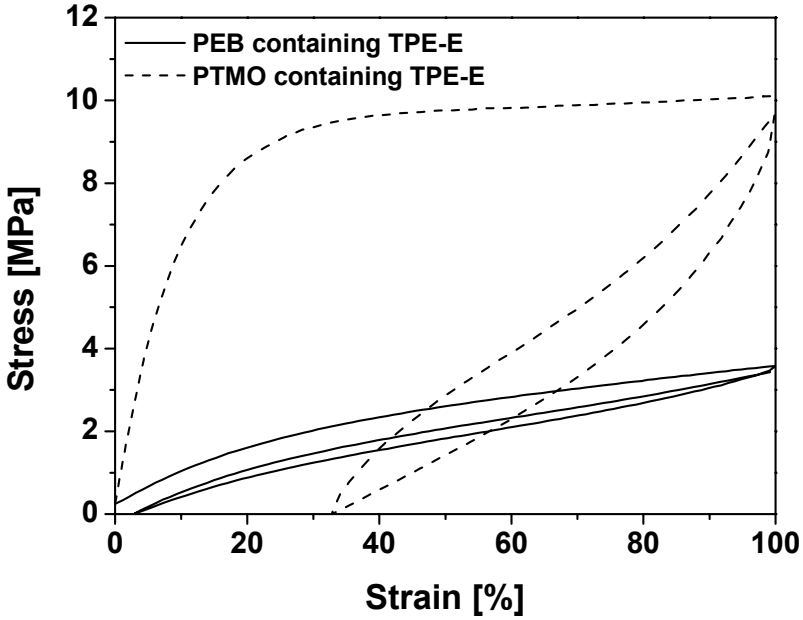

Figure 7. Hysteresis curves showing the first hysteresis cycle to a strain of 100% for a PTMO-based copoly(ether ester) containing 50% (w/w) PBT (dashed curve) and a PEB-based copoly(ether ester) containing 20% (w/w) PBT(solid curve).

Conclusion

Using various solid-state NMR techniques, detailed information on the phase behavior and molecular miscibility was obtained on copoly(ether ester)s based on PBT hard blocks and PEO-*b*-PEB-*b*-PEO soft blocks. Besides a crystalline PBT phase, we conclude that several phases with different molecular mobility are present in the amorphous phase, including a PEO-rich phase, a mixed PEO/PBT phase and a pure PEB phase. This microphase separation was found in all samples investigated. In addition, it was found that, at least for samples with 45% (w/w) of hard block, a 'pure' amorphous PBT phase is present. Hysteresis experiments showed that the copoly(ether ester)s with the PEO-*b*-PEB-*b*-PEO soft blocks have better elastic properties, *i.e.* a lower plastic deformation, compared to the conventionally used PBT-PTMO copoly(ether ester)s. Apparently incorporation of a predominantly non-polar soft block leads to a better phase separated structure in which the PBT crystallites form dispersed domains in a mobile amorphous matrix. This dispersion of hard PBT domains in an

amorphous matrix results in improved elastic properties compared to conventional copoly(ether ester)s with a co-continuous morphology.

Acknowledgment. Fruitful discussions with Dr. V. Litvinov and many colleagues at DSM Research are gratefully acknowledged.

References and Notes

(1) Adams, R. K.; Hoeschele, G. K.; Witsiepe, W. K. In *Thermoplastic Elastomers;* Holden, G.; Legge, N. R.; Quirk, R.; Schroeder, H. E., Eds.; Hanser: Munich, 1996, pp 191.

(2) van Berkel, R. W. M.; Borggreve, R. J. M. ; van der Sluis, C. L.; Werumeus Buning, G. H. Polyester-Based Thermoplastic Elastomers. In *Handbook of Thermoplastics*; Olabisi, O. Ed.; Marcel Dekker: New York, 1997, pp 397.

(3) Cella, R. J. *J. Polym. Sci., Polym. Symp.* **1973**, *42*, 727.

(4) Hoeschele, G. K.; Witsiepe, W. K. *Angew. Makromol. Chem.* **1973**, *29/30*, 267.

(5) Hoeschele, G. K. *Chimia* **1974**, *28*, 544.

(6) Seymour, R. W.; Overton, J. R.; Corley, L. S. *Macromolecules* **1975**, *8*, 331.

(7) Zhu, L.-L.; Wegner, G. *Macromol. Chem.* **1981**, *182*, 3625.

(8) Gabriëlse, W.; Soliman, M.; Dijkstra, K. *Macromolecules* **2001**, *34*, 1685.

(9) Schmidt, A; Veeman, S; Litvinov, V; Gabriëlse, W *Macromolecules* **1998**, *31*, 1652.

(10) Lilaonitkul, A.; West, J.; Cooper, S. L. *J. Macromol. Sci., Phys.* **1976**, *4*, 563.

(11) Castles Stevenson, J.; Cooper, S. L. *Macromolecules* **1988**, *21*, 1309.

(12) Bonart, R. *J. Macromol. Sci., Phys.* **1968**, *B2*, 115.

(13) Dieterich, D. *Polyurethane*; Hanser: Munich, 1983.

(14) Niesten, M. C. E. J.; Bosch, H.; Gaymans, R. J. *J. Appl. Polym. Sci.* **2001**, *81*, 1605.

(15) Schmalz, H.; Abetz, V.; Lange, R.; Soliman, M. *Macromolecules* **2001**, *34*, 795.

(16) Schmalz, H.; van Guldener, V.; Gabriëlse, W.; Lange, R.; Abetz, V. *Macromolecules* **2002**, *35*, 5491.

(17) Komoroski, R. A. *High Resolution NMR Spectroscopy of Synthetic Polymers in Bulk*; VCH: Weinheim, 1986.

(18) [A] Davis, J. H.; Jeffrey, K. R.; Bloom, M.; Valic, M. I.; Higgs, T. P. *Chem. Phys. Lett.* **1976**, *42*, 390; [B] Blinc, R.; Rutar, V.; Seliger, J.; Slak, J.; Smolej, V. *Chem. Phys. Lett.* **1977**, *48*, 576; [C] Hentschel, R.; Spiess, H. W. *J. Magn. Res.* **1979***, 35*, 157.

(19) Cory, D. G.; Ritchey, W. M. *Macromolecules* **1989**, *22*, 1611.

(20) Jelinski, L. W., Dumais, J. J.; Engel, A. K. *ACS Symp. Ser*. **1984,** *247*, p 55.

(21) Jelinski, L. W.; Dumais, J. J.; Engel, A. K. *Macromolecules* **1983**, *16*, 492.

3.2 PB-*b*-PI-*b*-PEO and PE-*b*-PEP-*b*-PEO Triblock Copolymers

3.2.1 Synthesis and Characterization of ABC Triblock Copolymers with Two Different Crystalline End Blocks: Influence of Confinement on Crystallization Behavior and Morphology

Holger Schmalz[a], Armin Knoll[b], Alejandro J. Müller[c], and Volker Abetz[a*]

a) Makromolekulare Chemie II, Universität Bayreuth, 95440 Bayreuth, Germany
b) Physikalische Chemie II, Universität Bayreuth, 95440 Bayreuth, Germany
c) Grupo de Polímeros USB, Departamento de Ciencia de los Materiales, Universidad Simón Bolívar, Caracas 1080-A, Venezuela

ABSTRACT: The preparation of polyethylene-*block*-poly(ethylene-*alt*-propylene)-*block*-poly(ethylene oxide) (PE-*b*-PEP-*b*-PEO) triblock copolymers by homogeneous catalytic hydrogenation of the precursor poly(1,4-butadiene)-*block*-poly(1,4-isoprene)-*block*-poly(ethylene oxide) (PB-*b*-PI-*b*-PEO) triblock copolymers, which were synthesized by sequential anionic polymerization, is described. Thermal analysis using differential scanning calorimetry (DSC) reveals differences in the crystallization behavior of the PEO and PE blocks arising from different morphological confinements active during crystallization. If the PEO block is confined into isolated spherical or cylindrical microdomains, crystallization can only be induced by large supercoolings resulting from the vast number of microdomains (spheres or cylinders) compared to the number of available heterogeneities. In contrast, crystallization of PE proceeds via heterogeneous nucleation regardless of the composition, which can be attributed to the miscibility of PEP and PE segments in the melt. Transmission electron microscopy (TEM) and scanning force microscopy (SFM) have been used to investigate the influence of different confinements, active in PE-*b*-PEP-*b*-PEO triblock copolymers, on the formed morphology. In addition, temperature dependent imaging by hot-stage SFM measurements following the melting of PEO blocks and annealing of PE crystallites within a PE-*b*-PEP-*b*-PEO triblock copolymer will be presented.

Introduction

Crystallization within block copolymer microdomains is an issue which has attracted increasing interest in recent years mainly focusing on diblock copolymers. The structure development in semicrystalline block copolymers, especially those having microphase-separated melts, is enriched by the presence of two competing self organizing mechanisms: microphase separation and crystallization. Depending on the segregation strength in the melt, crystallization can be either confined in lamellar, cylindrical or spherical microdomains for strongly segregated systems, or crystallization predominates the structure formation for weakly segregated or homogeneous systems. Three competing physical events determine the final microphase and crystalline morphology in amorphous-semicrystalline block copolymers: the microphase separation in the melt (order-disorder transition temperature T_{ODT}), the crystallization temperature (T_c) of the crystallizable block, and the vitrification (glass transition temperature T_g) of the amorphous block. In general three different situations can be observed. In diblock copolymers exhibiting a homogeneous melt ($T_{ODT} < T_c > T_g$), microphase separation is driven by crystallization if T_g of the amorphous block is lower compared to T_c of the crystallizable block. This results in a lamellar morphology where crystalline lamellae are sandwiched by the amorphous block layers regardless of the composition, as was shown for polyethylene-*block*-poly(ethylene-*alt*-propylene) (PE-*b*-PEP)[1-3], poly(ethylene oxide)-*block*-poly(methyl methacrylate) (PEO-*b*-PMMA)[4] and low molecular weight polyethylene-*block*-poly(3-methyl-1-butene) (PE-*b*-PMB)[5] diblock copolymers. In weakly segregated systems ($T_{ODT} > T_c > T_g$, soft confinement) crystallization often occurs with little morphological constraint enabling a "breakout" from the ordered melt structure. As a consequence, crystallization overwrites any preexisting melt structure resulting in a lamellar structure, as was demonstrated for polyethylene-*block*-poly(ethyl ethylene) (PE-*b*-PEE)[3,6,7], polyethylene-*block*-poly(head-to-head propylene) (PE-*b*-hhPP)[8], low molecular weight polybutadiene-*block*-poly(ε-caprolactone) (PB-*b*-PCL)[9-11], poly(ethylene oxide)-*block*-poly(butylene oxide) (PEO-*b*-PBO)[12], PEO-*b*-PEE and PEO-*b*-PEP[13], low molecular weight polyethylene-*block*-poly(styrene-*ran*-ethylene-*ran*-butylene) (PE-*b*-P(SEB),[14] and PE-*b*-PMB[5,15] diblock copolymers. However, confinement of crystallization within spherical or cylindrical microdomains is possible in strongly segregated systems and/or for highly entangled amorphous blocks (high molecular weight)[5,10,11,14-20]. A strictly confined crystallization within microdomains is observed for strongly segregated diblock copolymers with a glassy amorphous block ($T_{ODT} > T_g > T_c$, hard confinement). The initially formed melt

structure is preserved upon crystallization which was observed for PS and PEO containing block copolymers (PS-*b*-PEO, PEO-*b*-PS-*b*-PEO)[16,21-30], as well as polyethylene-*block*-poly(vinyl cylcohexane) (PE-*b*-PVCH)[7,31-34], PS-*b*-PCL[35-38], PS-*b*-PE[39], polystyrene-*block*-polytetrahydrofuran (PS-*b*-PTHF)[40], PMMA-*b*-PTHF[41-44] and poly(*tert*-butyl methacrylate)-*block*-poly(ethylene oxide) (P*t*BMA-*b*-PEO)[45] diblock copolymers.

Crystallization within block copolymer microdomains is not only affected by the strength of confinement but also by the structure of the microdomain, i.e. continuous (gyroid, lamellae) or dispersed (cylinders, spheres), and even by the size of the microdomain. Chen et al.[46] observed for PB-*b*-PEO/PB blends with varying amount of PB homopolymer a decrease in T_c(PEO) with decreasing PEO-content (domain size). Whereas in the blend with a lamellar structure T_c(PEO) = 30 °C, a large supercooling was necessary to induce PEO crystallization within PEO cylinders (T_c = -25 °C) or spheres (T_c = -35 °C). Similar results were obtained for other block copolymers, exhibiting confined crystallization within isolated spherical or cylindrical microdomains.[16,17,19,21,24] Confined crystallization within microdomains is often connected with a substantial decrease in crystallinity compared to the case of the corresponding homopolymers due to spatial restrictions.[10,11,17,21,22,28,29,40,42] In contrast, for PE containing block copolymers the degree of crystallinity is independent of the type of microdomain and comparable with PE homopolymer, which might be attributed to the usually very thin PE crystals (d ≈ 5 nm).[32,34] Crystallization can even be suppressed if the crystallizable block is confined into spheres or cylinders.[37,40,42] Investigations on crystallization kinetics revealed a strong influence of the type of confinement on the observed crystallization behavior.[14,24,33,40,47] If the crystallizable block is strongly confined into spherical or cylindrical microdomains unusual first-order crystallization kinetics, e.g. the Avrami exponent n = 1, has been observed and related to a homogeneous nucleation mechanism.[14,33,47] However, in some special cases even lower Avrami exponents have been detected.[24,40]

The crystallization in polymers usually occurs by heterogeneous nucleation, homogeneous nucleation or self-nucleation. In semicrystalline homopolymers crystallization in the bulk usually occurs on heterogeneous nuclei (catalyst debris, impurities, and other types of heterogeneities of unknown nature). In block copolymers the type of nucleation strongly depends on the type of microstructure. Crystallization in large or continuous domains is mostly induced by heterogeneous nucleation, because the probability that a heterogeneity is located within the crystallizable domain is large. However, crystallization in small isolated microdomains (spheres, cylinders) either proceeds in a fractionated manner, i.e. several

crystallization exotherms are observed in DSC, or crystallization can only be induced by homogeneous nucleation.[16-19,21,24,25,40,46,48-52] Microdomains that contain the heterogeneities usually active at low supercoolings in the bulk polymer will crystallize at identical temperatures compared to the bulk polymer. If less efficient heterogeneities are present in the microdomain, a larger supercooling is necessary to induce crystallization. Those microdomains that do not contain any heterogeneity will only be able to nucleate homogeneously (if the interphase does not affect the nucleation process). Especially in block copolymers, where the crystallizable block is confined into small isolated microdomains (spheres, cylinders) the number density of isolated microdomains is significantly higher than the number of available heterogeneities, thus favoring homogeneous nucleation.[16]

Besides the vast number of publications on amorphous ABC triblock copolymers there have been only few publications on ABC triblock copolymers with crystallizable blocks. Among them are reports on PS-*b*-PB-*b*-PCL and their hydrogenated analogues (PS-*b*-PE-*b*-PCL), in which a complex interplay between microphase separation and crystallizability has been found.[49,50,53-59] In addition, there have been investigations on polystyrene-*block*-polyisoprene-*block*-poly(ethylene oxide) (PS-*b*-PI-*b*-PEO)[60-63], PS-*b*-PEP-*b*-PE[64,65], poly(α-methylstyrene)-*block*-polyisobutylene-*block*-polypivalolactone (P(α-MeS)-*b*-PIB-*b*-PVL)[66] and linear[21] as well as star shaped[67] PS-*b*-PEO-*b*-PCL triblock copolymers.

In this contribution we will describe the synthesis of novel crystallizable ABC triblock copolymers comprising two different semicrystalline end blocks, polyethylene and poly(ethylene oxide), and a rubbery amorphous middle block poly(ethylene-*alt*-propylene) (PE-*b*-PEP-*b*-PEO). The synthesis includes anionic synthesis of the precursor poly(1,4-butadiene)-*block*-poly(1,4-isoprene)-*block*-poly(ethylene oxide) (PB-*b*-PI-*b*-PEO) triblock copolymers followed by homogeneous catalytic hydrogenation to yield the corresponding PE-*b*-PEP-*b*-PEO triblock copolymers. The influence of different types of confinements on the crystallization of PE and PEO will be examined using differential scanning calorimetry (DSC). Morphological investigations will be presented including wide-angle X-ray diffraction (WAXD), transmission electron microscopy (TEM) and scanning force microscopy (SFM). In addition, melting of the PEO block and annealing of PE crystallites within a PE-*b*-PEP-*b*-PEO triblock copolymer upon heating will be investigated at different temperatures applying hot-stage SFM measurements.

Experimental Section

Synthesis. Solvents and monomers for anionic polymerization were purified according to common procedures described elsewhere.[64,68] The synthesis of poly(1,4-butadiene)-*block*-poly(1,4-isoprene)-*block*-poly(ethylene oxide) (PB-*b*-PI-*b*-PEO) triblock copolymers was accomplished by sequential anionic polymerization of butadiene, isoprene, and ethylene oxide in benzene at 60 °C for butadiene and isoprene, and 40 °C for ethylene oxide using *sec*-BuLi as initiator. Polymerization of ethylene oxide in the presence of a lithium counterion was realized by using the recently established strong phosphazene base *t*-BuP_4 (Fluka, 1 M in hexane, [*sec*-BuLi] : [*t*-BuP_4] = 1 : 1)[27,69-73] The reaction was completed after 3 days and terminated with a mixture of methanol/acetic acid (1/5 : v/v) followed by precipitation in methanol. In our notation ($A_xB_yC_z^m$), the subscript numbers denote the mass fraction in percent, and the superscript gives the number-averaged molecular weight M_n in kg/mol of the block copolymer.

Hydrogenation. The PE-*b*-PEP-*b*-PEO triblock copolymers were synthesized by hydrogenation of the corresponding precursor PB-*b*-PI-*b*-PEO triblock copolymers. Homogeneous catalytic hydrogenation was carried out in degassed toluene (1.5 – 2 wt-% solution of polymer) at 100 °C and 90 bar H_2 pressure for 3 - 4 days using Wilkinson catalyst (1 mol-% with respect to the number of double bonds). Under the used conditions the PB block gets completely hydrogenated and the PI block shows an almost complete saturation with ca. 1% residual double bonds as revealed by ^{1}H-NMR. Purification was accomplished by precipitation into cold acetone followed by further purification in order to remove residual Wilkinson catalyst by refluxing a toluene solution with a small amount of concentrated hydrochloric acid, again followed by precipitation into cold acetone. Further purification was necessary due to the strong tendency of PEO to bind residual Wilkinson catalyst. Alternatively, several triblock copolymers were hydrogenated using diimide, generated *in-situ* by thermolysis of *p*-toluenesulfonyl hydrazide (TSH, Fluka).[74] The triblock copolymers were purified by filtration over basic aluminum oxide in order to remove residual *p*-toluenesulfonic acid (thermolysis product of *p*-toluenesulfonyl hydrazide) followed by precipitation into cold acetone. This method resulted in a complete hydrogenation of the PB block, whereas the PI block exhibits a degree of hydrogenation of ca. 70%.

Size Exclusion Chromatography (SEC). SEC experiments were performed on a Waters instrument calibrated with narrowly distributed polystyrene standards at 30 °C.[64] Molecular weights of the PB precursors were calculated from the apparent values obtained by SEC using given K and α values for PS and PB resulting in the equation $M_n(PB) = 0.696\ M_n(PS)^{0.985}$ (Mark-Houwink-Sakurada relation).[75]

Differential Scanning Calorimetry (DSC). For thermal analysis a Perkin Elmer DSC 7 with a CCA 7 liquid nitrogen cooling device was used. For all measurements a two point calibration with decane and indium was applied. All experiments were performed at a scanning rate of 10 °C/min. The displayed heating traces correspond to the second heating run in order to exclude effects resulting from any previous thermal history of the samples. Due to the vicinity of the melting endotherms of PEO and PE (problems involved with definition of the baseline for the PE endotherm), the degree of crystallinity for the PE blocks was extracted from the heat of crystallization. The degree of crystallinity for the PEO blocks was determined from the heat of fusion.

Wide Angle X-ray Diffraction (WAXD). WAXD patterns were taken from a Bruker-AXS D8 Advance diffractometer equipped with a scintillation counter and a Goebel mirror using CuK_α radiation at room temperature. Sample preparation was accomplished by compression molding between PTFE plates at 140 °C followed by cooling to room temperature.

Transmission Electron Microscopy (TEM). The bulk morphology of PE-*b*-PEP-*b*-PEO triblock copolymers was examined by bright field TEM using a Zeiss CEM 902 electron microscope operated at 80 kV. Films (around 0.5 mm thick) were prepared by casting from a 3 wt-% solution in toluene at 70 °C in order to avoid gelation upon solvent evaporation. After complete evaporation of the solvent (ca. 1 week) the films were slowly cooled to room temperature to induce crystallization of the PE and PEO blocks followed by further drying under vacuum at 40 °C for 2 days. Thin sections were cut at -130 °C using a Reichert-Jung Ultracut E microtome equipped with a diamond knife. Staining of amorphous PEO and PEP segments was accomplished by exposure of the thin sections to RuO_4 vapor for 30 - 40 min. Because of local conformational constraints active at microdomain interphases (reduced density) a preferential staining of the PEO/PEP microdomain interphase is observed. For the triblock copolymer $E_{19}EP_{40}EO_{41}$[138], which has been synthesized by hydrogenation of the

corresponding PB-*b*-PI-*b*-PEO triblock copolymer using TSH, OsO_4 vapor was used as staining agent (exposure for 1 min). Here, the PEP block contains ca. 30% residual double bonds (see hydrogenation section), which can be selectively stained using OsO_4.

Scanning Force Microscopy (SFM). Scanning force microscopy images were taken on a Digital Instruments Dimension 3100 microscope operated in TappingMode™ (free amplitude of the cantilever ≈ 20 nm; set point ratio ≈ 0.95). Measurements were performed on thin films prepared on polished silicon wafers by dip- or spin-coating from a 2 wt-% solution of the triblock copolymer in toluene. For temperature dependent measurements a D3/D5 SPC01 hot stage from Digital Instruments was used.

Results and Discussion

Synthesis. The PE-*b*-PEP-*b*-PEO triblock copolymers were prepared by homogeneous catalytic hydrogenation of the corresponding PB-*b*-PI-*b*-PEO triblock copolymers.

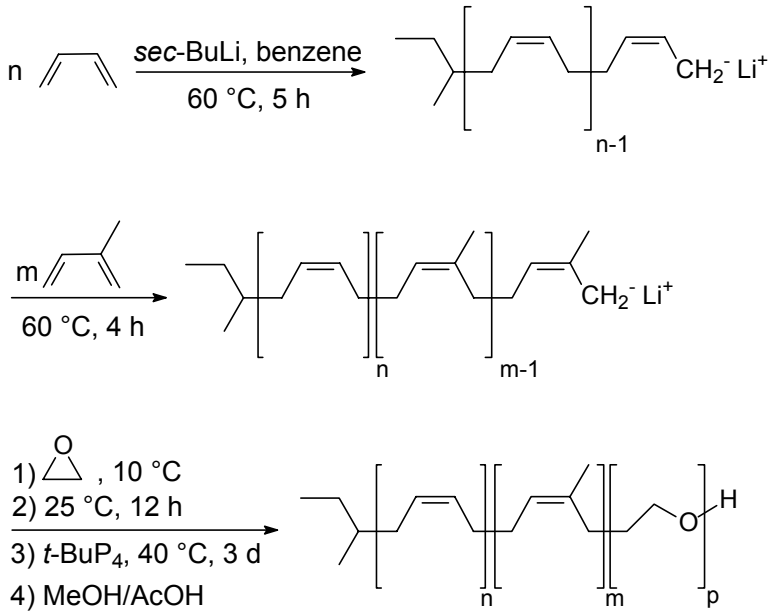

Scheme 1. Synthesis of poly(1,4-butadiene)-*block*-poly(1,4-isoprene)-*block*-poly(ethylene oxide) triblock copolymers (PB-*b*-PI-*b*-PEO) by sequential anionic polymerization.

The synthesis of PB-*b*-PI-*b*-PEO triblock copolymers was accomplished by sequential anionic polymerization of butadiene, isoprene, and ethylene oxide in benzene as depicted in Scheme 1. The polymerization of butadiene and isoprene in benzene at 60 °C leads to a preferentially 1,4-addition (Table 1), which especially for butadiene is indispensable to get the corresponding "pseudo polyethylene" structure after hydrogenation. Polymerization of ethylene oxide in the presence of a Li^+ counterion was realized using the recently established strong phosphazene base *t*-BuP_4. [27,69-73] SEC investigations (Figure 1) show that the reaction proceeds without any termination resulting in narrowly distributed PB-*b*-PI-*b*-PEO triblock copolymers (Table 1). Kinetic investigations on the ethylene oxide polymerization with sec-BuLi as initiator in the presence of the phosphazene base t-BuP_4 revealed the existence of an induction period.[76,77] As a result, reaction times of 2 – 3 days are necessary to get 100% conversion.

Table 1. Molecular Weight Characterization and Microstructure of PB-*b*-PI-*b*-PEO Triblock Copolymers

Triblock Copolymer	M_n[a] [kg/mol]	M_w/M_n[b]	PB-block[c]		PI-block[c]		
			%1,4	%1,2	%1,4	%1,2	%3,4
$B_{24}I_{56}EO_{20}^{67}$	67.3	1.01	89	11	88	6	6
$B_{11}I_{70}EO_{19}^{120}$	120	1.01	88	12	92	4	4
$B_{17}I_{57}EO_{26}^{130}$	130	1.01	89	11	92	4	4
$B_{19}I_{39}EO_{42}^{135}$	135	1.02	89	11	92	4	4

[a] Determined by ^{1}H-NMR spectroscopy using the molecular weight of the PB precursor obtained by SEC in THF calibrated against PS standards; for PB the molecular weight was calculated from the apparent value obtained by SEC using the equation $M_n(PB) = 0.696\ M_n(PS)^{0.985}$.

[b] Determined by SEC in THF calibrated against PS standards.

[c] Determined by ^{1}H-NMR spectroscopy in $CDCl_3$.

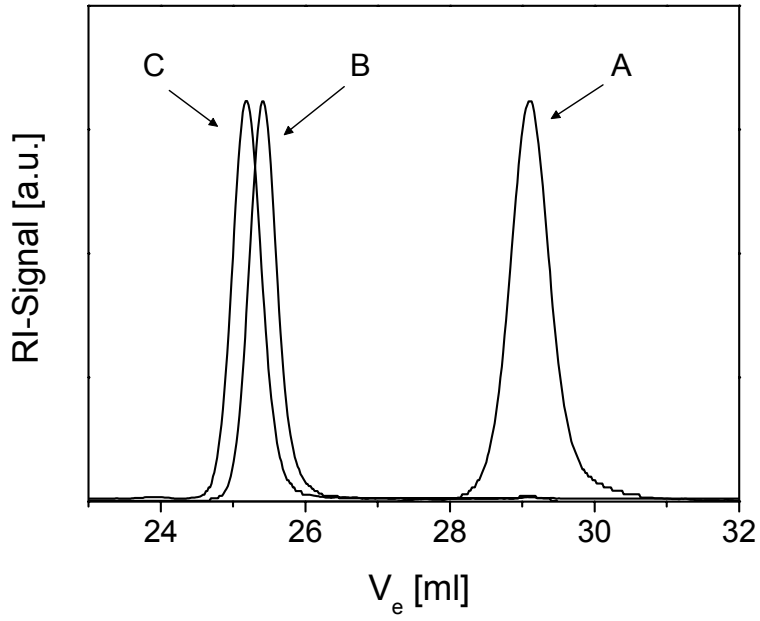

Figure 1. SEC traces of a synthesized PB-*b*-PI-*b*-PEO (C) triblock copolymer including the PB (A) and PB-*b*-PI (B) precursors, using THF as eluent and toluene as internal standard.

Homogeneous catalytic hydrogenation was carried out in toluene using Wilkinson catalyst $(Ph_3P)_3Rh(I)Cl$ (Scheme 2). The efficiency of the hydrogenation reaction was verified by ^{1}H-NMR spectroscopy showing a complete hydrogenation of the PB block and an almost complete saturation of the PI block with $\leq$ 1% residual double bonds (results not shown). For several triblock copolymers an alternative hydrogenation method was applied using *p*-toluenesulfonyl hydrazide (TSH). Using this method, a complete saturation of the PB block can be achieved, whereas the PI block exhibits a degree of hydrogenation of only ca. 70% due to sterical hindrance involved in the hydrogenation reaction.

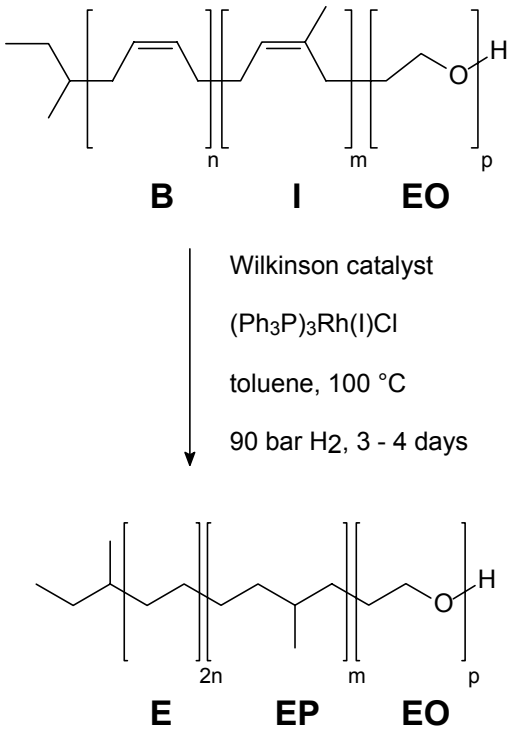

Scheme 2. Synthesis of PE-*b*-PEP-*b*-PEO triblock copolymers via homogeneous catalytic hydrogenation of the corresponding PB-*b*-PI-*b*-PEO triblock copolymers using Wilkinson catalyst.

Differential Scanning Calorimetry: PB-*b*-PI-*b*-PEO. Table 2 summarizes the thermal properties of the PB-*b*-PI-*b*-PEO and the corresponding hydrogenated PE-*b*-PEP-*b*-PEO triblock copolymers. The PB-*b*-PI-*b*-PEO triblock copolymers exhibit a glass transition temperature at ≈ –70 °C corresponding to a mixed phase of PB and PI. Consequently, the PB-*b*-PI-*b*-PEO triblock copolymers might be considered as diblock copolymers consisting of a PEO phase and a mixed PB/PI phase. The PEO blocks display a melting endotherm at approximately 60 – 66 °C and a degree of crystallinity of $\alpha \approx$ 70 – 85%, whereby the melting temperature increases with increasing PEO content (Figure 2A, Table 2). The degree of crystallinity was calculated assuming a heat of fusion for PEO of ΔH_m^0 = 196.6 J/g.[78] The crystallization of PEO occurs in all triblock copolymers with PEO contents < 30 wt-% at about -20 °C. However, the triblock copolymer with 26 wt-% PEO exhibits an additional small exotherm at 16 °C (Table 2, Figure 2B). From composition, a cylindrical PEO microstructure might be assumed and has been observed in the corresponding hydrogenated triblock copolymer $E_{18}EP_{57}EO_{25}$[133] (see discussion on $E_{18}EP_{57}EO_{25}$[133], Figure 4A). Thus, the high temperature exotherm (T_c = 16 °C) might be attributed to heterogeneous crystallization of PEO within interconnected PEO cylinders, and the low temperature exotherm (T_c = -21 °C)

to crystallization within isolated cylinders. In general, the crystallization exotherm exhibits a slight shift to higher temperatures with increasing PEO content and/or molecular weight of the PEO block. The observed crystallization temperatures in PB-*b*-PI-*b*-PEO triblock copolymers with PEO contents < 30 wt-% are significantly lower compared to the values observed in PEO homopolymer ($T_c \approx$ 40 °C).[16] This is a direct result from the vast number density of PEO microdomains ($\approx 10^{16}$ spheres/cm^3 or $\approx 10^{14}$ cylinders/cm^3) for $B_{11}I_{56}EO_{19}$[120] assuming a spherical (d ≈ 20 nm, see SFM section) or cylindrical microstructure (expecting an average length of 1μm for the PEO cylinders) compared to the number density of heterogeneous nuclei usually present in PEO homopolymers ($\approx 10^5$ nuclei/cm^3, for a spherulite radius of 100 μm[46]).[16] Similar results have been observed by Chen et al. for PB-*b*-PEO/PB blends.[46] The authors found that the crystallization temperature strongly depends on the volume of the dispersed PEO phase. If the PEO blocks are confined into cylinders crystallization occurs at approximately -25 °C, and for PEO spheres the crystallization temperature shifts to even lower temperatures (≈ -34 °C).

As a consequence of confinement, crystallization cannot proceed via heterogeneous nucleation, which is reflected in the observed large supercoolings necessary for crystallization in PB-*b*-PI-*b*-PEO triblock copolymers (PEO content < 30 wt-%). However, the crystallization temperatures observed for homogeneous nucleation in other PEO containing block copolymers ($T_c \approx$ -40 °C)[21] are significantly smaller than the observed values. Accordingly, the observed crystallization behavior cannot be attributed to a homogeneous nucleation mechanism. Self nucleation experiments show that domain II (self-nucleation domain) is completely absent for the PEO block in PB-*b*-PI-*b*-PEO triblock copolymers (PEO content < 30 wt-%).[79] Thus, nucleation induced by less efficient heterogeneities can be excluded and the observed crystallization behavior might be attributed to a nucleating property of the microdomain interphase. A similar result was obtained in self-nucleation experiments on the hydrogenated triblock copolymer $E_{24}EP_{57}EO_{19}$[69].[16]

Table 2. DSC Data for PB-*b*-PI-*b*-PEO and PE-*b*-PEP-*b*-PEO Triblock Copolymers[a]

Triblock Copolymer[b]	T_g [°C]	T_m(PEO) [°C]	T_{c1}(PEO)[c] [°C]	T_{c2}(PEO) [°C]	α(PEO) [%]	T_m(PE) [°C]	T_c(PE) [°C]	α(PE) [%]
$B_{24}I_{56}EO_{20}^{67}$	-69.5[d]	60.5	-23.9	-	84.5	-	-	-
$B_{11}I_{70}EO_{19}^{120}$	-65.9[d]	60.0	-22.2	-	71.4	-	-	-
$B_{17}I_{57}EO_{26}^{130}$	-67.5[d]	63.2	-21.0 (83)	16.1	70.4	-	-	-
$B_{19}I_{39}EO_{42}^{135}$	-68.7[d]	65.9	-25.0 (2)	37.5/19.8	77.8	-	-	-
$E_{24}EP_{57}EO_{19}^{69}$ (5.8)	-57.4	58.9	-26.4	-	80.2	93.4	66.5	27.4
$E_{11}EP_{71}EO_{18}^{123}$ (6.4)	-56.4	59.7	-25.4	-	65.0	89.0	50.0	38.1
$E_{11}EP_{71}EO_{18}^{123}$ [e]	-59.1	60.8	-25.3	-	70.3	89.6	53.5	37.9
$E_{18}EP_{57}EO_{25}^{133}$ (5.8)	-56.8	60.0	-21.1 (4)	26.8	56.9	92.9	64.6	21.2
$E_{19}EP_{40}EO_{41}^{138}$ (5.8)	-57.1	63.9	-24.0 (6)	37.6/23.6	72.1	94.4	69.4	20.3
$E_{19}EP_{40}EO_{41}^{138}$ [e]	-59.3	64.8	-22.6 (1)	39.0/22.6	69.9	94.0	71.4	19.8

[a] T_m = melting point of corresponding block (peak maximum), T_c = crystallization temperature of corresponding block (peak maximum), α = degree of crystallinity, and T_g = glass transition temperature.
[b] values in brackets give the content of ethyl branches within the PE block in mol-%.
[c] values in brackets give the fraction of crystallinity (in %).
[d] glass transition temperature of the mixed PB/PI phase.
[e] triblock copolymer was hydrogenated using *p*-toluenesulfonyl hydrazide.

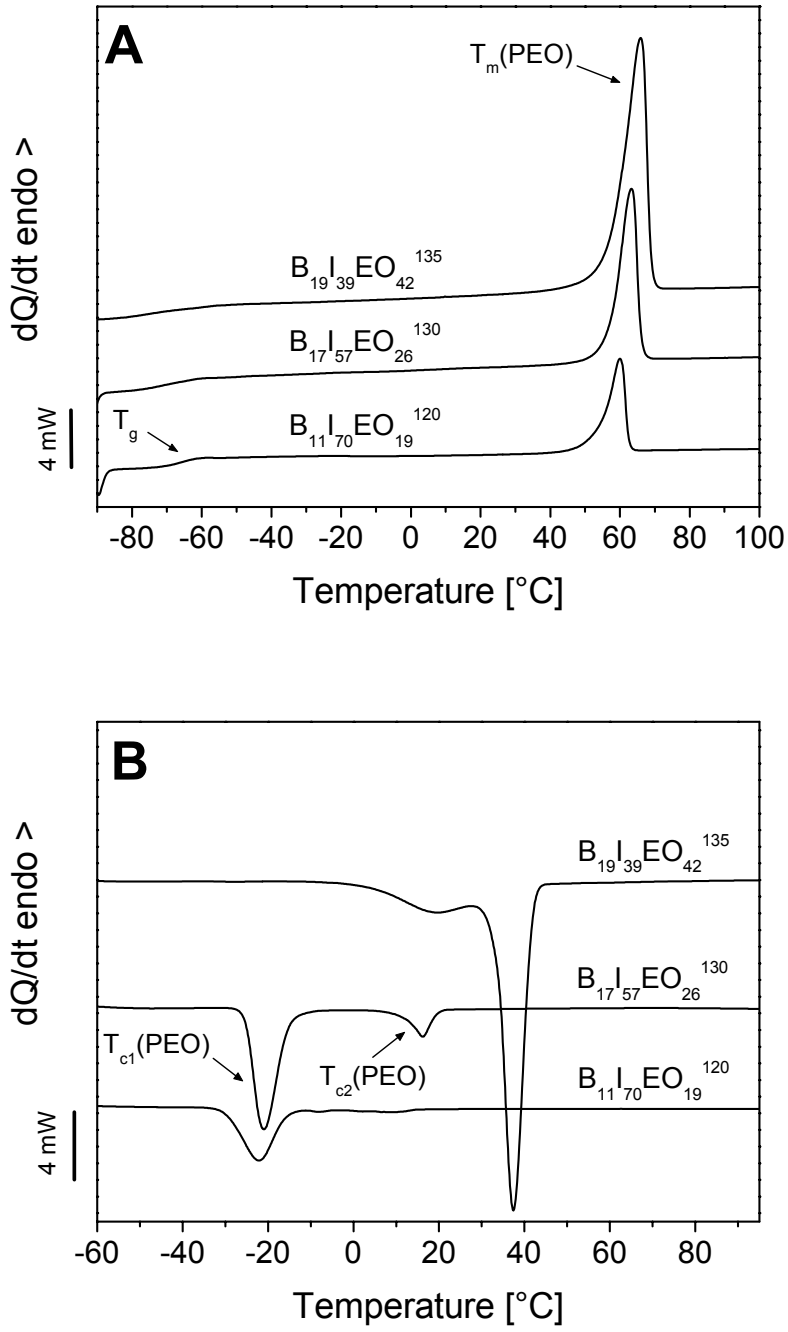

Figure 2. DSC heating (A) and cooling (B) traces for several PB-*b*-PI-*b*-PEO triblock copolymers.

In $B_{19}I_{39}EO_{42}^{135}$ the PEO blocks exhibit peak crystallization temperatures at 37 and 20 °C, which are close to the values observed in PEO homopolymer (Table 2, Figure 2B). From composition a lamellar domain structure might be expected, and has been observed by TEM investigations exhibiting crystalline PEO lamellae within a matrix of the miscible PB and PI segments (results no shown). However, a cylindrical microphase cannot completely be excluded due to uncertainties involved in the staining technique and problems involved in the

preparation of thin sections (cutting artefacts) due to the very soft samples (see also discussion on the corresponding hydrogenated triblock copolymer). The observation of a double exotherm might be attributed to crystallization within interconnected (higher T_c) and isolated (lower T_c) PEO lamellae, as was also concluded from the occurrence of a double exotherm in lamellar PE-*b*-PVCH diblock copolymers.[33] In conclusion, crystallization of PEO within $B_{19}I_{39}EO_{42}$[135] occurs with little morphological restrictions within lamellar PEO microdomains via heterogeneous nucleation.

PE-*b*-PEP-*b*-PEO. Any effects on the crystallization behavior of the PE-*b*-PEP-*b*-PEO triblock copolymers arising from residual Wilkinson catalyst could be excluded due to the applied purification procedure. The influence of Wilkinson catalyst debris on the crystallization of PEO is discussed elsewhere.[79] The PE-*b*-PEP-*b*-PEO triblock copolymers show melting endotherms for PE and PEO indicating microphase separation even for low molecular weights, which in the case of PE is induced by crystallization (Table 2, Figure 3A). Because of the small segmental interaction parameter χ of 0.007 at 120 °C for PE and PEP[80], crystallization of PE is expected to occur from a homogeneous mixture of PE and PEP segments.[1-3,81] In contrast, crystallization of the strongly incompatible PEO segments is confined into microphase-separated PEO domains.

The crystallization behavior of the PEO block within purified PE-*b*-PEP-*b*-PEO triblock copolymers is comparable to that discussed for the corresponding PB-*b*-PI-*b*-PEO triblock copolymers (Table 2). Crystallization of PEO in $E_{18}EP_{57}EO_{25}$[133] occurs nearly completely at 27 °C, whereas in the corresponding $B_{17}I_{57}EO_{26}$[130] triblock copolymer the major fraction of PEO crystallizes at -21 °C (Table 2, Figure 2B, 3B). Since effects from catalyst residues can be excluded, this effect might be attributed to differences in the cylindrical PEO microdomain structure, i.e. strongly interconnected PEO cylinders in $E_{18}EP_{57}EO_{25}$[133] favoring heterogeneous nucleation. Figure 4A shows the corresponding TEM micrograph obtained by staining a thin section of the sample with RuO_4 vapor. Thin sections were cut from a film cast from toluene solution at 70 °C, followed by slowly cooling to room temperature in order to induce crystallization of PE and PEO. The PEO blocks exhibit a distorted cylindrical structure (both top and side view of PEO cylinders visible), and interconnections between different PEO cylinders are clearly visible. Because of the used staining technique the interphase between PEO cylinders and the PEP matrix gets preferentially stained. This results in the visible dark shadow surrounding the PEO cylinders, whereby the PEP matrix appears only slightly gray. Furthermore, the PEO cylinders are obviously subdivided into small spherical

domains. These subdomains might be attributed to stacks of several PEO crystallites within the cylindrical PEO domains. One restriction of the used staining technique is the fact, that the crystalline PE domains, which are expected to be located within the PEP matrix, cannot be visualized.

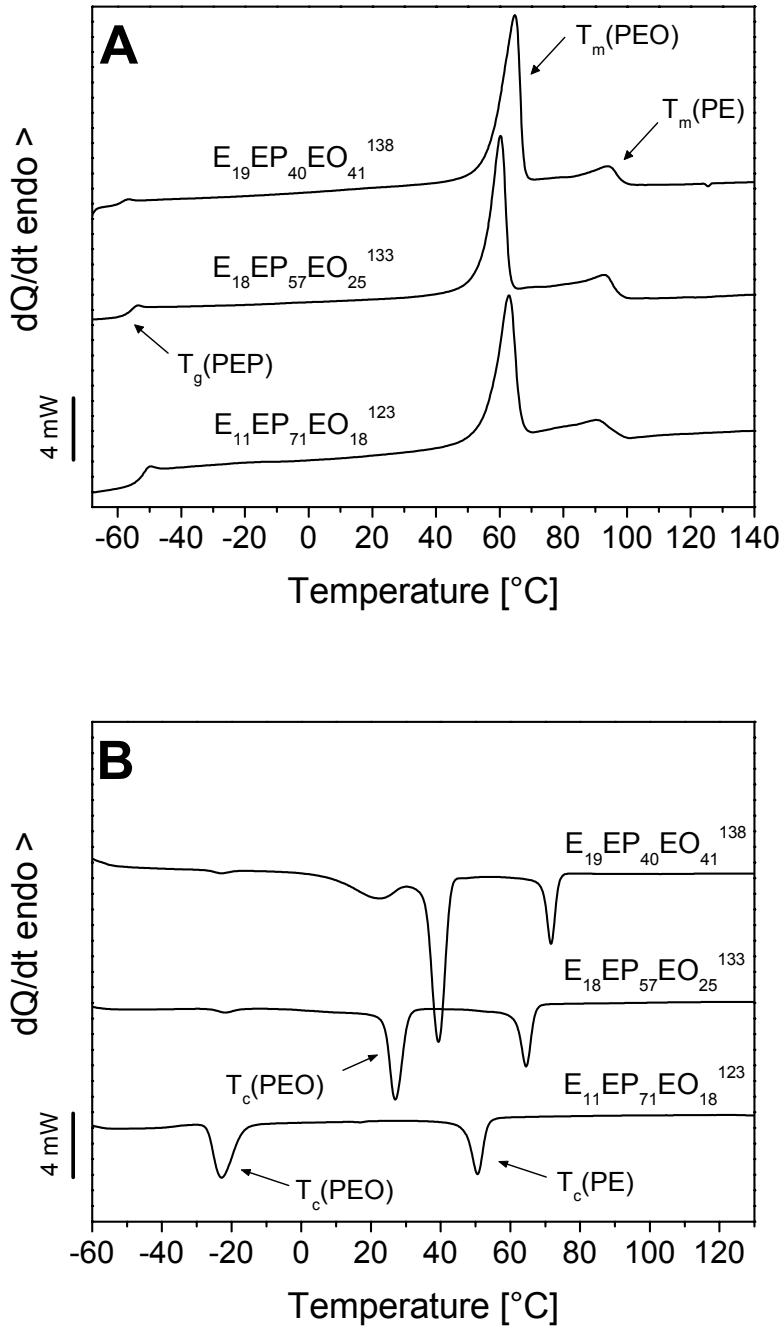

Figure 3. DSC heating (A) and cooling (B) traces for several PE-*b*-PEP-*b*-PEO triblock copolymers.

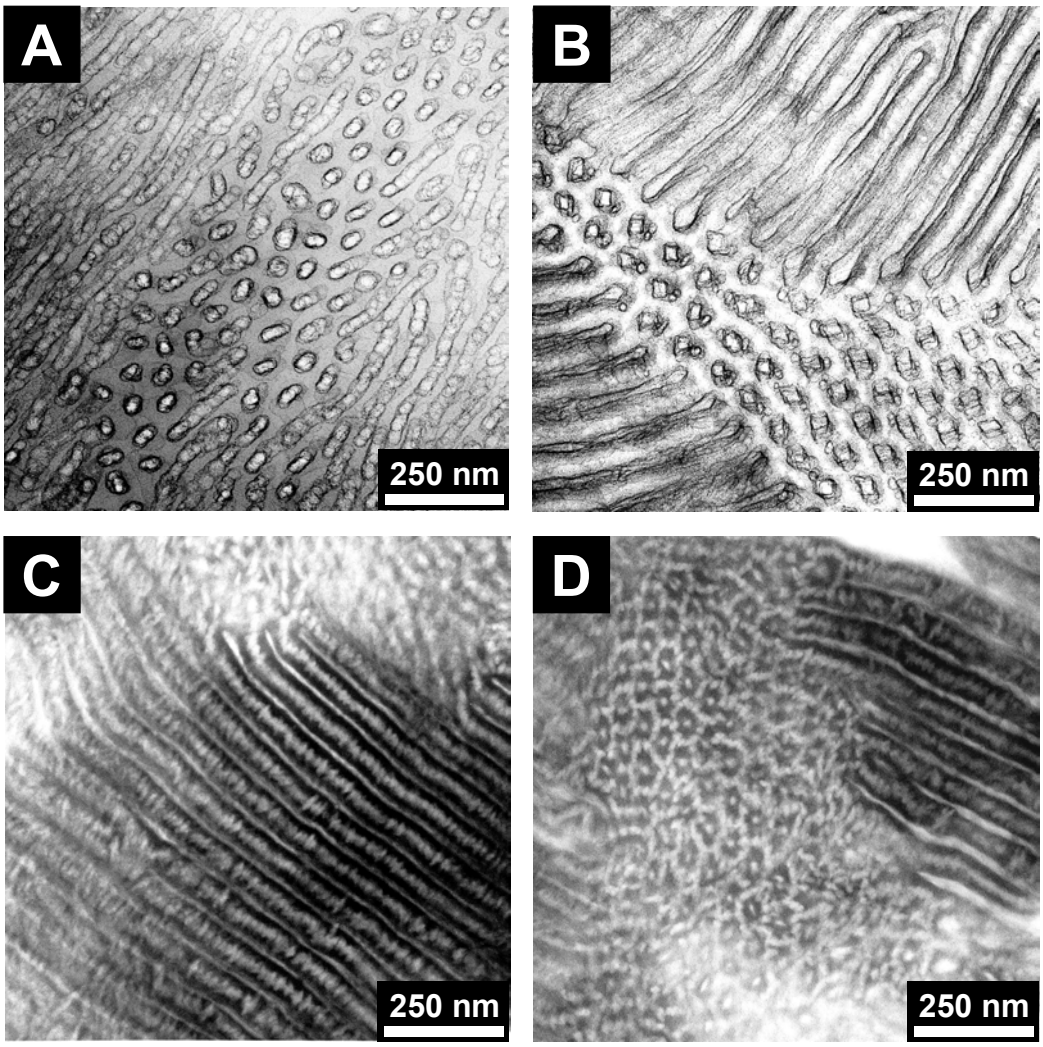

Figure 4. TEM micrographs of $E_{18}EP_{57}EO_{25}$[133] (A, RuO_4 staining), $E_{19}EP_{40}EO_{41}$[138] hydrogenated using Wilkinson catalyst (B, RuO_4 staining); and $E_{19}EP_{40}EO_{41}$[138] hydrogenated with TSH (C and D, OsO_4 staining).

The triblock copolymer $E_{19}EP_{40}EO_{41}$[138] exhibits a double exotherm for PEO which is in line with the observations in the corresponding $B_{19}I_{39}EO_{42}$[135] triblock copolymer (Table 2, Figure 2B and 3B). TEM investigations of the completely hydrogenated $E_{19}EP_{40}EO_{41}$[138] (hydrogenation with Wilkinson catalyst) show a cylindrical microdomain structure for the PEO blocks (Figure 4B). TEM investigations with lower magnifications show that the PEO cylinders can extent over several μm (results not shown). In contrast to the non-hydrogenated analogue showing a lamellar structure, the increased segregation strength in the hydrogenated triblock copolymer and the presence of a second crystalline block (PE) might be responsible for the change in the PEO microdomain structure. From the PEO cylinders, oriented perpendicular to the plane of observation, it can be deduced that the PEO cylinders exhibit a rectangular shape rather than a spherical shape, which might be attributed to the fact that the

PEO cylinders are semicrystalline. However, due to the staining technique (RuO_4 vapor) the crystalline PE domains cannot be visualized, as only the interphase between PEO cylinders and the PEP matrix gets preferentially stained (compare with Figure 4A).

As mentioned before, hydrogenation using *p*-toluenesulfonyl hydrazide results in an incomplete hydrogenation of the PI blocks within $B_{19}I_{39}EO_{42}$[135]. The residual double bonds in the PEP blocks of the hydrogenated $E_{19}EP_{40}EO_{41}$[138] triblock copolymer can be selectively stained with OsO_4 vapor. Figures 4C and 4D show TEM micrographs for $E_{19}EP_{40}EO_{41}$[138], prepared by hydrogenation with *p*-toluenesulfonyl hydrazide. In Figure 4C a projection along the thin white appearing PEO cylinders is shown. The fraction of PEO is apparently smaller as compared to Figure 4B. This might be attributed to the fact that only the crystalline PEO domains are visible, as the amorphous PEO segments get stained by OsO_4, too. Within the selectively stained PEP matrix (dark gray color) small white appearing domains are visible which are oriented perpendicular to the long direction of the PEO cylinders. This phase can be attributed to PE crystallites, as crystallization of PE occurs from a homogeneous mixture of PEP and PE segments. The TEM image in Figure 4D shows a projection perpendicular to the PEO cylinder axis. From this image it can be extracted, that PE crystallization is templated by the strongly segregated PEO cylinders, resulting in a hexagonally array of PE crystallites surrounding the PEO cylinders. Furthermore, the PE crystallites are apparently interconnected and form a continuous crystalline PE phase within the PEP matrix.

The PE block in PE-*b*-PEP-*b*-PEO triblock copolymers exhibits a melting temperature at approximately 90 °C and a degree of crystallinity between 20 and 38% (Table 2). The degree of crystallinity was calculated using the heat of fusion for a 100% crystalline PE of ΔH_m^0 = 276.98 J/g.[75] The DSC traces in Figure 3A display a relatively broad melting endotherm for the PE block reflecting a broad crystallite size distribution. The latter may arise from the ethyl branches within the PE block originating from the approximately 11% 1,2-units in the corresponding PB block of the non-hydrogenated triblock copolymer precursors (Table 1). PE-*b*-PEP-*b*-PEO triblock copolymers with ca. 20 wt-% PE exhibit crystallization temperatures at about 65 to 72 °C (Table 2, Figure 3B) reflecting a heterogeneous nucleation mechanism, since the observed values are very close to the crystallization temperature of ca. 73 °C observed in a hydrogenated polybutadiene with a similar content of ethyl branches.[16] However, the triblock copolymer $E_{11}EP_{71}EO_{18}$[123] exhibits a comparatively lower melting and crystallization temperature for the PE block. This might be attributed on one hand to the higher amount of ethyl branches in the PE block (Table 2),

resulting in thinner crystallites (lower T_m), and on the other hand to a slightly decreased segregation strength of the PE and PEP segments arising from the lower PE-content (lower T_c). Self-nucleation measurements on the PE block in PE-*b*-PEP-*b*-PEO triblock copolymers show that for all samples domain II (self-nucleation domain) is present, strongly underlining a heterogeneous nucleation mechanism.[79] In conclusion, crystallization of PE within PE-*b*-PEP-*b*-PEO triblock copolymers is induced by heterogeneous nucleation, even for very small PE contents (11 – 24 wt-%). In contrast to the confined crystallization of PEO within isolated microdomains (for low PEO contents), crystallization of PE occurs without confinement from a homogeneous mixture of PE and PEP segments, thus enabling heterogeneous nucleation.

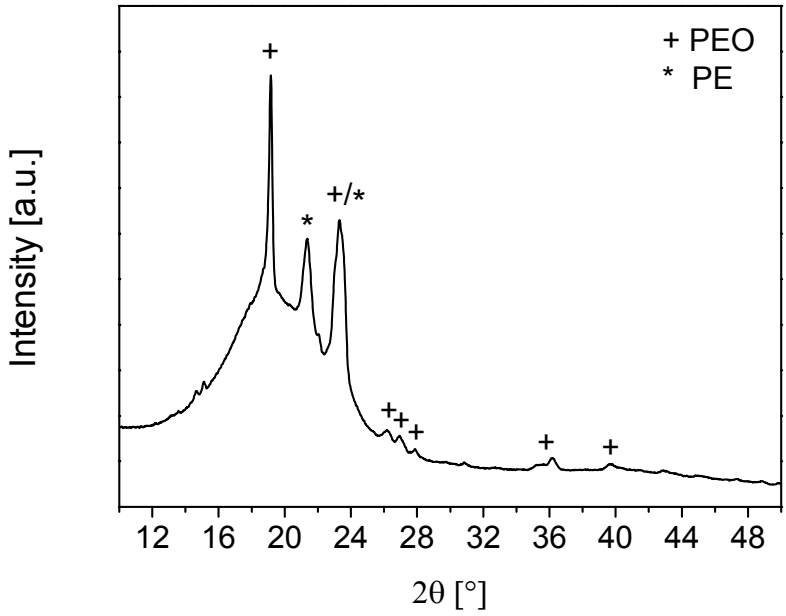

Figure 5. WAXD-pattern obtained for $E_{19}EP_{40}EO_{41}$[138] exhibiting reflex positions attributable to a triclinic modification of PEO and a orthorhombic modification of PE.

Wide Angle X-ray Diffraction (WAXD). To gain more insight into the crystal structure of the crystalline PE and PEO domains wide angle X-ray diffraction has been used. Figure 5 shows the diffraction pattern obtained for $E_{19}EP_{40}EO_{41}$[138]. The reflex positions at $2\theta = 19$, 23, $\approx$ 27, 36 and 40° reveal crystallization of PEO in its triclinic modification[82], which has also been observed for PS-*b*-PEO and PS-*b*-PEO-*b*-PCL block copolymers.[21] PE usually shows an orthorhombic crystal structure with corresponding reflex positions at 2θ = 21 and 24°.[34,83] Comparison with Figure 5 reveals a reflex position at $2\theta = 21°$ corresponding to PE in its orthorhombic modification, whereas the second reflex position at $2\theta = 24°$ is

superimposed with a reflex arising from the PEO crystals. In conclusion, WAXD shows that the PE and PEO blocks within PE-*b*-PEP-*b*-PEO triblock copolymers form well organized crystals exhibiting an orthorhombic and a triclinic crystal structure, respectively.

Scanning Force Microscopy (SFM). The influence of different confinements, being active during PE and PEO crystallization, on the formed morphology can be visualized using scanning force microscopy. The large differences in stiffness between amorphous and crystalline domains makes SFM a superior tool for investigating semicrystalline-amorphous block copolymers, without the need of special sample preparations. Most SFM investigations have been performed on crystallizable homopolymers[84-98] or semicrystalline-amorphous diblock copolymers[18,99-101], whereas only few reports concern the crystallization within semicrystalline ABC triblock copolymers.[59,64]

Figures 6A and 6B show the SFM topography and phase contrast images of $E_{11}EP_{71}EO_{18}$[123], respectively, prepared by dip-coating from a 2 wt-% solution of the triblock copolymer in toluene. Three different phases can be distinguished from the phase contrast image (Figure 6B). The bright appearing elongated domains correspond to crystalline PE lamellae viewed edge on, which are embedded in an amorphous matrix of the less bright appearing PEP blocks (hard materials usually induce a higher phase shift compared to soft materials). The PE crystallites are also clearly visible in the corresponding topography image (Figure 6A). Due to the miscibility of molten PE and PEP segments there is no confinement active during crystallization of PE. This results in the observed randomly distributed and strongly interconnected PE crystallites. Upon solvent evaporation during the dip-coating process first the PE segments start to crystallize from the homogeneous solution due to the low solubility of PE in toluene. This results in the formation of the observed continuous crystalline PE phase.

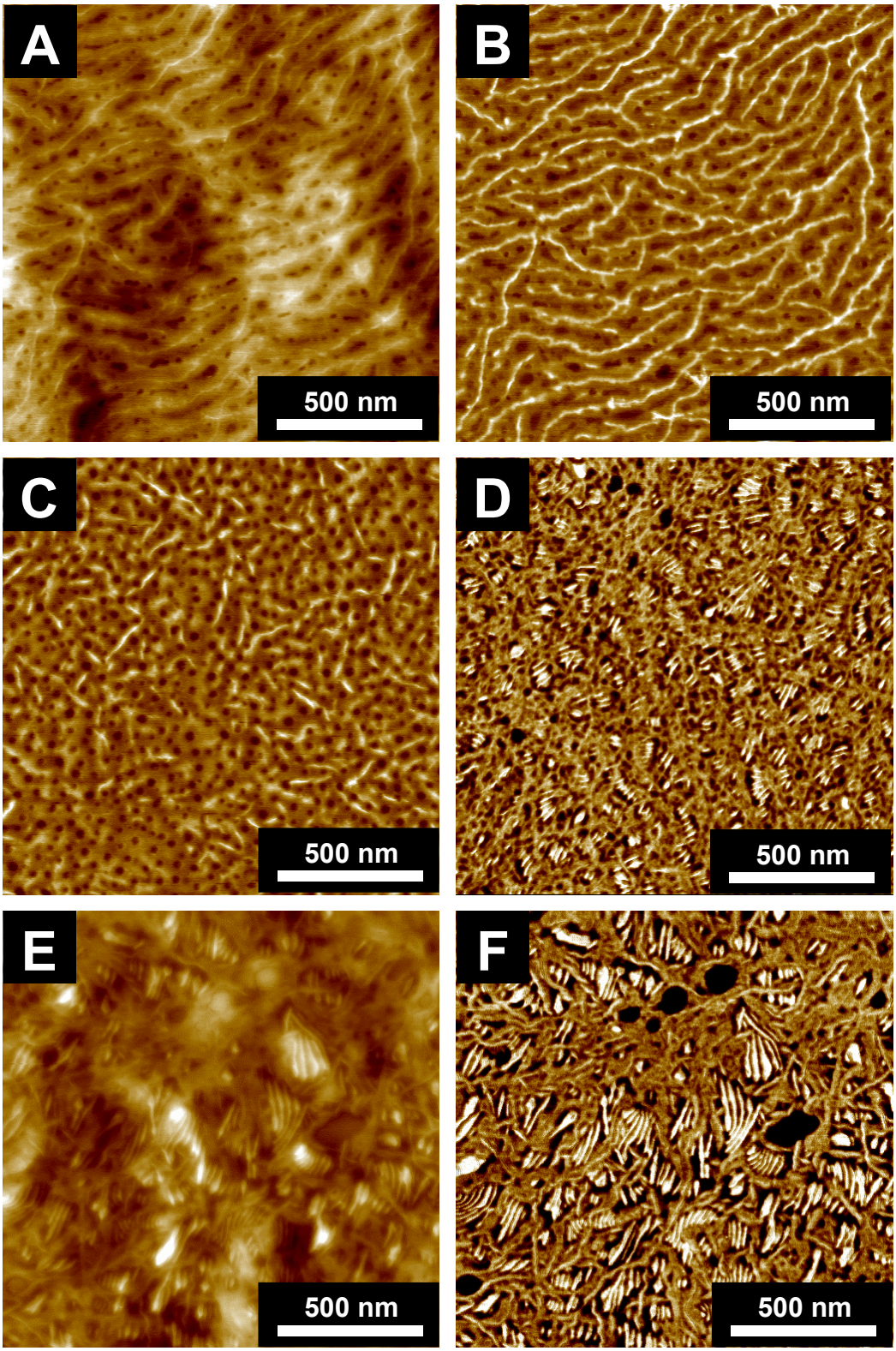

Figure 6. SFM topography and phase contrast images for $E_{11}EP_{71}EO_{18}$[123] (A, z = 20 nm; B, z = 15°; C, z = 20°: prepared from a warm toluene solution (≈ 40 °C)), and $E_{19}EP_{40}EO_{41}$[138] before (D, z = 20°) and after annealing at 91 °C for 5 min (E, z = 60 nm; F, z = 20°).

This assumption is underlined by the observation that higher concentrated solutions (3 - 4 wt-%) of the triblock copolymer form gels in toluene or o-xylene solutions at room temperature. As the PEO blocks are not able to crystallize at room temperature (Table 2, Figure 3B) this observation can only be explained by the formation of a continuous crystalline PE phase in the solution. Rheological investigations on a 3.6 wt-% solution of $E_{11}EP_{71}EO_{18}$[123] in o-xylene reveal a gel point at ca. 49 °C upon heating attributed to the melting of interconnected PE crystallites, which in turn results in a breakup of the physical network (results not shown). In addition, a third phase can be detected in the phase contrast image (Figure 6B). The dark appearing (low phase shift) spherical domains located in between the crystalline PE lamellae, which correspond to the dark spherical domains in the topography image (Figure 6A) can be attributed to amorphous PEO domains, as the PEO blocks are not able to crystallize at room temperature (Table 2, Figure 3B).

Since the formation of a continuous crystalline PE phase is induced by the gelation of the solution upon solvent evaporation in the dip-coating process, a thin film of $E_{11}EP_{71}EO_{18}$[123] was prepared by dip-coating from a warm toluene solution (≈ 40 °C). As can be seen from the corresponding phase contrast image (Figure 6C), the crystalline PE lamellae (bright appearing domains) are more isolated and exhibit smaller lengths as compared to Figure 6B. Moreover, the morphology appears more ordered as can be seen from the homogeneously distributed spherical PEO microdomains. With respect to the composition (18 wt-% PEO) PEO spheres or cylinders might be expected. The phase contrast image (Figure 6C) strongly suggests a spherical microdomain structure for the PEO block exhibiting an average diameter of 20 - 25 nm. However, cylindrical PEO microdomains cannot be excluded, as cylinders aligned perpendicular to the substrate surface would also result in the observation of an apparently spherical microdomain structure.

Increasing the PEO content to 41 wt-% in $E_{19}EP_{40}EO_{41}$[138] results in a completely different morphology with respect to the PEO domains as depicted in the corresponding phase contrast image (Figure 6D). Here the PEO blocks are able to crystallize at room temperature (T_c = 38 °C, Table 2). This results in a white appearing (high phase shift) PEO phase consisting of several stacks of crystalline PEO lamellae (viewed edge on), which are located in between the less bright appearing continuous crystalline PE phase. Figures 6E and 6F show the topography and phase contrast images of the same film, subjected to an annealing at 91 °C for 5 min, followed by cooling at a constant rate of –5 °C/min to room temperature. At 91 °C the PEO blocks are completely molten (Table 2, Figure 3A), whereas the PE blocks show annealing as revealed by DSC measurements (results not shown)[79]. Large PE crystallites grow

at the expense of smaller, less stable crystallites and surrounding molten PE segments, resulting in a more uniform crystallite size distribution without destroying the continuous crystalline PE structure, as is demonstrated by the corresponding phase contrast image (Figure 6F). Upon cooling from 91 °C the PEO blocks crystallize under the spatial confinement of the existing continuous crystalline PE phase. A comparison with the film prior to annealing (Figure 6D) reveals that the crystalline PEO domains are significantly larger and the crystallites exhibit a higher lateral extension when the PEO blocks are allowed to crystallize from the melt.

We have followed the morphological changes upon melting of the PEO blocks and annealing of the PE blocks in $E_{19}EP_{40}EO_{41}$[138] by hot-stage SFM measurements. Figure 7 shows phase contrast images of a thin film of $E_{19}EP_{40}EO_{41}$[138], prepared by spin-coating from a 2 wt-% solution of the triblock copolymer in toluene, taken at the same spot of the film at different temperatures upon heating. At 42.7 °C, a temperature well below the melting transition of the PEO and PE blocks (Table 2, Figure 3A), the crystalline PEO and PE domains are clearly visible (Figure 7A). It should be noted that the crystalline PE domains are expected to consist of several PE crystallites with different thickness, as from DSC a broad crystallite size distribution, reflected by the broad melting transition, can be derived (Figure 3A). However, it is not possible to resolve the resulting lamellar fine structure within the PE domains at this point due to the broad crystallite size distribution. Upon heating to 60.1 °C partial melting of the PEO block starts, as can be derived from the corresponding heating trace (Figure 3A). As a consequence, the average size of crystalline PEO domains decreases, which can be deduced from the comparison of the phase contrast images taken at 42.7 °C and 60.1 °C (circles in Figures 7A and 7B). At this temperature comparatively small crystallites are already completely molten as depicted by the arrows in Figures 7A and 7B.

A further increase in temperature to 65.7 °C, a temperature above the observed maximum in the melting transition (T_m = 64.8 °C, Table 2), results in a complete melting of PEO crystallites, and only the crystalline PE domains (T_m = 94 °C, Table 2) remain as depicted in Figure 7C. Further heating is connected with an annealing of PE crystallites which has been derived from self-nucleation experiments (results not shown)[79], i.e. larger crystallites grow at the expense of smaller, less stable crystallites or surrounding molten PE segments. Figure 7D shows the phase contrast image taken at 88.7 °C, a temperature revealing a large extent of annealing processes. Comparison with the phase contrast image taken at 65.7 °C (circle in Figure 7C) exhibits a significant change in the structure of the continuous crystalline PE phase. The lamellar fine structure within larger PE domains is now clearly visible. As a

result of reorganization during annealing, the PE crystallites exhibit an almost uniform thickness (Figure 7D).

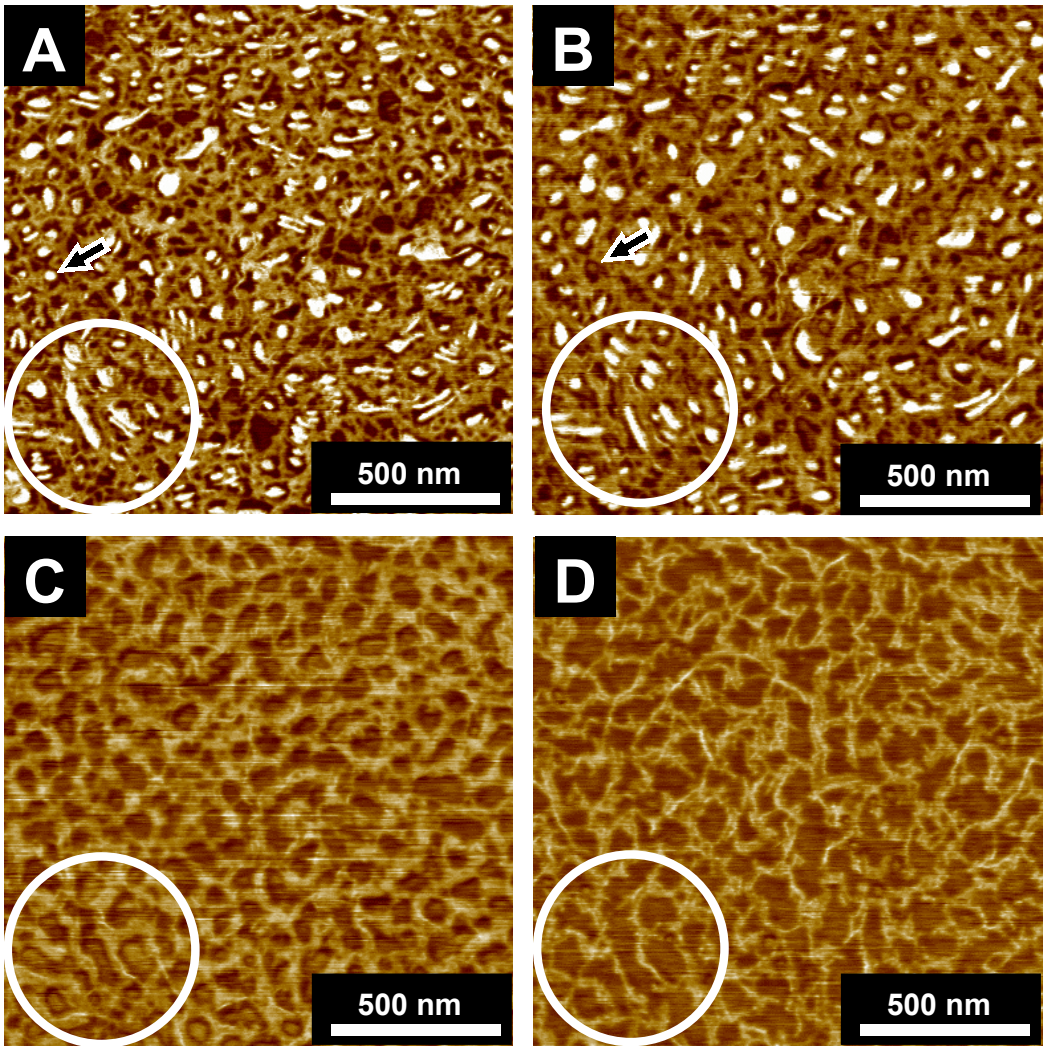

Figure 7. SFM phase contrast images of $E_{19}EP_{40}EO_{41}$[138] taken at 42.7 (A), 60.1 (B), 65.7 (C), and 88.7 °C (D); z = 25° for all images. The phase contrast images were taken at the same spot of the thin film upon heating; identical positions are marked with a white circle for clarity. The arrows highlight a small PEO crystallite which is already molten at 60.1 °C.

Conclusions

We have prepared several PE-*b*-PEP-*b*-PEO triblock copolymers with varying PEO content by homogeneous catalytic hydrogenation of the corresponding PB-*b*-PI-*b*-PEO triblock copolymers using Wilkinson catalyst. PB-*b*-PI-*b*-PEO triblock copolymers have been synthesized by sequential anionic polymerization in benzene, thus resulting in a high degree

of 1,4-addition for the PB and PI blocks. The anionic ring opening polymerization of ethylene oxide with Li^+ counterions was accomplished by using the strong phosphazene base *t*-BuP_4.

Thermal analysis utilizing DSC exhibits a different crystallization behavior for the PEO and PE blocks arising from different confinements active during crystallization. In PB-*b*-PI-*b*-PEO and PE-*b*-PEP-*b*-PEO triblock copolymers with PEO contents ≤ 20 wt-% the PEO blocks are confined within isolated spherical or cylindrical microdomains. As a result, large supercoolings are necessary to induce crystallization of PEO. The observed crystallization temperatures (-21 to -25 °C) in combination with self-nucleation experiments point to a weak nucleation of the microdomain interphase active upon PEO crystallization. In contrast, the PE blocks in PE-*b*-PEP-*b*-PEO triblock copolymers reflect a heterogeneous nucleation mechanism, which might be attributed to the non-confined crystallization of PE from a homogeneous mixture of PE and PEP segments in the melt.

TEM investigations on $E_{18}EP_{57}EO_{25}$[133] and $E_{19}EP_{40}EO_{41}$[138] reveal a cylindrical microstructure for the PEO blocks. The PE microstructure can be visualized by using a $E_{19}EP_{40}EO_{41}$[138] triblock copolymer containing residual olefinic double bonds within the PEP block, which can be selectively stained with OsO_4. In contrast to the cylindrical PEO microstructure, the PE block forms a continuous crystalline PE phase within the PEP matrix.

SFM investigations on thin films of PE-*b*-PEP-*b*-PEO triblock copolymers prepared from toluene solutions demonstrate the formation of a continuous crystalline PE phase arising from gelation upon film preparation. The PEO blocks form molten PEO spheres or cylinders in between the crystalline PE lamellae in triblock copolymers with PEO contents < 20 wt-%. In $E_{19}EP_{40}EO_{41}$[138] the PEO blocks crystallize within the restricted space provided in between the continuous crystalline PE phase. Utilizing hot-stage SFM measurements we were able to follow the melting of PEO domains and the annealing of PE crystallites upon heating of a thin film of $E_{19}EP_{40}EO_{41}$[138].

Acknowledgment. The authors thank A. Böker and Prof. G. Krausch (Physikalische Chemie II) for support concerning the SFM measurements, R. Lange (BASF AG) and Charles C. Han (NIST) for helpful discussions, and A. Göpfert (Makromolekulare Chemie II) for TEM investigations. Financial support by the German Israeli Foundation for Scientific Research and Development, DSM Research (Geleen), the Sonderforschungsbereich 481 funded by the Deutsche Forschungsgemeinschaft (DFG), and the Bayreuther Institut für Makromolekülforschung (BIMF) is gratefully acknowledged.

References and Notes

(1) Rangarajan, P.; Register, R. A.; Fetters, L. J. *Macromolecules* **1993**, *26*, 4640.

(2) Rangarajan, P.; Register, R. A.; Adamson, D. H.; Fetters, L. J.; Bras, W.; Naylor, S.; Ryan, A. J. *Macromolecules* **1995**, *28*, 1422.

(3) Ryan, A. J.; Hamley, I. W.; Bras, W.; Bates, F. S. *Macromolecules* **1995**, *28*, 3860.

(4) Richardson, P. H.; Richards, R. W.; Blundell, D. J.; MacDonald, W. A.; Mills, P. *Polymer* **1995**, *36*, 3059.

(5) Quiram, D. J.; Register, R. A.; Marchand, G. R.; Ryan, A. J. *Macromolecules* **1997**, *30*, 8338.

(6) Douzinas, K. C.; Cohen, R. E.; Halasa, A. F. *Macromolecules* **1991**, *24*, 4457.

(7) Hamley, I. W.; Patrick, J.; Fairclough, A.; Terrill, N. J.; Ryan, A. J.; Lipic, P. M.; Bates, F. S.; Towns-Andrews, E. *Macromolecules* **1996**, *29*, 8835.

(8) Rangarajan, P.; Register, R. A.; Fetters, L. J.; Bras, W.; Naylor, S.; Ryan, A. J. *Macromolecules* **1995**, *28*, 4932.

(9) Nojima, S.; Kato, K.; Yamamoto, S.; Ashida, T. *Macromolecules* **1992**, *25*, 2237.

(10) Rohadi, A.; Endo, R.; Tanimoto, S.; Sasaki, S.; Nojima, S. *Polym. Int.* **2000**, *32*, 602.

(11) Rohadi, A.; Tanimoto, S.; Sasaki, S.; Nojima, S. *Polym. J.* **2000**, *32*, 859.

(12) Ryan, A. J.; Fairclough, J. P. A.; Hamley, I. W.; Mai, S.-M.; Booth, C. *Macromolecules* **1997**, *30*, 1723.

(13) Hillmyer, M. A.; Bates, F. S. *Macromol. Symp.* **1997**, *117*, 121.

(14) Loo, Y.-L.; Register, R. A.; Ryan, A. J. *Macromolecules* **2002**, *35*, 2365.

(15) Quiram, D. J.; Register, R. A.; Marchand, G. R. *Macromolecules* **1997**, *30*, 4551.

(16) Müller, A. J.; Balsamo, V.; Arnal, M. L.; Jakob, T.; Schmalz, H.; Abetz, V. *Macromolecules* **2002**, *35*, 3048.

(17) Nojima, S.; Toei, M.; Hara, S.; Tanimoto, S.; Sasaki, S. *Polymer* **2002**, *43*, 4087.

(18) Reiter, G.; Castelein, G.; Sommer, J.-U.; Röttele, A.; Thurn-Albrecht, T. *Phys. Rev. Lett.* **2001**, *87*, 226101.

(19) Robitaille, C.; Prud'homme, J. *Macromolecules* **1983**, *16*, 665.

(20) Quiram, D. J.; Register, R. A.; Marchand, G. R.; Adamson, D. H. *Macromolecules* **1998**, *31*, 4891.

(21) Arnal, M. L.; Balsamo, V.; López-Carrasquero, F.; Contreras, J.; Carrillo, M.; Schmalz, H.; Abetz, V.; Laredo, E.; Müller, A. J. *Macromolecules* **2001**, *34*, 7973.

(22) Floudas, G.; Tsitsilianis, C. *Macromolecules* **1997**, *30*, 4381.

(23) Gervais, M.; Gallot, B. *Polymer* **1981**, *22*, 1129.

(24) Lotz, B.; Kovacs, A. J. *Polym. Prep. (Am. Chem. Soc., Div. Polym. Chem.)* **1969**, *10*, 820.

(25) O'Malley, J. J. *J. Polym. Sci., Polym. Symp.* **1977**, *60*, 151.

(26) Zhu, L.; Chen, Y.; Zhang, A.; Calhoun, B. H.; Chun, M.; Quirk, R. P.; Cheng, S. Z. D.; Hsiao, B. S.; Yeh, F.; Hashimoto, T. *Phys. Rev. B* **1999**, *60*, 10022.

(27) Zhu, L.; Cheng, S. Z. D.; Calhoun, B. H.; Ge, Q.; Quirk, R. P.; Thomas, E. L.; Hsiao, B. S.; Yeh, F.; Lotz, B. *Polymer* **2001**, *42*, 5829.

(28) Zhu, L.; Mimnaugh, B. R.; Ge, Q.; Quirk, R. P.; Cheng, S. Z. D.; Thomas, E. L.; Lotz, B.; Hsiao, B. S.; Yeh, F.; Liu, L. *Polymer* **2001**, *42*, 9121.

(29) Zhu, L.; Cheng, S. Z. D.; Huang, P.; Ge, Q.; Quirk, R. P.; Thomas, E. L.; Lotz, B.; Hsiao, B. S.; Yeh, F.; Liu, L. *Adv. Mater.* **2002**, *14*, 31.

(30) Zhu, L.; Huang, P.; Chen, W. Y.; Ge, Q.; Quirk, R. P.; Cheng, S. Z. D.; Thomas, E. L.; Lotz, B.; Hsiao, B. S.; Yeh, F.; Liu, L. *Macromolecules* **2002**, *35*, 3553.

(31) Hamley, I. W.; Fairclough, J. P. A.; Ryan, A. J.; Bates, F. S.; Towns-Andrews, E. *Polymer* **1996**, *37*, 4425.

(32) Loo, Y.-L.; Register, R. A.; Adamson, D. H. *J. Polym. Sci., Part B: Polym. Phys.* **2000**, *38*, 2564.

(33) Loo, Y.-L.; Register, R. A.; Ryan, A. J.; Dee, G. T. *Macromolecules* **2001**, *34*, 8968.

(34) Weimann, P. A.; Hajduk, D. A.; Chu, C.; Chaffin, K. A.; Brodil, J. C.; Bates, F. S. *J. Polym. Sci., Part B: Polym. Phys.* **1999**, *37*, 2053.

(35) Herman, J.-J.; Jerome, R.; Teyssie, P.; Gervais, M.; Gallot, B. *Makromol. Chem.* **1981**, *182*, 997.

(36) Heuschen, J.; Jerome, R.; Teyssie, P. *J. Polym. Sci., Part B: Polym. Phys.* **1989**, *27*, 523.

(37) Nojima, S.; Tanaka, H.; Rohadi, A.; Sasaki, S. *Polymer* **1998**, *39*, 1727.

(38) Nojima, S.; Kakihira, H.; Tanimoto, S.; Nakatami, H.; Sasaki, S. *Polym. J.* **2000**, *32*, 75.

(39) Cohen, R. E.; Cheng, P.-L.; Douzinas, K.; Kofinas, P.; Berney, C. V. *Macromolecules* **1990**, *23*, 324.

(40) Shiomi, T.; Tsukada, H.; Takeshita, H.; Takenaka, K.; Tezuka, Y. *Polymer* **2001**, *42*, 4997.

(41) Liu, L.-Z.; Li, H.; Jiang, B.; Zhou, E. *Polymer* **1994**, *35*, 5513.

(42) Liu, L.-Z.; Yeh, F.; Chu, B. *Macromolecules* **1996**, *29*, 5336.

(43) Liu, L. Z.; Jiang, B.; Zhou, E. *Polymer* **1996**, *37*, 3937.

(44) Liu, L. Z.; Xu, W.; Li, H.; Su, F.; Zhou, E. *Macromolecules* **1997**, *30*, 1363.

(45) Unger, R.; Reuter, H.; Höring, S.; Donth, E. *Polym. Plast. Technol. Eng.* **1990**, *29*, 1.

(46) Chen, H.-L.; Hsiao, S.-C.; Lin, T.-L.; Yamauchi, K.; Hasegawa, H.; Hashimoto, T. *Macromolecules* **2001**, *34*, 671.

(47) Loo, Y.-L.; Register, R. A. *Phys. Rev. Lett.* **2000**, *84*, 4120.

(48) O'Malley, J. J.; Crystal, R.; Erhardt, P. F. *Polym. Prep. (Am. Chem. Soc., Div. Polym. Chem.)* **1969**, *10*, 796.

(49) Balsamo, V.; von Gyldenfeldt, F.; Stadler, R. *Macromol. Chem. Phys.* **1996**, *197*, 3317.

(50) Balsamo, V.; Müller, A. J.; von Gyldenfeldt, F.; Stadler, R. *Macromol. Chem. Phys.* **1998**, *199*, 1063.

(51) Müller, A. J.; Arnal, M. L.; López-Carrasquero, F. *Macromol. Symp.*, in press.

(52) Arnal, M. L.; López-Carrasquero, F.; Laredo, E.; Müller, A. J., Manuscript in preparation.

(53) Balsamo, V.; Stadler, R. *Macromolecules* **1999**, *32*, 3994.

(54) Balsamo, V.; von Gyldenfeldt, F.; Stadler, R. *Macromolecules* **1999**, *32*, 1226.

(55) Balsamo, V.; Stadler, R. *Macromol. Symp.* **1997**, *117*, 153.

(56) Balsamo, V.; Paolini, Y.; Ronca, G.; Müller, A. J. *Macromol. Chem. Phys.* **2000**, *201*, 2711.

(57) Kim, G.; Han, C. C.; Libera, M.; Jackson, C. L. *Macromolecules* **2001**, *34*, 7336.

(58) Buzdugan, E.; Ghioca, P.; Stribeck, N.; Beckman, E. J.; Serban, S. *Macromol. Mater. Eng.* **2001**, *286*, 497.

(59) Balsamo, V.; Collins, S.; Hamley, I. W. *Polymer* **2002**, *43*, 4207.

(60) Koetsier, D. W.; Bantjes, A.; Feijen, J.; Lyman, D. J. *J. Polym. Sci., Part A: Polym. Chem.* **1978**, *16*, 511.

(61) Benson, R. S.; Wu, Q.; Ray, A. R.; Lyman, D. J. *J. Polym. Sci., Part A: Polym. Chem.* **1985**, *23*, 399.

(62) Mitov, Z. G.; Velichkova, R. S. *Eur. Polym. J.* **1992**, *28*, 771.

(63) Bailey, T. S.; Pham, H. D.; Bates, F. S. *Macromolecules* **2001**, *34*, 6994.

(64) Schmalz, H.; Böker, A.; Lange, R.; Krausch, G.; Abetz, V. *Macromolecules* **2001**, *34*, 8720.

(65) Park, C.; De Rosa, C.; Fetters, L. J.; Thomas, E. L. *Macromolecules* **2000**, *33*, 7931.

(66) Kwon, Y.; Kim, M. S.; Faust, R. *Polym. Prep. (Am. Chem. Soc., Div. Polym. Chem.)* **2001**, *42*, 483.

(67) Floudas, G.; Reiter, G.; Lambert, O.; Dumas, P. *Macromolecules* **1998**, *31*, 7279.

(68) Schmalz, H.; Abetz, V.; Lange, R.; Soliman, M. *Macromolecules* **2001**, *34*, 795.

(69) Eßwein, B.; Molenberg, A.; Möller, M. *Macromol. Symp.* **1996**, *107*, 331.

(70) Eßwein, B.; Möller, M. *Angew. Chem.* **1996**, *108*, 703.

(71) Eßwein, B.; Steidl, N. M.; Möller, M. *Macromol. Rapid Commun.* **1996**, *17*, 143.

(72) Förster, S.; Krämer, E. *Macromolecules* **1999**, *32*, 2783.

(73) Floudas, G.; Vazaiou, B.; Schipper, F.; Ulrich, R.; Wiesner, U.; Iatrou, H.; Hadjichristidis, N. *Macromolecules* **2001**, *34*, 2947.

(74) Hahn, S. F. *J. Polym. Sci., Part A: Polym. Chem.* **1992**, *30*, 397.

(75) Brandrup, J.; Immergut, E. H. *Polymer Handbook*, 3rd ed.; Wiley: New York, 1989.

(76) Lanzendörfer, M.; Schmalz, H.; Abetz, V.; Müller, A. H. E. *Polym. Prep. (Am. Chem. Soc., Div. Polym. Chem.)* **2001**, *42*, 329. Lanzendörfer, M. G.; Schmalz, H.; Abetz, V.; Müller, A. H. E. Application of FT-NIR Spectroscopy for Monitoring the Kinetics of Living Polymerizations. In *In-Situ Spectroscopy of Monomer and Polymer Synthesis*; Puskas, J. E.; Storey, R., Eds.; Kluwer Academic/Plenum: New York/Dordrecht, 2002, in press.

(77) Schmalz, H.; Lanzendörfer, M. G.; Abetz, V.; Müller, A. H. E. *Macromol. Chem. Phys.* **2003**, submitted.

(78) Wunderlich, B. *Macromolecular Physics*; Academic Press: New York, 1980; Vol. 3.

(79) Schmalz, H.; Müller, A. J.; Abetz, V. *Macromol. Chem. Phys.* **2003**, accepted.

(80) Bates, F. S.; Schultz, M. F.; Rosedale, J. H. *Macromolecules* **1992**, *25*, 5547.

(81) Kofinas, P.; Cohen, R. E. *Macromolecules* **1994**, *27*, 3002.

(82) Takahashi, Y.; Tadokoro, H. *Macromolecules* **1973**, *6*, 672.

(83) Howard, P. R.; Crist, B. *J. Polym. Sci., Part B: Polym. Phys.* **1989**, *27*, 2269.

(84) Sauer, B. B.; McLean, R. S.; Thomas, R. R. *Polym. Int.* **2000**, *49*, 449.

(85) Schultz, J. M.; Miles, M. J. *J. Polym. Sci., Part B: Polym. Phys.* **1998**, *36*, 2311.

(86) Beekmans, L. G. M.; Vancso, G. J. *Polymer* **2000**, *41*, 8975.

(87) Beekmans, L. G. M.; Vancso, G. J. *Polym. Mat. Sci. Eng.* **1999**, *81*, 260.

(88) Hobbs, J. K.; Miles, M. J. *Macromolecules* **2001**, *34*, 353.

(89) Lu, W.; Debelak, K.; Yang, C.; Collins, W. E.; Witt, A.; Lott, C. *Polym. Mat. Sci. Eng.* **1999**, 273.

(90) Beake, B. D.; Brewer, N. J.; Leggett, G. J. *Macromol. Symp.* **2001**, *167*, 101.

(91) Bliznyuk, V. N.; Kirov, K.; Assender, H. E.; Briggs, G. A. D.; Tsukahara, Y. *Polym. Prep. (Am. Chem. Soc., Div. Polym. Chem.)* **2000**, *41*, 1489.

(92) Sasaki, S.; Sakaki, Y.; Takahara, A.; Kajiyama, T. *Polymer* **2002**, *43*, 3441.

(93) Pearce, R.; Vancso, G. J. *Macromolecules* **1997**, *30*, 5843.

(94) Pearce, R.; Vancso, G. J. *Polymer* **1998**, *39*, 1237.

(95) Li, L.; Chan, C.-M.; Yeung, K. L.; Li, J.-X.; Ng, K.-M.; Lei, Y. *Macromolecules* **2001**, *34*, 316.

(96) Reiter, G.; Castelein, G.; Sommer, J.-U. *Phys. Rev. Lett.* **2001**, *86*, 5918.

(97) Reiter, G.; Sommer, J.-U. *J. Chem. Phys.* **2000**, *112*, 4376.

(98) Taguchi, K.; Miyaji, H.; Izumi, K.; Hoshino, A.; Miyamoto, Y.; Kokawa, R. *Polymer* **2001**, *42*, 7443.

(99) Hamley, I. W.; Wallwork, M. L.; Smith, D. A.; Fairclough, J. P. A. *Polymer* **1998**, *39*, 3321.

(100) Reiter, G.; Castelein, G.; Hoerner, P.; Riess, G.; Blumen, A.; Sommer, J.-U. *Phys. Rev. Lett.* **1999**, *83*, 3844.

(101) Reiter, G.; Castelein, G.; Hoerner, P.; Riess, G.; Sommer, J.-U.; Floudas, G. *Eur. Phys. J.* **2000**, *E 2*, 319.

3.2.2 Crystallization in ABC Triblock Copolymers with Two Different Crystalline End Blocks: Influence of Confinement on Self-Nucleation Behavior

Holger Schmalz[a], Alejandro J. Müller[b] and Volker Abetz[a*]

a) Makromolekulare Chemie II, Universität Bayreuth, 95440 Bayreuth, Germany
b) Grupo de Polímeros USB, Departamento de Ciencia de los Materiales Universidad Simón Bolívar, Caracas 1080-A, Venezuela

SUMMARY: The influence of different confinements active during crystallization within polybutadiene-*block*-polyisoprene-*block*-poly(ethylene oxide) (PB-*b*-PI-*b*-PEO) and the corresponding hydrogenated polyethylene-*block*-poly(ethylene-*alt*-propylene)-*block*-poly(ethylene oxide) (PE-*b*-PEP-*b*-PEO) triblock copolymers on the self-nucleation behavior of the crystallizable PEO and PE blocks is investigated by means of differential scanning calorimetry (DSC).
In triblock copolymers with PEO contents ≤ 20 wt-% crystallization of PEO is confined within small isolated microdomains (spheres or cylinders) and PEO crystallization takes place exclusively at high supercoolings. Self-nucleation experiments reveal an anomalous behavior in comparison to the classical self-nucleation behavior found in semicrystalline homopolymers. In these systems, *domain II* (exclusive self-nucleation domain) vanishes, and self-nucleation can only take place at lower temperatures in *domain* III_{SA}, when annealing is already active. The self-nucleation behavior of the PE blocks is significantly different compared to the PEO blocks. Regardless of the low PE content (10 – 25 wt-%) in the investigated PE-*b*-PEP-*b*-PEO triblock copolymers a classical self-nucleation behavior is observed, i. e. all three self-nucleation domains, usually present in crystallizable homopolymers, can be located. This is a direct result of the small segmental interaction parameter of the PEP and PE segments in the melt. As a consequence, crystallization of PE occurs without confinement from a homogeneous mixture of PE and PEP segments.

Keywords: block copolymers, confinement, self-nucleation, differential scanning calorimetry, morphology.

Introduction

Crystallization within confined dimensions is an issue which has attracted increasing interest. Well-defined block copolymers containing at least one crystallizable block are good model systems to study the influence of different confinements on the crystallization behavior of a particular block. In strongly segregated systems, where the crystallizable block is confined within small isolated microdomains, often a fractionated crystallization behavior or even exclusively crystallization induced by homogeneous nucleation is observed.[1-8] This can be attributed to the huge number density of isolated microdomains with respect to the number density of heterogeneities usually present in the system. On the contrary, crystallization of large or continuous domains mostly is induced by heterogeneous nucleation, because the probability of a heterogeneity to be located in the crystallizable domain is sufficiently high. In addition, the formed morphology depends in a very sensitive fashion on the strength of confinement exerted on the crystallizable block.[9] In strongly confined systems (high segregation strength) the melt phase morphology is preserved upon crystallization, i. e. crystallization takes place within the confined geometry of the microdomain. However, for weakly confined systems or systems exhibiting a homogeneous melt, the morphology is mainly determined by crystallization, i. e. a lamellar morphology with alternating crystalline and amorphous lamellae is observed (for more details see reference 2 and included references).

We have recently reported the synthesis and characterization of polybutadiene-*block*-polyisoprene-*block*-poly(ethylene oxide) (PB-*b*-PI-*b*-PEO) and the corresponding hydrogenated polyethylene-*block*-poly(ethylene-*alt*-propylene)-*block*-poly(ethylene oxide) (PE-*b*-PEP-*b*-PEO) triblock copolymers, the latter containing two different crystallizable end blocks.[2] Also the influence of cocrystallizing agents on the melting behavior of PEO in these systems was investigated.[10] Thermal analysis utilizing differential scanning calorimetry (DSC) revealed a different crystallization behavior for the PEO and PE blocks arising from different confinements active during crystallization. In triblock copolymers with PEO contents ≤ 20 wt.-% the strongly incompatible PEO blocks are confined within isolated spherical or cylindrical microdomains. As a result, a marked depression in crystallization temperature ($\Delta T_c \approx$ -40 °C) has been observed for the PEO blocks. In contrast, the PE blocks within PE-*b*-PEP-*b*-PEO triblock copolymers showed a crystallization temperature comparable to the value observed in PE homopolymers regardless of the low PE content

(< 25 wt.-%), thus reflecting a heterogeneous nucleation mechanism. This difference in crystallization behavior can be explained by the fact, that the PE segments crystallize from a homogeneous mixture of PEP and PE segments in the melt due to their low segmental interaction parameter of $\chi = 0.007$ at 120 °C.[11]

A more detailed study of the crystallization behavior and the influence of confinements can be accomplished by applying the self-nucleation (SN) technique developed by Fillon et al..[12] Self-nucleation consists of the partial melting of an initially crystalline "standard" state of the polymer at a given self-nucleation temperature (T_s). Upon subsequent cooling recrystallization takes place, using as nuclei the crystallographically "ideal" nuclei which are produced during partial melting, i. e. self-nuclei or crystal fragments of the same polymer under consideration. A detailed description of the SN technique will be given in the experimental section. Usually three self-nucleation domains can be located for crystallizable homopolymers as a function of the applied self-nucleation temperature: *domain I* or "complete melting domain", *domain II* or "self-nucleation domain", and *domain* III_{SA} or "self-nucleation and annealing domain". However, in block copolymers often an alteration of the usual self-nucleation behavior is found. This accounts especially for block copolymers where the crystallizable blocks are strongly confined into small isolated microdomains.[1, 13] As a consequence, the extremely high number of microdomains that need to be self-nucleated complicates the self-nucleation of the confined crystallizable block, which is reflected in the absence of *domain II*.

In this contribution, we investigate the self-nucleation behavior of the crystallizable blocks within PB-*b*-PI-*b*-PEO and PE-*b*-PEP-*b*-PEO triblock copolymers by applying the SN technique. The influence of different confinements active during crystallization of PE and PEO and the influence of the domain size on the self-nucleation behavior will be discussed. In addition, effects of catalyst debris, arising from the hydrogenation of PB-*b*-PI-*b*-PEO triblock copolymers using Wilkinson catalyst to yield the corresponding PE-*b*-PEP-*b*-PEO triblock copolymers, on the self-nucleation behavior of the PEO block are investigated.

Experimental section

Synthesis

PE-*b*-PEP-*b*-PEO triblock copolymers have been obtained by catalytic hydrogenation of the corresponding PB-*b*-PI-*b*-PEO triblock copolymer precursors which have been synthesized by sequential anionic polymerization of butadiene, isoprene, and ethylene oxide in benzene using *sec*-BuLi as initiator.[2, 14] Homogeneous catalytic hydrogenation was carried out in degassed toluene at 100 °C and 90 bar H_2 pressure for 3 – 4 days using Wilkinson catalyst ($(Ph_3P)_3Rh(I)Cl$). Under the applied conditions the PB block is hydrogenated completely and the PI block shows an almost complete saturation with ca. 1% residual double bonds. The PE-*b*-PEP-*b*-PEO triblock copolymers were subjected to a further purification prior to the self-nucleation experiments in order to exclude any influence of catalyst debris arising from the hydrogenation reaction. Purification was accomplished by refluxing a toluene solution of the triblock copolymer with a small amount of hydrochloric acid followed by precipitation in cold acetone. The nomenclature of the materials is as follows: $A_xB_yC_z^M$ denotes a triblock copolymer with the total molecular weight M in kg/mol of the three blocks A, B and C with the respective weight fractions (in %) of x, y, and z.

Differential scanning calorimetry (DSC)

Thermal analysis was performed on a Perkin Elmer DSC 7 with a CCA 7 liquid nitrogen cooling device. For all measurements a two point calibration with decane and indium was applied. All experiments were performed at a scanning rate of 10 °C/min with a reproducibility of ca. ± 0.1 °C. Due to the vicinity of the melting endotherms of PEO and PE (problems involved with definition of the baseline for the PE endotherm), the degree of crystallinity for the PE blocks was extracted from the heat of crystallization. The degree of crystallinity for the PEO blocks was determined as usual from the heat of fusion. The degrees of crystallinity were calculated assuming a heat of fusion for 100% crystalline PEO and PE of ΔH_m^0 = 196.6 J/g[15] and ΔH_m^0 = 276.98 J/g[16], respectively.

Self-nucleation (SN) experiments

Self-nucleation measurements were performed in analogy to the procedure described by Fillon et al..[12] This procedure is an extension of the classical self-nucleation experiments of Blundell et al.[17] to differential scanning calorimetry. The complete thermal treatment is depicted schematically in Figure 1, and will be explained in detail in the following.

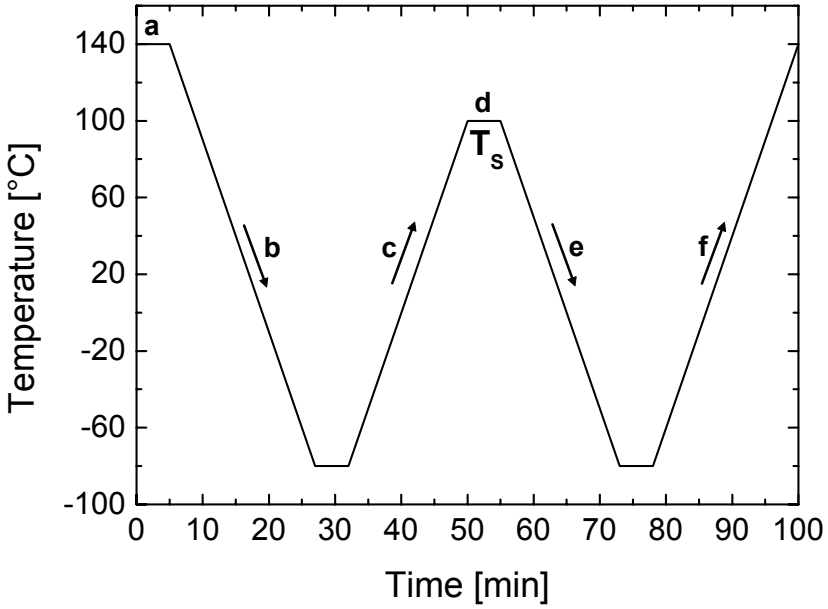

Figure 1. Schematic representation of the self-nucleation experiments conducted by means of DSC.

a) Erasure of any previous thermal history by heating the sample to 100 °C (for PB-*b*-PI-*b*-PEO) or 140 °C (for PE-*b*-PEP-*b*-PEO) for 5 min. This step erases all crystalline memory of the material as far as dynamic DSC experiments are concerned. Thus, upon heating the sample to 100 °C or 140 °C (or even higher temperatures) only temperature-resistant heterogeneous nuclei remain, and upon subsequent cooling the crystalline blocks (PEO and/or PE) will always crystallize at the same peak crystallization temperature (if the same cooling rate is used). This suggests that the nucleation density remains constant under the applied conditions, i. e. the selected melting temperature is efficient in erasing the crystalline memory of the material.

b) Creation of a "standard" thermal history by cooling at a rate of 10 °C/min to -80 °C. This step ensures that crystallization of the PEO and/or PE blocks always occurs under the same dynamic conditions.

c) Partial melting by heating to a so-called self-nucleation temperature, which will be labeled as T_s in the following.

d) Thermal conditioning at T_s for 5 min. Depending on T_s the crystalline PE or PEO domains will be completely molten, only self-nucleated, or self-nucleated and annealed.[12] If T_s is sufficiently high, no self-nuclei or crystal fragments can survive, then the sample is regarded to be under *domain I* or complete melting domain (as in step a above). When T_s is high enough to melt the sample almost completely, but low enough to leave some small crystal fragments that can act as self-nuclei during the subsequent cooling from T_s (see step e below), the sample is said to be under *domain II* or self-nucleation domain. If T_s is too low, only part of the crystal population will be molten. As a result, the remaining crystals will be annealed during the 5 min at T_s, while the rest of the polymer will be self-nucleated during the subsequent cooling from T_s (although some isothermal crystallization during the 5 min at T_s could also occur). In this regime the sample is considered to be under *domain* III_{SA} or self-nucleation and annealing domain. The distinction between the domains can be accomplished by careful observation of the subsequent cooling runs from T_s (step e) and the final heating runs (step f).

e) Subsequent cooling scan from T_s at a rate of 10 °C/min, where the effects of the thermal treatment will be reflected by the crystallization of the corresponding PE and PEO blocks. If self-nucleation takes place, a shift of the respective peak crystallization temperature of the PEO or PE blocks to higher temperatures as compared to the standard cooling run (step b) is expected.

f) Final heating scan to 100 °C (PB-*b*-PI-*b*-PEO) or 140 °C (PE-*b*-PEP-*b*-PEO), where the effects of the entire thermal history on the melting of the corresponding PEO and/or PE blocks will be apparent. For instance, if annealing takes place at T_s either a shift of the peak melting temperature to higher temperatures or the appearance of a second, higher melting peak is expected.

Transmission electron microscopy (TEM)

The bulk morphologies of $E_{11}EP_{71}EO_{18}$[123] and $E_{19}EP_{40}EO_{41}$[138] were examined by bright field TEM using a Zeiss CEM 902 electron microscope operated at 80 kV. Films (around 0.5 mm thick) were prepared by casting from a 3 wt.-% solution in toluene at 70 °C in order to avoid gelation upon solvent evaporation. After complete evaporation of the solvent (ca. 1 week) the films were slowly cooled to room temperature to induce crystallization of the PE and PEO blocks followed by further drying under vacuum at 40 °C for 2 days. Thin

sections were cut at -130 °C using a Reichert-Jung Ultracut E microtome equipped with a diamond knife. Selective staining of amorphous PEO and PEP segments within $E_{11}EP_{71}EO_{18}$[123] was accomplished by exposure of the thin sections to RuO_4 vapor for 30 – 40 min. For the triblock copolymer $E_{19}EP_{40}EO_{41}$[138], which has been synthesized alternatively by hydrogenation of the corresponding PB-*b*-PI-*b*-PEO triblock copolymer using *p*-toluenesulfonyl hydrazide, OsO_4 vapor was used as staining agent (exposure for 1 min). In contrast to the hydrogenation with Wilkinson catalyst, here the PEP block contains ca. 30% residual double bonds, which can be selectively stained using OsO_4 together with the amorphous PEO segments.

Results and discussion

Classical self-nucleation behavior

In crystallizable homopolymers usually all three different domains of self-nucleation can be defined, as has been derived for isotactic polypropylene (PP) by Fillon et al.[12] and was confirmed for other systems[13, 18-20]. A schematic illustration of the location of the three different self-nucleation domains is given in Figure 2.

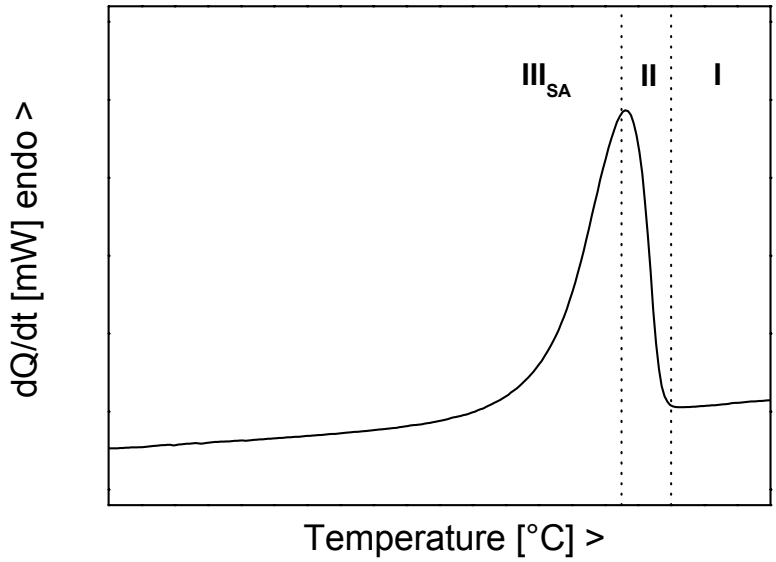

Figure 2. Schematic location of self-nucleation regimes for a crystallizable homopolymer.

In *domain I*, the remaining nuclei correspond to heterogeneous nuclei, i. e. thermally stable nuclei present in the melt. Upon cooling, crystallization always takes place at the same temperature. *Domain II* represents a T_s range, where the concentration of remaining crystal fragments varies dramatically with T_s. Small variations in T_s result in significant shifts of the crystallization peak to higher temperatures in the subsequent cooling run. In *domain* III_{SA} incomplete melting takes place, which is directly linked to the occurrence of considerable annealing of the remaining crystalline material. As mentioned above, for block copolymers the situation might be different, especially for systems where the crystallizable block is confined within isolated microdomains (spheres or cylinders). For example, self-nucleation experiments on PS-*b*-PB-*b*-PCL triblock copolymers and their hydrogenated analogues, PS-*b*-PE-*b*-PCL, showed that *domain II* is completely absent for systems where the crystallizable block is confined within small isolated microdomains (low contents of PE or PCL)[1, 13, 21].

Consequently, the crystallizable blocks cannot be nucleated by the self-seeding nuclei produced at self-nucleation temperatures corresponding to *domain II*. For self-nucleation a higher density of self-nuclei is necessary. As a result, T_s has to be lowered well into *domain* III_{SA}, where already partial melting and annealing is observed. In some cases, an even lower self-nucleation temperature is necessary in order to nucleate the confined crystallizable blocks. Here, *domain* III_{SA} was found to split in a pure annealing domain (*domain* III_A), without showing self-nucleation, and a self-nucleation and annealing domain (*domain* III_{SA}) at lower self-nucleation temperatures.[1, 13] Thus confinements active during crystallization within block copolymer microdomains can alter the usual self-nucleation behavior observed in semicrystalline homopolymers.

Self-nucleation behavior of the PEO block within PB-b-PI-b-PEO and purified PE-b-PEP-b-PEO triblock copolymers

PB-*b*-PI-*b*-PEO triblock copolymers. Table 1 shows the thermal properties of several PB-*b*-PI-*b*-PEO triblock copolymers with varying PEO content as derived from dynamic DSC experiments. For triblock copolymers with a PEO weight fraction ≤ 20 wt.-% large supercoolings are necessary to induce crystallization of the PEO blocks ($T_c \approx$ -20 °C). From the composition, a spherical or cylindrical microstructure for the PEO blocks might be expected.[2] Due to their softness ultrathin sections could not be obtained for the PB-*b*-PI-*b*-PEO triblock copolymers and we present only TEM results on their hydrogenated analogues. Figure 3 shows the TEM micrograph of $E_{11}EP_{71}EO_{18}^{123}$ (thin sections were cut at –130 °C), obtained by catalytic hydrogenation of the corresponding precursor $B_{11}I_{70}EO_{19}^{120}$ using Wilkinson catalyst.

Table 1. DSC data for PB-*b*-PI-*b*-PEO and PE-*b*-PEP-*b*-PEO triblock copolymers.[a]

Triblock Copolymer[b]	T_g [°C]	T_m(PEO) [°C]	T_c(PEO_I)[c] [°C]	T_c(PEO_{II}) [°C]	α(PEO) [%]	T_m(PE) [°C]	T_c(PE) [°C]	α(PE) [%]
$B_{24}I_{56}EO_{20}^{67}$	-69.5[d]	60.5	-23.9	-	84.5	-	-	-
$B_{11}I_{70}EO_{19}^{120}$	-65.9[d]	60.0	-22.2	-	71.4	-	-	-
$B_{17}I_{57}EO_{26}^{130}$	-67.5[d]	63.2	-21.0 (83)	16.1	70.4	-	-	-
$B_{19}I_{39}EO_{42}^{135}$	-68.7[d]	65.9	-25.0 (2)	37.5/19.8	77.8	-	-	-
$E_{24}EP_{57}EO_{19}^{69}$ (5.8)[e]	-58.6	57.2	-21.5 (17)	17.9	79.7	90.7	67.5	27.2
$E_{24}EP_{57}EO_{19}^{69}$	-57.4	58.9	-26.4	-	80.2	93.4	66.5	27.4
$E_{11}EP_{71}EO_{18}^{123}$ (6.4)[e]	-56.6	60.4	-23.0 (40)	19.6	64.3	88.9	50.8	37.4
$E_{11}EP_{71}EO_{18}^{123}$	-56.4	59.7	-25.4	-	65.0	89.0	50.0	38.1
$E_{18}EP_{57}EO_{25}^{133}$ (5.8)	-56.8	60.0	-21.1 (4)	26.8	56.9	92.9	64.6	21.2
$E_{19}EP_{40}EO_{41}^{138}$ (5.8)	-57.1	63.9	-24.0 (6)	37.6/23.6	72.1	94.4	69.4	20.3

[a] T_m = melting point of corresponding block (peak maximum), T_c = crystallization temperature of corresponding block (peak maximum), α = degree of crystallinity, and T_g = glass transition temperature.

[b] values in brackets give the content of ethyl branches within the PE block in mol-%.

[c] values in brackets give the fraction of crystallinity (in %).

[d] T_g of the mixed PB/PI phase.

[e] sample contains residual Wilkinson catalyst.

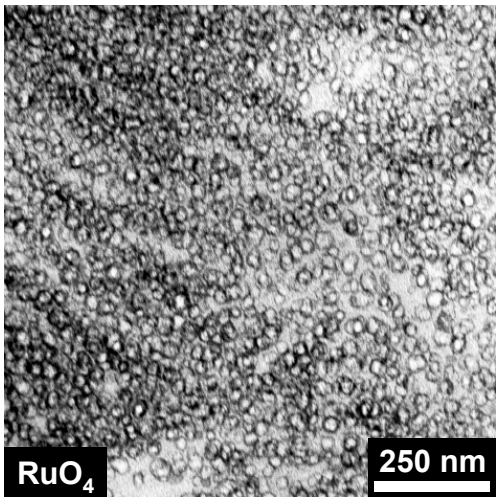

Figure 3. TEM micrograph of $E_{11}EP_{71}EO_{18}^{123}$. The crystalline PEO domains appear bright due to selective staining of amorphous PEP and PEO segments with RuO_4. Because of the used staining technique the crystalline PE domains cannot be visualized.

The use of RuO_4 results in a preferential staining of the amorphous PEP and PEO segments, while the PE segments cannot be visualized. Thus, the crystalline PEO domains appear bright and exhibit a distorted spherical structure, which clearly shows the confinement of the PEO blocks within isolated PEO domains and is the reason for the observed large supercoolings necessary to induce crystallization. From this it follows that also in the non-hydrogenated precursors the PEO domains are dispersed, because in those block copolymers PI and PB form a single, mixed domain building the matrix. Due to its dispersion PEO might crystallize after being nucleated by a weakly active heterogeneity, a weak nucleation of the microdomain interphase or by homogeneous nucleation. However, the observed crystallization temperatures (Table 1) are significantly higher compared to the crystallization temperatures observed in PEO containing block copolymers exhibiting exclusively homogeneous nucleation ($T_c \approx$ -40 °C)[3]. Therefore, homogeneous nucleation might not be responsible for the observed low crystallization temperatures. To gain more insight into the crystallization behavior of the PEO blocks confined into spherical or cylindrical microdomains within PB-*b*-PI-*b*-PEO triblock copolymers, self-nucleation experiments have been performed. Figures 4A and 4B show the corresponding cooling and heating traces for $B_{24}I_{56}EO_{20}^{67}$ obtained after thermal treatment at the indicated self-nucleation temperatures T_s.

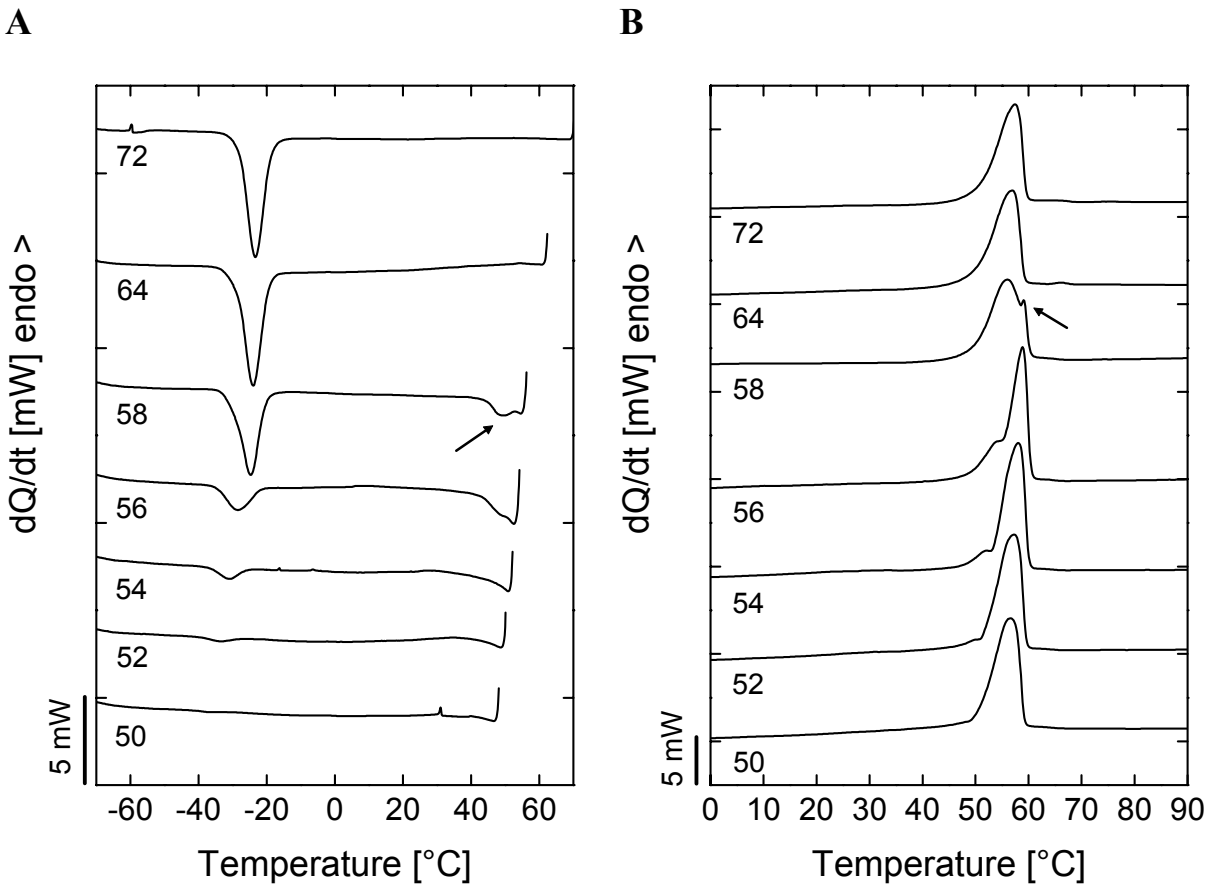

Figure 4. DSC cooling scans (A) for $B_{24}I_{56}EO_{20}$[67] after self-nucleation at the indicated T_s and subsequent heating scans (B).

For T_s > 58 °C no change in the peak crystallization temperature can be observed (Figures 4A and 5). Therefore, the PEO blocks are under *domain I* for T_s > 58 °C. At T_s = 58 °C the PEO blocks exhibit fractionated crystallization. A small fraction crystallizes right upon cooling, as indicated by the arrow in Figure 4A, whereby the larger fraction still crystallizes at the initial T_c (compare with T_s = 72 °C). Crystallization right upon cooling usually implies that self-nucleation and annealing are simultaneously present. This can be corroborated in the subsequent heating trace exhibiting a second high temperature melting peak (indicated by the arrow in Figure 4B). Therefore, from T_s = 58 °C downward, *domain* III_{SA}, or the self-nucleation and annealing domain, has been reached. A further decrease in T_s results in an increase of unmelted PEO. This in turn results in a higher amount of annealed crystals as indicated by the increase in size of the higher melting temperature endotherm, which also moves to lower values as T_s is decreased (Figure 4B). Furthermore, the low temperature crystallization exotherm decreases in size and shifts to lower temperatures as T_s is

decreased below 58 °C (Figure 4A), which can be verified more clearly in the plot of the observed crystallization temperatures (T_c) versus T_s (Figure 5).

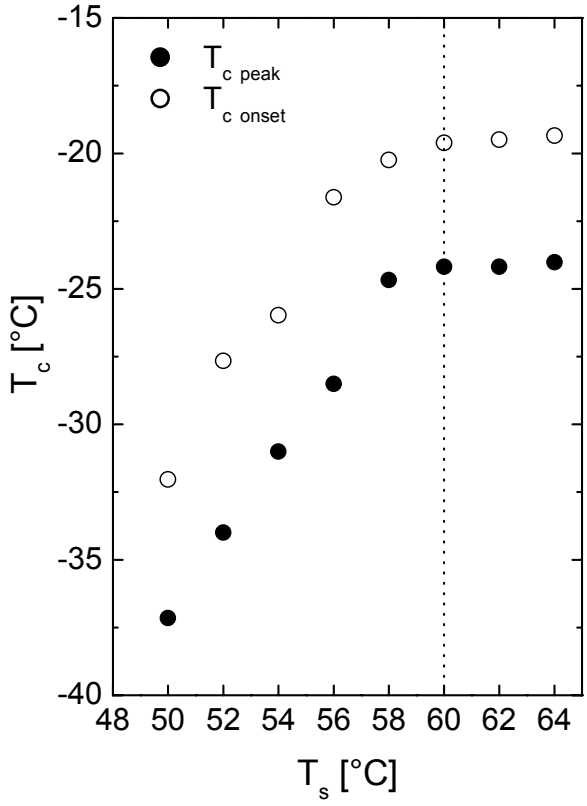

Figure 5. Variation of the crystallization temperatures with T_s for $B_{24}I_{56}EO_{20}$[67]. The dashed line corresponds to a change in the self-nucleation domain.

This can be attributed to the fact that after annealing only the thinner crystallites (formed by chains that crystallize at lower temperatures) remain molten and these chains will crystallize once more at comparatively lower temperatures upon subsequent cooling. This effect is characteristic for *domain* III_{SA} where self-nucleation and annealing takes place at the same time. Thus, *domain II* is completely absent in $B_{24}I_{56}EO_{20}$[67], as reflected by the direct transition from *domain I* into *domain* III_{SA} upon lowering T_s. The observed self-nucleation domains are depicted on the standard melting peak of the PEO block in Figure 6. A similar behavior was obtained for $B_{11}I_{70}EO_{19}$[120], showing an almost identical PEO content but a comparatively higher overall molecular weight (Table 2). The absence of *domain II* indicates that crystallization of PEO in these samples might be induced by nucleation of the microdomain interphase rather than by nucleation of a weakly active heterogeneity, but it is still difficult to ascertain this fact.

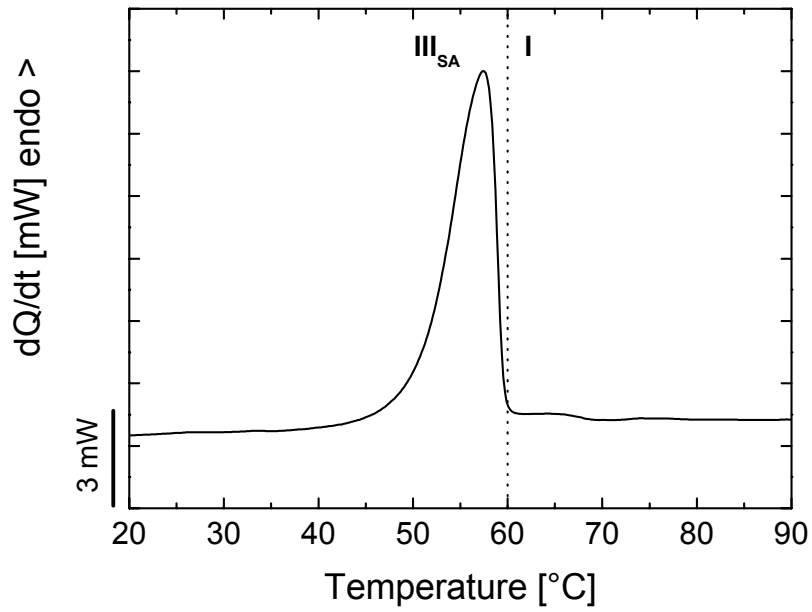

Figure 6. Location of self-nucleation domains in the standard melting peak for $B_{24}I_{56}EO_{20}^{67}$.

Table 2. Location of self-nucleation domains for PB-*b*-PI-*b*-PEO and PE-*b*-PEP-*b*-PEO triblock copolymers.

Triblock Copolymer	Self-nucleation domains [a]		
	PEO_I [b]	PEO_{II} [b]	PE
$B_{24}I_{56}EO_{20}^{67}$	$I \mid_{60} III_{SA}$	-	-
$B_{11}I_{70}EO_{19}^{120}$	$I \mid_{62} III_{SA}$	-	-
$B_{17}I_{57}EO_{26}^{130}$	$I \mid_{61} III_{SA}$	$I \mid_{65} II \mid_{63} III_{SA}$	-
$B_{19}I_{39}EO_{42}^{135}$	$I \mid_{63} III_A \mid_{59} III_{SA}$	$I \mid_{65} II \mid_{64} III_{SA}$	-
$E_{24}EP_{57}EO_{19}^{69\,c}$	$I \mid_{59} III_{SA}$	$I \mid_{63} II \mid_{59} III_{SA}$	$I \mid_{105} II \mid_{99} III_{SA}$
$E_{24}EP_{57}EO_{19}^{69}$	$I \mid_{59} III_{SA}$	-	$I \mid_{101} II \mid_{97} III_{SA}$
$E_{11}EP_{71}EO_{18}^{123\,c}$	$I \mid_{61} III_{SA}$	$I \mid_{63} II \mid_{61} III_{SA}$	$I \mid_{101} II \mid_{95} III_{SA}$
$E_{11}EP_{71}EO_{18}^{123}$	$I \mid_{61} III_{SA}$	-	$I \mid_{97} II \mid_{95} III_{SA}$
$E_{18}EP_{57}EO_{25}^{133}$	$I \mid_{59} III_{SA}$	$I \mid_{63} II \mid_{59} III_{SA}$	$I \mid_{101} II \mid_{97} III_{SA}$
$E_{19}EP_{40}EO_{41}^{138}$	$I \mid_{65} III_A \mid_{61} III_{SA}$	$I \mid_{67} II \mid_{65} III_{SA}$	$I \mid_{101} II \mid_{97} III_{SA}$

[a] numbers in subscripts give the transition temperature between the different self-nucleation domains.

[b] PEO_I corresponds to the exotherm at ca. –20 °C, and PEO_{II} corresponds to the high temperature exotherm ($T_c(PEO_I)$ and $T_c(PEO_{II})$ in Table 1).

[c] triblock copolymer contains residual Wilkinson catalyst.

$B_{19}I_{39}EO_{42}^{135}$, the PB-*b*-PI-*b*-PEO triblock copolymer with the highest PEO content under investigation, shows a double crystallization exotherm for PEO with peak temperatures of ≈ 20 and 37.5 °C, respectively. Only a tiny fraction (ca. 2%) of the PEO crystallizes at a T_c = -25 °C. From the composition a lamellar morphology might be expected and has been deduced from transmission electron microscopy (TEM) investigations, showing crystalline PEO lamellae within a matrix of the miscible PB and PI segments (results not shown). The unusual double exotherm might be explained by crystallization within isolated PEO lamellae (lower T_c) and crystallization within interconnected PEO lamellae (higher T_c). Here, the PEO blocks are not confined within small isolated spherical or cylindrical microdomains, as in the case of PB-*b*-PI-*b*-PEO triblock copolymers with PEO contents ≤ 20 wt.-%. This in turn is expected to have a significant influence on the self-nucleation behavior of the PEO block. Figures 7A and 7B show the corresponding cooling and heating traces obtained after thermal conditioning at the indicated T_s temperatures. First the self-nucleation behavior of the high temperature double crystallization exotherm will be discussed.

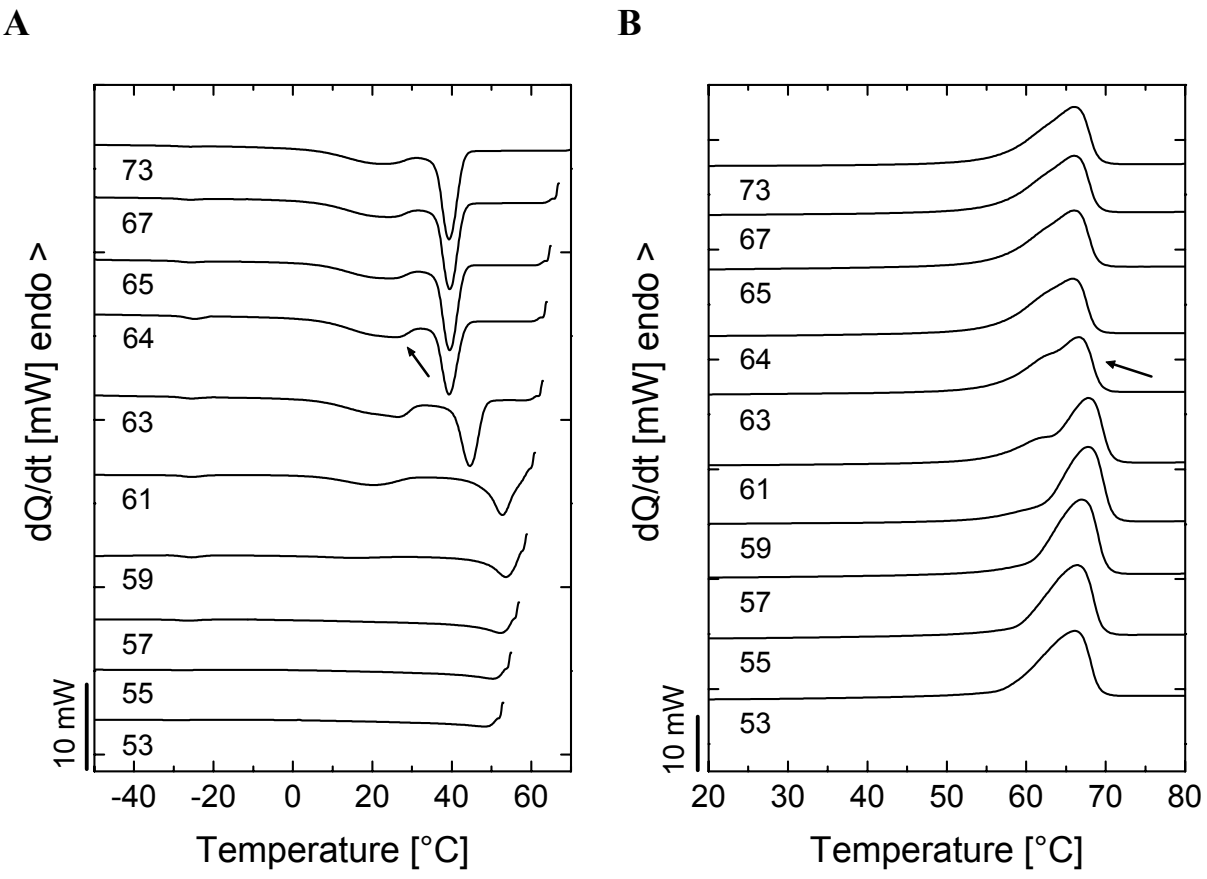

Figure 7. DSC cooling scans (A) for $B_{19}I_{39}EO_{42}^{135}$ after self-nucleation at the indicated T_s and subsequent heating scans (B).

For $T_s \geq 65$ °C no change in T_c(PEO) can be observed, i. e. the PEO blocks are under *domain I*. At $T_s = 64$ °C the lower crystallization peak of the double exotherm exhibits a slight shift to higher temperatures (Figure 7A), whereas in the subsequent heating run no indications for annealing can be detected (Figure 7B). This change is more obvious in the plot of T_c versus T_s depicted in Figure 8A.

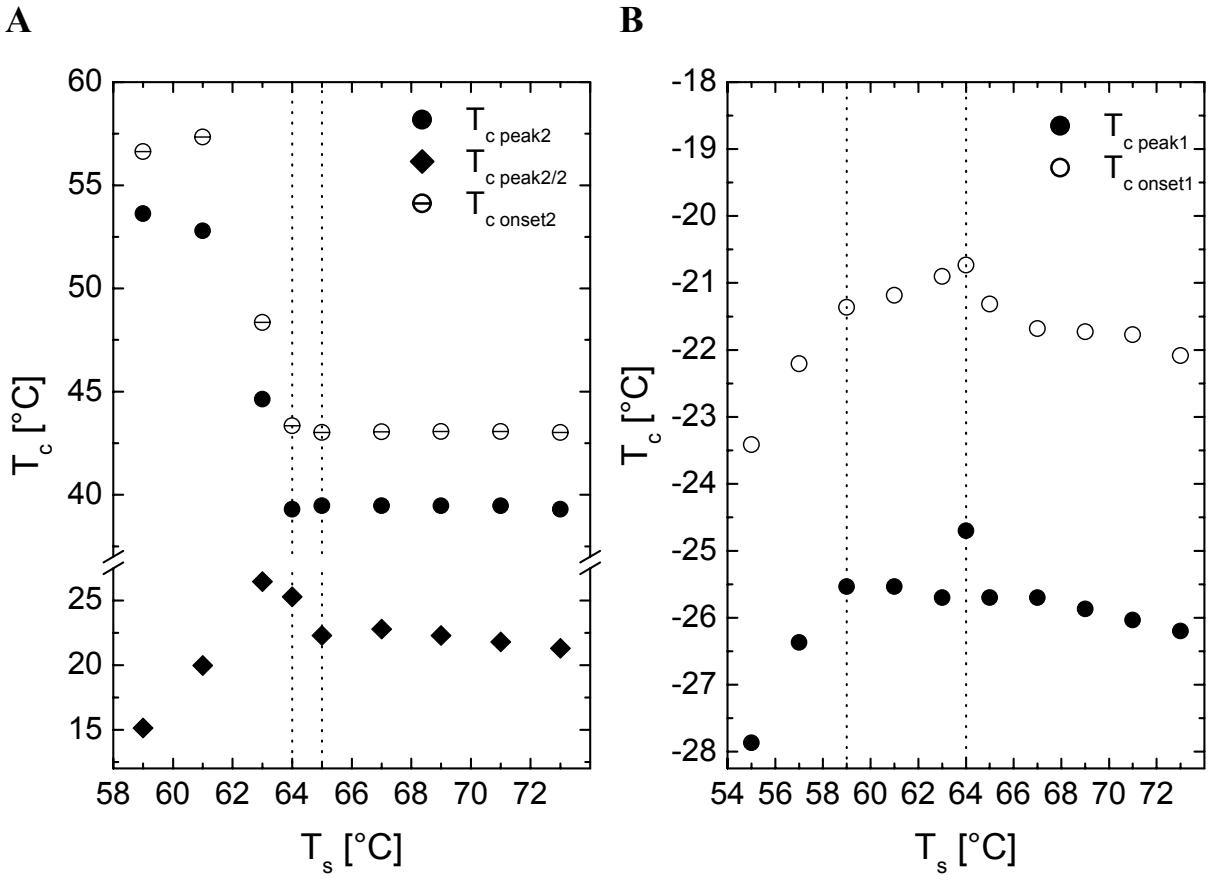

Figure 8. Variation of the crystallization temperatures with T_s for PEO crystallizing in exotherm II (A, $T_c(PEO_{II})$ in Table 1) and exotherm I (B, $T_c(PEO_I)$ in Table 1) within $B_{19}I_{39}EO_{42}$[135]. The dashed lines correspond to changes in self-nucleation domains.

The peak crystallization temperature of the exotherm at lower temperatures, labeled as $T_{c\ peak2/2}$ in Figure 8A, shows a clear shift to higher temperatures, indicating that self-nucleation occurs. In addition a slight shift to higher temperatures in the corresponding onset-temperature, labeled as $T_{c\ onset2}$ can be deduced. Thus, the PEO block is under *domain II* or self-nucleation domain at $T_s = 64$ °C. A further decrease in T_s of only 1 °C ($T_s = 63$ °C) already results in annealing as can be seen in the corresponding heating run from the slightly increased peak melting temperature and the "bimodal" character of the PEO melting

endotherm (Figure 7B). This is more pronounced for lower T_s temperatures exhibiting a shift of the complete melting endotherm to higher temperatures (see for example T_s = 59 °C). Consequently, *domain III*$_{SA}$ has already been reached at T_s = 63 °C. This slight variation in T_s induces a significant shift of the high temperature part of the double exotherm to higher temperatures whereas the lower temperature part exhibits only a slight shift (Figure 7A), which can be seen more clearly in Figure 8A. At T_s = 61 °C the major fraction of PEO crystallizes immediately upon cooling, whereas a small fraction still crystallizes at ca. 20 °C, showing that this population is less effectively nucleated by self-seeds. This seems reasonable, as this small fraction might be attributed to PEO segments located within isolated PEO lamellae and therefore needs a higher concentration of self-seeds to be nucleated. At T_s = 59 °C this fraction also crystallizes directly upon cooling as the corresponding exotherm at ca. 20 °C vanishes in the particular cooling trace (Figure 7A). In conclusion, the self-nucleation domains for the PEO fraction crystallizing in the double exotherm can be located as depicted in Figure 9A. All three self-nucleation domains can be located, whereas *domain II* exists only in a very sharp T_s range of 65 – 64 °C.

The low temperature crystallization exotherm at –25 °C might be attributed to a very small fraction of isolated PEO domains. This exotherm is so small that it cannot be readily appreciated at the scale used to plot the data in Figure 7. As the samples were not subjected to a special treatment previous to the self-nucleation experiments, the morphology is not perfectly ordered. The plot of T_c versus T_s for the PEO fraction crystallizing in the low temperature exotherm in Figure 8B shows no significant change in T_c for T_s temperatures $\geq$ 59 °C. The small variations are mainly attributable to uncertainties in data evaluation due to the very small heat of crystallization. This in turn implies that *domain II* is absent in this case, as no shift in T_c to higher temperatures with decreasing T_s is observed. Even for T_s < 64 °C where annealing already takes place (see corresponding heating traces in Figure 7B) no change in peak and onset crystallization temperatures can be detected down to a T_s = 59 °C (Figure 8B). Thus, at this temperature the annealed crystals present in the sample are not able to self-nucleate the PEO segments crystallizing in the low temperature exotherm. A T_s of 57 °C, i. e. higher concentration of self-seeds, is necessary to induce self-nucleation which is directly connected to a decrease in the observed T_c values (Figure 8B). Thus, for the PEO fraction crystallizing in the low temperature exotherm the self-nucleation domains can be located as depicted in Figure 9B. Upon lowering T_s a direct transition from *domain I* into *domain III*$_A$, without going through *domain II* is observed. In *domain III*$_A$ only annealing is

detected as the concentration of self-seeds is still too low to induce self-nucleation. Upon further lowering T_s *domain* III_{SA} is reached, where self-nucleation and annealing take place.

A

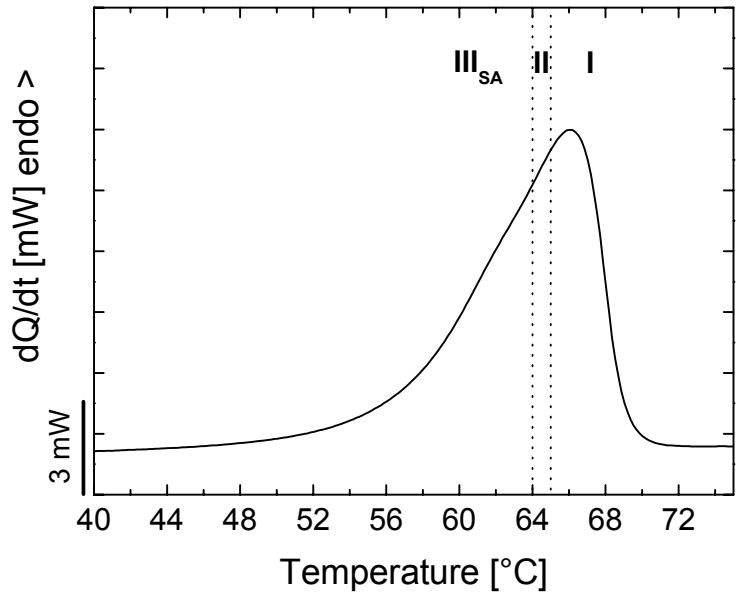

B

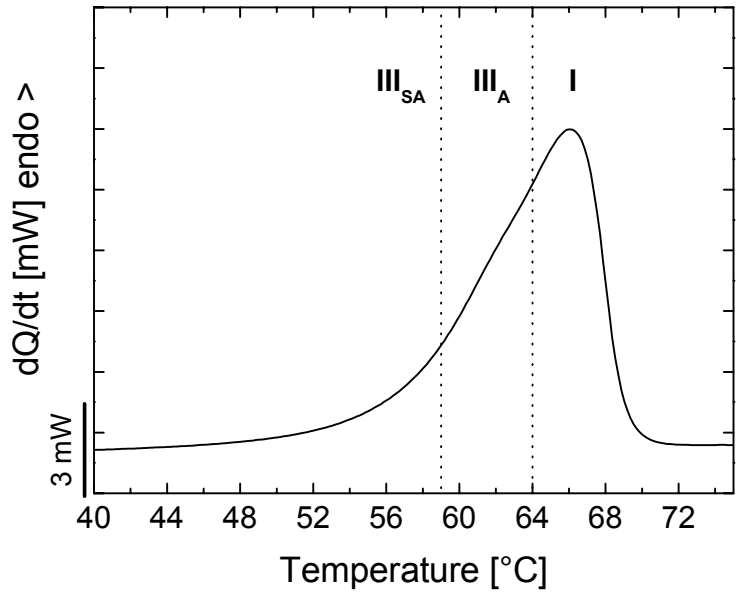

Figure 9. Location of self-nucleation regimes in the standard melting peak for PEO crystallizing in exotherm II (A, $T_c(PEO_{II})$ in Table 1) and exotherm I (B, $T_c(PEO_I)$ in Table 1) within $B_{19}I_{39}EO_{41}$[135].

The triblock copolymer $B_{17}I_{57}EO_{26}$[130] with an intermediate PEO content exhibits a fractionated crystallization (Table 1). The major PEO fraction crystallizes in the low temperature exotherm with a peak crystallization temperature of -21 °C. The self-nucleation behavior is identical to that observed in $B_{24}I_{56}EO_{20}$[67] and $B_{11}I_{70}EO_{19}$[120], i. e. *domain II* is completely absent (Table 2). In contrast, the PEO fraction crystallizing in the high temperature exotherm (T_c = 16.1 °C) shows a behavior similar to that observed for the PEO blocks in $B_{19}I_{39}EO_{42}$[135] crystallizing in the high temperature double exotherm. Here, all three self-nucleation domains are present (Table 2). From composition (26 wt.-% PEO) a cylindrical microdomain structure for PEO can be expected, as has been observed for the corresponding hydrogenated triblock copolymer[2] (results not shown). The differences in self-nucleation behavior observed for the two crystallization exotherms might be attributed to differences in the cylindrical microdomain structure, exhibiting either isolated or interconnected PEO cylinders. For PEO segments crystallizing within interconnected PEO cylinders a lower concentration of self-seeds is necessary to induce self-nucleation, i. e. *domain II* is present. However, for isolated PEO cylinders a comparatively higher concentration of self-seeds, i. e. lower T_s, is necessary. In this case self-nucleation can only occur when annealing processes are already active, i. e. *domain II* is absent.

PE-*b*-PEP-*b*-PEO triblock copolymers. In order to exclude any effects on the self-nucleation behavior of the PE-*b*-PEP-*b*-PEO triblock copolymers arising from residual Wilkinson catalyst, used in the hydrogenation reaction, all samples were subjected to a further purification step. This was accomplished by refluxing a toluene solution of the triblock copolymer with a small amount of hydrochloric acid. The PEO blocks in the purified PE-*b*-PEP-*b*-PEO triblock copolymers exhibit a similar self-nucleation behavior compared to the corresponding PB-*b*-PI-*b*-PEO triblock copolymers (Table 2). In PE-*b*-PEP-*b*-PEO triblock copolymers with PEO contents < 20 wt.-% *domain II* vanishes completely in analogy to the corresponding PB-*b*-PI-*b*-PEO triblock copolymers, emphasizing the strong influence of confinement on the self-nucleation behavior of the PEO blocks. In $E_{18}EP_{57}EO_{25}$[133] all three self-nucleation domains can be located for the PEO chains crystallizing in the high temperature exotherm, whereby *domain II* is absent for the low temperature exotherm. However, compared to $B_{17}I_{57}EO_{26}$[130] the fraction of PEO crystallizing in the high temperature exotherm is significantly higher for $E_{18}EP_{57}EO_{25}$[133] (Table 1). The self-nucleation behavior of the PEO blocks in $E_{19}EP_{40}EO_{41}$[138] is identical to that in $B_{19}I_{39}EO_{42}$[135]. For the low temperature exotherm again a split of *domain* III_{SA} into *domain* III_A and *domain* III_{SA} is observed. With regard to the non purified PE-*b*-PEP-*b*-PEO triblock copolymers a strong influence of residual

Wilkinson catalyst on the crystallization and self-nucleation behavior of the PEO block has been observed. This effect will be addressed in more detail in the appendix.

Self-nucleation behavior of the PE block within PE-b-PEP-b-PEO triblock copolymers

PE-*b*-PEP-*b*-PEO triblock copolymers with ca. 20 wt.-% PE exhibit crystallization temperatures at about 65 to 72 °C (Table 1) reflecting a heterogeneous nucleation mechanism, since the observed values are very close to the crystallization temperature of ca. 73 °C detected in a hydrogenated polybutadiene of similar branching content.[1] However, the triblock copolymer $E_{11}EP_{71}EO_{18}^{123}$ exhibits a comparatively lower melting and crystallization temperature for the PE block. This might be attributed on one hand to the higher amount of ethyl branches in the PE block (Table 1), resulting in thinner crystals (lower T_m), and on the other hand to a slightly decreased segregation strength of the PE and PEP segments arising from the lower PE-content (lower T_c). Due to the small value for the segmental interaction parameter χ of 0.007 at 120 °C for PE and PEP[11], crystallization of PE is expected to occur from a homogeneous mixture of PE and PEP segments.[22-25] Thus, in contrast to the PEO blocks, crystallization of PE should not be confined within isolated microdomains as it occurs from a homogeneous mixture of PE and PEP segments. This in turn, is expected to have a significant influence on the self-nucleation behavior of the PE blocks.

Figure 10 shows the TEM micrograph of $E_{19}EP_{40}EO_{41}^{138}$. As a result from hydrogenation with *p*-toluenesulfonyl hydrazide, the PEP block contains ca. 30% residual olefinic double bonds, which can be selectively stained with OsO_4. Consequently, the crystalline PE and PEO domains appear bright. The PE block forms a hexagonal array of interconnected PE crystallites, separated from the crystalline PEO cylinders by the selectively stained PEP block. This phase assignment has been proven by comparison of TEM images showing different projections with respect to the PEO cylinder long axis combined with TEM investigations of the completely hydrogenated $E_{19}EP_{40}EO_{41}^{138}$.[2] The hexagonal array of PE crystallites is often distorted, but interconnections between several PE crystallites are still clearly visible. Thus, TEM investigations show that crystallization of the PE block from a homogeneous mixture of PE and PEP segments in the melt results in the formation of a continuous semicrystalline PE phase.

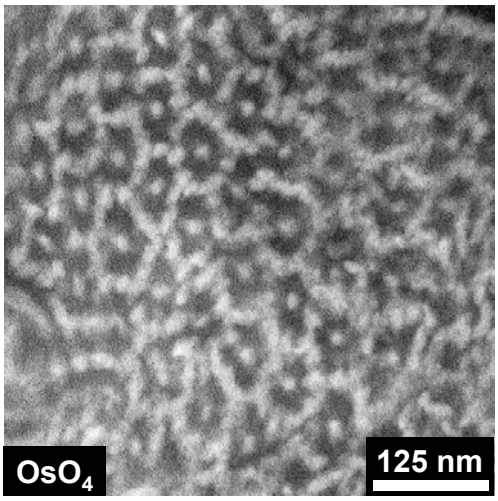

Figure 10. TEM micrograph of $E_{19}EP_{40}EO_{41}$[138]. The triblock copolymer contains 30% residual double bonds within the PEP block, which were selectively stained with OsO_4 together with the amorphous PEO segments.

Figures 11A and 11B show the corresponding cooling and heating traces obtained for self-nucleation experiments on the PE block within $E_{18}EP_{57}EO_{25}$[133]. From T_s = 111 °C to T_s = 101 °C the PE crystallization exotherm exhibits no change in $T_{c\ peak}$ and $T_{c\ onset}$, indicating that the PE block is under *domain I* (see also Figure 12). At T_s = 99 °C the exotherm shows a shift to higher temperatures, both in peak and onset crystallization temperature. This can be deduced in more detail in the plot of T_c versus T_s in Figure 12. Thus, *domain II* has been reached at T_s = 99 °C. Upon further decreasing T_s annealing takes place at T_s = 95 °C, as can be seen in the corresponding heating trace (Figure 11B). A closer look to the subsequent cooling run after self-nucleation at 95 °C (Figure 11A) reveals a split of the crystallization exotherm in a low temperature (labeled "a") and a high temperature (labeled "b") exotherm. While exotherm "b" shows a shift to higher temperatures upon lowering T_s (Figure 12), a small fraction of PE is left without self-nucleation in exotherm "a" and reveals a shift to lower temperatures. For $T_s < 91$ °C, the PE fraction that crystallizes in exotherm "b" at higher T_s values crystallizes now directly upon cooling, whereas the low temperature exotherm "a" is still present.

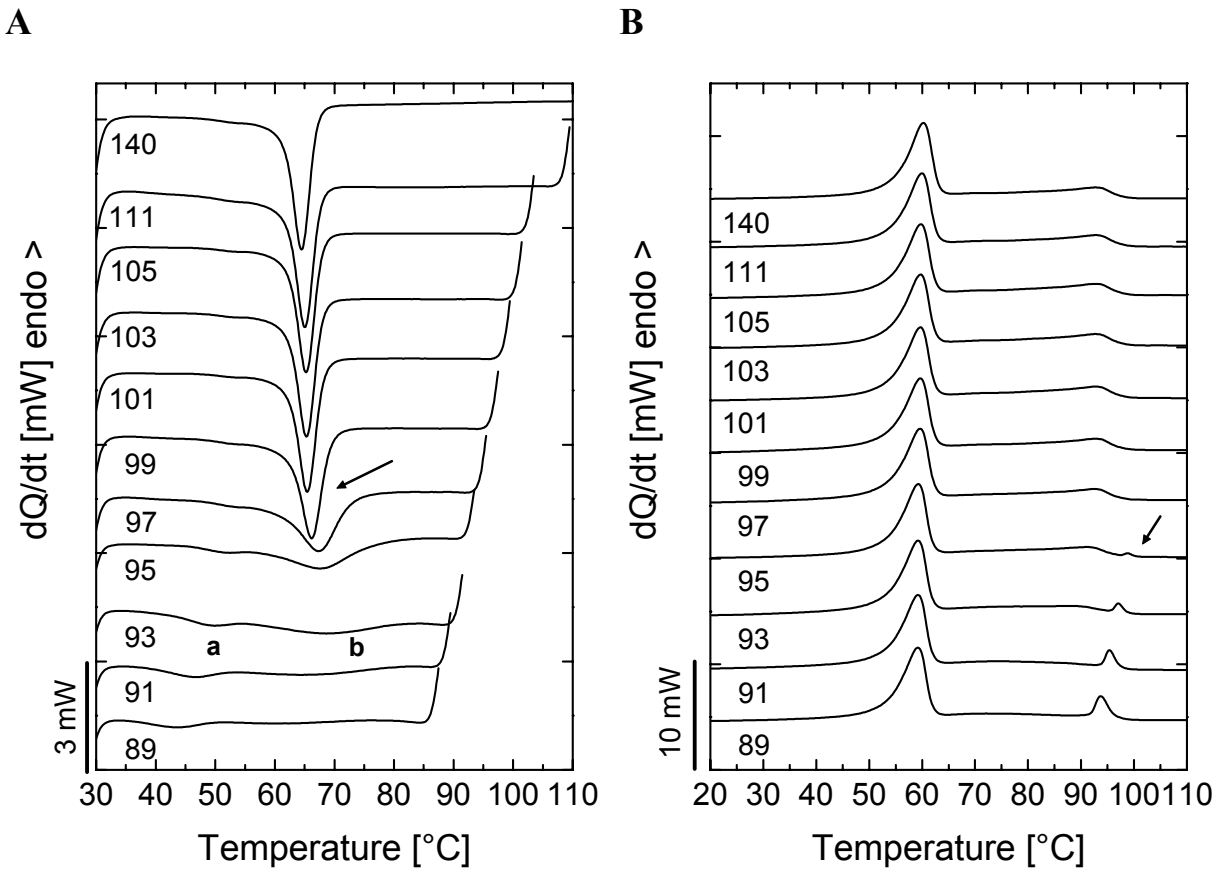

Figure 11. DSC cooling scans (A) for $E_{18}EP_{57}EO_{25}$[133] after self-nucleation at the indicated T_s and subsequent heating scans (B).

This bimodal crystallization of the PE block was observed for all investigated PE-*b*-PEP-*b*-PEO triblock copolymers. A similar result has been found for the strongly confined PE blocks within PS-*b*-PE-*b*-PCL triblock copolymers.[13] In that case, the bimodal crystallization has been interpreted as the result of the crystallization of two different parts of the PE chain. Those PE segments that are located close to the interphase experience a greater difficulty in being self-nucleated due to their restricted mobility. On the other hand, those PE segments that are located in the middle of the PE domain exhibit a higher mobility, and thus are able to be self-nucleated. In the present case a similar interpretation is difficult to envisage in view of the absence of a neighboring glassy block. Nevertheless, microphase separation between PE and PEP is driven by crystallization and results in a continuous PE phase consisting of interconnected PE crystallites, as has been shown by TEM investigations (Figure 10). As a result, the continuous PE phase exhibits a comparatively high interphase area with respect to an isolated microdomain (e. g. sphere). Consequently, the fraction of PE segments located

close to the domain interphase might be rather high, giving rise to the observed bimodal crystallization (even if this interphase is rubbery in the present case).

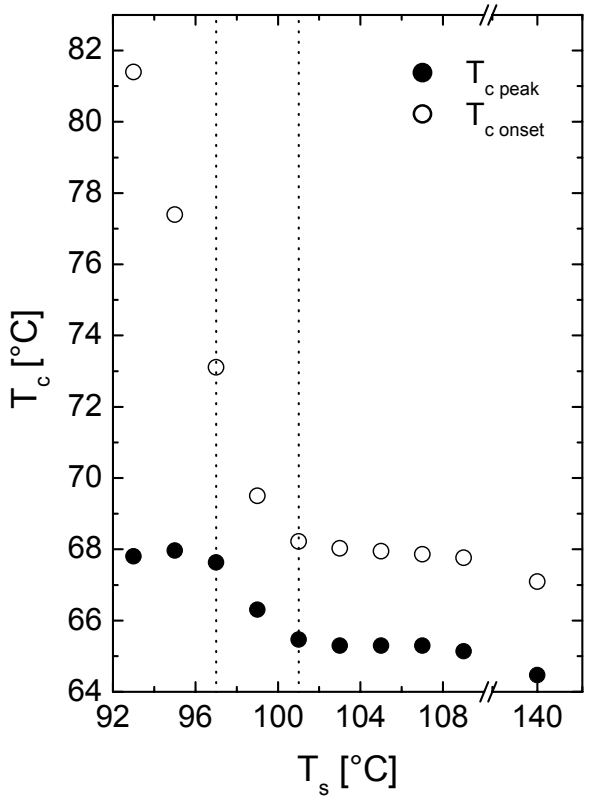

Figure 12. Variation of the PE crystallization temperatures with T_s for $E_{18}EP_{57}EO_{25}$[133]. The dashed lines correspond to changes in self-nucleation domains.

As a result, for the PE block in $E_{18}EP_{57}EO_{25}$[133] all three self-nucleation domains can be detected, as depicted in Figure 13. In contrast to the self-nucleation behavior of the PEO blocks within PE-*b*-PEP-*b*-PEO and PB-*b*-PI-*b*-PEO triblock copolymers, *domain II* is always present for the PE blocks, regardless of the very small PE contents between 10 and 25 wt.-% (Table 2). This is a direct result of the missing confinement during the crystallization of PE from a homogeneous mixture of PE and PEP segments.

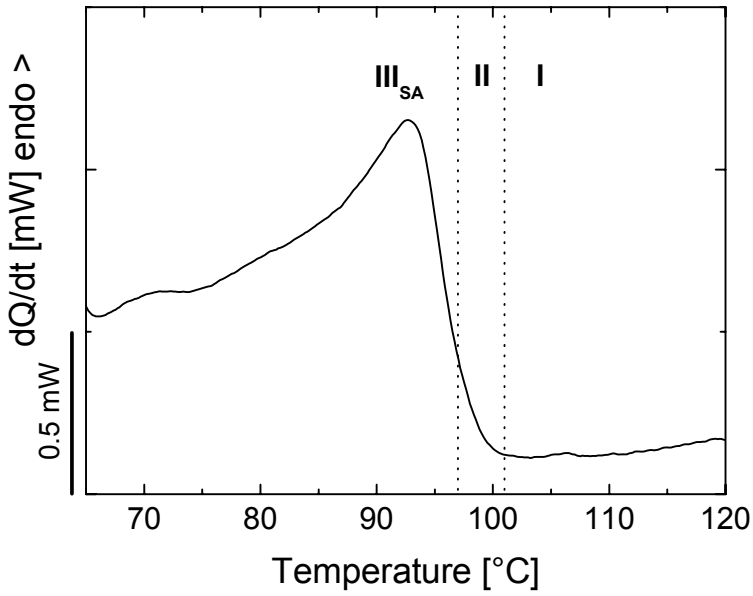

Figure 13. Location of self-nucleation regimes in the standard melting peak for PE within $E_{18}EP_{57}EO_{25}$[133].

Conclusions

We have investigated the influence of different confinements active during PEO and PE crystallization on the self-nucleation behavior of the corresponding blocks within PB-*b*-PI-*b*-PEO and PE-*b*-PEP-*b*-PEO triblock copolymers. In triblock copolymers with PEO contents ≤ 20 wt.-% crystallization of PEO occurs only at high supercoolings (T_c ca. –20 °C). Self-nucleation experiments show, that *domain II* is completely absent in these systems. This is a direct result of the confined crystallization of PEO within small isolated microdomains (spheres or cylinders). In order to induce self-nucleation of the confined PEO segments a high concentration of self-seeding nuclei is necessary, i. e. T_s has to be lowered well into *domain* III_{SA} to provide a sufficiently high concentration of self-seeds. Triblock copolymers with a higher PEO content exhibit fractionated crystallization in a high and a low temperature exotherm. For the high temperature exotherm all three self-nucleation domains are observed. Therefore, the concentration of self-seeds provided in *domain II* is sufficiently high to induce self-nucleation which might be attributed to the increasing size of the PEO domains (cylinders or lamellae) with increasing PEO content. In contrast, the PEO fraction that crystallizes in the low temperature exotherm shows a similar behavior compared to the PEO blocks in the triblock copolymers with PEO contents ≤ 20 wt.-%, i. e. *domain II* vanishes for these microdomains. This might be attributed to the fact, that still small isolated PEO microdomains

are present in the systems as the samples were not subjected to annealing prior to the self-nucleation experiments, i.e. the morphologies are not perfectly ordered.

The self-nucleation behavior of the PE blocks within PE-*b*-PEP-*b*-PEO triblock copolymers is significantly different as compared to the PEO blocks. Regardless of the low PE content (10 – 25 wt.-%) all three self-nucleation domains can be located for the PE blocks in the investigated triblock copolymers. This can be attributed to the fact that the PE segments crystallize from a homogeneous mixture of PEP and PE segments due to their low segmental interaction parameter. Consequently, there is no confinement active during PE crystallization resulting in the observation of all three self-nucleation domains.

Acknowledgment: Financial support by *DSM Research*, Geleen, the German Israeli Foundation for Scientific Research and Development (GIF) and the *Sonderforschungsbereich 481* funded by the *Deutsche Forschungsgemeinschaft (DFG)* is gratefully acknowledged.

Appendix

Effect of impurities on the self-nucleation behavior of the PEO block within PE-b-PEP-b-PEO triblock copolymers

The PE-*b*-PEP-*b*-PEO triblock copolymers were obtained by homogeneous catalytic hydrogenation of the corresponding PB-*b*-PI-*b*-PEO triblock copolymers using Wilkinson catalyst ($(Ph_3P)_3Rh(I)Cl$).[2] As a matter of fact the hydrogenated triblock copolymers contain some residues arising from the used Wilkinson catalyst due to the complex forming properties of the polar PEO blocks. This results in a significant change of the crystallization behavior of the PEO blocks as can be derived from the comparison of crystallization exotherms observed in $E_{24}EP_{57}EO_{19}$[69], which contains catalyst residues, and the corresponding precursor triblock copolymer $B_{24}I_{56}EO_{20}$[67] (Table 1). In $E_{24}EP_{57}EO_{19}$[69] the main fraction of PEO crystallizes at 17.9 °C, a temperature significantly higher than that observed for the non-hydrogenated triblock copolymer. Only a small fraction crystallizes in a similar manner compared to the non-hydrogenated triblock copolymer at –21.5 °C. Similar results were obtained for the triblock copolymer $E_{11}EP_{71}EO_{18}$[123] (Table 1). As the high temperature exotherm observed in $E_{24}EP_{57}EO_{19}$[69] and $E_{11}EP_{71}EO_{18}$[123] vanishes completely after purification (Table 1), it might be attributed to a nucleating property of Wilkinson catalyst residues, inducing heterogeneous nucleation of the PEO chains.

Figure 14A shows cooling traces for $E_{24}EP_{57}EO_{19}$[69] (with catalyst debris) obtained after thermal treatment at the indicated T_s values. The high temperature exotherm shows a clear shift to higher temperatures at T_s = 61 °C whereas the low temperature exotherm remains unchanged. This can be deduced more clearly in the corresponding plot of T_c versus T_s in Figure 14B. Thus, the PEO chains crystallizing in the high temperature exotherm are under *domain II* or self-nucleation domain. In contrast, the PEO segments that crystallize in the low temperature exotherm are still under *domain I*, since no self-nucleation can be detected for this population. At T_s = 57 °C the PEO chains crystallize directly upon cooling, reflecting that self-nucleation and annealing takes place at the same time. Moreover, the low temperature exotherm decreases in size and exhibits a shift of the peak crystallization temperature to lower values (Figure 14B). Thus at T_s = 57 °C *domain* III_{SA} has been reached for both populations which can also be corroborated from the corresponding heating trace, exhibiting a shift in the melting endotherm to higher temperatures (results not shown).

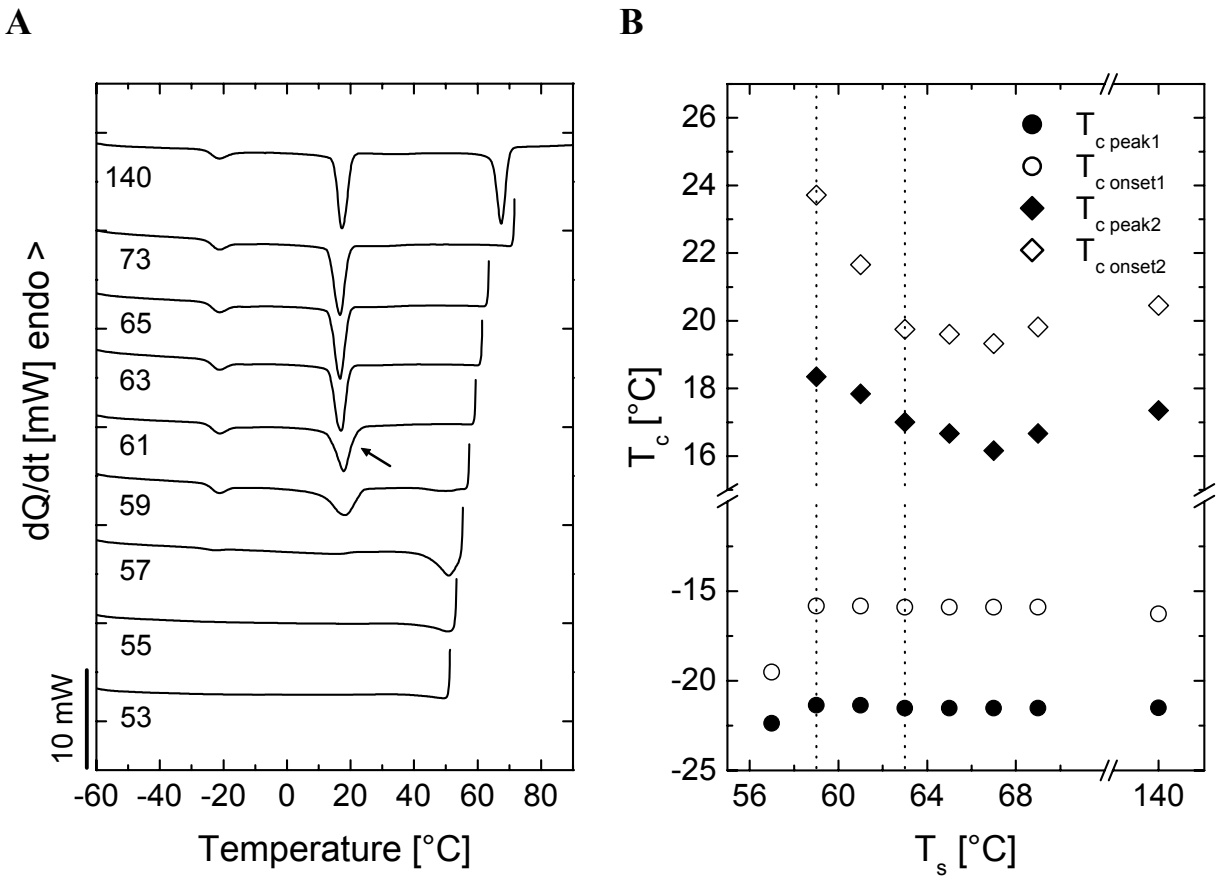

Figure 14. DSC cooling scans (A) for $E_{24}EP_{57}EO_{19}$[69], containing Wilkinson catalyst residues, after self-nucleation at the indicated T_s, and variation of crystallization temperatures with T_s (B). The dashed lines correspond to changes in self-nucleation domains.

In conclusion, for the PEO chains crystallizing in the high temperature exotherm all three self-nucleation domains can be located as depicted in Figure 15A. In contrast to the corresponding $B_{24}I_{56}EO_{20}$[67] triblock copolymer (Table 2) *domain II* is present, probably due to some nucleating property of catalyst residues in the PEO microdomains. However, the PEO fraction crystallizing in the low temperature exotherm exhibits an identical behavior compared to the PEO blocks in $B_{24}I_{56}EO_{20}$[67] (Figure 15B, Table 2). This might be rationalized by a lack of active catalyst residues in the corresponding PEO microdomain, resulting in the absence of *domain II*. Self-nucleation experiments on $E_{11}EP_{71}EO_{18}$[123] exhibit similar results (Table 2). In conclusion, Wilkinson catalyst debris, arising from the hydrogenation reaction, have a strong influence on the crystallization and self-nucleation behavior of the PEO block within PE-*b*-PEP-*b*-PEO triblock copolymers.

A

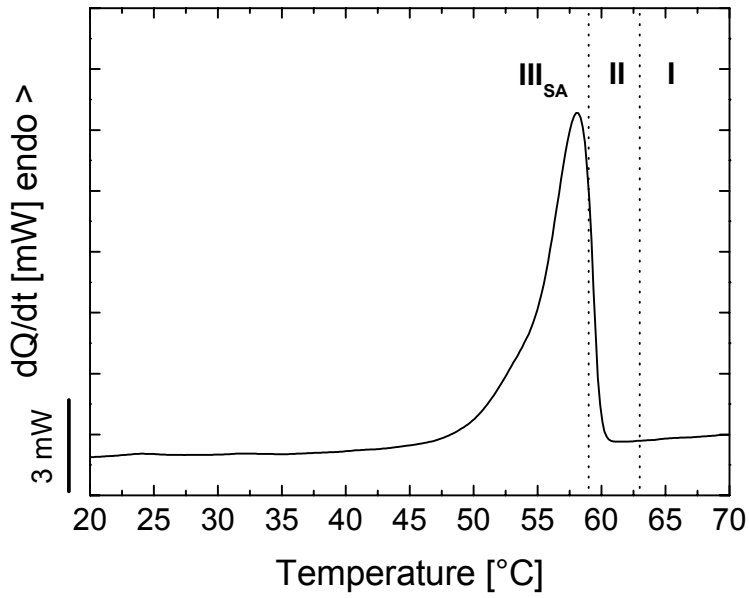

B

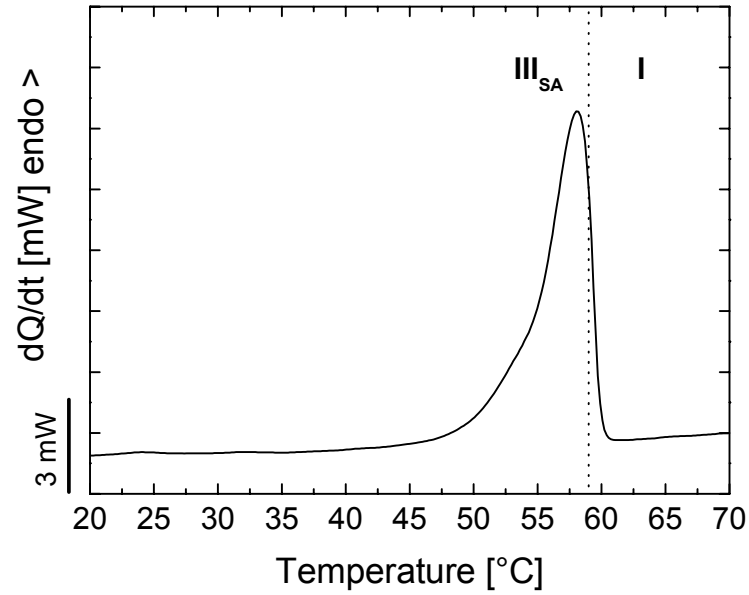

Figure 15. Location of self-nucleation regimes in the standard melting peak for PEO crystallizing in exotherm II (A, $T_c(PEO_{II})$ in Table 1) and exotherm I (B, $T_c(PEO_I)$ in Table 1) within $E_{24}EP_{57}EO_{19}$[69], containing Wilkinson catalyst residues.

References and notes

[1] A. J. Müller, V. Balsamo, M. L. Arnal, T. Jakob, H. Schmalz, V. Abetz, *Macromolecules* **2002**, *35*, 3048.

[2] H. Schmalz, A. Knoll, A. J. Müller, V. Abetz, *Macromolecules* **2002**, *35*, 10004.

[3] M. L. Arnal, V. Balsamo, F. López-Carrasquero, J. Contreras, M. Carrillo, H. Schmalz, V. Abetz, E. Laredo, A. J. Müller, *Macromolecules* **2001**, *34*, 7973.

[4] V. Balsamo, A. J. Müller, F. von Gyldenfeldt, R. Stadler, *Macromol. Chem. Phys.* **1998**, *199*, 1063.

[5] V. Balsamo, F. von Gyldenfeldt, R. Stadler, *Macromol. Chem. Phys.* **1996**, *197*, 3317.

[6] B. Lotz, A. J. Kovacs, *Polym. Prep. (Am. Chem. Soc., Div. Polym. Chem.)* **1969**, *10*, 820.

[7] S. Nojima, H. Kakihira, S. Tanimoto, H. Nakatami, S. Sasaki, *Polym. J.* **2000**, *32*, 75.

[8] C. Robitaille, J. Prud'homme, *Macromolecules* **1983**, *16*, 665.

[9] Y.-L. Loo, R. A. Register, A. J. Ryan, *Macromolecules* **2002**, *35*, 2365.

[10] H. Schmalz, V. Abetz, A. J. Müller, *Macromol. Symp.* **2002**, *183*, 179.

[11] F. S. Bates, M. F. Schultz, J. H. Rosedale, *Macromolecules* **1992**, *25*, 5547.

[12] B. Fillon, J. C. Wittmann, B. Lotz, A. Thierry, *J. Polym. Sci., Part B: Polym. Phys.* **1993**, *31*, 1383.

[13] V. Balsamo, Y. Paolini, G. Ronca, A. J. Müller, *Macromol. Chem. Phys.* **2000**, *201*, 2711.

[14] H. Schmalz, A. Böker, R. Lange, V. Abetz, *Polym. Mater. Sci. Eng.* **2001**, *85*, 478.

[15] B. Wunderlich, *"Macromolecular Physics", Vol. 3*, Academic Press, New York, 1980.

[16] J. Brandrup, E. H. Immergut, *"Polymer Handbook"*, 3rd Ed., Wiley, New York, 1989.

[17] D. J. Blundell, A. Keller, A. J. Kovacs, *J. Polym. Sci., Part B: Polym. Phys.* **1966**, *4*, 481.

[18] V. Balsamo, A. J. Müller, R. Stadler, *Macromolecules* **1998**, *31*, 7756.

[19] C. H. Molinuevo, G. A. Mendez, A. J. Müller, *J. Appl. Polym. Sci.* **1998**, *76*, 1725.

[20] M. A. Sabino, G. Ronca, A. J. Müller, *J. Mater. Sci.* **2000**, *35*, 5071.

[21] V. Balsamo, A. J. Müller, in *ANTEC Conference Proceedings, Vol. 3*, New York, **1999**, pp. 3756.

[22] P. Rangarajan, R. A. Register, L. J. Fetters, *Macromolecules* **1993**, *26*, 4640.

[23] P. Kofinas, R. E. Cohen, *Macromolecules* **1994**, *27*, 3002.

[24] P. Rangarajan, R. A. Register, D. H. Adamson, L. J. Fetters, W. Bras, S. Naylor, A. J. Ryan, *Macromolecules* **1995**, *28*, 1422.

[25] A. J. Ryan, I. W. Hamley, W. Bras, F. S. Bates, *Macromolecules* **1995**, *28*, 3860.

3.2.3 Thermal and Self-Nucleation Behavior of Molecular Complexes Formed by *p*-Nitrophenol and the Poly(ethylene oxide) End Block within an ABC Triblock Copolymer

H. Schmalz[a], V. Abetz[a]*, A. J. Müller[b]

a) Makromolekulare Chemie II, Universität Bayreuth, 95440 Bayreuth, Germany.
b) Grupo de Polímeros USB, Departamento de Ciencia de los Materiales, Universidad Simón Bolívar, Apartado 89000, Caracas 1080-A, Venezuela.

SUMMARY: We have been able to prepare a molecular complex between the poly(ethylene oxide) block of a poly(ethylene)-*b*-poly(ethylene-*alt*-propylene)-*b*-poly(ethylene oxide) triblock copolymer and *p*-nitrophenol (PNP). The composition of the copolymer employed was: 24% PE, 57% PEP and 19% PEO in weight percent. The pure copolymer exhibited a non-conventional thermal behavior since the PEO block displayed a fractionated crystallization process during cooling. The PEO block/PNP complex did not show any apparent crystallization during cooling, instead cold crystallization during heating was observed and an approximately 30 °C increase in melting point as compared to the neat PEO block within the copolymer. This caused an overlap in the melting regions of the PE block and the PEO block/PNP complex. The self-nucleation of the PE-*b*-PEP-*b*-PEO/PNP complex is very different from that of the neat triblock copolymer. An increased capacity for self-nucleation of the PEO block was produced by the complexation with PNP and therefore the three self-nucleation domains were clearly encountered for both the PE block and the PEO block/PNP complex. Self-nucleation was able to show that the two crystallizable blocks can be self-nucleated and annealed in an independent way, thereby ascertaining the presence of separate crystalline regions in the triblock copolymer. Through the use of PNP, both the crystallinity and the melting point of the PE-*b*-PEP-*b*-PEO triblock copolymer employed here can be substantially increased. Similar results were obtained by complexation of the same ABC triblock copolymer with resorcinol.

Introduction

The crystallization of polymers is known to depend very much on parameters like the size of crystallizable domains, the presence of heterogeneities, thermal history and other parameters. While polymers like polypropylene in the bulk state crystallize via the so-called heterogeneous nucleation, in blends it also may crystallize via homogeneous nucleation when the number of crystallizable domains exceeds the number of active heterogeneities originally present in the bulk polymer before dispersion [1-4]. In block copolymers with dispersed crystallizable domains (spheres or cylinders) there is a much higher number of domains per unit volume as compared to phase separated polymer blends. Thus in block copolymers there do exist various crystallization mechanisms within one sample, since different crystallizable microdomains will not all contain the same type of heterogeneity [4-13].

In this contribution we investigate the crystallization behavior of a triblock copolymer in which two short crystallizable end blocks, namely polyethylene (PE) and poly(ethylene oxide) (PEO) are separated by an amorphous poly(ethylene-*alt*-propylene) (PEP) middle block. As a method differential scanning calorimetry (DSC) is applied by means of self-nucleation experiments [14-15]. Moreover, it is well-known that PEO homopolymer can form well-defined complexes with low molecular weight components like *p*-nitrophenol leading to an increase of both melting and crystallization temperatures [16-17]. In the following it will be shown that such complexes can also be formed in a PEO containing block copolymer.

Experimental

The synthesis of the PE-*b*-PEP-*b*-PEO triblock copolymer (24% PE, 57% PEP and 19% PEO in weight percent with an overall M_n of 69 kg/mol) ($E_{24}EP_{57}EO_{19}^{69}$) was carried out by living anionic polymerization and subsequent hydrogenation using Wilkinson catalyst ($(Ph_3P)_3Rh(I)Cl$) [18]. Residual catalyst was removed by shortly heating a solution of the triblock copolymer in toluene with a small amount of concentrated aqueous HCl to reflux followed by precipitation into 2-propanol. $E_{24}EP_{57}EO_{19}^{69}$/PNP complex was prepared from toluene solution (molar ratio EO/PNP = 3/2). Details about DSC measurements and self-nucleation procedure can be found in refs. 12 and 13, which are based on ref. 14. Ts stands for self-nucleation temperature [12-14].

Results and Discussion

Figure 1 presents the typical crystallization and melting behavior of the $E_{24}EP_{57}EO_{19}^{69}$ triblock copolymer. The cooling scan displays an exotherm at around 65 °C where the PE block crystallizes. The PEO block needs a much higher supercooling in order to crystallize in view of a fractionated crystallization that has been reported for similar diblock and triblock copolymers containing small amounts of PEO [5-7, 11-13]. When the PEO component is well dispersed in the form of cylinders or spheres, the number of isolated microdomains (assuming that microphase segregation is complete and has occurred in the melt before crystallization) will be much higher than the number of heterogeneities that can cause nucleation at higher temperatures [11-13]. At least 10^{15} isolated PEO microdomains/cm^3 could be present, while for instance a bulk PEO homopolymer contains less than 10^6 heterogeneities/cm^3 [12-13]. Therefore fractionated crystallization takes place and in the case of the triblock copolymer of Fig. 1, the PEO block can only crystallize at approximately –25 °C (where most of the polymer crystallizes) and also at –45 °C (where only a very small fraction is crystallizing in Fig. 1). The crystallization at –25 °C is produced after nucleation by a weakly active heterogeneity present in the polymer [1, 12-13], while that at –45 °C is most probably due to the crystallization after homogeneous nucleation since PEO vitrifies at -56 °C under similar cooling conditions [1-3, 7, 11-13]. The subsequent melting trace of $E_{24}EP_{57}EO_{19}^{69}$ shows the melting endotherms of the PEO and the PE block at temperatures equivalent to those shown by homopolymers of similar molecular weight and microstructure [13].

Figure 1 also shows the DSC cooling and subsequent heating scans for the $E_{24}EP_{57}EO_{19}^{69}$/PNP complex. In the cooling trace only the PE block exhibits a crystallization exotherm upon cooling from the melt while the PEO block either does not crystallize or crystallizes in a small amount or in a wide temperature range that cannot be detected. The subsequent heating trace exhibits a very clear Tg at –55 °C that corresponds to the PEP block and a second Tg located at –35 °C that should correspond to the PEO block/PNP molecular complex. At a temperature close to 20 °C a cold crystallization exotherm for the PEO block/PNP complex develops and a very small endotherm can be observed at 55 °C which could be due to the melting of a small fraction of PEO block crystals that could not form part of the complex with PNP. Finally a complex and broad melting endotherm is displayed beyond 75 °C. The high temperature shoulder of this melting endotherm could correspond to the melting of the PE block that now overlaps with the melting of the PEO block/PNP complex. The melting temperature of PEO homopolymer increases when it co-crystallizes

with PNP as thicker and stable nonintegral-folded lamellae are formed [16-17]. Previous reports for PEO/PNP complexes of molar ratio 3/2 and with a PEO molecular weight of approximately 6000 g/mol indicate that these complexes have a melting temperature range of 75 - 95 °C depending on the crystallization temperatures employed [16].

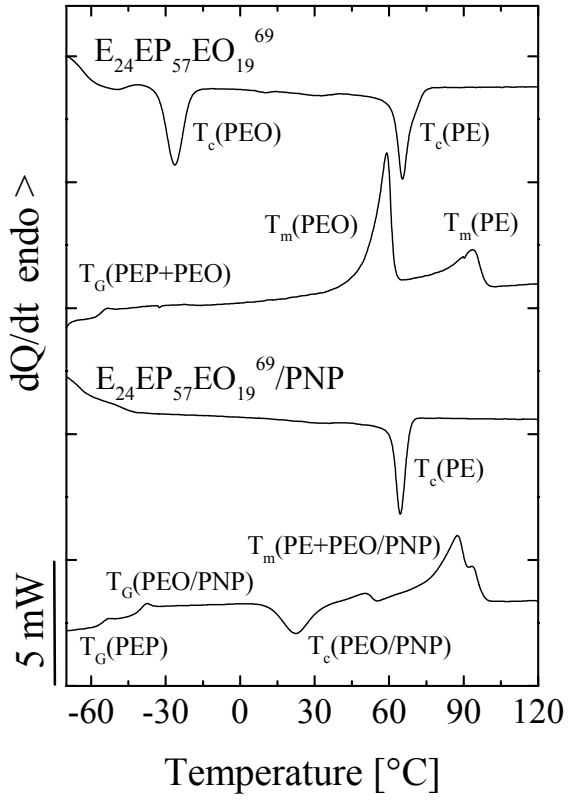

Figure 1. DSC cooling and heating scans at 10 °C/min for $E_{24}EP_{57}EO_{19}^{69}$ triblock copolymer (top) and for $E_{24}EP_{57}EO_{19}^{69}$/PNP complex (bottom).

The self-nucleation behavior of the $E_{24}EP_{57}EO_{19}^{69}$/PNP complex is displayed in Figure 2, where the cooling scans from selected Ts temperatures are shown in Fig. 2a while subsequent heating scans can be seen in Fig. 2b.

At a Ts of 104 °C or higher melting is complete and Domain I is reached by both the PE block and the PEO block/PNP complex. Only the PE block displays a clear crystallization exotherm upon cooling from 104 °C. A lowering of Ts causes self-nucleation of the PE block within Domain II as indicated by the shift of the crystallization temperature of the PE block to higher temperatures in the DSC cooling scans corresponding to Ts temperatures of 100 °C down to 96 °C. No apparent changes in the subsequent heating traces in Fig. 2b are observed up to Ts = 96 °C as expected for Domain II [13-14].

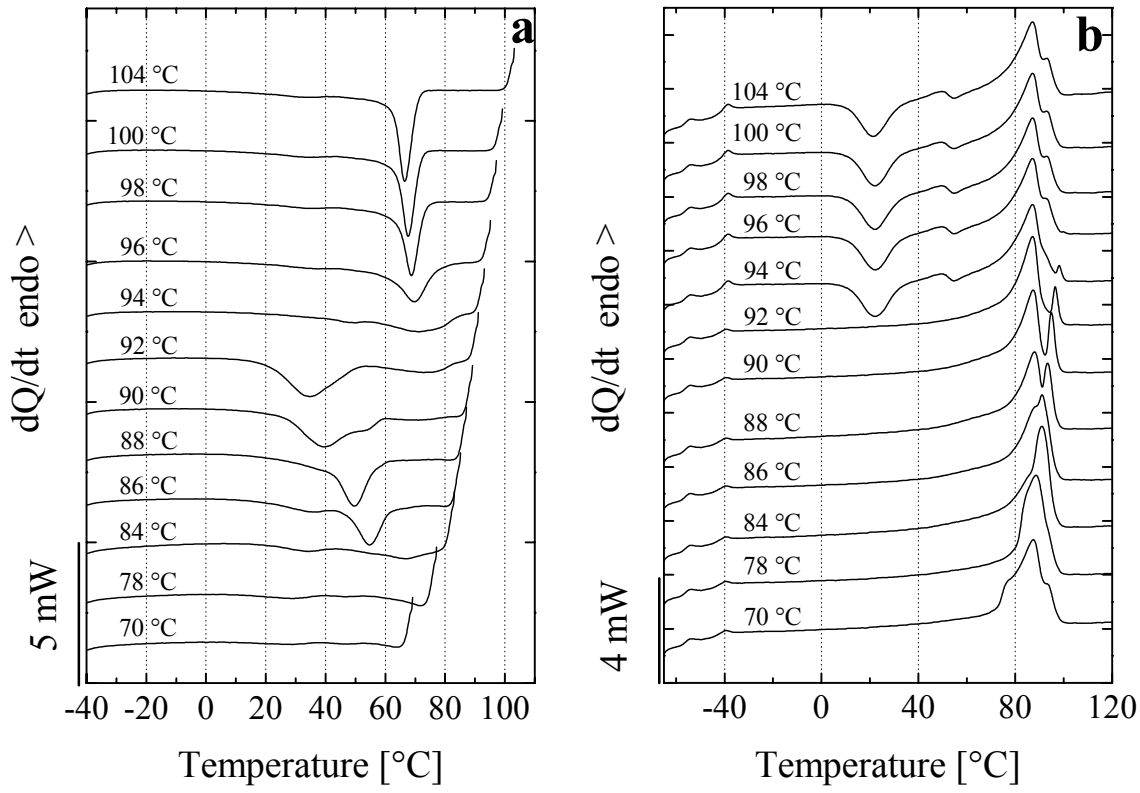

Figure 2. Self-nucleation behavior of $E_{24}EP_{57}EO_{19}^{69}$/PNP complex: a) DSC cooling scans from the indicated Ts temperatures and b) subsequent heating scans.

At a Ts temperature of 94 °C annealing of the PE block starts as Domain III is reached. This can be verified in Fig. 2b where a high temperature peak corresponding to the melting of annealed PE crystals can be observed. Apart from this additional melting peak, the rest of the DSC heating scan remains more or less unchanged indicating that the PEO block/PNP complex has not been altered by the applied heat treatments at Ts higher or equal to 94 °C (i.e., the PEO block/PNP complex is still in Domain I at such Ts temperatures).

The PEO block/PNP complex is self-nucleated at a Ts = 92 °C as can be seen in Fig. 2a where a very prominent exotherm that peaks at approximately 35 °C is readily apparent, therefore Domain II is reached for the PEO block/PNP complex. This behavior differs from that of the pure triblock copolymer, where Domain II for the PEO block disappears as a consequence of the fractionated crystallization process (for details of the self-nucleation behavior of $E_{24}EP_{57}EO_{19}^{69}$ see reference 13).

The produced self-nuclei at 92 °C are causing the crystallization of the PEO block/PNP complex during cooling and therefore on a subsequent heating scan (Fig. 2b) no cold crystallization is observed. This heating scan (for Ts = 92 °C) also shows how the amount of annealed PE crystals has grown with a reduction in Ts as compared with the heating scan after self-nucleation at 94 °C. The final transition from Domain II to Domain III for the PEO block/PNP complex probably occurs at Ts = 84 °C as judged by the immediate crystallization upon cooling from this Ts temperature in Fig. 2a and by the change in the corresponding melting endotherm in Fig. 2b [14].

Similar results were obtained by complexing the PEO block of the $E_{24}EP_{57}EO_{19}^{69}$ triblock copolymer with resorcinol.

Conclusions

We successfully prepared a molecular complex between the PEO block of a $E_{24}EP_{57}EO_{19}^{69}$ triblock copolymer and PNP. The PEO block/PNP complex did not show any apparent crystallization upon cooling from the melt, instead cold crystallization during heating was observed and an approximately 30 °C increase in melting point as compared to the neat PEO block within the copolymer. An increased capacity for self-nucleation of the PEO block was produced by the complexation with PNP and therefore the three self-nucleation domains were clearly observed for both the PE block and the PEO block/PNP complex. Self-nucleation was helpful to ascertain the presence of separate crystalline regions in the triblock copolymer. Through the use of PNP, both the crystallinity and the melting point of the $E_{24}EP_{57}EO_{19}^{69}$ triblock copolymer employed were substantially increased. Similar results were obtained by complexation of the same ABC triblock copolymer with resorcinol.

Acknowledgement

Financial support was given by CONICIT (Grant G97-000594) and by DSM Research.

References

[1] H. Frensch, P. Harnischfeger, B.-J. Jungnickel, *"Fractionated Crystallization in Incompatible Polymer Blends" in: Multiphase Polymers: Blends and Ionomers*, L. A. Utracky, R. A. Weiss, Eds., ACS Symp. Series, 395, 101 (1989).

[2] M. L. Arnal, M. E. Matos, R. A. Morales, O. O. Santana, A. J. Müller, *Macromol. Chem. Phys.* **1998**, *199*, 2275.

[3] M. L. Arnal, A. J. Müller, P. Maiti, M. Hikosaka, *Macromol. Chem. Phys.* **2000**, 201, 2493.

[4] Y. Loo, R. Register, A. J. Ryan, *Phys. Rev. Lett*. **2000**, *84*, 4120.

[5] B. Lotz, A. J. Kovacs, *Polym. Prep. (Am. Chem. Soc., Div. Polym. Chem.)* **1969**, *10*, 820.

[6] C. Robitaille, J. Prud´homme, *Macromolecules* **1983**, 16, 665.

[7] H. Chen, S. Hsiao, T. Lin, K. Yamauchi, H. Hasegawa, T. Hashimoto, *Macromolecules* **2001**, *34*, 671.

[8] P. A. Weimann, D. A. Hajduk, C. Chu, K. A. Chaffin, J. C. Brodil, F. S. Bates*, J. Polym. Sci., Part B: Polym. Phys*. **1999**, 37, 2053.

[9] V. Balsamo, F. von Gyldenfeldt, R. Stadler, *Macromol. Chem. Phys.* **1996**, *197*, 3317.

[10] V. Balsamo, A. J. Müller, F. von Gyldenfeldt, R. Stadler, *Macromol. Chem. Phys.* **1998**, *199*, 1063.

[11] M. L. Arnal, V. Balsamo, F. López-Carrasquero, J. Contreras, M. Carrillo, H. Schmalz, V. Abetz, E. Laredo, A. J. Müller, *Macromolecules* **2001**, *34*, 7973.

[12] A. J. Müller, M. L. Arnal, F. López-Carrasquero, submitted to *Macromol. Symp.* in 2001.

[13] A. J. Müller, V. Balsamo, M. L. Arnal, T. Jakob, H. Schmalz, V. Abetz, *Macromolecules* **2002**, *35*, 3048.

[14] B. Fillon, J. C. Wittman, B. Lotz, A. Thierry, *J. Polym. Sci., Part B: Polym. Phys*. **1993**, 31, 1383.

[15] V. Balsamo, Y. Paolini, G. Ronca, A. J. Müller, *Macromol. Chem. Phys.* **2000**, *201*, 2711.

[16] M. Dosiere, *J. Macromol. Sci.-Phys.***1996**, *B35*, 303.

[17] P. Damman, J. J. Point, *Macromolecules* **1993**, *26*, 1722.

[18] H. Schmalz, A. Böker, R. Lange, V. Abetz, *Polym. Mater. Sci. Eng.* **2001**, *85*, 478.

3.3 PS-*b*-PI-*b*-P(B/S) and PS-*b*-PEP-*b*-P(S/E) Triblock Copolymers

3.3.1 Synthesis and Properties of ABA and ABC Triblock Copolymers with Glassy (A), Elastomeric (B), and Crystalline (C) Blocks

Holger Schmalz[a], Alexander Böker[a,b], Ronald Lange[c], Georg Krausch[b] and Volker Abetz[a*]

a) Makromolekulare Chemie II, Universität Bayreuth, 95440 Bayreuth, Germany
b) Physikalische Chemie II and Bayreuther Zentrum für Kolloide und Grenzflächen (BZKG), Universität Bayreuth, 95440 Bayreuth, Germany
c) DSM Research, 6160 MD Geleen, The Netherlands

ABSTRACT: In this contribution we describe the synthesis, characterization and properties of polystyrene-*block*-poly(ethylene-*alt*-propylene)-*block*-polyethylene (PS-*b*-PEP-*b*-PE) and polystyrene-*block*-poly(ethylene-*alt*-propylene)-*block*-polystyrene (PS-*b*-PEP-*b*-PS) triblock copolymers. Morphological investigations using TEM, SEM and SFM reveal for the PS-*b*-PEP-*b*-PE triblock copolymers a morphology consisting of PS cylinders and PE crystallites within a matrix of the PEP block, whereas the PS-*b*-PEP-*b*-PS triblock copolymer shows interconnected, distorted PS cylinders in the PEP matrix. Mechanical characterization of these triblock copolymers demonstrated that for small strains the PS-*b*-PEP-*b*-PE triblock copolymers exhibit the aimed smaller plastic deformations, i.e. better elastic properties, compared to the polystyrene based ABA type thermoplastic elastomer. However, at high strains the PS-*b*-PEP-*b*-PS triblock copolymer shows a significantly better elastic recovery. The high plastic set at high elongations in PS-*b*-PEP-*b*-PE triblock copolymers is attributed to the weaker resistance of the PE crystallites compared to amorphous PS domains in the PS-*b*-PEP-*b*-PS triblock copolymer.

Introduction

Linear ABA triblock copolymers, with the A-block consisting of polystyrene whereas the B-block is typically polybutadiene or polyisoprene (PS-*b*-PB-*b*-PS or PS-*b*-PI-*b*-PS) are classic thermoplastic elastomers.[1-3] Due to the incompatibility between the two components microphase separation occurs whereby the polystyrene minority phase forms dispersed spheres or cylinders in a rubbery matrix of the middle block. Linear ABC triblock copolymers have been investigated by several groups and a huge variety of morphologies was found.[4-7] Besides classes of lamellar[8,9], cylindrical[10,11] and spherical morphologies[12] also cocontinuous morphologies were found[13-15], which all relate to the corresponding morphologies known from binary block copolymers. Fundamentally different from the diblock copolymer morphologies is the "knitting pattern" found for particular polystyrene-*block*-poly(ethylene-*stat*-butylene)-*block*-poly(methyl methacrylate) triblock copolymers.[16-18] A problem encountered in ABC triblock copolymers with short end blocks (i. e. end blocks forming spheres or cylinders) is the often occurrence of at least partial miscibility between the two end blocks. In such cases a two-phase morphology is obtained rather than a three-phase morphology. As a consequence, the B chain may loop back into the same end block domain rather than being forced to form a bridge between two different end block domains. This should have an influence on the elastic properties of such a material, since bridges and loops should behave different. In conclusion, ABC triblock copolymers with mixed end blocks should behave similar like ABA triblock copolymers both in terms of their morphological and mechanical properties.

ABC triblock copolymers offer the ability to build thermoplastic elastomers without any loops, if the A- and C-blocks are immiscible. Since the immiscibility is a function of the product $\chi_{AC} N_{AC}$, either strongly incompatible components or a high degree of polymerization have to be used (N_{AC} is the degree of polymerization of the A- and C-block and χ_{AC} is the segmental interaction parameter between the two species).[19] A high degree of polymerization, however, results in a high melt viscosity, which is disadvantageous in view of processing demands. For polystyrene-*block*-polybutadiene-*block*-poly(methyl methacrylate) (PS-*b*-PB-*b*-PMMA) triblock copolymers it was shown that only systems with a rather high molecular weight display microphase separated PS and PMMA domains under favorable conditions.[20,21]

Semicrystalline end blocks offer a way to achieve segregated end blocks at low molecular weights, since crystallization is a strong driving force for microphase separation.

Investigations on polyethylene-*block*-poly(ethylene-*alt*-propylene) (PE-*b*-PEP) diblock copolymers show that even for low molecular weights a microphase separated structure is obtained due to crystallization induced microphase separation.[22-24] Furthermore, this system exhibits a small value for the segmental interaction parameter χ of 0.007 at 120 °C (above the melting point of PE) resulting in a homogeneous melt in a wide composition range which is advantageous in view of processing.[25]

ABA triblock copolymers with polyethylene as crystallizable A-block have already been investigated with respect to their morphology and mechanical properties.[26-33] Morton and coworkers compared polyethylene-*block*-polyisoprene-*block*-polyethylene (PE-*b*-PI-*b*-PE) and polyethylene-*block*-poly(ethylene-*stat*-butylene)-*block*-polyethylene (PE-*b*-PEB-*b*-PE) triblock copolymers with polystyrene based thermoplastic elastomers. The polyethylene containing thermoplastic elastomers exhibit better solvent resistance and show a homogeneous melt in the case of the PE-*b*-PEB-*b*-PE systems. Triblock copolymers with polyethylene contents up to 30 wt-% show an elastomeric behavior with low plastic deformations after elongation, whereas systems with higher polyethylene content exhibit more plastic properties. Compared to the polystyrene based thermoplastic elastomers the plastic deformations even for the systems with 30 wt-% polyethylene are higher especially for high extensions. This may be attributed to a weaker resistance of crystalline domains to distortion compared to polystyrene domains in this case. The Young´s modulus increases with increasing polyethylene content, whereby the tensile strength mainly depends on the molecular weight of the polyethylene block.

In this contribution we compare ABC triblock copolymers with a glassy and a semicrystalline end block with an ABA triblock copolymer with glassy end blocks. Here we describe the synthesis and the properties of polystyrene-*block*-poly(ethylene-*alt*-propylene)-*block*-polyethylene (PS-*b*-PEP-*b*-PE) triblock copolymers. Tensile testing in comparison to a polystyrene-*block*-poly(ethylene-*alt*-propylene)-*block*-polystyrene (PS-*b*-PEP-*b*-PS) triblock copolymer is performed in order to investigate the influence of a crystalline end block on the mechanical properties. A special synthetic procedure allows us to synthesize PS-*b*-PEP-*b*-PS and PS-*b*-PEP-*b*-PE triblock copolymers with identical A- and B- blocks, only differing in the type of the C-block. This excludes any effects on the mechanical properties resulting from the molecular weight or composition of the triblock copolymers. The miscibility of polyethylene and poly(ethylene-*alt*-propylene) in the melt provides us with systems exhibiting a two-phase melt instead of a three-phase melt. This should in turn result in a reduced melt viscosity, and

hence in a better processability. Furthermore, the low solubility of the polyethylene block compared to a polystyrene block should also lead to a higher solvent resistance of the corresponding triblock copolymers.

It should be noted that in general ABA and ABC triblock copolymers with a similar overall composition with respect to the end blocks must have different morphologies, when A and C are immiscible. For example, when A and C form cylinders, they must be arranged on a tetragonal lattice or a hexagonal lattice having a different symmetry compared to the hexagonally packed cylinders of the corresponding ABA triblock copolymer. The situation is similar in a lattice of A and C spheres in a B matrix. Thus, an investigation of mechanical properties in dependence on the presence or absence of loops without changing the morphology is impossible when comparing ABA and ABC triblock copolymers. It is the aim of this contribution to show a way to generate ABC triblock copolymers with short microphase separated end blocks and compare them with a reference ABA triblock copolymer.

Experimental Section

Materials. Benzene (Acros) was purified by successive distillation over CaH_2 and potassium and kept in a dry nitrogen atmosphere until use. Styrene (Acros) was distilled from CaH_2 under nitrogen, stirred over Bu_2Mg and condensed into storage ampoules. Butadiene (Linde) was passed over columns with molecular sieve and activated alumina, followed by storage over Bu_2Mg under purified nitrogen before use. Isoprene (Fluka) was stirred over Bu_2Mg under purified nitrogen for 12 h, condensed onto *n*-BuLi followed by stirring at 0 °C for 1 h before being condensed into glass ampoules. Toluene (p. a., Merck), *sec*-BuLi (Acros, 1.3 M in cyclohexane/hexane : 92/8), *n*-BuLi (Aldrich, 1.6 M in hexane), Bu_2Mg (Aldrich, 1 M in heptane), and Wilkinson catalyst $(Ph_3P)_3Rh(I)Cl$ (Aldrich) were used as received.

Synthesis. The synthesis of PS-*b*-PI-*b*-PB and PS-*b*-PI-*b*-PS triblock copolymers was accomplished by sequential anionic polymerization of styrene, isoprene and butadiene or styrene in benzene at 40 °C (for styrene) and 60 °C (for butadiene and isoprene) with *sec*-BuLi as initiator. The use of benzene as a solvent results in a high 1,4-addition for butadiene and isoprene which particularly for butadiene is indispensable to get a “pseudo polyethylene” structure after hydrogenation. The combination of two laboratory autoclaves (Büchi) allowed

us to synthesize ABC triblock copolymers with identical A- and B-blocks, but different C-blocks by dividing the living AB diblock copolymer precursor into two fractions. This enables us to study the influence of the C end block on the morphological and mechanical properties of ABC triblock copolymers by keeping all other parameters, like molecular weight and relative composition, constant.

Hydrogenation. The PS-*b*-PEP-*b*-PE and PS-*b*-PEP-*b*-PS triblock copolymers were synthesized by hydrogenation of the corresponding precursor polystyrene-*block*-poly(1,4-isoprene)-*block*-poly(1,4-butadiene) (PS-*b*-PI-*b*-PB) and polystyrene-*block*-poly(1,4-isoprene)-*block*-polystyrene (PS-*b*-PI-*b*-PS). Homogeneous catalytic hydrogenation was carried out in degassed toluene (1.5 – 2 wt-% solution of polymer) at 100 °C and 90 bar H_2 pressure for 3 days using Wilkinson catalyst (1 mol-% with respect to the number of double bonds). Purification was accomplished by precipitation in methanol. The extend of hydrogenation was verified using ^{1}H-NMR spectroscopy (Bruker AC 250 spectrometer). Under the used conditions the polybutadiene blocks are hydrogenated completely and the polyisoprene blocks show an almost complete saturation with $\leq$ 1% residual double bonds.

Size Exclusion Chromatography (SEC). SEC experiments were performed on a Waters instrument calibrated with narrowly distributed polystyrene standards at 30 °C. Four PSS-SDV columns (5µm, Polymer Standards Service, Mainz) with a porosity range from 10^2 to 10^5 Å were used together with a differential refractometer and a UV-detector at 254 nm. Measurements on the non-hydrogenated triblock copolymers were performed in THF with a flow rate of 1 ml/min using toluene as internal standard.

Differential Scanning Calorimetry (DSC). For thermal analysis a Perkin Elmer DSC 7 with a CCA 7 liquid nitrogen cooling device was used. For all measurements a two point calibration with chloroform and indium was applied. All experiments were performed at a heating rate of 10 K/min, unless otherwise specified. The displayed heating trace corresponds to the second heating run in order to exclude effects resulting from any previous thermal history of the samples.

Dynamic Mechanical Analysis. Dynamic shear experiments were performed with an Advanced Rheometric Expansion System (ARES, Rheometrics) in the plate-plate configuration with a plate diameter of 25 mm and a gap of ~ 1 mm. Temperature dependent measurements of G' and G'' were performed at a scanning rate of 1 K/min at a constant frequency of 1 rad/s. It was made sure that all experiments were done in the linear viscoelastic regime.

Mechanical Testing. Mechanical testing was carried out using an Instron 5565 and a Zwick (equipped with optical extensometers) tensile testing machine. Young´s modulus was determined at a testing speed of 0.2 mm/min at small elongations (0 – 0.5%), elongations at break were measured at 20 mm/min. Hysteresis measurements were performed at a testing speed of 20 mm/min for elongations to 100 (3 times), 200, 300, 400 and 500% followed by extension to break. No holding time between the cycles was applied. Test specimens according to ISO 37:1994 were used. Preparation was accomplished by compression molding into plates at 140 – 150 °C followed by cooling to room temperature (≈ -1.5 K/min). It was made sure that the cutting of test specimens always occurred in the same direction in order to exclude any effects resulting from different orientation within the test samples.

Transmission Electron Microscopy (TEM). The bulk morphology of the triblock copolymers was examined by bright field TEM using a Zeiss CEM 902 electron microscope operated at 80 kV. Films of PS-*b*-PI-*b*-PS triblock copolymers (around 0.5 mm thick) were prepared by casting from a 2 wt-% solution in $CHCl_3$ and allowed to slowly evaporate over a period of 2 weeks followed by drying under vacuum for 1 day. In addition, compression molded samples, which were used for mechanical testing, were also taken for morphological investigations. Thin sections were cut at - 130 °C using a Reichert-Jung Ultracut E microtome equipped with a diamond knife. Selective staining of the PI domains was achieved by exposure of the sections to OsO_4 vapor for 60 s, while the thin sections of hydrogenated triblock copolymers were exposed to RuO_4 vapor for 45 min to selectively stain the PS domains.

Scanning Electron Microscopy (SEM). SEM images were taken on a LEO 1530 Gemini instrument equipped with a field emission cathode possessing a lateral resolution of approximately 2 nm. Thin films of PS-*b*-PEP-*b*-PE were prepared by dip coating onto a polished silicon wafer from a 1 mg/ml solution of the triblock copolymer in toluene. The

films were stained with RuO_4 vapor for 45 min prior to SEM imaging in order to visualize the PS domains.

Scanning Force Microscopy (SFM). Scanning force microscopy images were taken on a Digital Instruments Dimension 3100 microscope operated in TappingMode™ (free amplitude of the cantilever: 20 nm; set point ratio: 0.95). Measurements were performed on thin films prepared on polished silicon wafers by dip coating from a 1 mg/ml solution of the polymer in toluene or by spin coating using a 5 wt-% solution of the respective polymer in toluene. Selective swelling of the PS-microdomains in PS-*b*-PEP-*b*-PE triblock copolymer thin films was accomplished by exposing a vacuum dried film to toluene vapor for 1 min. In addition, measurements were performed on compression molded samples, which were prepared similar to the samples used for mechanical testing. SFM imaging was carried out on smooth cut surfaces obtained by cutting with a diamond knife at -130 °C using a Reichert-Jung Ultracut E microtome.

Small Angle X-ray Scattering (SAXS). SAXS measurements were performed on compression molded samples using a Bruker-AXS Nanostar instrument with a sealed X-ray tube (Cu, $\lambda = 1.5418$ Å) operated at 40 mA and 40 kV and equipped with crossed Goebel mirrors and a 2D Histar detector.

Results and Discussion

Synthesis. The PS-*b*-PEP-*b*-PE and PS-*b*-PEP-*b*-PS triblock copolymers were prepared by homogeneous catalytic hydrogenation of the corresponding PS-*b*-PI-*b*-PB and PS-*b*-PI-*b*-PS triblock copolymers which were synthesized by sequential anionic synthesis.

Scheme 1 shows the synthesis of PS-*b*-PI-*b*-PB and PS-*b*-PI-*b*-PS triblock copolymers with identical PS- and PI-blocks by combination of two laboratory autoclaves. First the sequential anionic polymerization of styrene and isoprene was performed in benzene. Subsequently, the resulting solution of living PS-*b*-PI diblock copolymer precursors was divided into two fractions. Further addition of styrene or butadiene, respectively, leads to the formation of the corresponding PS-*b*-PI-*b*-PS and PS-*b*-PI-*b*-PB triblock copolymers.

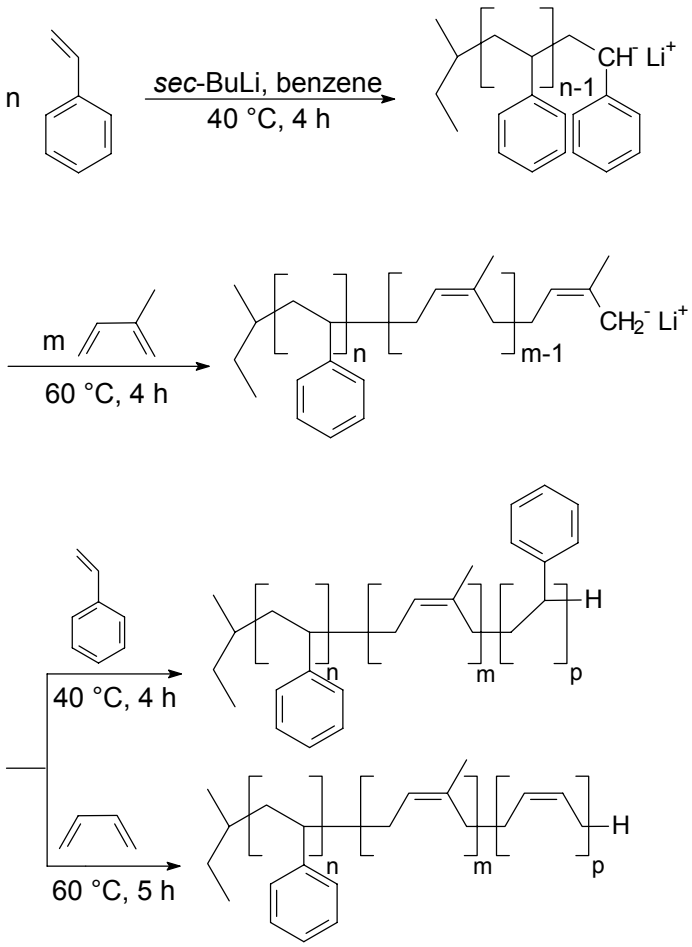

Scheme 1. Synthesis of polystyrene-*block*-poly(1,4-isoprene)-*block*-polystyrene (PS-*b*-PI-*b*-PS) and polystyrene-*block*-poly(1,4-isoprene)-*block*-poly(1,4-butadiene) (PS-*b*-PI-*b*-PB) with identical PS- and PI-blocks by combination of two laboratory autoclaves.

Polymerization in benzene results in a high 1,4-content for butadiene and isoprene as depicted in Table 1. In our nomenclature ($A_xB_yC_z^m$) the subscripts give the weight percentage of the corresponding block, and the superscript is the molar mass of the triblock copolymer in kg/mol. SEC shows that dividing the living PS-*b*-PI diblock copolymer precursor proceeds without any termination resulting in narrowly distributed PS-*b*-PI-*b*-P(S/B) triblock copolymers (Figure 1, Table 1). However, for the PS-*b*-PI-*b*-PB triblock copolymers the addition of butadiene to the living PS-*b*-PI precursor gives rise to a very small amount of chain termination (< 6%) as can be seen from the shoulder at higher elution volumes (Figure 1) which might be attributed to residual impurities in the butadiene. Due to the very small extend of chain termination the residual PS-*b*-PI precursor is not expected to influence the mechanical properties of the PS-*b*-PI-*b*-PB triblock copolymer after hydrogenation.

Table 1. Molecular Weight Characterization and Microstructure of PS-*b*-PI-*b*-P(B/S) Triblock Copolymers

triblock	M_n[a] [kg/mol]	M_w/M_n[b]	PB-block[c]		PI-block[c]		
			%1,4	%1,2	%1,4	%1,2	%3,4
$S_{14}I_{57}B_{29}^{109}$	109	1.02	89	11	92	4	4
$S_{14}I_{64}B_{22}^{119}$	119	1.02	87	13	92	4	4
$S_{14}I_{65}S_{21}^{117}$	117	1.01	-	-	92	4	4

[a] Determined by ^{1}H-NMR spectroscopy using the molecular weight of the PS precursor obtained by SEC in THF calibrated against PS standards.
[b] Determined by SEC in THF calibrated against PS standards.
[c] Determined by ^{1}H-NMR spectroscopy in $CDCl_3$.

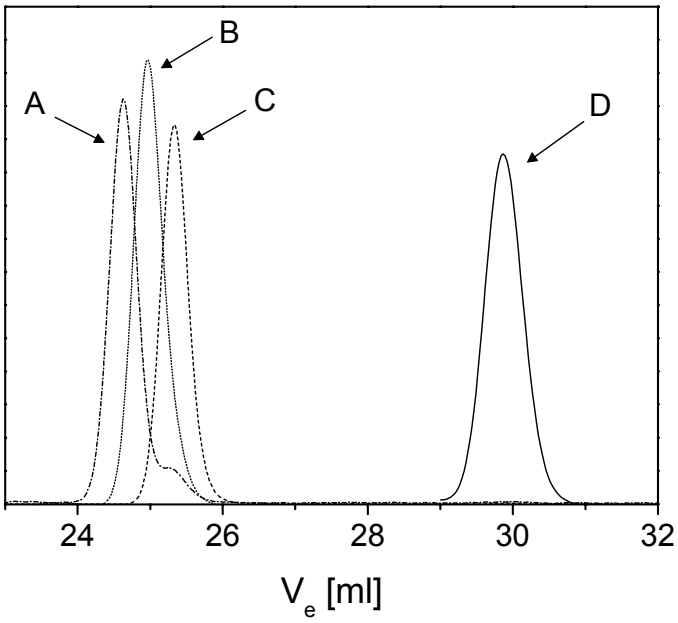

Figure 1. SEC traces of a PS-*b*-PI-*b*-PS (B) and a PS-*b*-PI-*b*-PB (A) triblock copolymer with identical PS and PI blocks, synthesized by connection of two laboratory autoclaves, including the PS (D) and PS-*b*-PI (C) precursors using THF as eluent and toluene as internal standard.

Homogeneous catalytic hydrogenation was carried out in toluene using the Wilkinson catalyst $(Ph_3P)_3Rh(I)Cl$ at 100 °C and 90 bar H_2 pressure. Under these conditions the PB-block gets completely hydrogenated and the PI-block exhibits an almost complete saturation with less than 1% residual double bonds, as monitored by the disappearance of the corresponding signals of the vinylic protons in ^{1}H-NMR (not shown). Hydrogenation at lower temperatures (60 °C) leads only to a partially hydrogenated PI-block, whereas the PB-block gets completely saturated.

Thermal Properties. The PS-*b*-PEP-*b*-PS and PS-*b*-PEP-*b*-PE triblock copolymers exhibit glass transition temperatures at approximately –55 °C for the PEP block and at about 100 °C for the PS block, reflecting a strongly microphase separated structure (Table 2). The PE blocks in PS-*b*-PEP-*b*-PE triblock copolymers reveal a melting endotherm at ca. 90 °C and degrees of crystallinity of $\alpha \sim 31\%$. The degree of crystallinity was calculated using the heat of fusion for a 100% crystalline PE of $\Delta H_m^0 = 276.98$ J/g.[34]

Table 2. DSC Data of PS-*b*-PEP-*b*-P(E/S) Triblock Copolymers[a]

triblock	$T_{G,\,PEP}$ [°C]	$T_{G,\,PS}$ [°C]	$T_{m,\,PE}$ [°C]	$T_{c,\,PE}$ [°C]	α_{PE} [%]
$S_{14}EP_{66}S_{20}^{119}$	-55.5	102.4	-	-	-
$S_{14}EP_{64}E_{22}^{122}$	-56.0	99.3[b]	88.0	57.6	31.9
$S_{13}EP_{57}E_{30}^{112}$	-56.0	100.4[b]	88.7	59.8	31.0

[a] T_m = melting point (peak maximum), T_c = crystallization temperature (peak maximum), α = degree of crystallinity, and T_G = glass transition temperature.
[b] Determined by dynamic mechanical analysis (maximum G'', 1 rad/s, 1 K/min).

The DSC heating trace for $S_{13}EP_{57}E_{30}^{112}$ (Figure 2) displays a relatively broad melting endotherm for the PE block indicating a broad crystallite size distribution. The latter may arise from the approximately 11% 1,2-units in the corresponding PB block of the non-hydrogenated triblock copolymer precursor (Table 1). The corresponding cooling trace (Figure 2) shows that crystallization of the PE block occurs at ca. 60 °C.

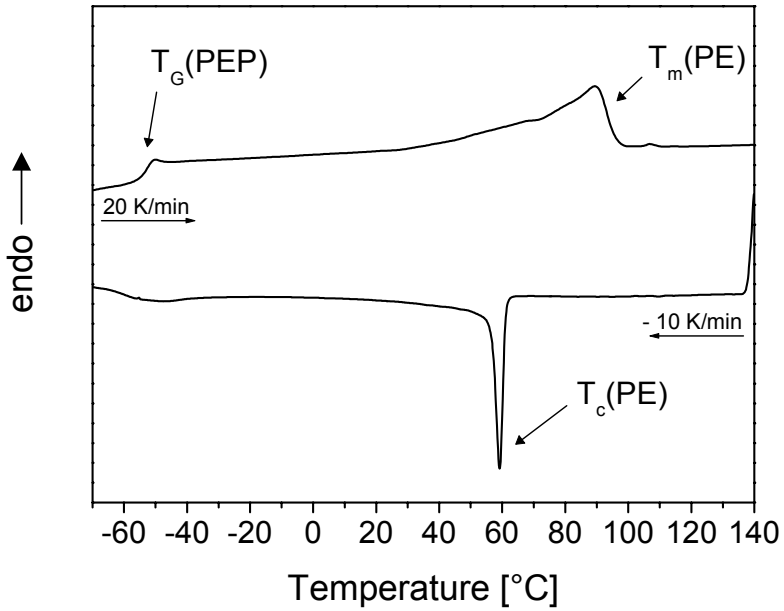

Figure 2. DSC heating and cooling traces for $S_{13}EP_{57}E_{30}^{112}$.

The melting and crystallization temperatures of the PE block in the PS-*b*-PEP-*b*-PE triblock copolymers exhibit a slight increase with increasing molecular weight of the PE block (Table 2). In addition, the degree of crystallinity α(PE) shows a slight increase with increasing molecular weight of the triblock copolymer, which might be attributed to a higher incompatibility between the PEP and PE block due to the increasing values of χN. From DSC measurements it is not possible to detect a glass transition temperature of the PS block in PS-*b*-PEP-*b*-PE triblock copolymers. In Figure 3 a temperature dependent dynamic shear experiment on $S_{13}EP_{57}E_{30}{}^{112}$ is shown. The sharp drop in the storage modulus G' at ca. –50 °C is related to the glass transition temperature of the PEP block which corresponds to the transition temperature obtained by DSC (Table 2, Figure 2). Upon further heating, melting of the crystalline PE block results in an additional drop in G' at ca. 90 °C which is in line with the observed melting endotherm in DSC. The glass transition temperature of the PS block is indicated by a small maximum in the loss modulus G'' at ca. 100 °C. The corresponding drop in G' is not visible, probably due to the low PS content of only 13 wt-%.

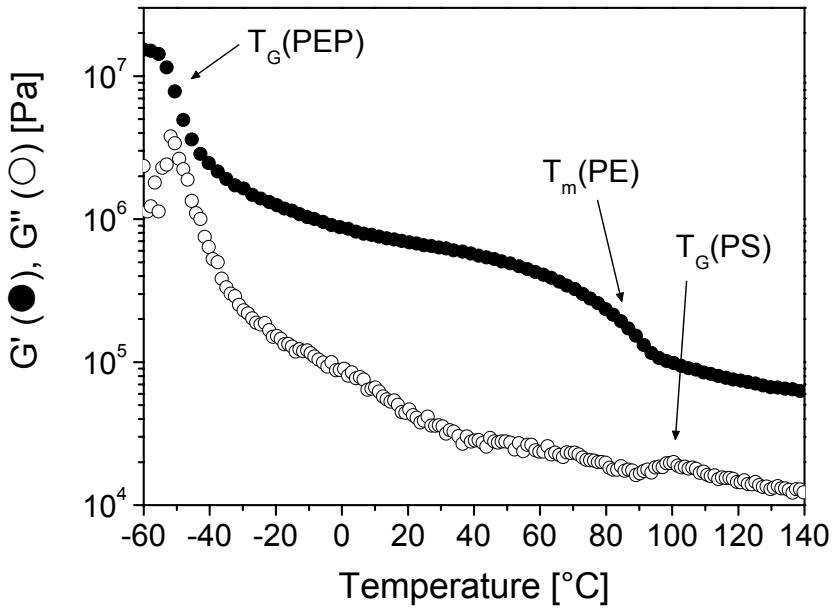

Figure 3. Temperature dependent dynamic shear experiments on $S_{13}EP_{57}E_{30}{}^{112}$.

Concerning the solubility, PS-*b*-PEP-*b*-PE triblock copolymers show a better solvent resistance compared to PS-*b*-PEP-*b*-PS triblock copolymers, which are in general soluble in organic solvents. In $CHCl_3$ and toluene small amounts of PS-*b*-PEP-*b*-PE triblock copolymers are soluble at room temperature, whereas higher concentrated solutions (> 0.02 g/ml) can only be obtained at elevated temperatures and exhibit gelation upon cooling.

Morphology. TEM investigations on $S_{14}I_{65}S_{21}^{117}$ (precursor of $S_{14}EP_{66}S_{20}^{119}$) cast from $CHCl_3$ solution show a cylindrical morphology with hexagonally packed PS-cylinders within a matrix of PI (selectively stained with OsO_4 vapor) as shown in Figure 4A. With regard to the performed mechanical testing the morphology of the compression molded samples is of special interest. Figure 4B shows a TEM image of $S_{14}I_{65}S_{21}^{117}$, prepared by compression molding in an identical way as for the tensile testing. The PS domains exhibit a strongly distorted cylindrical structure without showing any long range order. The TEM image of the corresponding hydrogenated triblock copolymer $S_{14}EP_{66}S_{20}^{119}$ (Figure 4C), also prepared by compression molding, exhibits a similar morphology consisting of strongly distorted PS-cylinders. In both systems the formation of interconnected PS-cylinders is possible due to the strongly distorted PS-domains.

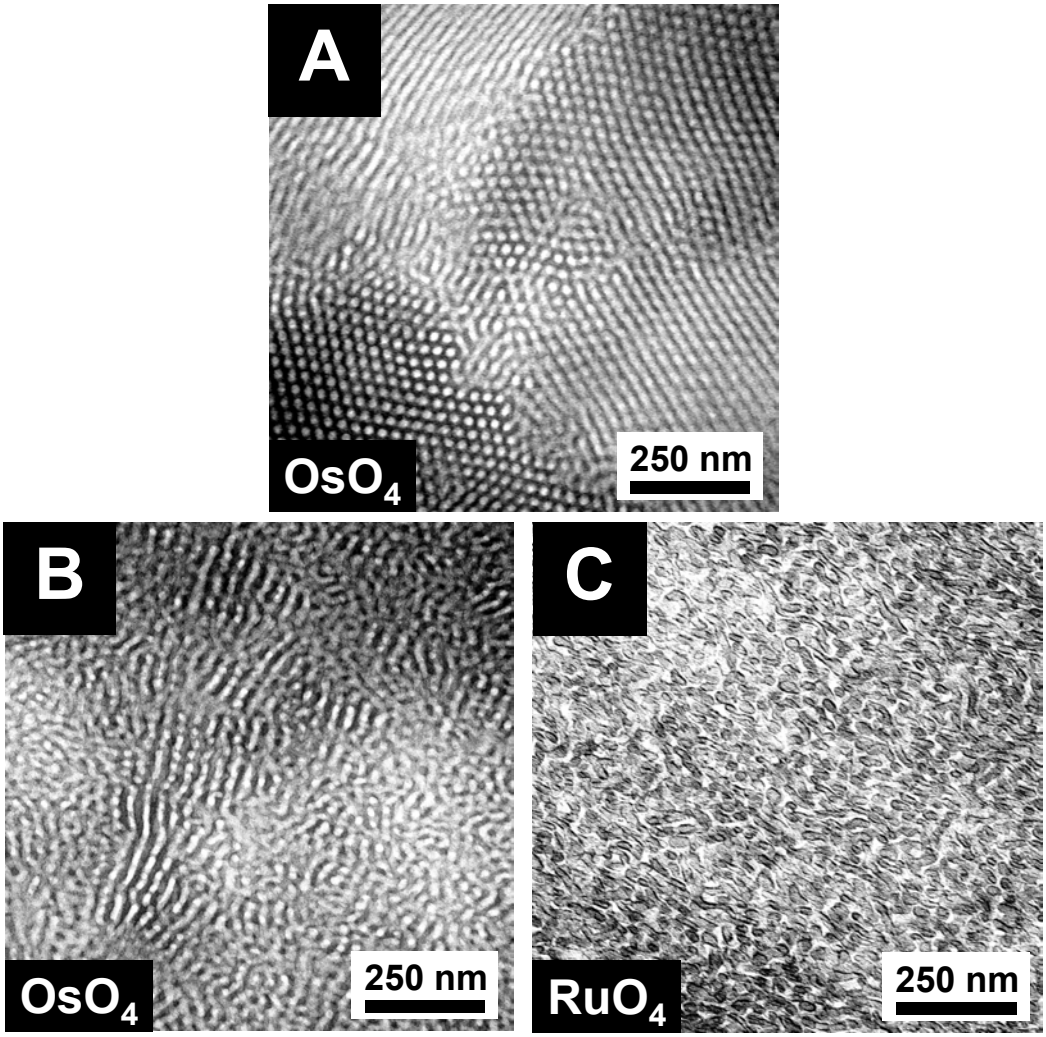

Figure 4. TEM images of (A) $S_{14}I_{65}S_{21}^{117}$ cast from $CHCl_3$; (B) $S_{14}I_{65}S_{21}^{117}$ prepared by compression molding, selective staining of PI was achieved by exposure to OsO_4 vapor; and (C) $S_{14}EP_{66}S_{20}^{119}$ prepared by compression molding, stained with RuO_4 for visualization of PS.

Morphological investigations on PS-*b*-PEP-*b*-PE triblock copolymers using conventional TEM techniques encounter the problem that the PS and PE domains cannot be visualized simultaneously.[35] Detection of the PS-domains is possible by selective staining of PS with RuO_4 vapor. The PE crystallites can be visualized by underfocus phase contrast bright field TEM investigations of the unstained samples. In order to gain a more detailed insight into the morphology of our PS-*b*-PEP-*b*-PE triblock copolymers we prepared thin films by dip and spin coating from dilute solutions. Figure 5A shows the SEM image of such a thin film of $S_{13}EP_{57}E_{30}^{112}$ prepared from toluene solution (1mg/ml). The white dot- and worm-like structures represent the PS domains selectively stained by exposure to RuO_4 vapor. As the PE block is expected to form crystalline lamellae, it is very likely that according to the composition the PS block forms cylinders in the PEP matrix. The cause of the obvious distortion of the PS cylinders will be explained in the following.

Figure 5B shows a SFM phase contrast image of a vacuum dried thin film of $S_{13}EP_{57}E_{30}^{112}$ dip coated from toluene solution (1mg/ml). In this picture we can distinguish between at least two different phases. The bright elongated domains with rough boundaries correspond to PE crystallites which induce a high phase shift within a matrix of PEP, which appears darker in the phase contrast. In addition, we can identify a third phase which is located in between the PE crystallites. This phase can be visualized more clearly by exposure of the film to toluene vapor for 1 min as shown in Figure 5C (circles in Figure 5B/C). As toluene is a selective solvent for polystyrene we can conclude that the bright dot- and worm-like structures can be attributed to PS cylinders in a PEP matrix located between PE crystallites. Obviously, the swelling of the PS domains with toluene also changes the interaction between the tip and the sample surface significantly which leads to a distinct phase shift. As during film preparation the PE crystallizes before solidification of the PS cylinders, the latter have to cope with the confined geometry given by the PE “crystal lamellae” which leads to the observed distortions in the PS domains.

Further evidence for our phase assignment is given by the SFM images of a spin coated film of $S_{14}EP_{64}E_{22}^{122}$ (5 wt-% solution in toluene, film thickness = 22.6 nm) as shown in Figures 5D/E. The phase image exhibits the same characteristics as the one shown in Figure 5C. In addition, we compare the phase to the respective topography. In both images we can identify the PS domains (as the lower parts in the topography and the bright areas in the phase). This is in exact agreement with previous investigations[36] where it was shown that the block with the best solubility in the solvent from which the film was prepared showed the highest shrinkage upon film drying.

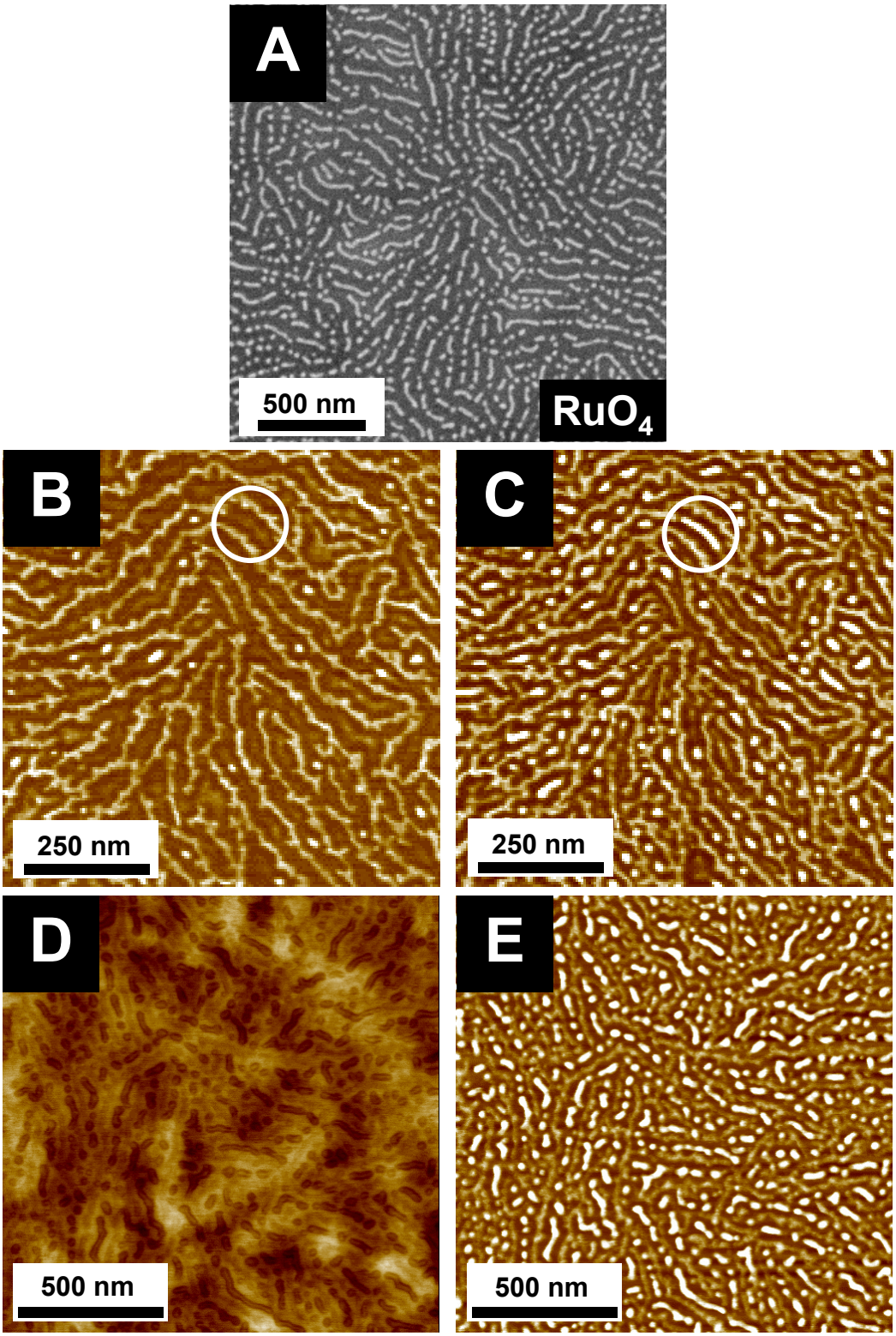

Figure 5. (A) SEM image of a dip coated film of $S_{13}EP_{57}E_{30}^{112}$ onto a silicon wafer. (B) and (C) TappingMode SFM phase contrast images of a thin film of $S_{13}EP_{57}E_{30}^{112}$ dip-coated onto a silicon wafer: (B) dry film; (C) same spot of the film after 1 min exposure to toluene vapor, visualizing the PS-cylinders; z = 20°. TappingMode SFM height (D, z = 15 nm) and phase (E, z = 50°) image of a thin film of $S_{14}EP_{64}E_{22}^{122}$ spin-coated from a 5 wt-% solution in toluene onto a silicon wafer.

SFM investigations on thin films of $S_{14}EP_{64}E_{22}^{122}$ spin coated from a 10 wt-% solution in toluene (film thickness = 55.6 nm) exhibit an identical morphology (results not shown). From the independence of morphology on film thickness we can conclude that the SiO_x surface of the silicon wafer does not show a significant influence on the morphology of the investigated samples. Therefore we can deduce that by using TappingMode SFM we are able to identify all three components of our triblock copolymers from topography and phase informations in combination with the influence of selective solvents.

Morphological investigations on PS-*b*-PEP-*b*-PE triblock copolymers were also performed on compression molded samples, prepared in a similar way as the samples for tensile testing. Figure 6A shows a bright field TEM image of $S_{13}EP_{57}E_{30}^{112}$. Selective staining with RuO_4 vapor visualizes the PS-domains appearing as dark dots and worms, revealing a distorted cylindrical morphology. The PS-domains do not show a preferential orientation as might possibly arise from the compression molding process. In the SFM phase contrast image, depicted in Figure 6B, clearly three different phases can be distinguished as in the case of the spin coated sample of $S_{14}EP_{64}E_{22}^{122}$ (Figure 5E). From the results obtained by solvent vapor treatment the bright (higher phase shift) appearing dots and worms can be attributed to PS cylinders in a matrix of the darker appearing PEP block. The third, less bright appearing phase, corresponds to crystalline PE domains.

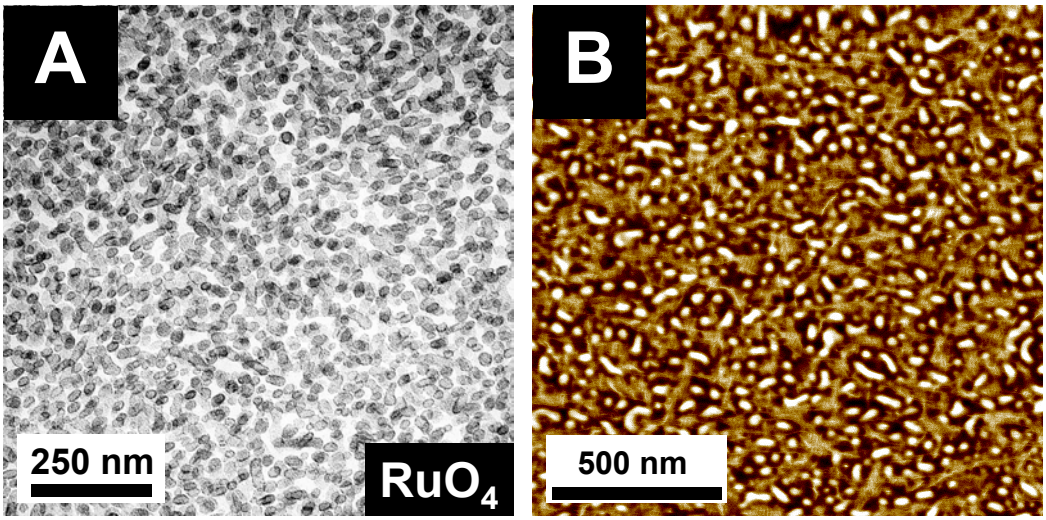

Figure 6. Morphology of $S_{13}EP_{57}E_{30}^{112}$ prepared by compression molding: (A) TEM image; (B) SFM phase contrast image (z = 15°).

Compression molded samples of $S_{14}EP_{64}E_{22}^{122}$ show an identical overall morphology and differ only in the amount of crystalline PE. Compared to the solvent cast films of $S_{13}EP_{57}E_{30}^{112}$ (Figure 5C) and $S_{14}EP_{64}E_{22}^{122}$ (Figure 5E) the PE crystallites in the compression molded sample (Figure 6B) are significantly smaller in length and exhibit a more distorted structure. In contrast to the film preparation from solution, the PS solidifies first upon cooling from the melt due to its higher glass transition temperature of ca. 100 °C compared to the crystallization temperature of the PE block of ca. 60 °C (Table 2). Due to the already existing glassy PS domains the PE blocks have to cope with the confined geometry given by the PS cylinders upon crystallization. This results in the formation of PE crystallites showing smaller dimensions as compared to the PE crystallites formed by crystallization from solution. In conclusion, PS-*b*-PEP-*b*-PE triblock copolymers prepared by compression molding show a similar morphology compared to the solvent cast films, i. e. dispersed PS cylinders and PE crystallites within a matrix of the PEP block.

From the TEM and SFM investigations on compression molded samples of PS-*b*-PEP-*b*-PS (Figure 4C) and PS-*b*-PEP-*b*-PE (Figures 6A/B) triblock copolymers no preferential orientation resulting from the melt processing can be detected, as was also confirmed by SEM and 2D-SAXS (not shown).

Mechanical Properties. In order to investigate the influence of a crystalline end block on the elastic properties of triblock copolymers, we performed hysteresis measurements on PS-*b*-PEP-*b*-PE triblock copolymers in comparison to a PS-*b*-PEP-*b*-PS triblock copolymer (Table 3). The remaining plastic deformation (ε_{plast}) was determined for extensions to 100, 200, 300, 400 and 500%, whereby the first cycle was conducted 3 times. In Figure 7 the hysteresis measurements performed on $S_{13}EP_{57}E_{30}^{112}$ are shown. As in the case of $S_{14}EP_{64}E_{22}^{122}$ no yield point is observed. This finding might be attributed to dispersed PS and PE domains within a matrix of the PEP block, as revealed by TEM and SFM investigations (Figure 6A/B). The insert to Figure 7 shows that for extensions to 100% the remaining plastic deformation is nearly constant for all 3 cycles.

Table 3. Mechanical Properties of PS-*b*-PI-*b*-PS and PS-*b*-PEP-*b*-P(E/S) Triblock Copolymers[a]

triblock copolymer	$\varepsilon_{plast}(100)/1$ [%]	$\varepsilon_{plast}(100)/2$ [%]	$\varepsilon_{plast}(100)/3$ [%]	$\varepsilon_{plast}(200)$ [%]	$\varepsilon_{plast}(300)$ [%]	$\varepsilon_{plast}(400)$ [%]	$\varepsilon_{plast}(500)$ [%]	E [MPa]	ε_{br} [%]
$S_{14}I_{65}S_{21}^{117}$ [b]	11.4 (0.10)	12.0 (0.19)	12.5 (0.52)	19.6 (0.12)	28.3 (0.91)	34.2 (0.26)	40.9 (0.25)	-	1399 (189)
$S_{14}EP_{66}S_{20}^{119}$ [b]	14.2 (0.97)	14.6 (1.26)	14.7 (1.36)	22.4 (0.76)	29.2 (1.04)	42.9 (6.39)	58.1 (4.32)	65.9 (2.00)	844 (14.4)
$S_{14}EP_{64}E_{22}^{122}$ [b]	6.79 (0.89)	7.36 (0.63)	7.75 (0.56)	14.6 (1.11)	26.3 (1.04)	42.5 (0.89)	60.6 (1.83)	9.40 (0.01)	613 (22.8)
$S_{13}EP_{57}E_{30}^{112}$ [b]	7.04 (0.07)	8.06 (0.16)	8.60 (0.10)	17.3 (0.12)	32.7 (0.71)	53.4 (0.92)	76.2 (1.55)	9.83 (0.56)	898 (48.0)
$S_{13}EP_{57}E_{30}^{112}$ [b,c]	7.44 (0.12)	8.16 (0.03)	8.55 (0.10)	16.0 (0.05)	29.6 (0.65)	47.2 (0.32)	67.7 (1.28)	8.53 (0.07)	-
$S_{14}EP_{66}S_{20}^{119}$ [d]	14.1 (1.04)	14.7 (1.08)	15.0 (1.10)	21.5 (1.89)	25.5 (2.74)	27.5 (2.72)	42.6	43.1 (4.21)	-
$S_{14}EP_{64}E_{22}^{122}$ [d]	5.20 (0.39)	5.73 (0.41)	6.03 (0.47)	11.4 (0.86)	20.8 (1.26)	35.5 (1.23)	57.3	10.3 (1.18)	-
$S_{13}EP_{57}E_{30}^{112}$ [d]	5.69 (1.05)	6.36 (1.06)	6.62 (1.08)	13.5 (1.49)	26.2 (1.43)	46.5 (1.19)	72.8	9.70 (0.94)	-

[a] $\varepsilon_{plast}(X)$ = remaining plastic deformation after an extension to X %, no holding time in between the steps of the hysteresis measurement; E = Young´s modulus; ε_{br} = elongation at break; the values in parenthesis give the standard deviations.

[b] Measurements were performed on an Instron 5565 tensile testing machine without optical extensometers.

[c] Sample annealed at 83 °C under vacuum for 12 h.

[d] Measurements were performed on a Zwick tensile testing machine equipped with optical extensometers.

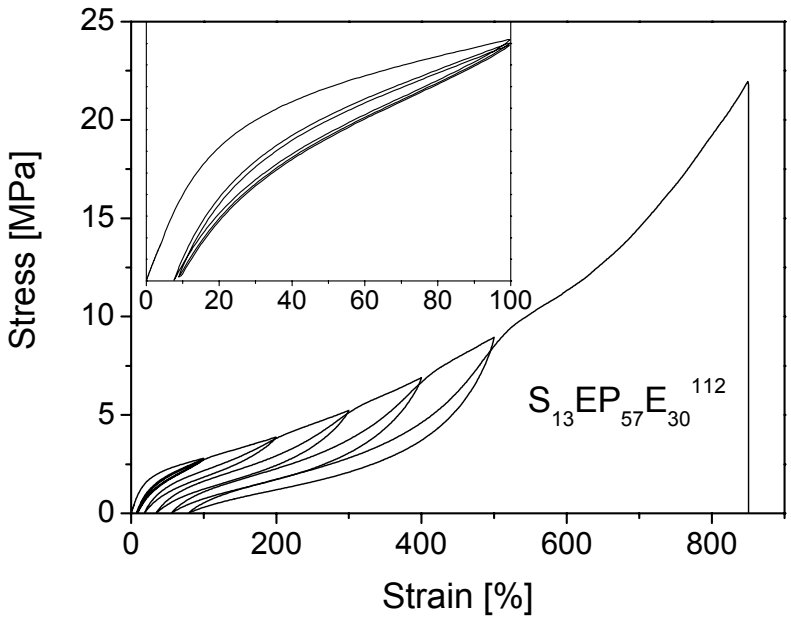

Figure 7. Hysteresis measurements on $S_{13}EP_{57}E_{30}^{112}$.

The PS-*b*-PEP-*b*-PS triblock copolymer shows a different stress-strain behavior (Figure 8). As can be clearly seen from the insert to Figure 8 a yield point is observed at a strain of 7.7% which may result from the break up of partially interconnected PS domains (see also Figure 4C). At the yield point formation of a neck occurs, which runs through the sample with increasing strain up to an elongation of ca. 150%. At this point the strain is again distributed homogeneously over the whole sample. In addition, the Young´s modulus is much larger as compared to the PS-*b*-PEP-*b*-PE triblock copolymers (Table 3). For well oriented "single crystal"-type PS-*b*-PB-*b*-PS triblock copolymers with cylindrical (PS) morphology it is known, that the mechanical properties strongly depend on the direction of the applied strain with regard to the oriented PS-cylinders.[37] On elongations parallel to the cylinder axis, the stress-strain curves display a yield behavior, whereas on perpendicular elongations no yield point is observed. Samples of PS-*b*-PEP-*b*-P(S/E) triblock copolymers for TEM and SFM investigations were prepared in a way that we look on the sample along the direction of the afterwards applied strain in mechanical testing. For both PS-*b*-PEP-*b*-PS (Figure 4C) and PS-*b*-PEP-*b*-PE (Figure 6A/B) the strongly distorted PS-cylinders show no preferential orientation with respect to the direction of strain (perpendicular to the plane of the TEM or SFM image). Therefore it can be concluded, that the different stress-strain behavior results from differences in the morphology and not from different orientations. In the PS-*b*-PEP-*b*-PS triblock copolymer the PS-cylinders might be partially interconnected resulting in the

observed yielding behavior. In contrast, for PS-*b*-PEP-*b*-PE triblock copolymers the PS and PE domains are dispersed within a matrix of PEP and no yield point is observed. The observed minimum at 450% strain (Figure 8) arises from the strong tendency of $S_{14}EP_{66}S_{20}^{119}$ to sample slippage especially at high strain values. This effect was also observed for the PE containing triblock copolymers. Compared to $S_{13}EP_{57}E_{30}^{112}$ (Figure 7) and $S_{14}EP_{64}E_{22}^{122}$ (results not shown) the stress values for elongations beyond 100% are always lower for $S_{14}EP_{66}S_{20}^{119}$ (Figure 8). This might result from the suppressed loop formation in PS-*b*-PEP-*b*-PE triblock copolymers due to the strong incompatibility of the end blocks. However, one has to take into account that the morphologies of PS-*b*-PEP-*b*-PS and PS-*b*-PEP-*b*-PE triblock copolymers are not identical.

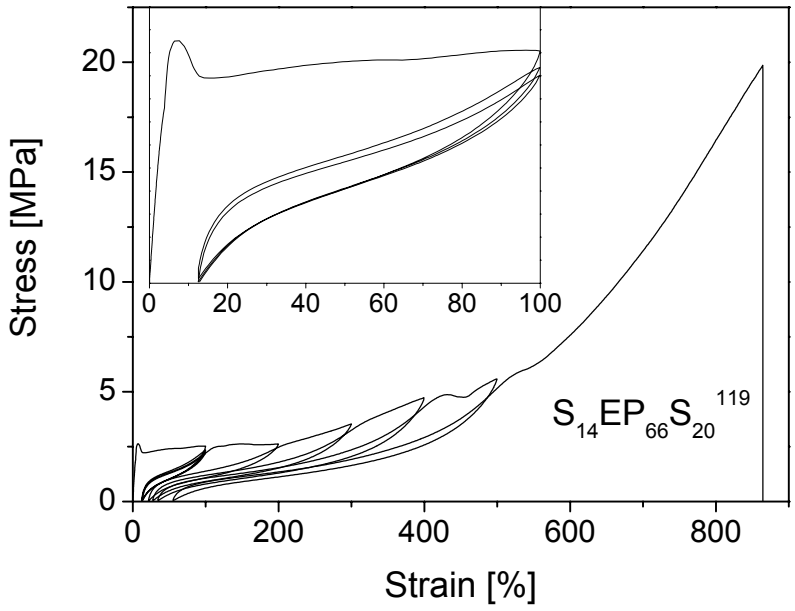

Figure 8. Hysteresis measurements on $S_{14}EP_{66}S_{20}^{119}$.

Figure 9 shows a comparison of the plastic deformations (ε_{plast}) obtained from hysteresis measurements on PS-*b*-PEP-*b*-PS and PS-*b*-PEP-*b*-PE triblock copolymers. For elongations up to 200% both PS-*b*-PEP-*b*-PE triblock copolymers exhibit a smaller plastic deformation (ε_{plast}), i. e. better elastic recovery, compared to $S_{14}EP_{66}S_{20}^{119}$ with respect to the measurements conducted without optical extensometers (Figure 9, Table 3). The comparatively high plastic deformation of $S_{14}EP_{66}S_{20}^{119}$ for small strains may also be attributed to the observed necking, which goes along with successive break up of

interconnected PS-cylinders and is expected to continue with increasing strain (post-neck or drawing regime) resulting in an accumulation of plastic deformation.

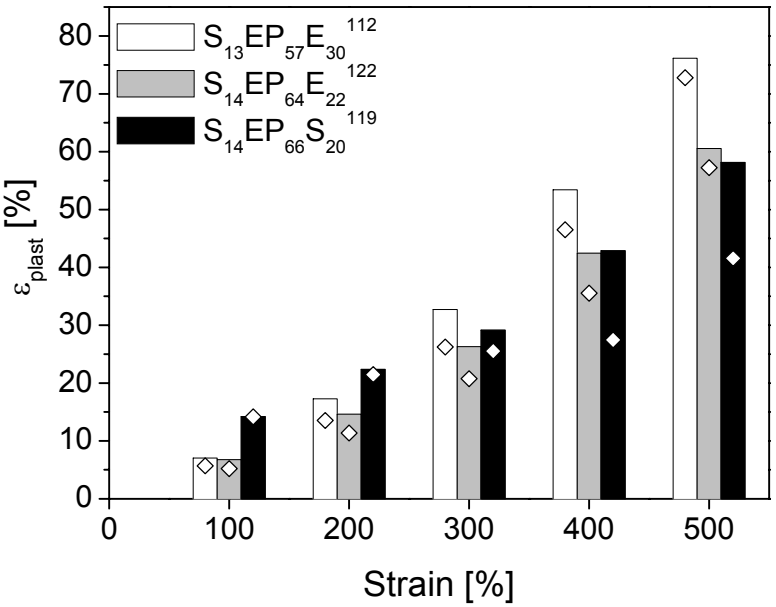

Figure 9. Comparison of plastic deformations (ε_{plast}) obtained from hysteresis measurements with (◊) and without (bars) optical extensometers.

Especially the triblock copolymer with a lower PE weight fraction ($S_{14}EP_{64}E_{22}^{122}$) shows better elastic properties, i. e. lower ε_{plast}, which is likely to result from a better resistance of the PE crystallites against disruption. Up to 300% strain, the plastic deformation is lower compared to $S_{14}EP_{66}S_{20}^{119}$ and nearly equal for higher strains. A comparison of the plastic deformations of $S_{14}I_{65}S_{21}^{117}$ with $S_{14}EP_{66}S_{20}^{119}$ shows that the non-hydrogenated triblock copolymer exhibits slightly better elastic recovery (Table 3). Annealing of $S_{13}EP_{57}E_{30}^{112}$ at 83 °C for 12 h results in a slight improvement of the elastic recovery especially at high elongations as depicted in Figure 10. This effect can be attributed to a more uniform crystallite size distribution for the PE block in the annealed sample resulting from the transformation of small (less stable) crystallites into bigger (more stable) ones. This was also detected by DSC, revealing an increased melting temperature of PE and a more narrow melting endotherm in the annealed sample (result not shown).

One has to take into account that the PS-*b*-PEP-*b*-PS and PS-*b*-PEP-*b*-PE triblock copolymers show slippage especially at high elongations which strongly affects the determined plastic deformations. Therefore we also conducted hysteresis measurements with optical extensometers which are insensitive to sample slippage. The obtained plastic deformations are depicted as diamonds (◊) in Figure 9. For strains up to 300% the use of

optical extensometers confirms the behavior described above. In contrast, for higher elongations the recovery of $S_{14}EP_{66}S_{20}^{119}$ gets significantly better compared to the PE containing triblock copolymers reflecting the strong effect of slippage observed for $S_{14}EP_{66}S_{20}^{119}$ on the measurements without optical extensometers.

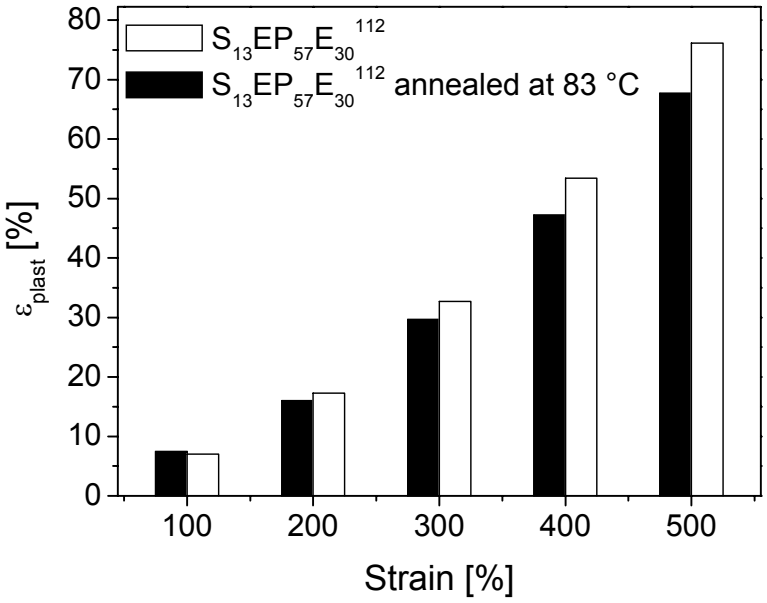

Figure 10. Comparison of plastic deformations (ε_{plast}) of $S_{13}EP_{57}E_{30}^{112}$ before and after annealing at 83 °C for 12h.

In conclusion, for strains up to 300% PS-*b*-PEP-*b*-PE triblock copolymers exhibit a slightly improved elastic recovery compared to the PS-*b*-PEP-*b*-PS triblock copolymer. However, for higher strains the PE crystallites in PS-*b*-PEP-*b*-PE triblock copolymers apparently suffer greater distortions than the amorphous PS domains in the PS-*b*-PEP-*b*-PS triblock copolymer leading to higher plastic deformations. The improved elastic recovery at low strains for the PE containing triblock copolymers might be attributed to the suppressed loop formation in this system due to the strong incompatible end blocks. Another possibility for the observed behavior might arise from the different morphologies of PS-*b*-PEP-*b*-PS and PS-*b*-PEP-*b*-PE triblock copolymers. In addition, the observed yielding and necking for $S_{14}EP_{66}S_{20}^{119}$ and $S_{14}I_{65}S_{21}^{117}$ triblock copolymers, which might be related to the break up of interconnected PS-cylinders, also results in an increased plastic deformation.

In general for PS-*b*-PEP-*b*-PE triblock copolymers the elastic recovery is better for systems with a lower PE weight fraction. This result is in agreement to the results obtained by Morton et al. for PE-*b*-PI-*b*-PE and PE-*b*-PEB-*b*-PE triblock copolymers.[29-31] The

investigated triblock copolymers with approximately 30 wt-% PE exhibit relatively good elastic recovery, whereas the systems with higher PE contents show unusually high unrecovered deformations, i. e. cold drawing. For high strains they have also detected a much higher plastic set for the PE containing triblock copolymers compared to PS-*b*-PB-*b*-PS triblock copolymers, which was attributed to a smaller resistance of the PE crystallites against distortion compared to amorphous PS domains, especially at high elongations.

Conclusions

We have compared the morphologies and mechanical properties of PS-*b*-PEP-*b*-PE triblock copolymers with a PS-*b*-PI-*b*-PS and the corresponding hydrogenated PS-*b*-PEP-*b*-PS triblock copolymer. SFM investigations on PS-*b*-PEP-*b*-PE triblock copolymers in combination with selective swelling of the PS domains by exposure to toluene vapor enables us to simultaneously detect the PS and PE domains which is not possible by using conventional TEM techniques. Due to the imcompatibility of the end blocks the formation of loops is suppressed resulting in a morphology consisting of dispersed PS cylinders and PE crystallites within a matrix of the PEP block. Morphological investigations on compression molded samples exhibit a distorted cylindrical structure of the PS block for PS-*b*-PI-*b*-PS and PS-*b*-PEP-*b*-PS, making the formation of loops and interconnected PS cylinders possible.

Comparison of plastic deformations obtained from hysteresis measurements on PS-*b*-PEP-*b*-PE and PS-*b*-PEP-*b*-PS triblock copolymers reveals better elastic properties, i. e. smaller plastic deformations, for the PE containing triblock copolymers at small strains. Different reasons may be responsible for that: the restricted loop formation in PS-*b*-PEP-*b*-PE triblock copolymers, the different morphologies of the compared systems or a combination of both effects. In contrast to the behavior at small strains, for high strain values the PS-*b*-PEP-*b*-PS triblock copolymer exhibits a significantly better elastic recovery. This might be attributed to a weaker resistance of crystalline PE domains against disruption compared to amorphous PS domains. In general, the elastic recovery of PS-*b*-PEP-*b*-PE triblock copolymers improves with decreasing content of crystalline PE.

Acknowledgment. We thank K. Matussek, R. Giesa and J. van Elburg for assistance with mechanical testing, A. J. Müller (Universidad Simón Bolívar, Caracas) for helpful discussions concerning the DSC measurements, C. Drummer for SEM and A. Göpfert for TEM investigations. Financial support was given by DSM Research, Geleen and the German Israeli Foundation for Scientific Research and Development (GIF). This work was partially supported by the Deutsche Forschungsgemeinschaft (SFB 481) and by the Bayreuther Institut für Makromolekülforschung (BIMF).

References and Notes

(1) Morton, M. *Encyclopedia of Polymer Science and Technology*; John Wiley & Sons: New York, 1971, Vol. 15, pp 508.

(2) Morton, M. *Anionic Polymerization: Principles and Practice*; Academic Press: New York, 1983.

(3) Holden, G.; Legge, N. R. *Styrenic Thermoplastic Elastomers*, In *Thermoplastic Elastomers: A Comprehensive Review*; 2nd ed.; Holden, G., Legge, N. R., Quirk, R. P. and Schroeder, H. E., Ed.; Hanser: Munich, 1996, p 47.

(4) Mogi, Y.; Nomura, M.; Kotsuji, H.; Ohnishi, K.; Matsushita, Y.; Noda, I. *Macromolecules* **1994**, *27*, 6755.

(5) Riess, G.; Hurtrez, G.; Bahadur, P. *Block Copolymers*, In *Encycl. Polym. Sci. Eng.*, 1985; Vol. 2, pp 324.

(6) Bates, F. S.; Fredrickson, G. H. *Physics Today* **1999**, *52*, 32.

(7) Abetz, V., In *Supramolecular Polymers*; Ciferri, A., Ed.; Marcel Dekker: New York, 2000, chapter 6, pp 215.

(8) Kane, L.; Spontak, R. J. *Macromolecules* **1994**, *27*, 663.

(9) Stadler, R.; Auschra, C.; Beckmann, J.; Krappe, U.; Voigt-Martin, I.; Leibler, L. *Macromolecules* **1995**, *28*, 3080.

(10) Gido, S. P.; Schwark, D. W.; Thomas, E. L.; do Carmo Goncalves, M. *Macromolecules* **1993**, *26*, 2636.

(11) Breiner, U.; Krappe, U.; Abetz, V.; Stadler, R. *Macromol. Chem. Phys.* **1997**, *198*, 1051.

(12) Breiner, U.; Krappe, U.; Jakob, T.; Abetz, V.; Stadler, R. *Polym. Bull.* **1998**, *40*, 219.

(13) Shefelbine, T. A.; Vigild, M. E.; Matsen, M. W.; Hajduk, D. A.; Hillmyer, M. A.; Cussler, E. L.; Bates, F. S. *J. Am. Chem. Soc.* **1999**, *121*, 8457.

(14) Abetz, V.; Goldacker, T. *Macromol. Rapid Commun.* **2000**, *21*, 16.

(15) Hückstädt, H.; Göpfert, A.; Abetz, V. *Polymer* **2000**, *41*, 9089.

(16) Breiner, U.; Krappe, U.; Stadler, R. *Macromol. Rapid Commun.* **1996**, *17*, 567.

(17) Breiner, U.; Krappe, U.; Thomas, E. L.; Stadler, R. *Macromolecules* **1998**, *31*, 135.

(18) Ott, H.; Abetz, V.; Altstädt, V. *Macromolecules* **2001**, *34*, 2121.

(19) Abetz, V.; Stadler, R.; Leibler, L. *Polym. Bull.* **1996**, *37*, 135.

(20) Brinkmann, S.; Stadler, R.; Thomas, E. L. *Macromolecules* **1998**, *31*, 6566.

(21) Brinkmann-Rengel, S.; Abetz, V.; Stadler, R.; Thomas, E. L. *Kautschuk Gummi Kunststoffe* **1999**, *52*, 806.

(22) Kofinas, P.; Cohen, R. E. *Macromolecules* **1994**, *27*, 3002.

(23) Rangarajan, P.; Register, R. A.; Fetters, L. J. *Macromolecules* **1993**, *26*, 4640.

(24) Rangarajan, P.; Register, R. A.; Adamson, D. H.; Fetters, L. J.; Bras, W.; Naylor, S.; Ryan, A. J. *Macromolecules* **1995**, *28*, 1422.

(25) Bates, F. S.; Schultz, M. F.; Rosedale, J. H. *Macromolecules* **1992**, *25*, 5547.

(26) Falk, J. C. *Macromolecules* **1971**, *4*, 152.

(27) Falk, J. C.; Schlott, R. J. *Angew. Makromol. Chem.* **1972**, *21*, 17.

(28) Mohajer, Y.; Wilkes, G. L.; Wang, I. C.; McGrath, J. E. *Polymer* **1982**, *23*, 1523.

(29) Morton, M.; Lee, N.-C.; Terrill, E. R. *Polym. Prep.* **1981**, *22*, 136.

(30) Morton, M.; Lee, N.-C.; Terrill, E. R. *ACS Symposia Series, Elastomers and Rubber Elasticity* **1982**, *193*, 101.

(31) Morton, M. *Rubber Chem. Tech.* **1983**, *56*, 1096.

(32) Morton, M.; Quirk, R. P. *Anionic Triblock Copolymers*, In *Thermoplastic Elastomers: A Comprehensive Review*; 2nd ed.; Holden, G., Legge, N. R., Quirk, R. P. and Schroeder, H. E., Ed.; Hanser: Munich, 1996, pp 71.

(33) Séguéla, R.; Prud'homme, J. *Polymer* **1989**, *30*, 1446.

(34) Brandrup, J.; Immergut, E. H. *Polymer Handbook*; *3rd* ed.; Wiley: New York, 1989.

(35) Park, C.; De Rosa, C.; Fetters, L. J.; Thomas, E. L. *Macromolecules* **2000**, *33*, 7931.

(36) Elbs, H.; Fukunaga, K.; Stadler, R.; Sauer, G.; Magerle, R.; Krausch, G. *Macromolecules* **1999**, *32*, 1204.

(37) Odell, J. A.; Keller, A. *Polym. Eng. Sci.* **1977**, *17*, 544.

3.3.2 Thermoplastic Elastomers Based on Semicrystalline Block Copolymers

H. Schmalz,[a] V. Abetz, [a *] R. Lange[b]

a) Makromolekulare Chemie II, Universität Bayreuth, 95440 Bayreuth, Germany
b) DSM-Research, 6160 MD Geleen, The Netherlands,
present address: BASF-AG, ZKS/B1, 67056 Ludwigshafen, Germany

ABSTRACT: Thermoplastic elastomers are used in a wide range of applications due to easy processing by conventional methods like injection molding and extrusion. ABC triblock copolymers with two hard domain forming end blocks in a rubbery matrix of B are one way to approach thermoplastic elastomers. In this contribution we will compare polystyrene-*block*-poly(ethylene-*alt*-propylene)-*block*-polyethylene (PS-*b*-PEP-*b*-PE) and polystyrene-*block*-poly(ethylene-*alt*-propylene)-*block*-polystyrene (PS-*b*-PEP-*b*-PS) triblock copolymers with similar middle block content with respect to their morphological and mechanical properties. Transmission electron microscopy (TEM) and scanning force microscopy (SFM) reveal for the PS-*b*-PEP-*b*-PE triblock copolymers a morphology consisting of PS cylinders and PE crystallites within a matrix of the PEP block. Mechanical characterization of these triblock copolymers demonstrated that for small strains the PS-*b*-PEP-*b*-PE triblock copolymers exhibit the aimed smaller plastic deformations, *i.e.* better elastic properties, compared to the polystyrene based ABA type thermoplastic elastomers. However, at high strains the PS-*b*-PEP-*b*-PS triblock copolymers show a significantly better elastic recovery.

Introduction

Thermoplastic elastomers or TPE's combine the properties of irreversible crosslinked elastomers with the easy processing of thermoplastic materials. This enables product designs not easily achieved for conventional rubbers.

One type of TPE's is based on linear ABA and ABC triblock copolymers, where A and C form hard, dispersed domains in an elastomeric B matrix. A well-known example for ABA block copolymers are systems with the A-block consisting of polystyrene whereas the B-block is typically polybutadiene or polyisoprene (PS-*b*-PB-*b*-PS or PS-*b*-PI-*b*-PS).[1,2] Due to the incompatibility between the two components microphase separation occurs, whereby the polystyrene minority phase forms dispersed spheres or cylinders in a rubbery matrix of the middle block. As a consequence, the B chain may loop back into the same end block domain rather than being forced to form a bridge between two different end block domains. This should have an influence on the elastic properties of such materials, since bridges and loops behave mechanically different. In order to force the end blocks into different domains, they should be incompatible with each other, i.e. the ABA must be replaced by an ABC system. A problem encountered in ABC triblock copolymers with short end blocks (*i. e.* end blocks forming spheres or cylinders) is the usually insufficient degree of incompatibility between A and C, $\chi_{AC} \cdot N_{AC}$ (N_{AC} is the degree of polymerization of the A- and C-block and χ_{AC} is the segmental interaction parameter between the two species).[3,4] Semicrystalline end blocks offer a way to achieve segregated end blocks at low molecular weights, since crystallization is a strong driving force for microphase separation. Investigations on polyethylene-*block*-poly(ethylene-*alt*-propylene) (PE-*b*-PEP) diblock copolymers show that even for low molecular weights a microphase separated structure is obtained due to crystallization induced microphase separation.[5-7] Furthermore, this system exhibits a small value for the segmental interaction parameter χ of 0.007 at 120 °C (above the melting point of PE) resulting in a homogeneous melt in a wide composition range which is advantageous in view of processing.[8] This is also true for PE-*b*-PEB-*b*-PE triblock copolymers, which were compared with polystyrene based thermoplastic elastomers.[9,10] Recently first results on a comparison between polystyrene-*block*-poly(ethylene-*alt*-propylene)-*block*-polyethylene (PS-*b*-PEP-*b*-PE) with the corresponding PS-*b*-PEP-*b*-PS block copolymer were published, which showed superior mechanical properties for PS-*b*-PEP-*b*-PS at higher elongations, while at lower elongations the PS-*b*-PEP-*b*-PE showed better properties.[11] This behavior was assigned to the suppression of loops in the case of PS-*b*-PEP-*b*-PE, which might lead to a better elastic

recovery at low strains, while the weaker mechanical resistance of the PE blocks at larger strains results in better properties of the PS-*b*-PEP-*b*-PS.

In this contribution we give an overview of the morphological and mechanical properties of PS-*b*-PEP-*b*-PE triblock copolymers with a glassy and a semicrystalline end block in comparison to the corresponding PS-*b*-PEP-*b*-PS triblock copolymers with two glassy end blocks.

Experimental Section

Synthesis. Details of the synthesis of the PS-*b*-PEP-*b*-PS and PS-*b*-PEP-*b*-PE triblock copolymers via living anionic polymerization and subsequent catalytic hydrogenation are given in ref. [11]. The nomenclature of these triblock copolymers is $A_xB_yC_z^M$, where x, y, z are the weight percentages of the blocks A, B, C and M is the total molecular weight in kg/mol.

Differential Scanning Calorimetry (DSC). For thermal analysis a Perkin Elmer DSC 7 with a CCA 7 liquid nitrogen cooling device was used. For all measurements a two point calibration with decane and indium was applied. All experiments were performed at a scanning rate of 10 °C/min. The degree of crystallinity of the PE block within PS-*b*-PEP-*b*-PE triblock copolymers was calculated using the heat of fusion for a 100% crystalline PE of $\Delta H_m^0 = 276.98$ J/g.[12]

Transmission Electron Microscopy (TEM). The bulk morphology of the triblock copolymers was examined by bright field TEM using a Zeiss CEM 902 electron microscope operated at 80 kV. Films were prepared by compression molding in an identical manner as the samples for mechanical testing, unless indicated otherwise. Thin sections were cut at -130 °C using a Reichert-Jung Ultracut E microtome equipped with a diamond knife. Selective staining of the PI domains was achieved by exposure of the sections to OsO_4 vapor for 60 s, while the thin sections of hydrogenated triblock copolymers were exposed to RuO_4 vapor for 45 min to selectively stain the PS domains.

Scanning Force Microscopy (SFM). Scanning force microscopy images were taken on a Digital Instruments Dimension 3100 microscope operated in Tapping Mode™ (free amplitude of the cantilever: 20 nm; set point ratio: 0.95). Measurements on PS-*b*-PEP-*b*-PE triblock copolymers were performed on thin films prepared on polished silicon wafers by spin coating from a 5 mg/ml solution of the polymer in toluene.

Mechanical Testing. Mechanical testing was carried out using a Zwick tensile testing machine equipped with optical extensometers. Young´s modulus was determined at a testing speed of 20 mm/min at small elongations (0 – 4%), elongations at break were measured at the same rate. Hysteresis measurements were performed at a testing speed of 20 mm/min for elongations to 100, 200, 300, 400 and 500% followed by extension to break. No holding time between the cycles was applied. Test specimens according to ISO 37:1994 were used. Preparation was accomplished by compression molding into plates at 140 – 150 °C followed by cooling to room temperature. It was made sure that the cutting of test specimens always occurs in the same direction in order to exclude any effects resulting from different orientation within the test samples.

Results and Discussion

Thermal Properties. Table 1 summarizes the thermal properties of the synthesized PS-*b*-PEP-*b*-PS and PS-*b*-PEP-*b*-PE triblock copolymers. The triblock copolymers exhibit glass transition temperatures at ca. –55 °C for the PEP blocks and ca. 100 °C for the PS blocks, reflecting a strong microphase separation. The glass transition temperature of the PEP blocks is almost independent of composition, whereas the PS blocks show a decrease in glass transition temperature with decreasing PS content. This effect is more pronounced for PS-*b*-PEP-*b*-PE triblock copolymers. In the case of PE, microphase separation is induced by crystallization, as the PE segments are expected to crystallize from a homogeneous mixture of PEP and PE segments due to their low segmental interaction parameter in the melt.[8] With increasing PE content, the PS-*b*-PEP-*b*-PE triblock copolymers exhibit a shift in the peak melting and crystallization temperature to higher values. This effect is more obvious in the detected peak crystallization temperatures. A higher PE content results in a slightly increased segregation strength between the PE and PEP segments in the melt and thus in the observed increase in peak crystallization temperature. Depending on composition, the PE blocks exhibit a degree of crystallinity between ca. 20 and 30%. $S_{13}EP_{76}E_{11}^{121}$, the triblock copolymer with the lowest PE content, shows a comparatively small degree of crystallinity and a marked depression in the melting and crystallization temperature.

Table 1. DSC Data of PS-*b*-PEP-*b*-P(E/S) Triblock Copolymers[a]

triblock	T_g (PEP) [°C]	T_g (PS) [°C]	T_m (PE) [°C]	T_c (PE) [°C]	α (PE) [%]
$S_{14}EP_{66}S_{20}^{119}$	-55.5	102.4	-	-	-
$S_{13}EP_{77}S_{10}^{119}$	-57.7	98.4	-	-	-
$S_8EP_{71}S_{21}^{121}$	-58.7	97.9[b]	-	-	-
$S_{13}EP_{76}E_{11}^{121}$	-57.5	98.3[b]	86.6	51.0	21.0
$S_8EP_{71}E_{21}^{121}$	-58.0	72.3[b]	89.6	56.8	25.8
$S_{14}EP_{64}E_{22}^{122}$	-56.0	99.3[b]	88.0	57.6	31.9
$S_{13}EP_{57}E_{30}^{112}$	-56.0	100.4[b]	88.7	59.8	31.0
$S_{33}EP_{37}E_{30}^{115}$	-57.6	105.4	90.4	65.2	25.2

[a] T_m = melting point (peak maximum), T_c = crystallization temperature (peak maximum), α = degree of crystallinity, and T_g = glass transition temperature.
[b] Determined by dynamic mechanical analysis (maximum G'', 1 rad/s, 1 °C/min).

Morphology. Figure 1A shows the TEM micrograph of $S_8I_{71}S_{21}^{119}$, the precursor of $S_8EP_{71}S_{21}^{121}$, prepared by compression molding in an identical manner as compared to the preparation of test specimens for tensile testing. Due to selective staining of the PI blocks, the PS blocks appear white and exhibit a distorted cylindrical microstructure. With respect to the PS cylinders, both top and side view are visible, no preferential orientation can be detected. Figure 1B shows the TEM image of the corresponding $S_8EP_{71}E_{21}^{121}$ triblock copolymer, in which one PS block of the respective $S_8EP_{71}S_{21}^{121}$ triblock copolymer is replaced by a PE block. Due to the lack of olefinic double bonds staining was achieved using RuO_4 vapor, which preferentially stains the PS blocks. Consequently, the PS domains appear dark and exhibit a similar distorted cylindrical microstructure as compared to $S_8I_{71}S_{21}^{119}$ (Figure 1A). Due to the small PS content of 8 wt-%, interconnections between the PS cylinders are not visible. As a result of the used staining technique, the crystalline PE domains, which are expected to be located within the matrix of the PEP blocks, are not visible. Figures 1C and 1D show the TEM images of $S_{13}EP_{76}E_{11}^{121}$ and $S_{33}EP_{37}E_{30}^{115}$, respectively. As a matter of increasing PS content in the PS-*b*-PEP-*b*-PE triblock copolymers (Figures 1B - 1D), the size of the PS domains increases. In all three triblock copolymers, the PS blocks exhibit a distorted cylindrical microstructure, without showing a preferential orientation of the PS cylinders. Furthermore, sample preparation by compression molding obviously restricts the formation of PS cylinders with a considerable length, as the PS cylinders exhibit only short lengths. This is more pronounced for $S_{33}EP_{37}E_{30}^{115}$, which might be expected to show relatively long cylinders with respect to the composition.

Alternatively, samples of $S_{13}EP_{76}E_{11}^{121}$ and $S_{33}EP_{37}E_{30}^{115}$ were prepared by casting from toluene solution. Due to the tendency of the triblock copolymer solutions in toluene to form gels upon solvent evaporation, film casting was performed at 70 °C to avoid gelation. After complete evaporation of the solvent, the films were allowed to cool to room temperature in order to induce crystallization of the PE blocks. Figure 1E shows the TEM micrograph of $S_{13}EP_{76}E_{11}^{121}$, prepared by solvent casting. Comparison with the sample prepared by compression molding (Figure 1C) reveals that the cylindrical PS microdomains are more nicely developed. However, the PS cylinders are still strongly distorted and exhibit no significant preferential orientation.

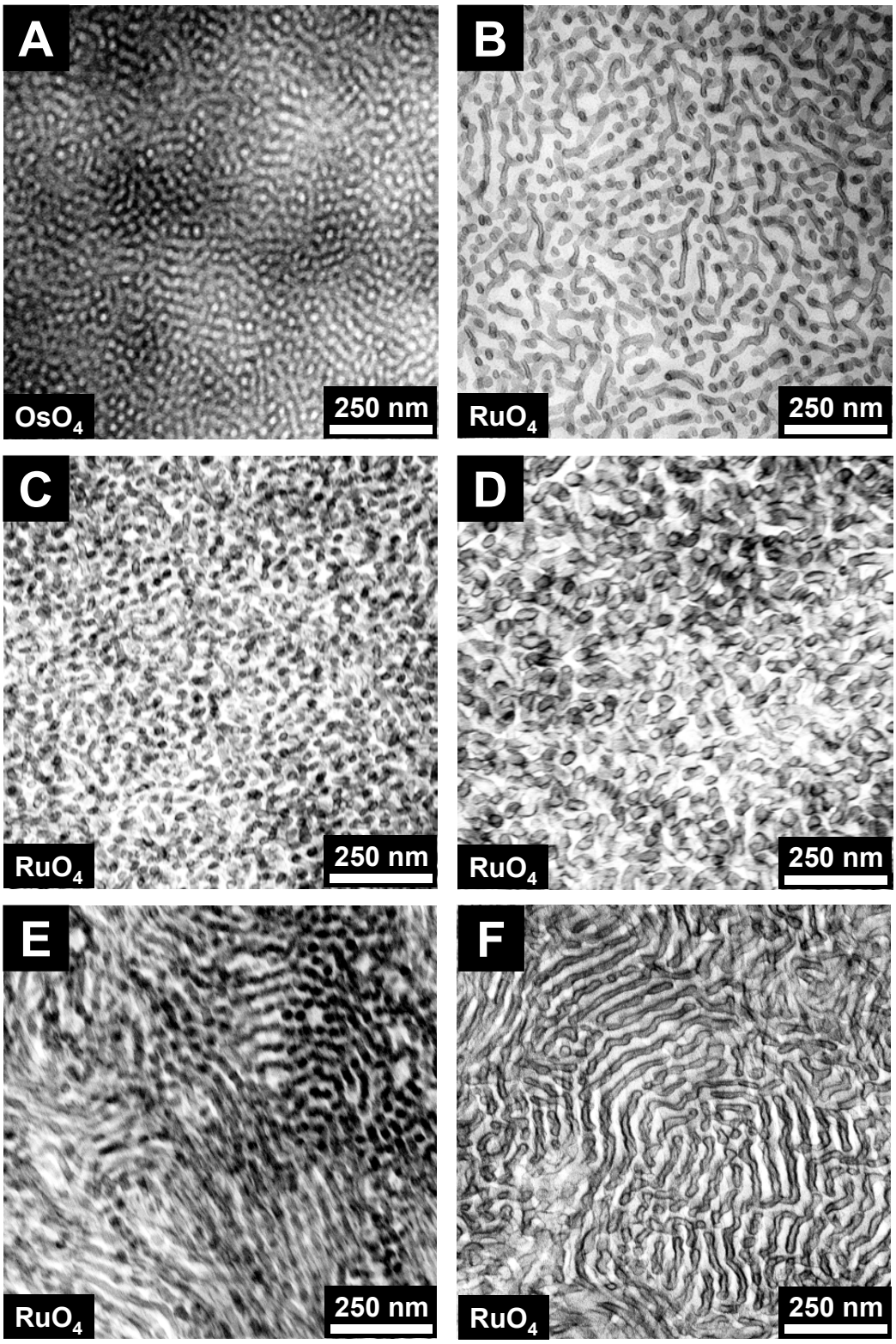

Figure 1. TEM micrographs of $S_8I_{71}S_{21}^{119}$ (A), $S_8EP_{71}E_{21}^{121}$ (B), $S_{13}EP_{76}E_{11}^{121}$ (C), and $S_{33}EP_{37}E_{30}^{115}$ (D), samples prepared by compression molding; and TEM micrographs of $S_{13}EP_{76}E_{11}^{121}$ (E), and $S_{33}EP_{37}E_{30}^{115}$ (F), samples prepared by casting from toluene solution at 70 °C.

Also $S_{33}EP_{37}E_{30}^{115}$ shows better developed and longer cylinders, when being prepared by solvent casting (Figure 1F) in comparison to compression molding (Figure 1D). Furthermore, a preferential orientation along the cylinder long axis can be observed and even interconnections between different PS cylinders are visible. This is expected to exert a significant influence on the mechanical properties as will be discussed in detail in the section on mechanical testing.

Due to problems involved in the staining technique, the crystalline PE domains cannot be visualized using TEM investigations. In order to gain more insight into the structure of the crystalline PE blocks within PS-*b*-PEP-*b*-PE triblock copolymers, scanning force microscopy (SFM) has been used. The large differences in stiffness between amorphous and crystalline domains makes SFM a superior tool for investigating semicrystalline-amorphous block copolymers, without the need of special sample preparations. Figures 2A and 2B show the topography and phase contrast images obtained for a thin film of $S_{33}EP_{37}E_{30}^{115}$ spin-coated from toluene solution, respectively. From the phase contrast image (Figure 2B) three different phases can be distinguished. The bright appearing domains (high phase shift) correspond to PS domains, which are located in between a continuous crystalline PE phase, which appears less bright with respect to the PS domains. These domains are also visible in the corresponding topography image (Figure 2A). The third phase, appearing dark in the phase contrast image, corresponds to the PEP blocks, as the amorphous PEP is expected to show a low phase shift due to the low glass transition temperature. This phase assignment has been previously proven by selective swelling of PS domains with toluene vapor in combination with scanning electron microscopy investigations.[11] Furthermore, the PS domains exhibit a strongly distorted structure with respect to a cylindrical microstructure, which might be expected from composition and TEM investigations (Figures 1D and 1F). As during film preparation the PE crystallizes before solidification of the PS cylinders (low solubility of PE in toluene results in gelation), the latter have to cope with the confined geometry given by the PE "crystal lamellae" which leads to the observed distortions in the PS domains. In contrast, when the film is prepared by solvent casting at 70 °C, first the PS solidifies upon solvent evaporation (T_g = 105.4 °C) followed by crystallization of the PE blocks during subsequent cooling to room temperature. As a consequence, the PS domains can form a well developed cylindrical microstructure as depicted in the corresponding TEM micrograph (Figure 1F).

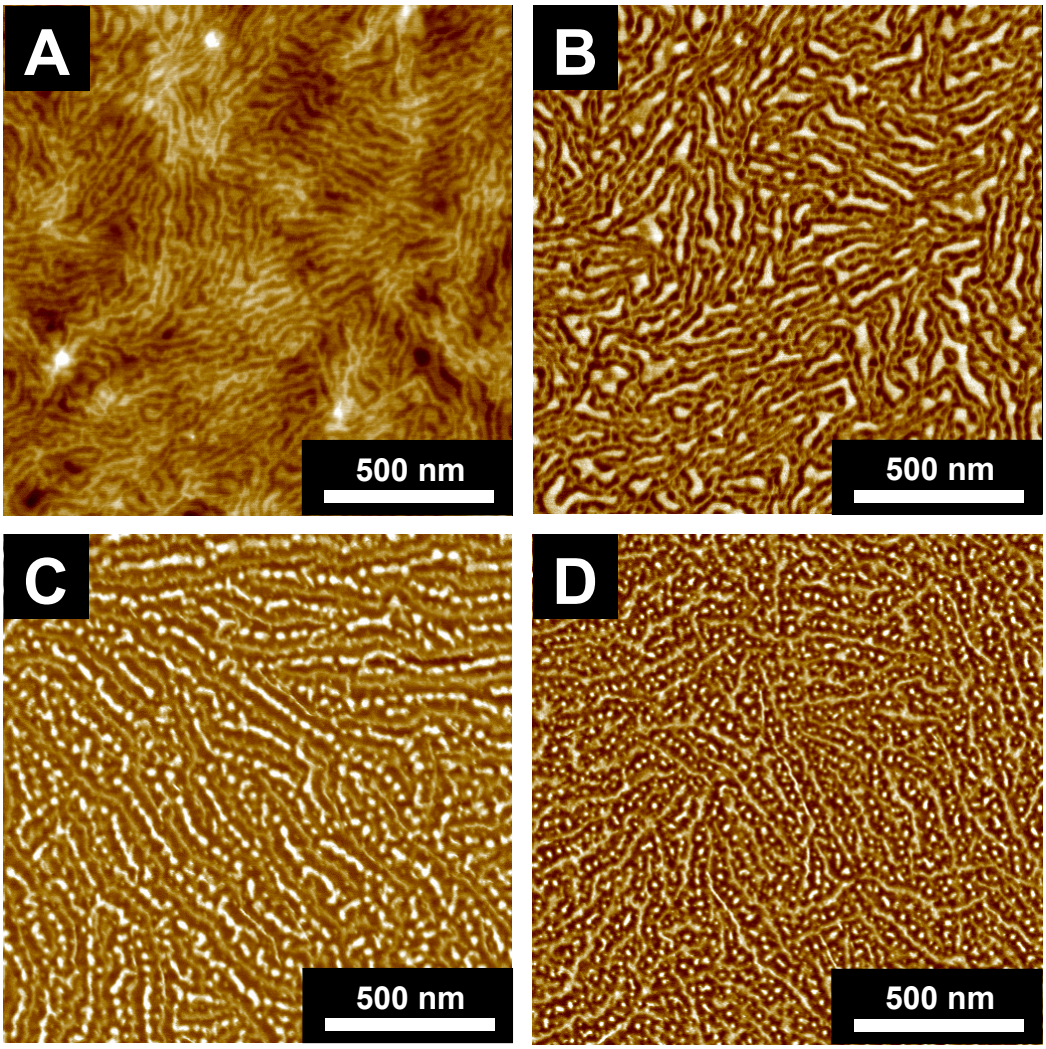

Figure 2. SFM topography and phase contrast images of $S_{33}EP_{37}E_{30}^{115}$ (A, z = 15 nm; B, z = 20°), $S_{13}EP_{76}E_{11}^{121}$ (C, z = 20°), and $S_8EP_{71}E_{21}^{121}$ (D, z = 10°).

Figures 2C and 2D show phase contrast images of $S_{13}EP_{76}E_{11}^{121}$ and $S_8EP_{71}E_{21}^{121}$, respectively. As expected from composition, the PEP block forms the matrix, appearing dark in the corresponding phase contrast images (low phase shift). The bright spherical and worm-like PS domains (high phase shift) are again located in between a network of interconnected PE crystallites (viewed edge on). Comparison of Figures 2C and 2D reveals that the size of the PS domains decreases as might be expected from the decreasing PS content. Furthermore the PS domains in $S_8EP_{71}E_{21}^{121}$ exhibit an almost exclusively spherical structure. However, cylindrical PS microdomains cannot be excluded, as cylinders aligned perpendicular to the substrate surface would also appear like spheres. A closer look to the crystalline PE domains shows, that the crystallite thickness in $S_{13}EP_{76}E_{11}^{121}$ (Figure 2C) is slightly decreased compared to $S_8EP_{71}E_{21}^{121}$ (Figure 2D). This corresponds to the lower melting temperature of the PE block within $S_{13}EP_{76}E_{11}^{121}$ compared to $S_8EP_{71}E_{21}^{121}$ (Table 1).

Mechanical Properties. In order to investigate the influence of a crystalline end block on the elastic properties of triblock copolymers, we performed hysteresis measurements on PS-*b*-PEP-*b*-PE triblock copolymers in comparison to PS-*b*-PEP-*b*-PS triblock copolymers with comparable compositions (Table 2). As an example, the hysteresis measurement performed on $S_{33}EP_{37}E_{30}^{115}$, prepared by solvent casting from toluene at 70 °C, is shown in Figure 3. The remaining plastic deformation (ε_{plast}) increases with increasing applied strain. In contrast to $S_{33}EP_{37}E_{30}^{115}$, prepared by compression molding, and the other PS-*b*-PEP-*b*-PE triblock copolymers (results not shown), the solvent cast sample of $S_{33}EP_{37}E_{30}^{115}$ shows a clear yield point. This might be attributed to the preferential orientation of PS cylinders and the interconnections between different PS cylinders in this sample, as has been deduced from TEM investigations on the solution cast film (Figure 1F). At the yield point interconnections between cylinders or cylinders oriented parallel to the strain direction break up. In contrast, the PS-*b*-PEP-*b*-PE triblock copolymers, prepared by compression molding, exhibit a distorted cylindrical microstructure without any preferential orientation (Figures 1B - 1D). As a consequence, no yield point is observed for these polymers. This results in a higher plastic deformation at any strain value for $S_{33}EP_{37}E_{30}^{115}$ prepared from solution, compared to the compression molded sample, and also accounts for the significantly higher Young´s modulus of the solution cast sample (Table 2). A similar effect has been observed for "single-crystal"-type PS-*b*-PB-*b*-PS triblock copolymers with cylindrical (PS) morphology.[13] Upon elongation parallel to the cylinder axis, the stress-strain traces display a yielding behavior, whereas on perpendicular elongations no yield point is observed. The possibility that also interconnected PE crystallites might be responsible for the observed behavior can be ruled out, since $S_{13}EP_{57}E_{30}^{112}$, exhibiting an equivalent PE content, shows no yield point. The mechanical properties of $S_{13}EP_{76}E_{11}^{121}$ do not show a significant influence of the sample preparation technique. This might be attributed to the fact that as well for the compression molded sample, as for the solution cast sample a distorted cylindrical microstructure was observed by TEM (Figures 1C and 1E).

Table 2. Mechanical Properties of PS-*b*-PEP-*b*-P(E/S) Triblock Copolymers[a]

triblock copolymer	$\varepsilon_{plast}(100)$ [%]	$\varepsilon_{plast}(200)$ [%]	$\varepsilon_{plast}(300)$ [%]	$\varepsilon_{plast}(400)$ [%]	$\varepsilon_{plast}(500)$ [%]	E [MPa]	ε_{br} [%]
$S_{14}EP_{66}S_{20}$[119]	14.1 (1.04)	21.5 (1.89)	25.5 (2.74)	27.5 (2.72)	42.6	43.1 (4.21)	470 (23.7)
$S_{13}EP_{77}S_{10}$[119]	6.96 (0.04)	10.1 (0.08)	12.6 (0.15)	14.6 (0.05)	-	12.8 (1.38)	483 (16.8)
$S_8EP_{71}S_{21}$[121]	6.59 (0.73)	9.75 (0.78)	12.6 (0.85)	15.4 (0.75)	20.1 (1.31)	14.9 (3.68)	502 (50.8)
$S_{13}EP_{76}E_{11}$[121]	4.14 (0.12)	8.27 (0.24)	12.9 (0.33)	-	-	8.70 (0.48)	295 (6.99)
$S_{13}EP_{76}E_{11}$[121 b]	3.72 (0.72)	7.00 (0.60)	10.8	14.6	-	9.31 (0.69)	271 (94.7)
$S_8EP_{71}E_{21}$[121]	3.07 (0.15)	7.79 (0.14)	15.3 (0.14)	28.9 (0.16)	47.6 (0.17)	8.34 (0.06)	-
$S_{14}EP_{64}E_{22}$[122]	5.20 (0.39)	11.4 (0.86)	20.8 (1.26)	35.5 (1.23)	55.0 (2.03)	10.3 (1.18)	782
$S_{13}EP_{57}E_{30}$[112]	5.69 (1.05)	13.5 (1.49)	26.2 (1.43)	46.5 (1.19)	71.5 (1.14)	9.70 (0.94)	646 (22.1)
$S_{33}EP_{37}E_{30}$[115]	15.6 (0.54)	35.7 (0.79)	69.9 (1.00)	118 (0.88)	183 (1.52)	62.6 (6.08)	563
$S_{33}EP_{37}E_{30}$[115 b]	19.7 (2.47)	42.2 (3.74)	76.2 (0.88)	127 (6.03)	194 (14.1)	136 (8.58)	748 (169)

[a] $\varepsilon_{plast}(X)$ = remaining plastic deformation after an extension to X%, no holding time in between the steps of the hysteresis measurement; E = Young´s modulus; ε_{br} = elongation at break; the values in parenthesis give the standard deviations.

[b] Samples were prepared by solvent casting from toluene at 70 °C, followed by cooling to room temperature.

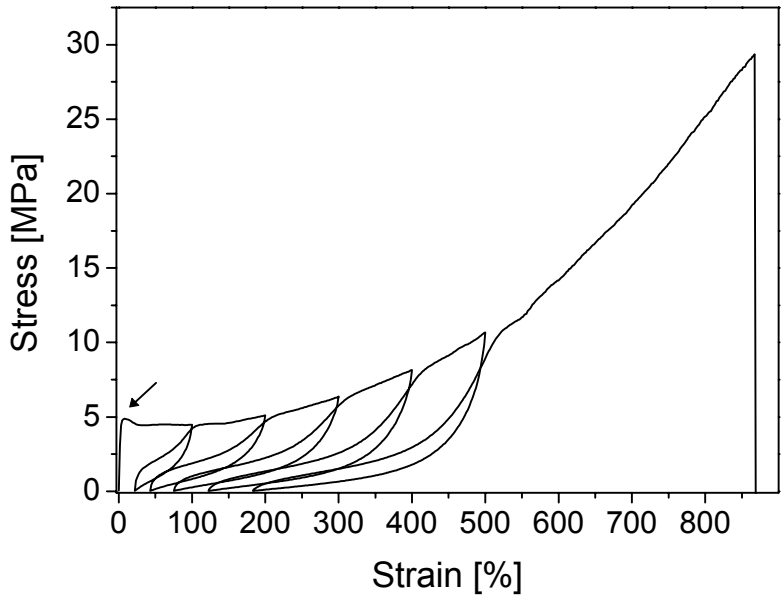

Figure 3. Hysteresis measurements on $S_{33}EP_{37}E_{30}^{115}$, prepared by solvent casting from toluene at 70 °C.

Figure 4 shows a comparison of plastic deformations (ε_{plast}) for various PS-*b*-PEP-*b*-PS and PS-*b*-PEP-*b*-PE triblock copolymers. For elongations < 300% the PS-*b*-PEP-*b*-PE triblock copolymers reveal significantly smaller plastic deformations compared to the corresponding PS-*b*-PEP-*b*-PS triblock copolymers with comparable composition, i. e. the elastic recovery is improved (see also Table 2). This might result from the suppressed loop formation in PS-*b*-PEP-*b*-PE triblock copolymers due to the strong incompatibility of the end blocks. However, one has to take into account that the morphologies of PS-*b*-PEP-*b*-PS and PS-*b*-PEP-*b*-PE triblock copolymers are not identical. At strain values ≥ 300% the situation is reversed and the PS-*b*-PEP-*b*-PS triblock copolymers exhibit a better elastic recovery (Figure 4, Table 2). An exception is the triblock copolymer $S_{14}EP_{64}E_{22}^{122}$, exhibiting a better elastic recovery at 300% strain compared to $S_{14}EP_{66}S_{20}^{119}$. The comparatively high plastic deformations for $S_{14}EP_{66}S_{20}^{119}$, especially for low strain values (Table 2), might be rationalized by the observation of yielding and necking[11], which goes along with successive breakup of interconnected PS cylinders and is expected to continue with increasing strain (postneck or drawing regime). The improved elasticity of PS-*b*-PEP-*b*-PS triblock copolymers with respect to PS-*b*-PEP-*b*-PE triblock copolymers at high elongations might be attributed to a weaker resistance of crystalline PE domains against disruption compared to amorphous PS domains, especially at high strains.

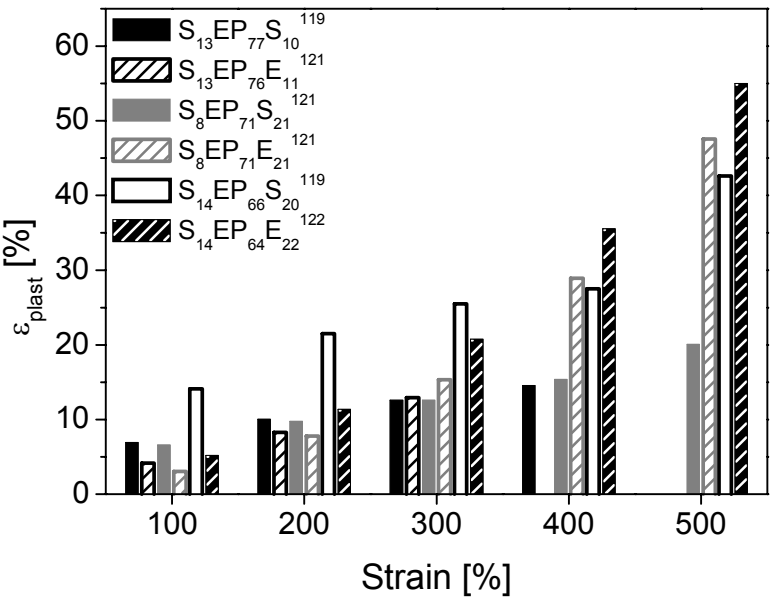

Figure 4. Comparison of plastic deformations (ε_{plast}) of PS-*b*-PEP-*b*-PS and PS-*b*-PEP-*b*-PE triblock copolymers.

The relationship between composition and elastic properties of PS-*b*-PEP-*b*-PE triblock copolymers is illustrated in Figure 5. A comparison of PS-*b*-PEP-*b*-PE triblock copolymers with similar PS content but varying PE content reveals an improvement in elastic recovery with decreasing PE content (Figure 5, Table 2). The triblock copolymer $S_{13}EP_{76}E_{11}^{121}$ exhibits a comparatively low elongation at break, which can be attributed to the low PE content. As deduced from the lower melting temperature of the PE block (Table 1), the crystallites are thinner compared to the systems with higher PE contents. As a consequence, the PE crystallites are less stable against disruption upon elongation, resulting in the observed lower elongation at break. In addition, lowering the PS content while keeping the PE content constant, also results in an improved elastic recovery which can be deduced by comparing the plastic deformations of $S_{14}EP_{64}E_{22}^{122}$ and $S_8EP_{71}E_{21}^{121}$ (Figure 5, Table 2). In general for PS-*b*-PEP-*b*-PE triblock copolymers with comparable PS content the elastic recovery is better for systems with a lower PE weight fraction. This result is in agreement with the results obtained by Morton et al. for PE-*b*-PI-*b*-PE and PE-*b*-PEB-*b*-PE triblock copolymers.[9, 14, 15] The investigated triblock copolymers with approximately 30 wt-% PE exhibit relatively good elastic recovery, whereas the systems with higher PE contents show unusually high unrecovered deformations, i. e. cold drawing. For high strains they have also detected a significantly higher plastic set for the PE containing triblock copolymers compared to PS-*b*-PB-*b*-PS triblock copolymers, which was attributed to a smaller resistance of the PE crystallites against distortion compared to amorphous PS domains, too.

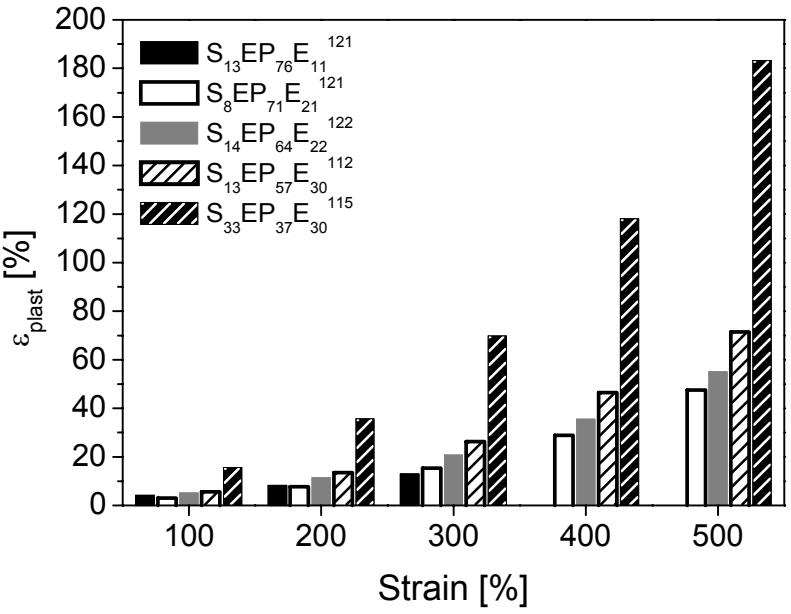

Figure 5. Comparison of plastic deformations (ε_{plast}) of PS-*b*-PEP-*b*-PE triblock copolymers with varying composition.

Acknowledgements. The authors thank A. Böker and Prof. G. Krausch (Physikalische Chemie II) for support concerning the SFM measurements, and A. Göpfert (Makromolekulare Chemie II) for TEM investigations. Financial support by the German Israeli Foundation for Scientific Research and Development (GIF), DSM Research Geleen, the SFB 481 funded by the Deutsche Forschungsgemeinschaft (DFG) and the Bayreuther Institut für Makromolekülforschung (BIMF) is gratefully acknowledged.

References and Notes

1. Morton M. Anionic Polymerization: Principles and Practice. New York: Academic Press, 1983.
2. Holden G, Legge NR. Styrenic Thermoplastic Elastomers. In: Holden G, Legge NR, Quirk RP, Schroeder HE, editors. Thermoplastic Elastomers: A Comprehensive Review; 2nd ed. Munich: Hanser, 1996, p. 47.
3. Abetz V, Stadler R, Leibler L. Order-Disorder and Order-Order Transitions in AB and ABC Block Copolymers. Description by a Simple Model. Polym Bull 1996; 37: 135 - 142.
4. Brinkmann-Rengel S, Abetz V, Stadler R, Thomas EL. Thermoplastic Elastomers Based on ABA- and ABC-Triblock Copolymers. Kautschuk Gummi Kunststoffe 1999; 52: 806 - 813.
5. Kofinas P, Cohen RE. Morphology of Highly Textured Poly(ethylene)/Poly(ethylene-propylene) (E/EP) Semicrystalline Diblock Copolymers. Macromolecules 1994; 27: 3002 - 3008.
6. Rangarajan P, Register RA, Fetters LJ. Morphology of Semicrystalline Block Copolymers of Ethylene-(Ethylene-*alt*-Propylene). Macromolecules 1993; 26: 4640 - 4645.
7. Rangarajan P, Register RA, Adamson DH, Fetters LJ, Bras W, Naylor S, Ryan AJ. Dynamics of Structure Formation in Crystallizable Block Copolymers. Macromolecules 1995; 28: 1422 - 1428.
8. Gehlsen MD, Almdal K, Bates FS. Order-Disorder Transition: Diblock Versus Triblock Copolymers. Macromolecules 1992; 25: 939 - 943.
9. Morton M. Structure-Property Relations in Amorphous and Crystallizable ABA Triblock Copolymers. Rubber Chem Tech 1983; 56: 1096 - 1110.
10. Morton M, Quirk RP. Anionic Triblock Copolymers. In: Holden G, Legge NR, Quirk RP, Schroeder HE, editors. Thermoplastic Elastomers: A Comprehensive Review; 2nd ed. Munich: Hanser, 1996, p. 71.
11. Schmalz H, Böker A, Lange R, Krausch G, Abetz V. Synthesis and Properties of ABA and ABC Triblock Copolymers with Glassy (A), Elastomeric (B), and Crystalline (C) End Blocks. Macromolecules 2002; 34: 8720 - 8729.
12. Brandrup J, Immergut EH. Polymer Handbook, 3rd ed.; New York: Wiley, 1989.
13. Odell JA, Keller A. Structural and Mechanical Properties of an S-B-S Copolymer. Polym Eng Sci 1977; 17: 544.
14. Morton M, Lee N-C, Terrill ER. Elastomeric Polydiene ABA Triblock Copolymers with Crystalline End Blocks. Polym Prepr 1981; 22: 136 - 137.
15. Morton M, Lee N-C, Terrill ER. Elastomeric Polydiene ABA Triblock Copolymers with Crystalline End Blocks. ACS Symp Ser Elastomers and Rubber Elasticity 1982; 193: 101 - 118.

3.4 Anionic Polymerization of Ethylene Oxide in the Presence of the Phosphazene Base *t*-BuP_4 – Kinetic Investigations Using In-Situ FT-NIR Spectroscopy and MALDI-ToF MS

Holger Schmalz, Michael G. Lanzendörfer, Volker Abetz*, Axel H. E. Müller*

Makromolekulare Chemie II, Universität Bayreuth, D-95440 Bayreuth, Germany

Dedicated to Prof. Dr. H. Höcker on the occasion of his 65th birthday

ABSTRACT: Fourier-transform near infrared (FT-NIR) fiber-optic spectroscopy was successfully used to monitor the anionic polymerization of ethylene oxide (EO). Kinetic data are provided for the polymerization of EO with the *sec*-BuLi/*t*-BuP_4 initiating system under different reaction conditions. In addition, the influence of different initiators and reaction conditions on the polymerization of EO is investigated. Online monitoring using NIR spectroscopy reveals an unexpected induction period present in EO homopolymerizations as well as in the synthesis of PEO containing block copolymers with [Li/*t*-BuP_4]$^+$ counterions. The resulting polymers are characterized by SEC. A low molecular weight polystyrene-*block*-poly(ethylene oxide) (PS-*b*-PEO) diblock copolymer was synthesized to gain more insight into the observed induction period by matrix assisted laser desorption ionization time of flight mass spectrometry (MALDI-ToF MS) on samples taken during EO polymerization. The induction period is believed to be a result of different factors involved in the formation of active centers, like break up of lithium alkoxide aggregates by the phosphazene base *t*-BuP_4, and chain length effects. It depends on reaction temperature, concentration of the phosphazene base *t*-BuP_4, as well as the structure of the initiator.

Introduction

The anionic polymerization of ethylene oxide (EO) has been intensively studied using several alkali metal counterions like Na^+, K^+, and Cs^+.[1-6] For lithium counterions, however, only initiation but no propagation has been observed under conventional reaction conditions.[7, 8] This effect was attributed to the strong aggregation of lithium alkoxides resulting from the comparatively high charge density of the lithium cation. However, recent investigations using MALDI-ToF MS show that for sufficiently long reaction times (several weeks) formation of EO oligomers (dimers and trimers) can be observed.[9] In general, the strength of aggregates decreases with decreasing charge density (increasing size) of the counterion, i. e. in the row Li^+, Na^+, K^+, Rb^+, Cs^+. Investigations on the anionic polymerization of ethylene oxide with alkali naphthalide initiators in tetrahydrofuran show an aggregation number of 4 for Na^+ counterions, whereas for K^+ and Cs^+ an aggregation number of 3 was found.[2] In addition, there is a report stating that polymerization of ethylene oxide with Li^+ counterions is possible by adding tetramethylethylenediamine (TMEDA) as complexing agent for Li^+, but there are no further hints concerning this reaction.[10]

Recently Eßwein et al. showed that in the presence of a strong Lewis base like the phosphazene base *t*-BuP_4 polymerization of ethylene oxide with Li^+ counterions can be achieved.[11-13] In this case the phosphazene base *t*-BuP_4 forms a strong complex with Li^+ resulting in a break up of the strong lithium alkoxide aggregates, and thus making the polymerization of ethylene oxide possible. Furthermore, because of the strongly basic character of the phosphazene base *t*-BuP_4 even alcohols can be used as initiators. Anionic polymerization of ethylene oxide in the presence of Li^+ counterions is of particular interest for the synthesis of PEO containing block copolymers by sequential anionic polymerization.[11, 14-18] Since most of the applicable monomers are commonly polymerized using organolithium initiators, the use of *t*-BuP_4 has the advantage that the block copolymer can be prepared without an exchange of the cation. In former procedures[19-21] the living chain end with a Li^+ counterion was first end capped with ethylene oxide to obtain the corresponding OH-functionality followed by purification and reactivation of the terminal OH-group with potassium naphthalide or cumyl potassium for the anionic ring opening polymerization of ethylene oxide. Especially for the anionic polymerization of butadiene it is indispensable to use organolithium initiators in order to achieve a high amount of 1,4-addition. This is important for the synthesis of polyethylene containing block copolymers via hydrogenation of the corresponding 1,4-polybutadiene containing block copolymers. For example, poly(1,4-

butadiene)-*block*-poly(1,4-isoprene)-*block*-poly(ethylene oxide) triblock copolymers can be synthesized in a one-pot procedure using the phosphazene base *t*-BuP$_4$.[16, 18] Subsequent hydrogenation results in the formation of polyethylene-*block*-poly(ethylene-*alt*-propylene)-*block*-poly(ethylene oxide), a triblock copolymer with two semicrystalline end blocks.

Concerning the kinetics of ethylene oxide polymerization in the presence of Li^+ counterions using the phosphazene base *t*-BuP$_4$ only little information is given in the literature.[12, 13] Monitoring the EO pressure during the course of the reaction, Eßwein and coworkers found a linear first-order dependence in monomer consumption using the initiating system *n*-BuLi/*t*-BuP$_4$. The resulting PEO homopolymers exhibited narrow molecular weight distributions. No information is given with respect to the temperature dependence of the reaction and the influence of the Li^+/*t*-BuP$_4$ ratio on polymerization. As ethylene oxide is a hazardous toxic monomer we were interested in a valuable non-destructive tool for the determination of additional kinetic data, also with respect to block copolymer synthesis. Recently we developed an online spectroscopic method to follow EO conversions during polymerization using FT-NIR spectroscopy in combination with a fiber-optic equipment.[22, 23] In contrast to earlier kinetic investigations[12, 13] we found an unexpected induction period for the homopolymerization of ethylene oxide with the initiating system *sec*-BuLi/*t*-BuP$_4$ under our reaction conditions. With increasing temperature (40 – 60 °C) the polymerization rate increased and the induction period decreased. Once the polymerization had started, a linear first-order dependence on monomer concentration was found and the reaction was complete after a few hours. This observation explains why usually ethylene oxide is allowed to react for 2 - 3 days when using the phosphazene base *t*-BuP$_4$.[14, 15, 17] In this contribution we will present a more detailed investigation on the nature of the observed induction period and its dependence on reaction temperature, the ratio of Li^+/*t*-BuP$_4$, type and concentration of initiator, and the sequence of reactant addition. In addition, we will discuss the effect of different initiating systems on the kinetics and molecular weight distribution, including the synthesis of polystyrene-*block*-poly(ethylene oxide) (PS-*b*-PEO) diblock copolymers. MALDI-ToF investigations on samples taken during the synthesis of a low molecular weight PS-*b*-PEO diblock copolymer in combination with kinetic investigations are used to gain more information about the observed induction period.

Experimental

Materials. Tetrahydrofuran (Merck) was purified by successive distillation over CaH_2 and K and kept under dry nitrogen before usage. Ethylene oxide (Linde) was condensed onto CaH_2 and stirred at 0 °C for 3 h before being transferred into glass ampoules. Styrene (Acros) was distilled from CaH_2 under nitrogen, stirred over Bu_2Mg and condensed into storage ampoules. 1,1-Diphenylethylene (Aldrich) was purified by stirring with *sec*-BuLi followed by distillation. The phosphazene base *t*-BuP_4 (Fluka, 1 M in hexane), *sec*-BuLi (Acros, 1.3 M in cyclohexane/hexane: 92/8), *t*-BuOH (Aldrich, anhydrous), *t*-BuOLi (Aldrich, 1 M in THF), pyridine (Aldrich, anhydrous), and 3,5-dinitro benzoylchloride (Fluka) were used as received.

Online Pressure and Temperature Monitoring. Online monitoring of pressure and temperature during the course of reaction was accomplished using a Büchi data system with pressure and temperature controller together with the Büchi log'n see software.

Online FT-NIR Spectroscopy. NIR spectra were recorded with a Nicolet Magna 560 FT-IR optical bench equipped with a white light source and a PbS detector. Online monitoring was accomplished using a laboratory autoclave (Büchi) equipped with an all glass low-temperature immersion transmission probe (Hellma) with an optical path length of 10 mm and connected to the spectrometer via 2 m fiber-optical cables. The probe was fed through a port in the stainless steel top plate of the reactor and immersed into the reaction mixture. More detailed information about the setup can be found elsewhere.[23] Data processing was performed with Nicolet's OMNIC Series software. Each spectrum was accumulated from 32 scans with a resolution of 4 cm^{-1}. The total collection time per spectrum was about 22 s.

The FT-NIR spectrum of ethylene oxide in THF was obtained by solvent subtraction in order to yield a pure component spectrum and to determine conversions since THF has strong absorptions close to the overtone vibrations of ethylene oxide (Figure 1). Solvent subtraction gives a relatively flat baseline at wavenumbers higher than approx. 6200 cm^{-1} and thus provides a prerequisite for a quantitative conversion determination. Specific monomer absorptions for EO were detected at 6070, 4665 and 4547 cm^{-1}. The strongest vibration is located at 4547 cm^{-1} and not separated from other vibrations (4665 cm^{-1}, EO; 4500 cm^{-1}, solvent cutoff). Thus, the first overtone C-H stretching of EO at 6070 cm^{-1} was chosen for

conversion determination. In addition, peak heights were used instead of peak areas for evaluation, since they usually gave less noise.

Conversions, X_p, were calculated using the following equation:

$$X_p = \frac{A_0 - A_t}{A_0 - A_\infty}$$

where A_t is the absorbance at time t, A_0 = initial absorbance, and A_∞ = absorbance at full conversion. The apparent rate constants of propagation were extracted from the linear regime in the corresponding first-order time-conversion plots ($-\ln(1-X_p)$ versus t), by the slope of the linear fit at values of $1 \leq -\ln(1-X_p) \leq 2$. The given induction times were calculated from the linear fit, i. e. they reflect the point of intersection of the linear fit line with the time axis.

Matrix Assisted Laser Desorption Ionization Time of Flight Mass Spectrometry (MALDI-ToF MS). MALDI-ToF MS was performed on a Bruker Reflex III with a UV laser operating at 337 nm and an accelerating voltage of 20 kV. 2,5-Dihydroxybenzoic acid (DHB) was used as matrix for the PEO homopolymers together with lithium trifluoromethanesulfonate as cationizing agent. 1,8,9-trihydroxyanthracene (dithranol) and silver triflate as cationizing agent were used in the case of the low molecular weight PS-*b*-PEO diblock copolymer. Samples were dissolved in THF (10 mg/mL) and mixed with matrix (20 mg/mL in THF) and salt (10 mg/mL in THF) at a mixing ratio of 10 : 2 – 1 : 1 (v/v, matrix : analyte : salt). 1 μL of this mixture was spotted onto the target and allowed to dry. 200 – 500 laser shots were accumulated for a spectrum. All samples were measured after complete drying without removing the phosphazene base to keep the composition unchanged without loss of low molecular weight fractions.

Size Exclusion Chromatography (SEC). SEC experiments were performed on a Waters instrument calibrated with narrowly distributed poly(ethylene oxide) standards for the PEO homopolymers and polystyrene standards for the PS-*b*-PEO diblock copolymers at 30 °C. Four PSS-SDV gel columns (5 μm) with a porosity range from 10^2 to 10^5 Å were used together with a differential refractometer and a UV detector at 254 nm. Measurements were performed in THF with a flow rate of 1 ml/min using toluene as internal standard. The total molecular weights of the PS-*b*-PEO diblock copolymers were determined by means of ^{1}H-

NMR spectroscopy using the molecular weight of the corresponding PS precursor, obtained by SEC calibrated with PS standards.

Polymerizations. Polymerizations were carried out in a thermostated laboratory autoclave (Büchi) under dry nitrogen atmosphere.

Ethylene oxide (EO) polymerizations with *sec*-BuLi as initiator were performed in THF solution using the phosphazene base *t*-BuP_4.[11, 12] *Sec*-BuLi was added to THF at –78 °C followed by addition of EO. After stirring for 30 min the reaction mixture was heated to 40 °C –60 °C (depending on the experiment) and the reaction was started by addition of *t*-BuP_4 (time $t = 0$) after the reaction temperature was reached ($[sec\text{-BuLi}]_0 = [t\text{-BuP}_4] = 2.34 \cdot 10^{-3}$ M; $[EO]_0 = 0.53$ M). Experiments with varying *sec*-BuLi/*t*-BuP_4 ratio were performed at 50 °C. For the reaction with diphenylhexyl lithium (DPHLi) as initiator, first DPHLi was prepared in THF at -78 °C by the reaction of *sec*-BuLi with DPE ([*sec*-BuLi] /[DPE] = 1 /1.1) followed by addition of EO. After stirring at –78 °C for 30 min the reaction mixture was heated to 50 °C and polymerization of EO was started by addition of *t*-BuP_4 ([DPHLi] /[*t*-BuP_4] = 1 /1). Polymerizations with *t*-BuOH and *t*-BuOLi as initiator were performed in a similar way. In this case the initiator was added to THF at 10 °C followed by addition of ethylene oxide. After rising the temperature to 50 °C the polymerization of ethylene oxide was initiated by addition of the phosphazene base *t*-BuP_4 ($[initiator]_0/[t\text{-BuP}_4] = 1/1$). For some experiments simultaneous gravimetric investigations were performed using septum-sealed flasks containing MeOH/AcOH (1/5 v/v) as termination agent. After complete conversion the reaction was terminated with a mixture of MeOH/AcOH (1/5 v/v). For all EO homopolymerizations identical concentrations of initiator and monomer were used, unless otherwise specified. Kinetic investigations were performed using the same charge of *t*-BuP_4 in order to exclude any effects arising from different purity.

For EO polymerization initiated with a PEO macroinitiator a monohydroxy functionalized PEO homopolymer with an number-average molecular weight of 8670 g/mol was used ($[EO_{197}] = 2.7 \cdot 10^{-3}$ M, [EO] = 0.496 M, $[Li^+]$ /[*t*-BuP_4] = 1 /1, T = 50 °C). The PEO homopolymer was synthesized in THF at 50 °C using DPHLi as initiator along with the phosphazene base *t*-BuP_4. Purification of the PEO homopolymer was accomplished by ultrafiltration in order to remove excess phosphazene base, followed by freeze-drying with benzene for 3 times. The terminal OH groups of the PEO homopolymer were deprotonated by titration with DPHLi (prepared from DPE and *sec*-BuLi) in THF at 10 °C, until the red color of DPHLi remained for at least 45 min. After addition of EO the reaction mixture was heated

to 50 °C and allowed to react for 2 d in order to verify wether a PEO macroinitiator is able to start EO polymerization without the presence of the phosphazene base *t*-BuP_4. As no conversion was observed, the polymerization of EO was started by addition of *t*-BuP_4.

The synthesis of PS-*b*-PEO diblock copolymers was accomplished by sequential anionic polymerization of styrene and ethylene oxide in THF. First styrene was polymerized at -78 °C for 1 h using *sec*-BuLi as initiator. After addition of ethylene oxide followed by stirring at -78 °C for 1 h the temperature was raised to 40 or 60 °C. Subsequently the polymerization of ethylene oxide was started by addition of the phosphazene base *t*-BuP_4 ([*sec*-BuLi]$_0$/[*t*-BuP_4] = 1/1; $S_{118}EO_{2038}$: [*sec*-BuLi] = 6.05 10^{-4} M, [EO] = 1.17 M, [S] = 8.70 10^{-2} M, T = 40 °C; $S_{19}EO_{38}$: [*sec*-BuLi] = 7.46 10^{-3} M, [EO] = 0.394 M, [S] = 0.179 M, T = 60 °C). In our nomenclature A_xB_y, the indices denote the number-average degrees of polymerization of the blocks. Simultaneous gravimetric investigations were performed in the same way as for the EO homopolymerizations.

Selective labeling of terminal OH groups in PEO homopolymer with a UV chromophore was accomplished by esterification with 3,5-dinitrobenzoylchloride. The reaction was carried out in anhydrous THF using pyridine as catalyst at 40 °C for 1 d, followed by deactivation with methanol. A 10-fold excess of 3,5-dinitro benzoylchloride with respect to the number of expected OH groups was used. After filtration of the crude reaction mixture, the polymer was recovered by precipitation in hexane.

Results and Discussion

In order to check the applicability of FT-NIR spectroscopy to monitor EO polymerization, we recorded an NIR spectrum of pure EO in THF using background subtraction (Figure 1).

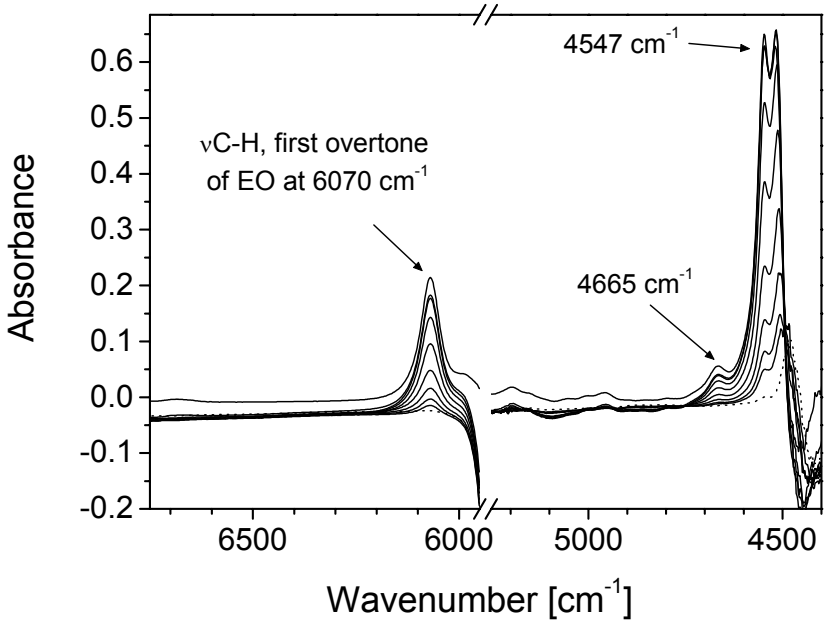

Figure 1. Pure component FT-NIR spectra of EO during polymerization in THF at 60 °C obtained by solvent subtraction at t = 0, 200, 400, 600, 620, 640, 680, 700 and 800 min.

EO shows specific monomer signals at 6070, 4665, and 4547 cm^{-1} that can be attributed to combinations of fundamental vibrations.[24] All three bands might be used for data evaluation as they show a simultaneous drop in intensity with increasing reaction time (Figure 1 and 2). However, the signal at 4547 cm^{-1} is too close to the solvent cutoff and not separated from the absorption at 4665 cm^{-1} (Figure 1). Therefore the band at 6070 cm^{-1} was used for the determination of conversion. The region between 6000 and 5400 cm^{-1} is inaccessible due to solvent interference and is not expected to show monomer signals.[24, 25]

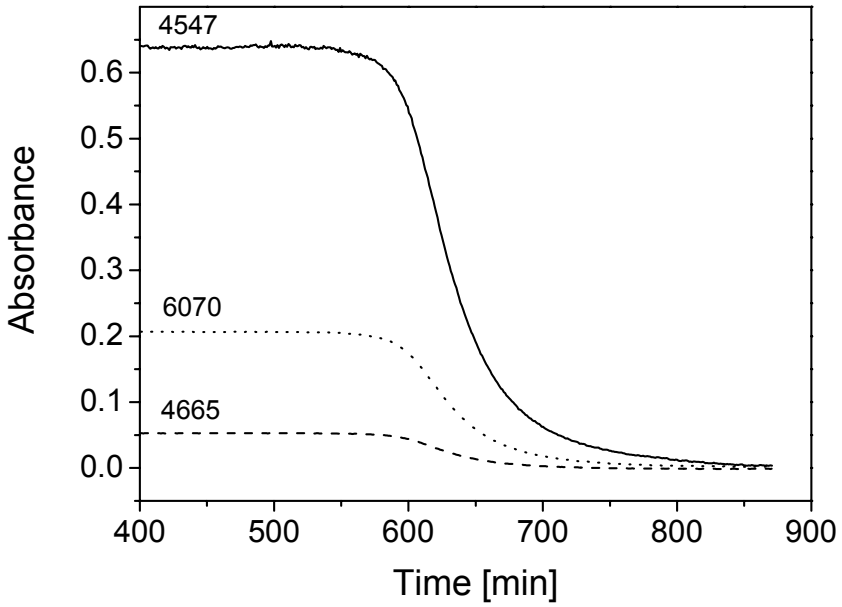

Figure 2. Evaluation of peak heights for specific EO signals at 4547, 4665, and 6070 cm^{-1} during EO homopolymerization at 60 °C using *sec*-BuLi/*t*-BuP_4 as initiating system.

To make sure that the concentration range used for EO polymerizations is consistent within Beer's law, we recorded the NIR spectra of a series of known concentrations of EO in THF and constructed a calibration curve (Figure 3). It is clearly demonstrated that the absorption shows a linear dependence on EO concentration in THF.

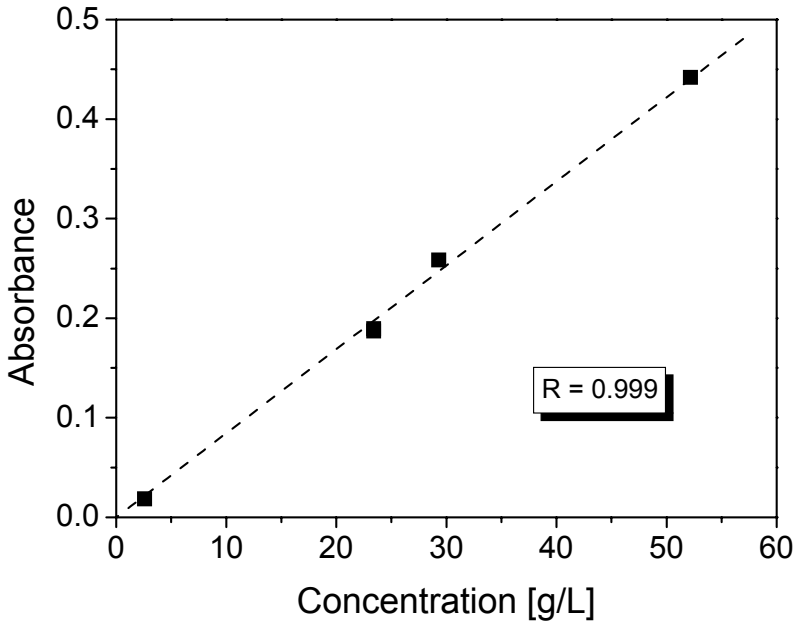

Figure 3. Linear dependence of specific EO absorption at 6070 cm^{-1} on EO concentration.

Kinetic runs were conducted in a way that first the initiator was added to THF followed by addition of EO. After reaching the final reaction temperature the polymerization of EO was initiated by addition of the phosphazene base *t*-BuP_4 (time t = 0). Figure 4 shows the first-order time-conversion plots that were constructed using the NIR data and compared to gravimetric measurements for EO homopolymerizations with the *sec*-BuLi/*t*-BuP_4 initiating system at different temperatures. Both NIR and gravimetric analysis exhibit excellent agreement for this monomer. Unexpectedly, we observed a long induction period of the polymerization under our reaction conditions, whereas no induction period was reported in previous kinetic investigations.[12, 13] When increasing the temperature from 40 °C to 60 °C the polymerization rate increased, i. e. the slope in the first-order time-conversion plot increased, and the induction period decreased (Figure 4).

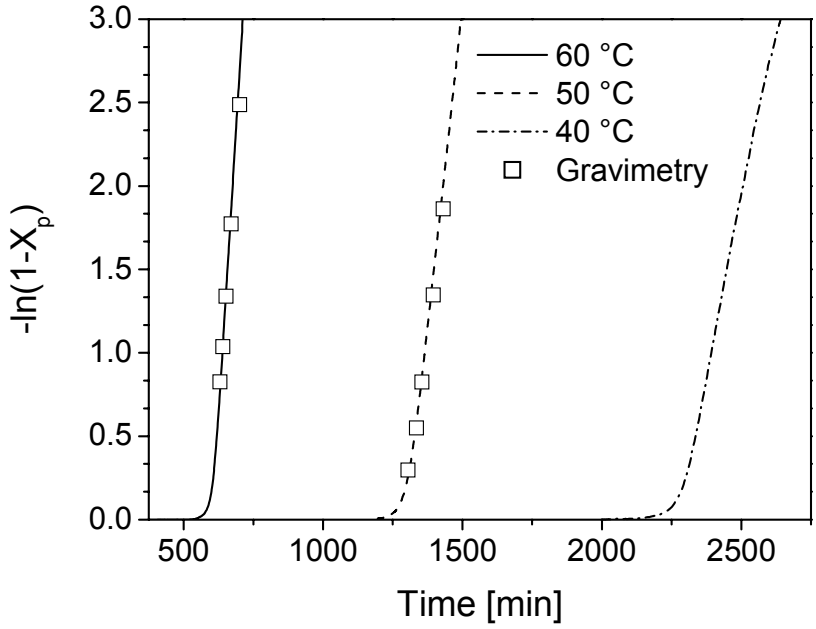

Figure 4. First-order time-conversion plots in EO homopolymerizations at different reaction temperatures indicating long induction periods. For comparison, gravimetric data (□) are given for the reactions at 50 and 60 °C ([*sec*-BuLi]$_0$ = 2.34 · 10^{-3} M, [*sec*-BuLi]/[*t*-BuP_4] = 1/1, [EO] = 0.53 M).

Once the polymerization had started, a linear first-order dependence in monomer concentration was found for polymerizations at 50 and 60 °C. The first-order plot at 40 °C is slightly curved for conversions higher than approx. 80%. The apparent rate constants of propagation were calculated from the slopes in the linear range of the first-order plots (Table 1).

The absolute rate constants were calculated according to the equation

$$k_p = \frac{k_{app}}{f[I_0]}$$

where f is the initiator efficiency defined as $f = M_{n\ th}/M_{n\ exp}$ (see Table 4).

Table 1. Kinetic Data for EO Homopolymerizations at Different Temperatures

	40 °C	50 °C	60 °C
k_{app} [10^{-3}/min]	8.86	14.5	27.4
k_p[L/mol·s]	0.173	0.291	0.562
t_{ind} [min]	2300	1230	600

From the apparent rate constants of propagation an Arrhenius plot was constructed (results not shown) and the activation energy of propagation (E_a) in the presence of the [Li/*t*-BuP_4]$^+$ counterion was determined as E_a = 51.0 ± 4.4 kJ/mol with a frequency exponent of logA = 7.74 ± 0.70 L/mol·s. Compared to other counterions this initiating system shows a slightly lower activation energy of propagation together with a lower frequency exponent (Table 2).

Table 2. Comparison of Activation Energies of Propagation (E_a) and Logarithm of the Frequency Exponent (logA) for EO Homopolymerizations with Different Counterions in THF

counterion	E_a [kJ/mol]	logA [L/mol·s]
K^{+} [5]	79.2	12
Cs^{+} [5]	49.9	8.1
[Li/*t*-BuP_4]$^+$	51.0 ± 4.4	7.74 ± 0.70

The observed induction period might arise from the formation of strong lithium alkoxide aggregates, which were formed by the reaction of *sec*-BuLi with EO prior to the addition of *t*-BuP_4. Consequently, the phosphazene base *t*-BuP_4 has to break up the aggregates by complexation of the Li^+ counterion in order to enable the polymerization of EO. This might result in an association-dissociation pre-equilibrium which is responsible for the detected induction period (Equation 1).

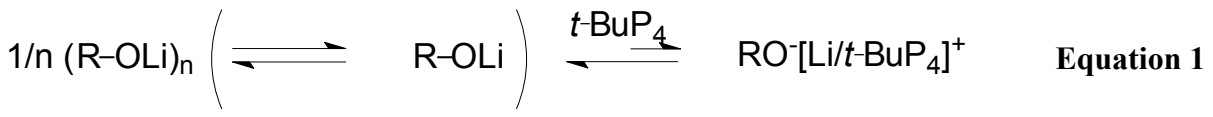

Equation 1

If such an equilibrium is active the induction period should also depend on the amount of added phosphazene base *t*-BuP$_4$. Figure 5 shows first-order time-conversion plots for EO homopolymerizations with different ratios of *sec*-BuLi/*t*-BuP$_4$ at 50 °C.

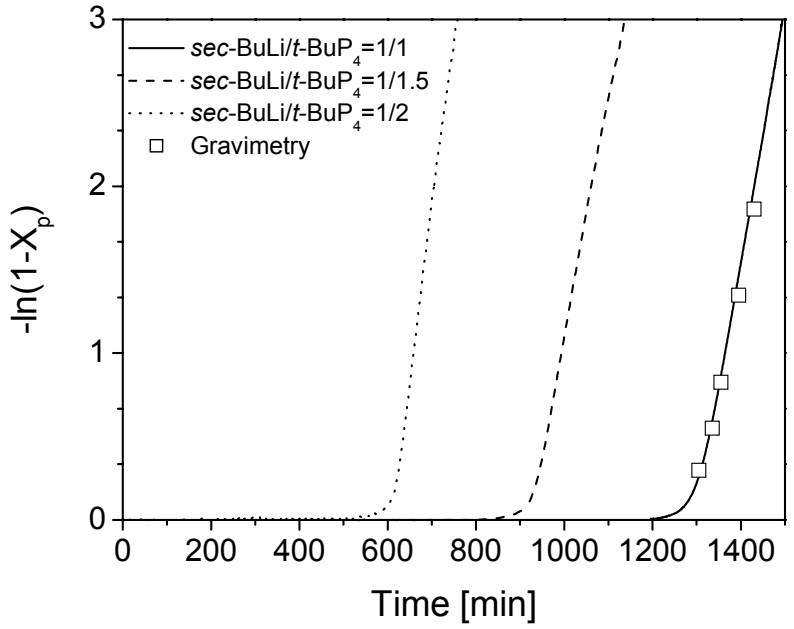

Figure 5. Dependence of induction period and apparent rate of EO polymerization on the *sec*-BuLi/*t*-BuP$_4$ ratio at 50 °C in THF ([*sec*-BuLi]$_0$ = 2.34 · 10^{-3} M, [EO] = 0.53 M). For comparison, gravimetric data (□) are given for the reaction with [*sec*-BuLi]/[*t*-BuP$_4$] = 1/1.

The observed induction periods decrease with increasing amount of added phosphazene base, e. g. a ratio of [*sec*-BuLi]/[*t*-BuP$_4$] = 1/2 reduces the induction period from 1300 min to about 600 min (Table 3). The observed reduction is linear in the investigated concentration range. However, this is not the case for the propagation rates, which exhibit only a small increase with increasing concentration of *t*-BuP$_4$. A linear extrapolation of the observed induction times (Table 3) versus the ratio of [*sec*-BuLi]/[*t*-BuP$_4$] indicates that at a ratio of [*sec*-BuLi]/[*t*-BuP$_4$] = 1/3 no induction time should be observed. However, using a large excess of *t*-BuP$_4$ with respect to the initiator ([DPHLi]/[*t*-BuP$_4$] = 1/4) also results in the observation of a short induction time (ca. 320 min, results not shown). Thus, even for a large excess of *t*-BuP$_4$ an induction time is still present. These results underline the assumption that association-dissociation processes are involved in EO polymerization with organolithium initiators in the presence of *t*-BuP$_4$.

Table 3. Kinetic Data for EO Homopolymerizations Using Different Ratios of *sec*-BuLi/*t*-BuP$_4$

	sec-BuLi/*t*-BuP$_4$		
	1/1	1/1.5	1/2
k_{app} [10^{-3}/min]	14.5	14.9	21.8
k_p[L/mol·s]	0.291	0.326	0.347
t_{ind} [min]	1230	930	610

To ensure that the induction period determined by online FT-NIR fiber-optic spectroscopy does not arise from the used instrumentation we have also monitored the pressure and temperature profile during the reaction. Figure 6 shows a comparison of online FT-NIR absorbance, pressure and temperature monitoring for an EO homopolymerization at 50 °C using the *sec*-BuLi/*t*-BuP$_4$ initiating system ([*sec*-BuLi]/[*t*-BuP$_4$] = 1/2). The pressure profile and specific EO absorption show a simultaneous drop around 600 min combined with a slight increase in temperature. This excellent agreement between different methods confirms that the observed induction period arises from the reaction itself and is not influenced by the used instrumentation.

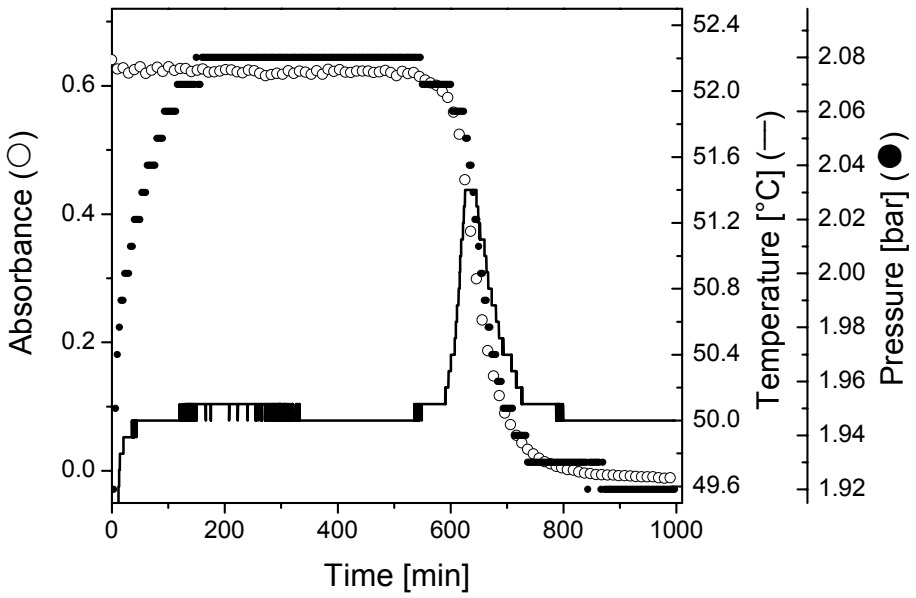

Figure 6. Temperature and pressure profile compared with NIR monomer signal (at 6070 cm^{-1}) during EO homopolymerization ([*sec*-BuLi]$_0$ = 2.34 · 10^{-3} M, [*sec*-BuLi]/[*t*-BuP$_4$] = 1/2, [EO] = 0.53 M; T = 50 °C).

The molecular characteristics of the synthesized PEO homopolymers using *sec*-BuLi as initiator are summarized in Table 4. For all samples the detected molecular weights by means of SEC are significantly higher compared to the expected values. For example, the PEO homopolymer obtained with *sec*-BuLi as initiator at 50 °C exhibits a number average molecular weight of M_n = 29,000 g/mol, which is ca. three times higher than the targeted M_n of 10,000 g/mol. This implies that only one third of the initiator molecules was active, i. e. termination or side reactions occur. Similar results were obtained for all EO homopolymerizations using *sec*-BuLi as initiator (Table 4).

Table 4. Molecular Characteristics of Synthesized PEO Homopolymers

Initiator I	[I]:[*t*-BuP$_4$]	T [°C]	M_n(calc.) [g/mol]	M_n(SEC)[a] [g/mol]	M_w/M_n[a]	f[b]
sec-BuLi	1/1	40	10,000	27,500	1.09	0.37
sec-BuLi	1/1	50	10,270	29,000	1.10	0.36
sec-BuLi	1/1	60	10,300	29,700	1.10	0.35
sec-BuLi	1/1.5	50	9,640	29,600	1.12	0.33
sec-BuLi	1/2	50	10,250	22,900	1.09	0.45
t-BuOLi	1/1	50	9,670	6,760	1.08	1.43
DPHLi	1/1	50	10,230	10,900	1.05	0.94
t-BuOH	1/1	50	9,890	6,970	1.19	1.42

[a] Obtained by SEC in THF using PEO standards.
[b] f = initiator efficiency.

Figure 7 shows SEC traces for samples taken during EO polymerization at 50 °C using the *sec*-BuLi/*t*-BuP$_4$ initiating system ([*sec*-BuLi]/[*t*-BuP$_4$] = 1/1). All samples show a bimodal distribution which is present from the beginning of the reaction and thus indicates the presence of two differently active growing species, which might be produced by side reactions during reaction of *sec*-BuLi with EO at -78 °C and during the subsequent induction period and polymerization of EO. With increasing conversion the samples get more narrowly distributed but still show a bimodality.

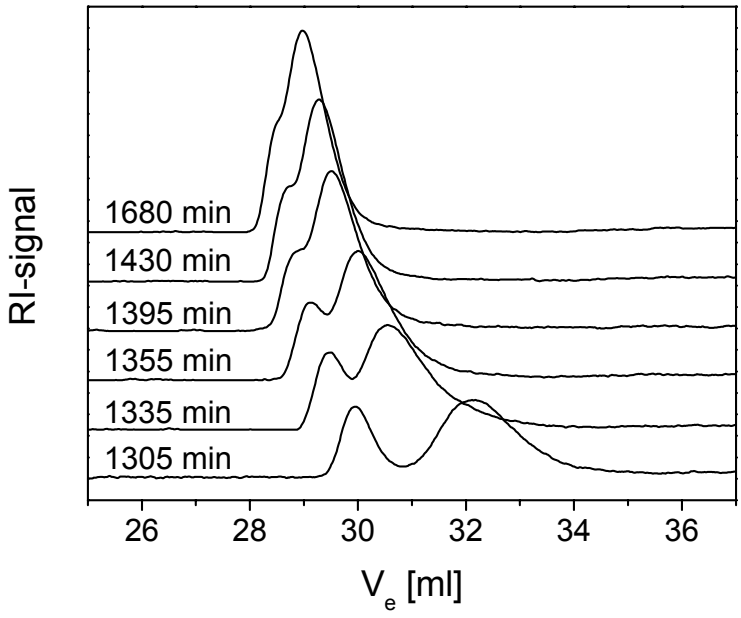

Figure 7. SEC traces for samples taken during EO homopolymerization at 50 °C ([*sec*-BuLi]/[*t*-BuP_4] = 1/1).

A further indication for side reactions is given in Figure 8 showing a comparison of RI and UV signals for the sample taken at 1305 min. The lower molecular weight fraction of the RI signal (higher retention time) exhibits a weak UV signal at 254 nm, which is unexpected since the initiator and the EO monomer units are not considered to show any UV absorption.

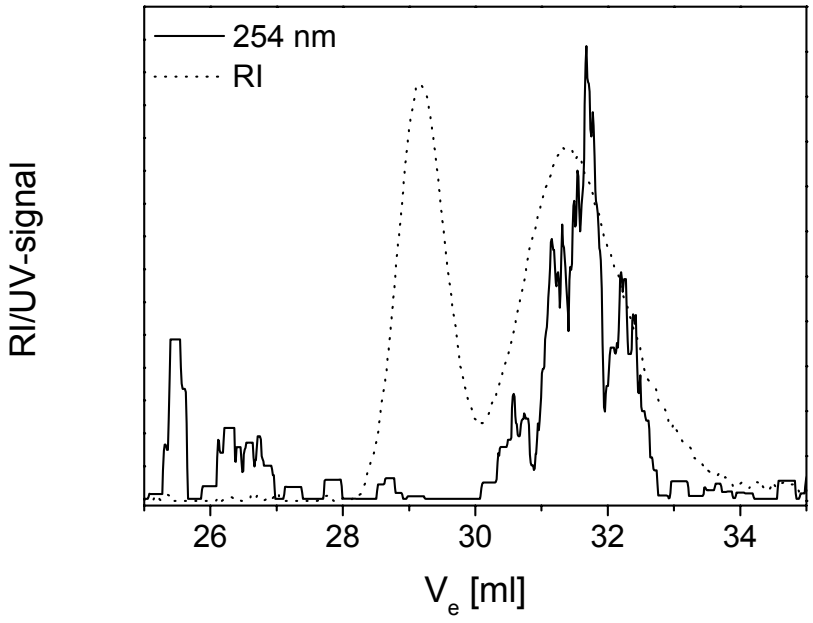

Figure 8. Comparison of RI- and UV-signal for the sample taken at 1305 min during EO homopolymerization at 50 °C ([*sec*-BuLi]/[*t*-BuP_4] = 1/1).

It is well known from literature that organolithium compounds can cause side reactions with cyclic ethers, like THF, especially at elevated temperatures. For THF the side reaction has been attributed to a deprotonation of THF by the organolithium compound followed by decomposition of the resulting THF anion under formation of ethylene and the corresponding lithium enolate.[26-29] From this background a similar side reaction during EO polymerization using *sec*-BuLi as initiator might be derived as depicted in Scheme 1.

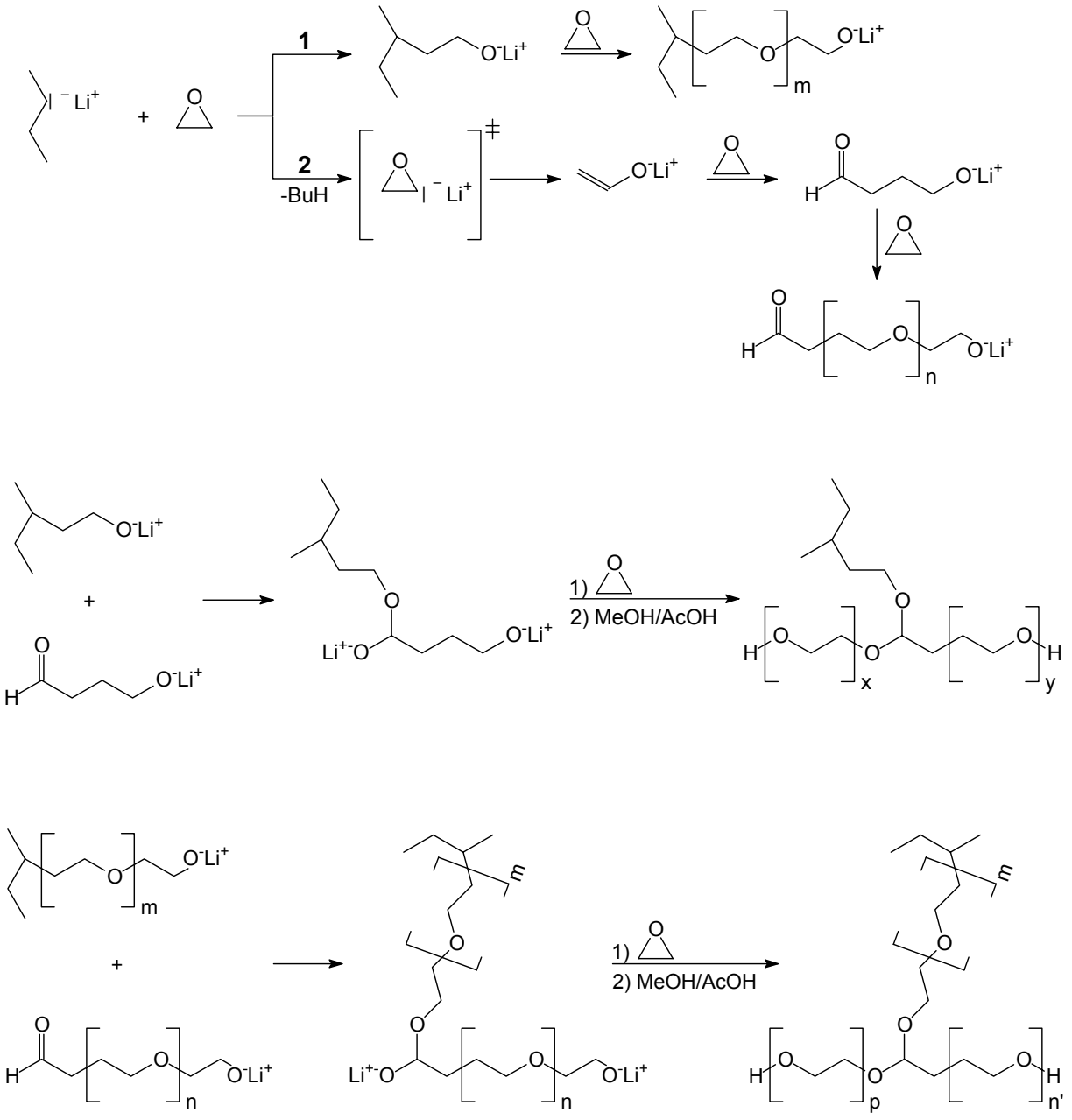

Scheme 1. Illustration of possible side-reactions during EO polymerization initiated with *sec*-BuLi.

At -78 °C solutions of *sec*-BuLi in THF are stable for a sufficient time, which excludes side reactions arising from the reaction of *sec*-BuLi with THF. As EO is a very reactive monomer, two possible reactions might occur between EO and *sec*-BuLi (Scheme 1). Pathway 1 is the expected ring opening of EO by a nucleophilic attack of *sec*-BuLi, resulting in the formation of lithium(3-methyl pentanolate), which in turn is able to initiate the homopolymerization of EO. The alternative pathway 2 includes first deprotonation of EO to yield the corresponding metastable EO anion, which rearranges under formation of lithium enolate. Subsequent addition of one EO unit results in the formation of the lithium salt of 4-hydroxy butanal, which is again able to initiate homopolymerization of EO. This aldehyde function might be responsible for the observation of a UV absorption in the lower molecular weight fraction within the sample taken at 1305 min (Figure 8). The formylmethyl group can be further attacked by lithium(3-methyl pentanolate) as depicted in Scheme 1, under formation of a bifunctional initiator for EO homopolymerization. Consequently, the chain exhibits two growing centers which in turn results in the formation of PEO chains with a higher molecular weight with regard to the expected value for 100% initiator efficiency. It has to be mentioned, that this side reaction, resulting in the formation of a bifunctional initiator, does not necessarily occur within the observed induction time as depicted in Scheme 1. It is also possible that first the initiators, formed in pathways 1 and 2, initiate the polymerization of EO, resulting in the formation of growing PEO chains with a terminal formylmethyl group (pathway 2) or a terminal *sec*-butyl function (pathway 1). The nucleophilic attack of one growing PEO chain (with a terminal *sec*-butyl function) to the aldehyde function of a second PEO chain again results in the formation of a PEO chain exhibiting two growing centers (Scheme 1).

Alternatively, coupling can also take place between two living PEO chains having terminal formylmethyl functions. As one terminal aldehyde function remains after coupling subsequent coupling reactions are possible, resulting in growing PEO chains with more than two active centers. These PEO chains, exhibiting two or even more active growing sites, might be responsible for the higher molecular weight fraction observed in Figure 8. In addition, loop formation by backbiting to a formylmethyl function might occur. The formation of an aldehyde function has also been observed for EO homopolymerizations initiated by potassium solutions in THF containing 18-crown-6.[30] However, in this case the mechanism is completely different. Electron transfer from potassium to EO results in the formation of an EO radical-anion, which shows disproportionation under formation of lithium

ethanolate and the corresponding lithium enolate. Subsequent polymerization of EO results in the formation of PEO chains containing ethoxy or formylmethyl groups.

In order to verify if the proposed side reaction occurs, the sample taken at 1335 min was functionalized with 3,5-dinitro benzoylchloride, a strong UV chromophore. Those PEO chains exhibiting two or more active growing centers during polymerization (higher molecular weight fraction in Figure 8) are expected to have at least two terminal OH groups, which can be selectively labeled with the UV chromophore. As a result, the UV signal of this fraction, which counts the labeled OH end groups, should be significantly higher than the corresponding normalized RI signal. For normalization the RI signal at a given elution volume was divided by the corresponding molecular weight, which was extracted from the PEO calibration of the SEC instrument. Thus the molecular weight dependence of the RI signal is ruled out and the resulting distribution reflects a frequency distribution of PEO chains eluting at a given elution volume. Figure 9 shows the comparison of UV- and normalized RI-signal for the sample taken at 1335 min during EO homopolymerization at 50 °C using *sec*-BuLi as initiator ([*sec*-BuLi]/[*t*-BuP_4] = 1/1).

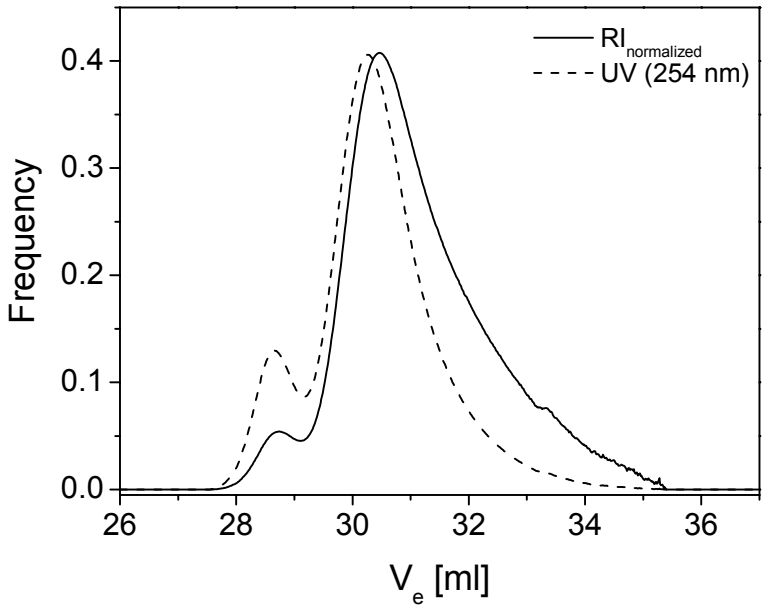

Figure 9. Comparison of normalized RI signal and the corresponding UV signal for the 3,5-dinitro benzoyl labeled sample taken at 1335 min during EO homopolymerization at 50 °C ([*sec*-BuLi]/[*t*-BuP_4] = 1/1).

It can be clearly seen, that the UV signal of the higher molecular weight fraction is more than twice as high as the corresponding normalized RI signal. This in turn underlines the presence of the proposed side reactions in Scheme 1, which is thought to be responsible for the observed discrepancy in calculated and observed molecular weights for EO homopolymerizations using *sec*-BuLi as initiator (Table 4).

The MALDI-ToF spectrum of the sample taken at 1305 min shows more than one distribution (Figure 10). The main series (A) can be assigned to the initiator derived species. However, branched structures (D) unfortunately have identical masses (see Table 5). The series (B) can be attributed to PEO chains with terminal formylmethyl groups. Thus, MALDI-ToF investigations underline the proposed side reactions (Scheme 1). Another minor series (C) is visible at a mass difference of –18 to series (B) and might be formed by loss of H_2O from (B) under MALDI conditions.

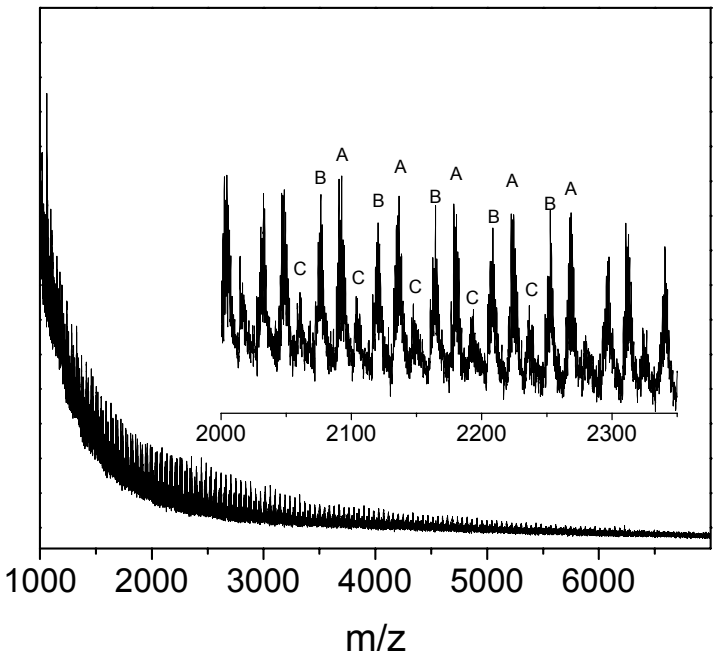

Figure 10. MALDI-ToF MS of PEO homopolymer initiated with *sec*-BuLi. (Sample taken at 1305 min during EO homopolymerization at 50 °C ([*sec*-BuLi]/[*t*-BuP_4] = 1/1).

Table 5. Theoretical and Experimental Masses for Proposed Structures in Scheme 1

	structure	theoretical mass [g/mol]	experimental mass [g/mol]
A	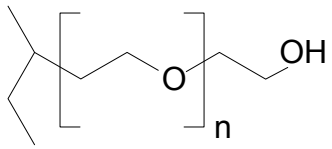	$C_6H_{13}O$ + n C_2H_4O + H + Cation n = 48: $C_{102}H_{206}O_{49}Li^7$ M = 2222.38	M = 2222.61
B	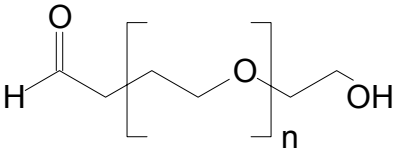	$C_4H_7O_2$ + n C_2H_4O + H + Cation n = 48: $C_{100}H_{200}O_{50}Li^7$ M = 2208.33	M = 2208.60
D	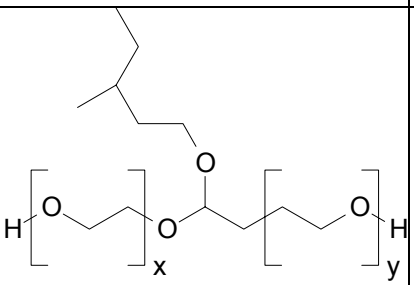	$C_8H_{16}O_2$ + (x + y) C_2H_4O + H_2 + Cation x + y = 47: $C_{102}H_{206}O_{49}Li^7$ M = 2222.38	M = 2222.61

Investigations on EO homopolymerizations using the initiating system *sec*-BuLi/*t*-BuP_4 have always revealed an induction period. However, a similar induction period was not reported for *n*-BuLi/*t*-BuP_4 and 1-octanol/*t*-BuP_4 initiating systems.[12, 13] To examine the characteristics of the observed induction period in more detail, the influence of different initiators on the kinetics of EO polymerization in the presence of the phosphazene base *t*-BuP_4 was investigated. Figure 11 shows the first-order time-conversion plots in EO homopolymerization at 50 °C using different initiating systems. All experiments with organolithium initiators (*sec*-BuLi, *t*-BuOLi and DPHLi) exhibit an induction period, which depends on the structure of the initiator. Under the same reaction conditions the use of *t*-BuOLi as initiator results in a significantly increased induction period with respect to *sec*-BuLi, whereas the polymerization using DPHLi reveals a shorter induction period (Figure 11, Table 6). In addition, an induction period in EO polymerization was also found in the synthesis of PS-*b*-PEO diblock copolymers as depicted in Table 6. In conclusion, the dependence of the induction period on the type of organolithium initiator might result from differences in the association behavior of the used and formed lithiumalkoxides in our investigation.

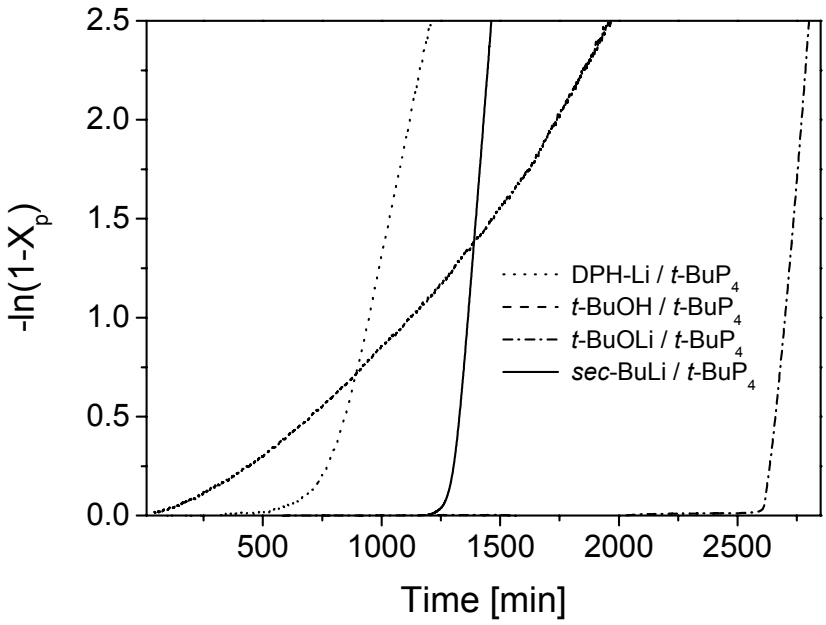

Figure 11. First-order time-conversion plots in EO homopolymerizations at 50 °C using different initiating systems ([initiator] = $2.34 \cdot 10^{-3}$ M, [initiator]/[*t*-BuP_4] = 1/1, [EO] = 0.53 M).

Table 6. Kinetic Data for EO Polymerizations Using Different Initiators

	T [°C]	k_{app} [10^{-3}/min]	k_p [L/mol·s]	t_{ind} [min]
sec-BuLi	50	14.5	0.291	1230
t-BuOLi	50	14.1	0.070	2530
DPHLi	50	5.78	0.043	780
$S_{118}Li$	40	0.725	0.020	740
$S_{19}Li$	60	5.92	0.013	270
t-BuOH	50	1.24	0.006	0
$EO_{197}Li$	50	1.90	0.012	1155

In contrast to the results obtained with organolithium initiators, the polymerization with the *t*-BuOH/*t*-BuP_4 initiating system does not show any induction period (Figure 11, Table 6) which is in agreement with the previous investigation on 1-octanol/*t*-BuP_4[12, 13]. However, the first-order time-conversion plot (Figure 11) is not linear but shows an increase in slope with increasing conversion. This might result from a slow initiation reaction, as the initiator *t*-BuOH, which was added first, has first to be deprotonated by the phosphazene base *t*-BuP_4 in order to initiate EO polymerization. This should also result in a broadening of the molecular weight distribution.

Figure 12 illustrates the SEC traces for PEO homopolymers obtained by using different initiators. The tailing of the first maximum towards low molecular weights for the PEO homopolymer synthesized with *t*-BuOH/*t*-BuP_4 as initiating system is likely due to slow initiation, whereas the small second maximum is attributed to traces of water from the very hygroscopic phosphazene base or the used *t*-BuOH. Under the same conditions the *t*-BuOLi/*t*-BuP_4 system yielded a narrow distribution. However, the obtained molecular weight is significantly smaller compared to the targeted molecular weight, which might be attributed to uncertainties in concentration of the used commercial *t*-BuOLi solution (Table 4). End capping of *sec*-BuLi with DPE is known to reduce the nucleophilicity of the carbanion, and is a widely used method in anionic polymerization. The polymerization with the DPHLi/*t*-BuP_4 initiating system results in the formation of PEO with targeted M_n and narrow molecular weight distribution (Figure 12, Table 4). In conclusion, end capping of *sec*-BuLi with DPE is a versatile method to avoid the side reactions occurring in EO homopolymerizations with the *sec*-BuLi/*t*-BuP_4 initiating system.

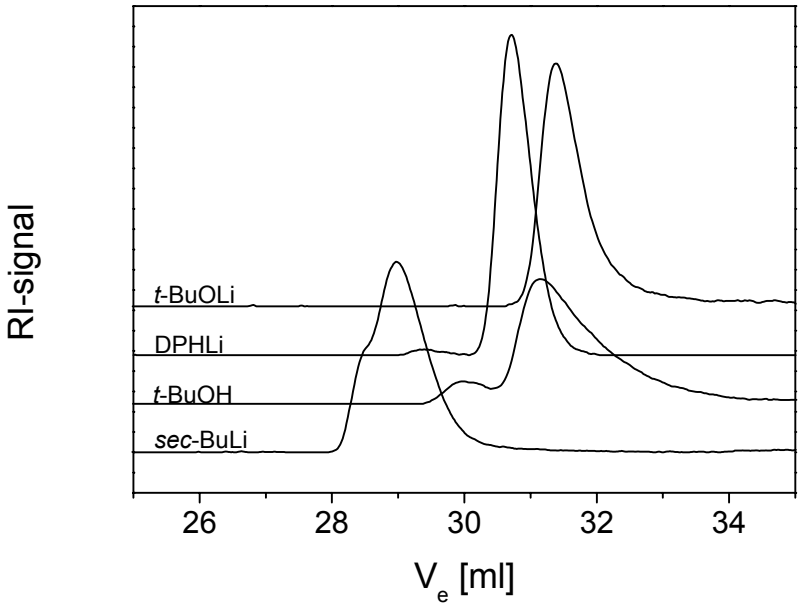

Figure 12. SEC traces for EO homopolymerizations using different initiating systems at 50 °C.

A closer look to the corresponding SEC trace (Figure 12) reveals a small signal at significantly higher molecular weights. This higher molecular weight fraction might be attributed to PEO chains initiated by traces of water, since the phosphazene base is strongly hygroscopic. A further evidence for this assumption is the fact that this higher molecular

weight fraction shows no UV absorption (results not shown), as would be expected if the chains were intiated by DPHLi. Initiation by an excess of *sec*-BuLi remaining from the reaction of *sec*-BuLi and DPE can also be ruled out, since in EO homopolymerizations, using a two-fold excess of DPE with respect to *sec*-BuLi, again a higher molecular weight signal was observed (results not shown).

In addition, reports on the synthesis of PEO-containing block copolymers using the phosphazene base *t*-BuP_4[11, 14, 15, 17] and our own experiments on PB-*b*-PI-*b*-PEO[16, 18] and PS-*b*-PEO block copolymers did not show any traces of termination or bimodality in the SEC analysis. Figure 13 shows the SEC traces for two PS-*b*-PEO diblock copolymers including the polystyrene precursors. The molecular characteristics of the diblock copolymers obtained by SEC are given in Table 7. Obviously there is no termination of the living polystyryllithium occurring in the block copolymer synthesis and the distributions are monomodal exhibiting a low polydispersity. In conclusion, the discrepancy in theoretical and experimental M_n and the bimodal distribution observed for EO homopolymerizations with the *sec*-BuLi/*t*-BuP_4 initiating system arises from side reactions between *sec*-BuLi and EO even at –78 °C (Scheme 1), and is not attributed to chain termination during the course of EO polymerization and/or the presence of differently active growing species.

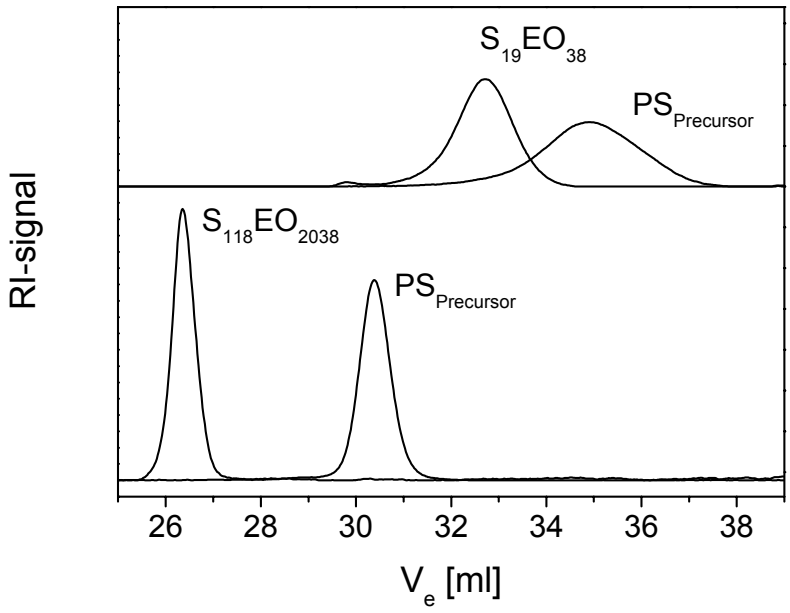

Figure 13. SEC traces for the synthesized PS-*b*-PEO diblock copolymers.

Kinetic analysis shows that even in the synthesis of PS-*b*-PEO diblock copolymers an induction period is existent as verified by real time FT-NIR spectroscopy (Table 6). For one of these block copolymers conditions were chosen that lead to the formation of a low molecular weight PS-*b*-PEO diblock copolymer ($S_{19}EO_{38}$, Table 7). During the blocking reaction samples were taken for further investigations by MALDI-ToF mass spectrometry.

Table 7. Molecular Characteristics of the Synthesized PS-*b*-PEO Diblock Copolymers

PS-*b*-PEO	T [°C]	M_n(PS)[a] [g/mol]	M_n(PEO)[b] [g/mol]	M_n [g/mol]	M_n(MALDI) [g/mol]	M_w/M_n[a]
$S_{118}EO_{2038}$	40	12,300	89,800	102,100	-	1.01
$S_{19}EO_{38}$	60	1,940	1,690	3,630	3,330	1.09

[a] Determined by SEC in THF using PS standards.
[b] Calculated from ^{1}H-NMR spectra using the M_n of the PS precursor obtained by SEC.

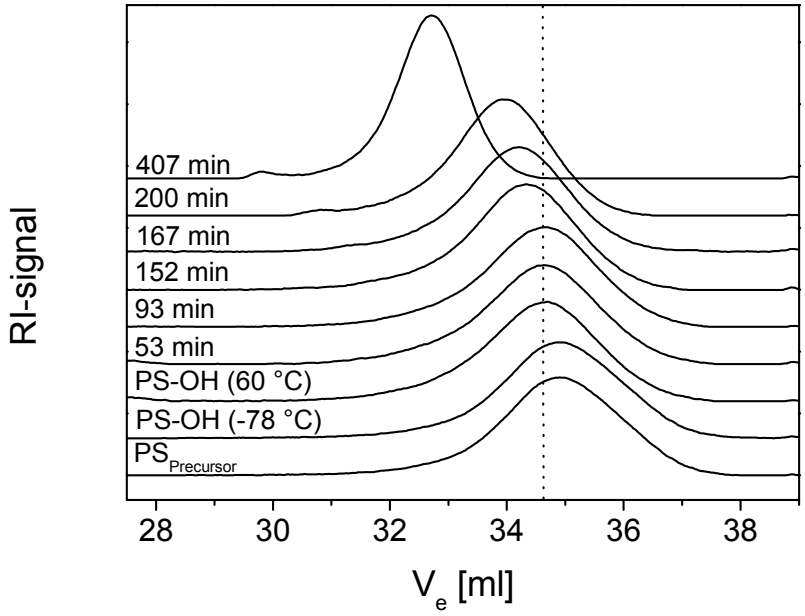

Figure 14. SEC traces showing the course of EO polymerization for the synthesis of $S_{19}EO_{38}$.

Figure 14 shows the SEC traces of the samples taken during polymerization of the PEO block in the synthesis of $S_{19}EO_{38}$, including the PS precursor. It can be clearly seen, that for reaction times < 152 min no significant shift to higher molecular weights occurs which corresponds well to the observed induction period of 270 min (Table 6). Upon increasing the reaction time, the distribution exhibits a continuous shift to higher molecular weights (lower values of V_e). Comparison of the SEC traces of the final PS-*b*-PEO diblock copolymer (407 min) with the corresponding PS precursor shows that the distribution shifts completely

to higher molecular weights, i. e. no termination of living PS precursor occurs during the course of EO polymerization.

MALDI-ToF has proven its ability to detect different end groups or functionalities at polymers. Figure 15 shows the polystyrene precursor and the resulting $S_{19}EO_{38}$ diblock copolymer. The conditions were chosen in a way that the copolymer sequences can still be resolved by MALDI-ToF spectrometry.

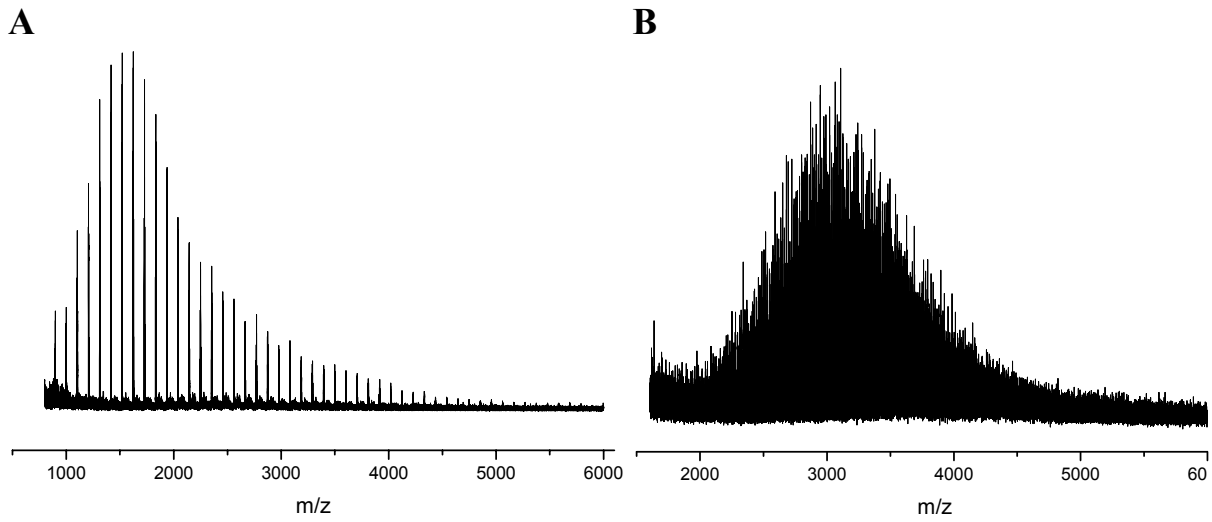

Figure 15. MALDI-ToF mass spectra of the PS-precursor (A) and the resulting $S_{19}EO_{38}$ diblock copolymer (B) prepared by sequential anionic synthesis.

Figure 16 shows that after initial functionalization of the PS macroinitiator with one EO unit no growth could be detected for reaction times < 93 min. The MALDI mass spectrum of the EO endcapped polystyrene (PS-OH, Figure 16) exhibits that end capping is quantitative, since signals corresponding to the PS precursor are absent. For reaction times ≥ 93 min EO polymerization takes place and polystyrene chains with two EO units are detectable. Here, the higher sensitivity of MALDI-ToF compared to SEC is clearly reflected, as in the corresponding SEC investigations a first shift of the distribution to higher molecular weights could only be detected for the sample taken at 152 min (Figure 14). The spectra even allow to resolve a number of copolymer compositions up to chains bearing 7 EO units while the initial EO_1 end capped chains have almost disappeared. Thus, the induction period in EO polymerization during the synthesis of PS-*b*-PEO diblock copolymers which was detected by FT-NIR and SEC investigations, is verified by MALDI-ToF MS for a diblock copolymer.

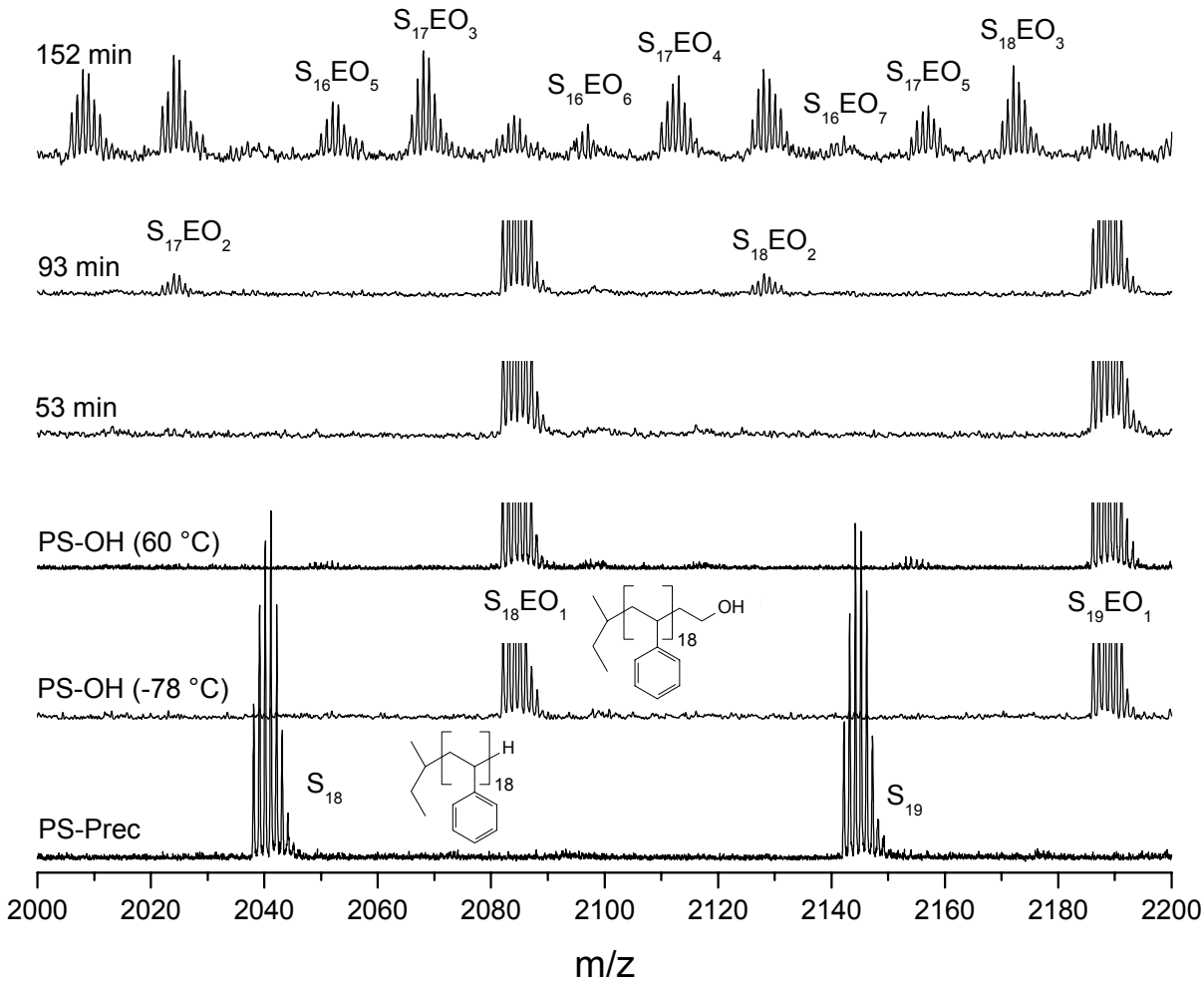

Figure 16. MALDI-ToF mass spectra of samples taken during EO polymerization of $S_{19}EO_{38}$. Spectra are measured in reflectron mode using AgTFA as cationizing agent and dithranol as matrix.

In order to gain more insight into the observed induction period we performed EO homopolymerizations with varying initiator concentrations at 50 °C, using DPHLi as initiator (Table 8). The concentration of EO was kept constant, and a ratio of $[DPHLi]_0/[t\text{-}BuP_4] = 1/1$ was used for all reactions. The apparent rate constant of propagation (k_{app}) decreases with decreasing initiator concentration, which can also be seen from the decreasing slope in the corresponding first-order time-conversion plots (Figure 17).

Table 8. Kinetic Data and Molecular Characteristics for EO Homopolymerizations with DPHLi as Initiator at 50 °C[a]

[I] [mol/l]	k_{app} [10^{-3}/min]	k_p [L/mol·s]	t_{ind} [min]	M_n(calc.) [g/mol]	M_n(SEC)[b] [g/mol]	f[c]
$2.34 \cdot 10^{-3}$	4.12	0.031	680	10,000	10,300	0.97
$1.21 \cdot 10^{-3}$	3.15	0.057	740	20,000	26,200	0.76
$5.63 \cdot 10^{-4}$	1.62	0.054	630	40,000	45,000	0.89

[a] New batch of *t*-BuP_4, [DPHLi]/[*t*-BuP_4] = 1/1.
[b] Determined by SEC in THF using PEO standards.
[c] f = initiator efficiency.

However, the observed induction periods are nearly independent on initiator concentration. A closer look onto the first-order time-conversion plot for the lowest initiator concentration (Figure 17, M_n = 40,000 g/mol) reveals that even in the beginning of the reaction a small conversion takes place. This course of conversion is similar to that expected for a slow initiation. This fact might be attributed to the used small initiator concentration, which in turn should result in an easier break-up of lithium alkoxide aggregates during the induction period.

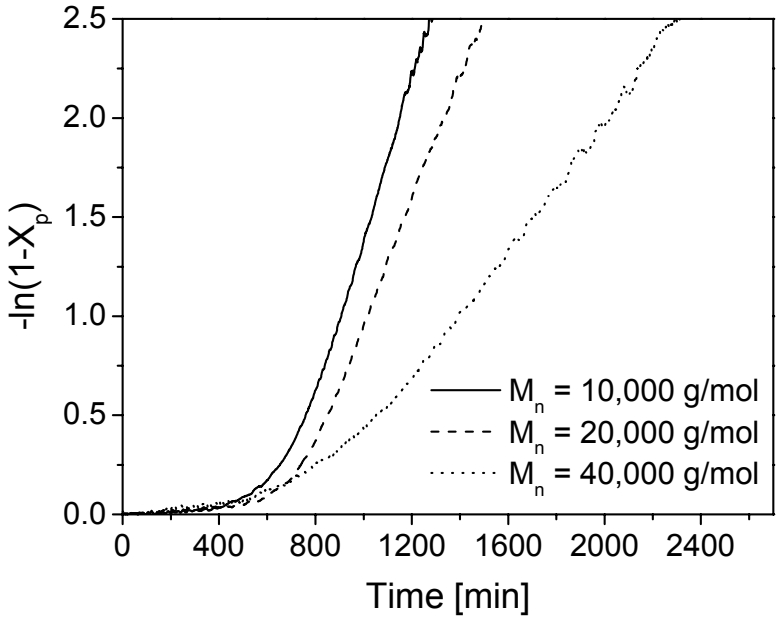

Figure 17. First-order time-conversion plots in EO homopolymerizations at 50 °C with varying initiator concentration, using DPHLi as initiator ([DPHLi]/[*t*-BuP_4] = 1/1).

To extract a reaction order with respect to the initiator concentration, we have used the kinetic expression given in Equation 2, assuming that the initiator corresponds to a DPHLi/*t*-BuP_4 complex.

$$-\frac{d[EO]}{dt} = k_p[I]^a[EO]^b = k_{app}[EO]^b$$ **Equation 2**

I = DPHLi/*t*-BuP_4 complex

Consequently, the reaction order with respect to the initiator concentration was extracted from a plot of ln k_{app} versus ln$[I]_0$ with a slope of a = 0.66 (correlation coefficient, r = 0.98). The obtained fractional reaction order with respect to the initiator concentration gives a further indication that associates are involved in EO homopolymerization with organolithium initiators and the phosphazene base *t*-BuP_4. In the polymerization of methyl methacrylate with Li^+ counterion in THF reaction orders changing from 0.6 to 0.9 were attributed to the coexistence of aggregated and non-aggregated ion pairs.[31]

The discussed dependence of the induction period on reaction temperature, on the amount of added phosphazene base *t*-BuP_4, and on the type of the used initiator points to a dissociation-association pre-equilibrium, which might be responsible for the observed induction periods. In order to induce polymerization of EO, the strong lithium alkoxides have first to be broken up by the phosphazene base *t*-BuP_4. In order to check this assumption a control experiment was performed as depicted in Scheme 2.

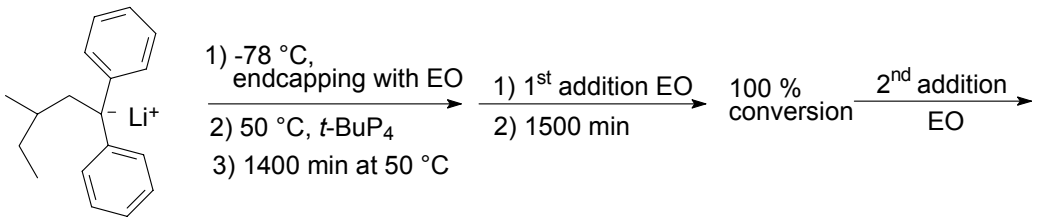

Scheme 2

First, the initiator DPHLi was end-capped with EO to form the corresponding alkoxide at –78 °C. Excess EO was removed by evacuating the reaction mixture, followed by addition of dry nitrogen. This procedure was performed several times in order to ensure complete removal of excess EO. Subsequently, the reaction mixture was heated to 50 °C, followed by stirring for 1400 min after addition of the phosphazene base *t*-BuP_4, in order to induce complex formation between the initiator and the phosphazene base *t*-BuP_4. If the induction period arises from complex formation, the induction period should vanish if EO is added after 1400 min, a time which is significantly longer than the observed induction period (Table 6). However, the corresponding first-order time-conversion plot (Figure 18A) shows that an induction period (505 min) is still present. In conclusion, complex formation between lithium

alkoxides and *t*-BuP$_4$ is not the only factor contributing to the observed induction period. After complete EO conversion (verified by FT-NIR), a 2nd batch of EO was added to the reaction mixture (Scheme 2). Here, the living PEO homopolymer, formed after addition of the 1st batch of EO, acts as macroinitiator for the polymerization of the 2nd batch of EO. The apparent short induction period (Figure 18 B) that was observed for the second EO addition is the result of adding and mixing times which can therefore be neglected. The lack of a significant induction period might be attributed to a chain length effect, as PEO is known to be a good complexation agent for alkali metal cations.[32-37] Furthermore, it has been found that complexation of the RO^-M^+ ion pair by the growing PEO chain results in an autoacceleration in the early stage of EO polymerization (degree of polymerization DP < 4 - 6).[38, 39] Consequently, complexation of the Li^+ counterion by the PEO macroinitiator might result in an additional weakening of lithium alkoxide aggregates.

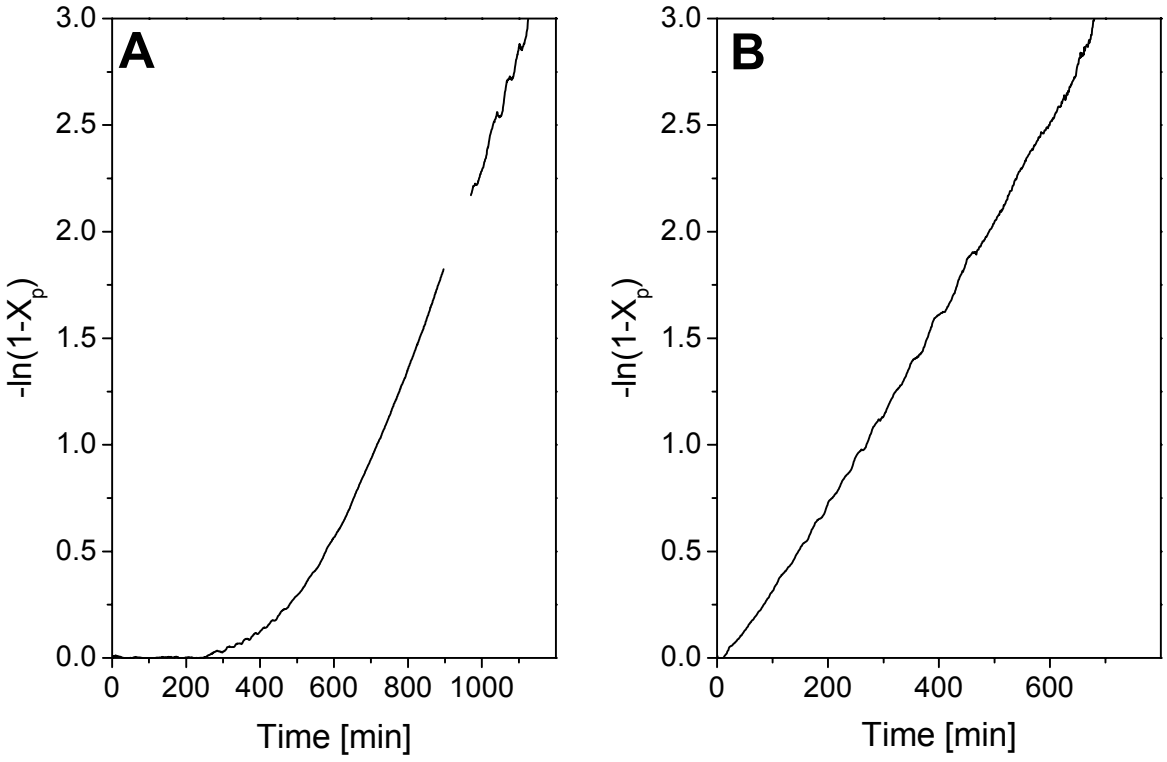

Figure 18. First-order time-conversion plots in EO homopolymerization at 50 °C with DPHLi as initiator for the 1st addition (A) and the 2nd addition (B) of EO ([DPHLi]/[*t*-BuP$_4$] = 1/1, [DPHLi] = 2.34 · 10^{-3} M, [EO1] = 0.524 M, [EO2] = 0.385 M, f = 0.77).

The apparent rate constants of propagation are almost identical for the 1st and 2nd batch of EO (k_{app} = 4.56·10^{-3} min^{-1}, k_p = 0.042 L/mol·s). This is reasonable, as the concentration of initiator is identical for both polymerizations.

For further investigations on the above discussed chain length effect a PEO homopolymer (DP_n = 197; M_n = 8,670 g/mol) prepared with DPHLi as initiator in the presence of the phosphazene base *t*-BuP_4 was used as macroinitiator for EO homopolymerization. Reactivation of the terminal OH groups of the PEO homopolymer for anionic polymerization of EO was accomplished by titration with DPHLi. After complete titration the reaction mixture was heated to 50 °C followed by addition of EO and *t*-BuP_4. Figure 19 shows the corresponding first-order time-conversion plot.

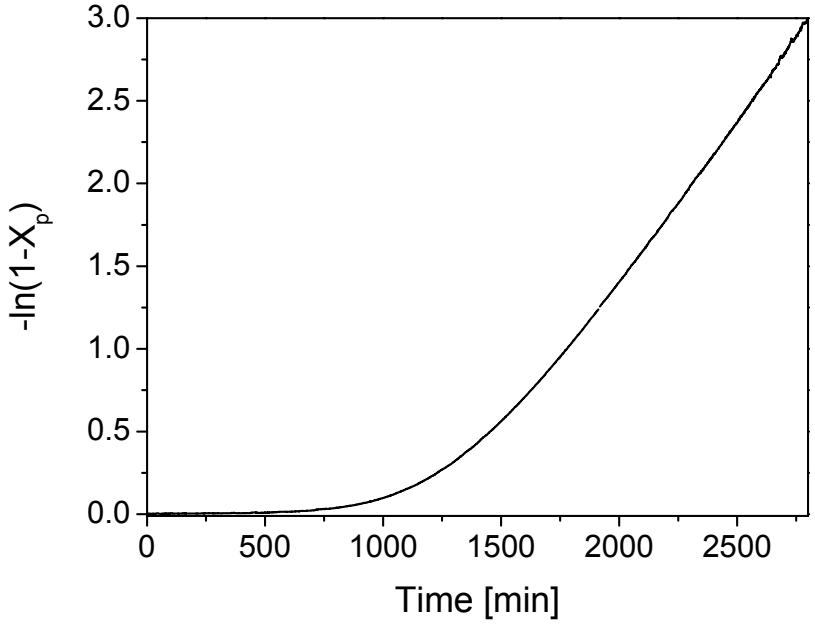

Figure 19. First-order time-conversion plot in EO homopolymerization using a PEO-Li macroinitiator (M_n = 8,670 g/mol) at 50 °C ($[PEOLi]_0 = 2.71 \cdot 10^{-3}$ M, [PEOLi]/[*t*-BuP_4] = 1/1, [EO] = 0.50 M).

Again, a long induction period (1155 min) is observed which is significantly longer compared to EO homopolymerizations with DPHLi as initiator under comparable conditions. In addition, the rate constant of propagation is also lower compared to the experiments with DPHLi as initiator (Table 6). An incomplete initiation, which might be responsible for the observed differences in induction period and rate constant of propagation, can be ruled out, as the molecular weight distribution of the PEO macroinitiator is shifted almost completely to higher molecular weights upon EO polymerization (Figure 20). In conclusion, even the use of a PEO macroinitiator results in the observation of an induction period. Thus, a chain length effect is not alone responsible for the observed induction period.

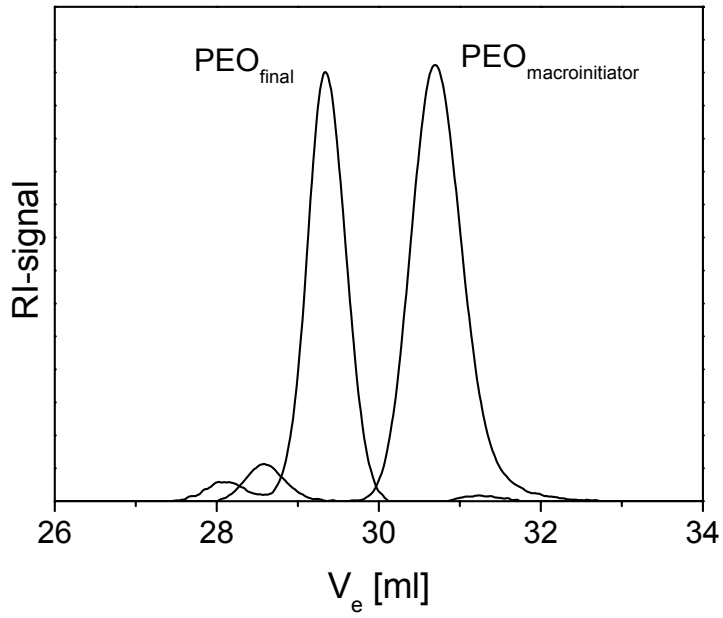

Figure 20. SEC traces of the final PEO homopolymer and the PEO macroinitiator used in EO homopolymerization at 50 °C ([PEOLi]/[*t*-BuP_4] = 1/1).

Our experiments on EO homopolymerization using organolithium initiators along with the phosphazene base *t*-BuP_4 revealed the presence of an induction period. This induction period shows a complex dependence on reaction temperature, amount of added phosphazene base, the type of initiator, and sequence of addition of reactants. From these observations, it might be concluded that a dissociation-association pre-equilibrium is responsible for the detected induction period. Lithium alkoxides form strong aggregates which first have to be destroyed by the phosphazene base *t*-BuP_4 in order to induce EO polymerization. However, if the initiator is allowed to react with the phosphazene base prior to EO addition for a long time, again an induction period is present. In addition, polymerizations using a PEO macroinitiator exclude the possible influence of a chain length effect, as again an induction period is detected. In conclusion, the observed induction period cannot be explained by a simple dissociation-association pre-equilibrium or a chain length effect. Obviously there are additional factors influencing the formation of the active site during the induction period, which are not accessible by the performed kinetic investigations.

Ethylene oxide can act as a complexing agent of alkaline cations, as has been shown by Hogen-Esch et al..[40] This resulted in the formulation of a "push-pull mechanism" for the anionic polymerization of EO.[3, 41] This mechanism implies electrophilic activation of EO by dipole-dipole interactions between the RO^-M^+ ion pair and EO. The observed increase in the rate of propagation with increasing size of the counterion can be explained by an increasing

interionic distance in RO^-M^+, i. e. increasing dipole moment and thus higher electrophilic activation of EO. The inactivity of lithium alkoxides in EO polymerization might be attributed on one hand to the formation of strong aggregates (inactive in EO polymerization), and on the other hand to the small interionic distance in RO^-Li^+, i. e. weak electrophilic activation of EO. As a consequence the break-up of aggregates by the phosphazene base *t*-BuP_4 during the observed induction period is only the first step in enabling EO polymerization. Subsequently, the complexation of Li^+ by *t*-BuP_4 also increases the interionic distance in RO^-Li^+, which should result in a higher dipole moment and thus a more efficient electrophilic activation of EO, i. e. enabling polymerization of EO. However, *t*-BuP_4 is a very bulky base which might result in a decrease in reactivity due to shielding of the active center. A similar effect was observed for EO polymerization with K^+ and Cs^+ counterions in the presence of cryptands.[3, 41] Cryptated ion pairs exhibit a lower reactivity compared to the corresponding non complexed ion pairs due to shielding of the active center by the cryptand. In conclusion, this shielding effect might decrease the activation of the RO^-Li^+ ion pair by complexation with *t*-BuP_4. This in turn might result in a very low rate constant of EO propagation, which contributes to the observed induction period. Despite the low rate constant of propagation, PEO oligomers will be formed during the induction period if the reaction time is sufficiently long. This assumption is underlined by the observation of PEO oligomers (dimers and trimers) in the functionalization reaction of polystyryllithium with EO after several weeks, even in the absence of *t*-BuP_4.[9] Consequently, the growing PEO chain is able to contribute to the Li^+ complexation, as PEO is known to be a good complexing agent for alkaline cations.[32-37] Furthermore, it has been observed that complexation of the RO^-M^+ ion pair by the growing PEO chain results in an autoacceleration in the very beginning of the EO polymerization (degree of polymerization DP < 4 - 6).[38, 39] In conclusion, the increasing contribution of PEO oligomers (DP = 4 – 6), formed during the end of the induction period, to the complexation of Li^+ might result in a weakening of the shielding effect arising from the bulky phosphazene base *t*-BuP_4 due to competition between *t*-BuP_4 and PEO for free coordination sites. Thus, once PEO oligomers with a DP of 4 – 6 are formed during the induction period, EO polymerization can proceed. However, EO homopolymerization using a PEO macroinitiator also results in the observation of an induction period. This suggests, that EO itself is involved in a more complex way into the formation of the active growing site during the induction period, which can be attributed to its good complexing properties for alkaline cations.

Conclusions

Investigations on EO polymerization using organolithium initiators in the presence of the *t*-BuP_4 base revealed an induction period which can be significantly reduced by adjusting the reaction conditions. Possible side reactions of strong lithium alkyls with the monomer can be minimized by simply decreasing the strenghts of the anion using DPE as capping agent. This has some relevance for block copolymer synthesis when for example a strong macro-anion acts as initiator. The variations of reaction conditions neither eliminate the induction period nor did we fully understand its reason. The experimental data give some explanations but the exact role of the *t*-BuP_4 base is still speculative.

Acknowledgment

The authors thank DSM Research and Deutsche Forschungsgemeinschaft (SFB 481) for financial support.

References and Notes

[1] P. Sigwalt, S. Boileau, *J. Polym. Sci., Polym. Symp.* **1978**, *62*, 51.

[2] K. S. Kazanskii, A. A. Solovyanov, S. G. Entelis, *Eur. Polym. J.* **1971**, *7*, 1421.

[3] S. Boileau, in *Comprehensive Polymer Science, Vol. 3* (Ed.: G. Allen), Pergamon, Oxford, 1989, pp. 467.

[4] H. Reuter, S. Hörig, J. Ulbricht, *Eur. Polym. J.* **1989**, *25*, 1113.

[5] A. A. Solovyanov, K. S. Kazanskii, *Polym. Sci. USSR (Engl. Transl.)* **1972**, *A14*, 1186.

[6] S. Penczek, A. Duda, *Makromol. Chem., Macomol. Symp.* **1993**, *67*, 15.

[7] H. L. Hsieh, Quirk, R. P., *"Anionic Polymerization - Principles and Practical Applications"*, Marcel Dekker Inc., New York, 1996.

[8] C. Wesdemiotis, M. A. Arnould, Y. Lee, R. P. Quirk, *Polym. Prep. (Am. Chem. Soc., Div. Polym. Chem.)* **2000**, *41*, 629.

[9] R. P. Quirk, R. T. Mathers, C. Wesdemiotis, M. A. Arnould, *Macromolecules* **2002**, *35*, 2912.

[10] K. Gonsalves, M. D. Marvin, D. Rausch, *J. Polym. Sci., Part A: Polym. Chem.* **1986**, *24*, 1419.

[11] B. Eßwein, M. Möller, *Angew. Chem.* **1996**, *108*, 703.

[12] B. Eßwein, A. Molenberg, M. Möller, *Macromol. Symp.* **1996**, *107*, 331.

[13] B. Eßwein, PhD thesis, University of Ulm (Ulm, Germany), **1998**.

[14] S. Förster, E. Krämer, *Macromolecules* **1999**, *32*, 2783.

[15] G. Floudas, B. Vazaiou, F. Schipper, R. Ulrich, U. Wiesner, H. Iatrou, N. Hadjichristidis, *Macromolecules* **2001**, *34*, 2947.

[16] H. Schmalz, A. Böker, R. Lange, V. Abetz, *Polym. Mater. Sci. Eng.* **2001**, *85*, 478.

[17] L. Zhu, S. Z. D. Cheng, B. H. Calhoun, Q. Ge, R. P. Quirk, E. L. Thomas, B. S. Hsiao, F. Yeh, B. Lotz, *Polymer* **2001**, *42*, 5829.

[18] H. Schmalz, A. Knoll, A. J. Müller, V. Abetz, *Macromolecules* **2002**, *35*, 10004.

[19] J. Allgaier, A. Poppe, L. Willner, D. Richter, *Macromolecules* **1997**, *30*, 1582.

[20] M. A. Hillmyer, F. S. Bates, *Macromolecules* **1996**, *29*, 6994.

[21] D. H. Adamson, *Polym. Prepr. (Am. Chem. Soc., Div. Polym. Chem.)* **2000**, *41*, 1231.

[22] M. Lanzendörfer, H. Schmalz, V. Abetz, A. H. E. Müller, *Polym. Prepr. (Am. Chem. Soc., Div. Polym. Chem.)* **2001**, *42*, 329.

[23] M. G. Lanzendörfer, H. Schmalz, V. Abetz, A. H. E. Müller, in *In-Situ Spectroscopy of Monomer and Polymer Synthesis* (Eds.: J. E. Puskas, R. Storey), Kluwer Academic/Plenum, New York/Dordrecht, 2002, in press.

[24] J. W. Linnett, *J. Chem. Phys.* **1938**, *6*, 692.

[25] L. G. Bonner, *J. Chem. Phys.* **1937**, *5*, 704.

[26] A. Rembaum, S.-P. Siao, N. Indictor, *J. Polym. Sci.* **1962**, *56*, 17.

[27] R. B. Bates, L. M. Kroposki, D. E. Potter, *J. Org. Chem.* **1972**, *37*, 560.

[28] P. Tomboulian, D. Amick, S. Beare, K. Dumke, D. Hart, R. Hites, A. Metzger, R. Nowak, *J. Org. Chem.* **1973**, *38*, 322.

[29] G. Bianchi, C. De Micheli, R. Gandolfi, *Angew. Chem., Int. Ed. Engl.* **1979**, *18*, 721.

[30] A. Stolarzewicz, Z. Grobelny, G. N. Arkhipovich, K. S. Kazanskii, *Makromol. Chem., Rapid Commun.* **1989**, *10*, 131.

[31] D. Kunkel, A. H. E. Müller, L. Lochmann, M. Janata, *Makromol. Chem., Macromol. Symp.* **1992**, *60*, 315.

[32] G. N. Arkhipovich, S. A. Dubrovskii, K. S. Kazanskii, A. N. Shupik, *Vysokomol. Soedin., Ser A* **1981**, *23*, 1653.

[33] G. N. Arkhipovich, S. A. Dubrovskii, K. S. Kazanskii, N. V. Ptitsina, A. N. Shupik, *Eur. Polym. J.* **1982**, *18*, 569.

[34] G. N. Arkhipovich, Y. A. Ugolkova, K. S. Kazanskii, *Polym. Bull.* **1984**, *12*, 181.

[35] H.-J. Buschmann, *Makromol. Chem.* **1986**, *187*, 423.

[36] D. K. Dimov, I. M. Panayotov, V. N. Lazarov, C. B. Tsvetanov, *J. Polym. Sci., Part A: Polym. Chem.* **1982**, *20*, 1389.

[37] N. V. Ptitsina, A. N. Shupik, K. S. Kazanskii, G. N. Arkhipovich, *Dokl. Akad. Nauk SSSR* **1979**, *247*, 1412.

[38] K. S. Kazanskii, *Pure Appl. Chem.* **1981**, *53*, 1645.

[39] A. A. Solovyanov, K. S. Kazanskii, *Eur. Polym. J.* **1971**, *7*, 142.

[40] C. J. Chang, R. F. Kiesel, T. E. Hogen-Esch, *J. Am. Chem. Soc.* **1973**, *95*, 8446.

[41] S. Boileau, A. Deffieux, D. Lassalle, F. Menezes, B. Vidal, *Tetrahedr. Lett.* **1978**, *20*, 1767.

4 Summary

In this work the synthesis and characterization of two novel types of thermoplastic elastomers (TPEs) is described. The first type comprises multiblock copoly(ether ester)s with semicrystalline hard segments and triblock copolymer soft segments. The second class of investigated TPEs are systems based on ABA triblock copolymers with two glassy end blocks and ABC triblock copolymers with one or two semicrystalline end blocks. The motivation of this work is the development of TPEs with improved elastic properties compared to commercially available systems.

The basic idea about increasing the elasticity of conventional copoly(ether ester)s based on poly(butylene terephthalate) (PBT) hard segments and polyether soft segments, e. g. poly(tetramethylene oxide) (PTMO), is the replacement of the continuous PBT hard phase in these systems by a disperse PBT hard phase. It is shown, that the incorporation of nonpolar segments is possible by using poly(ethylene oxide)-*block*-poly(ethylene-*stat*-butylene)-*block*-poly(ethylene oxide) (PEO-*b*-PEB-*b*-PEO) triblock copolymers, where the polar PEO blocks act as compatibilizer between the nonpolar PEB segments and the polar PBT segments during the melt polycondensation. Dynamic shear experiments in combination with small angle X-ray scattering (SAXS) show an enhanced microphase separation induced by the nonpolar PEB segments. As a consequence, the PBT segments crystallize from a microphase-separated melt, which in turn results in the formation of a disperse PBT hard phase, as has been shown by transmission electron microscopy (TEM) and scanning force microscopy (SFM). Mechanical testing reveals a significantly improved elastic recovery compared to that of conventional PBT-based copoly(ether ester)s with PTMO soft segments. This can be attributed to the fact that a disperse PBT hard phase shows a higher resistance against irreversible distortion compared to the case of a continuous PBT hard phase. From the combination of results obtained from differential scanning calorimetry (DSC) and dynamic mechanical analysis (DMA) a structure model for this new type of copoly(ether ester)s has been derived and confirmed by solid-state NMR investigations. The morphology consists of a semicrystalline PBT hard phase and an amorphous soft segment phase, which is divided into a pure PEB phase, a PEO-rich phase besides a mixed PBT/PEO phase, and a pure amorphous PBT phase.

In the second part of this thesis ABC triblock copolymers with one or two semicrystalline end blocks have been investigated, taking advantage of crystallization as a strong driving force for microphase separation. Two main aspects were addressed: i) the

interplay between morphology and crystallization, and ii) the comparison of ABA and ABC triblock copolymers with glassy (A), elastomeric (B) and crystalline (C) blocks.

Several polyethylene-*block*-poly(ethylene-*alt*-propylene)-*block*-poly(ethylene oxide) (PE-*b*-PEP-*b*-PEO) triblock copolymers with two different semicrystalline end blocks have been synthesized by a combination of sequential anionic polymerization of butadiene, isoprene, and ethylene oxide (PB-*b*-PI-*b*-PEO) and subsequent homogeneous catalytic hydrogenation. The PB-*b*-PI-*b*-PEO triblock copolymers have been synthesized in a one-pot strategy by using the phosphazene base *t*-BuP_4, which enables the polymerization of ethylene oxide in the presence of lithium counterions. Kinetic investigations on the ethylene oxide polymerization using in-situ near infrared fiber-optic spectroscopy reveal an unexpected induction period. It has been found that the induction period depends in a complex fashion on the reaction temperature, amount of added phosphazene base *t*-BuP_4, type of initiator, and the sequence of reactant addition. It is concluded that the induction period is a result of different factors like break up of lithium alkoxide aggregates by the phosphazene base *t*-BuP_4, chain length effect of the growing PEO chain on Li^+ complexation, and contribution of ethylene oxide itself in the formation of the active growing site.

Thermal characterization of the PB-*b*-PI-*b*-PEO and PE-*b*-PEP-*b*-PEO triblock copolymers utilizing DSC and special self-nucleation techniques reveals a strong influence of the confinement active during crystallization on the crystallization and self-nucleation behavior of the semicrystalline PEO and PE blocks. In PE-*b*-PEP-*b*-PEO triblock copolymers with low PEO contents large supercoolings are necessary to induce crystallization of PEO. Furthermore, the self-nucleation behavior of the PEO blocks is different compared to that of semicrystalline homopolymers, i. e. domain II (self-nucleation domain) is absent. This is a direct result of the confinement of the PEO blocks into small isolated microdomains. In contrast, for the PE blocks a heterogeneous nucleation mechanism and the presence of all three self-nucleation domains, usually present in crystallizable homopolymers, is observed. Because of the miscibility of the PE and PEP segments in the melt, the PE segments crystallize without any confinement from a homogeneous mixture of PE and PEP segments, resulting in the observed behavior. In addition, it is shown that the melting temperature of PEO within PE-*b*-PEP-*b*-PEO triblock copolymers can be significantly increased by complexation of the PEO segments with *p*-nitrophenol or resorcinol.

In TPEs based on ABA triblock copolymers with glassy end blocks, e. g. polystyrene-*block*-poly(ethylene-*alt*-propylene)-*block*-polystyrene (PS-*b*-PEP-*b*-PS) triblock copolymers, the middle block chains can either loop back into the same PS domain or form bridges by the

connection of two different PS domains. However, only the bridges contribute to the elastic properties and the loops do not, which limits the elastic recovery of theses systems. The influence of a semicrystalline end block on the mechanical properties has been investigated by comparison of polystyrene-*block*-poly(ethylene-*alt*-propylene)-*block*-polyethylene (PS-*b*-PEP-*b*-PE) and the corresponding PS-*b*-PEP-*b*-PS triblock copolymers with two glassy PS end blocks. For small elongations (< 300%) the PE containing triblock copolymers exhibit a significantly improved elastic recovery compared to that of the PS-*b*-PEP-*b*-PS triblock copolymers. This can be attributed to the increased bridge fraction in the PS-*b*-PEP-*b*-PE triblock copolymers induced by the immiscibility of the two different end blocks. In contrast, for high elongations (< 300%) the situation is reversed and the triblock copolymers with two glassy PS end blocks reveal better elastic properties. Obviously, glassy PS domains show a higher resistance against distortion compared to that of semicrystalline PE domains, especially at high strains. In general, the elastic properties of the PS-*b*-PEP-*b*-PE triblock copolymers are improved for systems exhibiting a low content of the PS and/or PE blocks.

The morphology of the PS-*b*-PEP-*b*-PE and PE-*b*-PEP-*b*-PEO triblock copolymers has been investigated applying TEM and SFM. The large differences in stiffness between crystalline and amorphous domains makes SFM the superior tool for morphological investigations. This especially applies for the characterization of the semicrystalline PE blocks, which cannot be visualized simultaneously to the other triblock components by conventional TEM investigations due to problems involved in the staining technique. Furthermore, hot-stage SFM has been used to follow the melting of the PEO blocks and the annealing of the PE blocks within a PE-*b*-PEP-*b*-PEO triblock copolymer.

5 Zusammenfassung

In der vorliegenden Arbeit wird die Synthese und Charakterisierung von zwei neuartigen Vertretern der thermoplastischen Elastomere (TPE´s) beschrieben. Die erste Klasse stellen Multiblock-Copolyetherester mit teilkristallinen Hartsegmenten und Dreiblockcopolymer-Weichsegmenten dar. Weiterhin wurden TPE´s auf der Basis von ABA Dreiblockcopolymeren mit zwei glasartigen Endblöcken und ABC Dreiblockcopolymeren mit einem oder zwei teilkristallinen Endblöcken untersucht. Die Zielsetzung dieser Arbeit ist die Entwicklung von TPE´s, die im Vergleich zu kommerziell erhältlichen Systemen eine verbesserte Elastizität aufweisen.

Die grundlegende Strategie zur Verbesserung der elastischen Eigenschaften von konventionellen Copolyetherestern mit Hartsegmenten aus Polybutylenterephthalat (PBT) und Polyether-Weichsegmenten, z. B. Polytetramethylenoxid (PTMO), ist der Austausch der kontinuierlichen PBT-Hartphase in diesen Systemen durch eine dispergierte Hartphase. Es wird gezeigt, daß die Verwendung von Polyethylenoxid-*block*-Poly(ethylen-*stat*-butylen)-*block*-Polyethylenoxid (PEO-*b*-PEB-*b*-PEO) Dreiblockcopolymeren einen Einbau von unpolaren PEB-Segmenten ermöglicht, wobei die PEO-Blöcke während der Schmelzpolykondensation als Phasenvermittler zwischen den unpolaren PEB-Segmenten und den polaren PBT-Segmenten fungieren. Dynamische Scherexperimente und Röntgenkleinwinkelstreuung (SAXS) ergeben eine ausgeprägte Mikrophasenseparation in der Schmelze, die durch die unpolaren PEB-Weichsegmente hervorgerufen wird. Die PBT-Segmente kristallisieren folglich aus einer mikrophasenseparierten Schmelze heraus. Dies führt zur Ausbildung einer dispergierten PBT-Hartphase, wie durch Transmissions-elektronenmikroskopie (TEM) und Rasterkraftmikroskopie (SFM) gezeigt wird. Mechanische Untersuchungen ergeben erheblich verbesserte elastische Rückstelleigenschaften im Vergleich zu herkömmlichen Copolyetherestern mit PBT-Hartsegmenten und PTMO-Weichsegmenten. Dies läßt sich auf die erhöhte Widerstandsfähigkeit einer dispergierten PBT-Hartphase gegenüber irreversibler Verformung, im Vergleich zu der einer kontinuierlichen PBT-Hartphase, zurückführen. Aus den Ergebnissen der differentiellen Wärmeflußkalorimetrie (DSC) und dynamisch mechanischen Analyse (DMA) läßt sich ein Strukturmodell für diese neuartigen Copolyetherester ableiten, das durch Festkörper-NMR Untersuchungen bestätigt worden ist. Die Copolyetherester bestehen aus einer teilkristallinen PBT-Hartphase und einer amorphen Weichsegmentphase, die in eine reine PEB-Phase, eine

PEO-reiche Phase neben einer PEO/PBT-Mischphase und eine reine amorphe PBT-Phase unterteilt ist.

Der zweite Teil dieser Arbeit befaßt sich mit ABC Dreiblockcopolymeren mit einem oder zwei teilkristallinen Endblöcken, wobei hier die Kristallisation als starke Triebkraft für Mikrophasenseparation genutzt wurde. Hierbei wurden zwei Hauptaspekte untersucht: i) das Zusammenspiel zwischen Strukturbildung und Kristallisation und ii) der Vergleich von ABA und ABC Dreiblockcopolymeren mit glasartigen (A), elastomerartigen (B) und kristallinen (C) Blöcken.

Polyethylen-*block*-Poly(ethylen-*alt*-propylen)-*block*-Polyethylenoxid (PE-*b*-PEP-*b*-PEO) Dreiblockcopolymere wurden durch eine Kombination von sequentieller anionischer Polymerisation von Butadien, Isopren und Ethylenoxid (PB-*b*-PI-*b*-PEO) und nachfolgender homogener katalytischer Hydrierung hergestellt. Die Synthese der PB-*b*-PI-*b*-PEO Dreiblock-copolymere in einer Ein-Topf Strategie wurde durch die Verwendung der Phosphazenbase *t*-BuP_4 ermöglicht, welche die Polymerisation von Ethylenoxid in der Gegenwart von Lithiumgegenionen erlaubt. Kinetische Untersuchungen der Ethylenoxidpolymerisation mit der Hilfe von „in-situ“ Nahinfrarot-Faseroptik-Spektroskopie ergeben eine unerwartete Induktionsperiode. Diese hängt in komplexer Weise von der Reaktionstemperatur, Menge der Phosphazenbase *t*-BuP_4, Art des Initiators und der Reihenfolge, in der die Reaktanten zugegeben werden, ab. Zusammenfassend läßt sich sagen, daß die Induktionsphase offensichtlich von mehreren Faktoren beeinflußt wird, wie z. B. dem Aufbrechen von Lithiumalkoxid-Aggregaten durch die Phosphazenbase *t*-BuP_4, einem möglichen Kettenlängeneffekt der wachsenden PEO Kette auf die Li^+-Komplexierung und einem Einfluß von Ethylenoxid selbst auf die Ausbildung des aktiven Zentrums.

Thermische Untersuchungen mittels DSC und speziellen Selbstnukleierungs-messungen zeigen, daß das Kristallisations- und Selbstnukleierungsverhalten der PEO- und PE-Blöcke in PB-*b*-PI-*b*-PEO und PE-*b*-PEP-*b*-PEO Dreiblockcopolymeren stark davon abhängt, inwieweit der jeweilige Block bei der Kristallisation eingeengt ist. In PE-*b*-PEP-*b*-PEO Dreiblockcopolymeren, die einen geringen PEO-Anteil aufweisen, sind sehr große Unterkühlungen nötig um die Kristallisation von PEO zu induzieren. Desweiteren unterscheidet sich das Selbstnukleierungsverhalten der PEO-Blöcke wesentlich von dem Verhalten teilkristalliner Homopolymere, was sich in der Abwesenheit von Domäne II (Selbstnukleierungs-Domäne) widerspiegelt. Dieses Verhalten resultiert aus der Einengung der PEO Blöcke in kleine isolierte Mikrodomänen während der Kristallisation. Im Gegensatz dazu beobachtet man für die PE-Blöcke einen heterogenen Nukleierungsmechanismus.

Desweiteren sind alle drei Selbstnukleierungs-Domänen, die man üblicherweise bei teilkristallinen Homopolymeren beobachtet, vorhanden. Dies läßt sich dadurch erklären, daß aufgrund der Mischbarkeit von PE- und PEP-Segmenten in der Schmelze die Kristallisation von PE ohne jegliche Einengung aus einer homogenen Mischung von PE- und PEP-Segmenten heraus erfolgt. Zusätzlich wird gezeigt, daß der Schmelzpunkt von PEO in PE-*b*-PEP-*b*-PEO Dreiblockcopolymeren durch Komplexierung mit *p*-Nitrophenol oder Resorcin erheblich erhöht werden kann.

In TPE´s, die auf ABA Dreiblockcopolymeren mit glasartigen Endblöcken basieren, z. B. Polystyrol-*block*-Poly(ethylen-*alt*-propylen)-*block*-Polystyrol (PS-*b*-PEP-*b*-PS), können die Mittelblockketten entweder in die gleiche PS-Domäne zurückfalten (Schlaufen) oder Brücken bilden, indem sie zwei unterschiedliche PS-Domänen verknüpfen. Allerdings sind nur die Brücken elastisch aktiv, wodurch die elastischen Eigenschaften dieser Systeme eingeschränkt sind. Der Einfluß eines teilkristallinen Endblocks auf die mechanischen Eigenschaften wurde anhand von Polystyrol-*block*-Poly(ethylen-*alt*-propylen)-*block*-Polyethylen (PS-*b*-PEP-*b*-PE) Dreiblockcopolymeren untersucht, die mit den entsprechenden PS-*b*-PEP-*b*-PS Dreiblockcopolymeren mit zwei glasartigen PS-Endblöcken verglichen wurden. Bei kleinen Dehnungen (< 300%) zeigen die PE-haltigen Dreiblockcopolymere wesentlich bessere elastische Rückstelleigenschaften im Vergleich zu denen der PS-*b*-PEP-*b*-PS Dreiblockcopolymere. Dies läßt sich auf die Unverträglichkeit der beiden Endblöcke zurückführen, die zu einer Erhöhung des Brückenanteils in den PS-*b*-PEP-*b*-PE Dreiblockcopolymeren führt. Bei Dehnungen über 300% beobachtet man ein gegensätzliches Verhalten, wobei jetzt die PS-*b*-PEP-*b*-PS Dreiblockcopolymere bessere elastische Eigenschaften aufweisen. Dieses Verhalten beruht offenbar darauf, daß die glasartigen PS-Domänen eine erhöhte Resistenz gegenüber irreversibler Deformation aufweisen als teilkristalline PE-Domänen, was insbesondere bei hohen Dehnungen zum tragen kommt. Im Allgemeinen geht eine Verringerung des PS und/oder PE Anteils mit einer Verbesserung der elastischen Eigenschaften einher.

Die Morphologie der PS-*b*-PEP-*b*-PE und PE-*b*-PEP-*b*-PEO Dreiblockcopolymere ist mittels TEM und SFM untersucht worden. Aufgrund des großen Härteunterschiedes zwischen kristallinen und amorphen Bereichen ist SFM für morphologische Untersuchungen besonders gut geeignet. Dies gilt speziell für die Charakterisierung der teilkristallinen PE-Blöcke, die durch konventionelle TEM-Untersuchungen aufgrund von Kontrastierungsproblemen nicht sichtbar gemacht werden können. Weiterhin ist es gelungen mit Hilfe von

temperaturabhängigen SFM-Messungen das Aufschmelzen der PEO-Blöcke sowie das Tempern der PE-Blöcke in einem PE-*b*-PEP-*b*-PEO Dreiblockcopolymer zu verfolgen.

6 Appendix

List of Synthesized Diblock and Triblock Copolymers

Sample	M_w/M_n	PB %-1,4	PI %-14
PB-*b*-PI-*b*-PEO			
$B_{24}I_{56}EO_{20}^{67}$	1.01	89	88
$B_{11}I_{70}EO_{19}^{120}$	1.01	88	92
$B_{17}I_{57}EO_{26}^{130}$	1.01	89	92
$B_{19}I_{39}EO_{42}^{135}$	1.02	89	92
PS-*b*-PI-*b*-PS			
$S_8I_{71}S_{21}^{119}$	1.01	-	92
$S_{14}I_{76}S_{10}^{116}$	1.01	-	92
$S_{14}I_{65}S_{21}^{117}$	1.01	-	92
PS-*b*-PI-*b*-PB			
$S_8I_{71}B_{21}^{118}$	1.01	90	92
$S_{14}I_{75}B_{11}^{117}$	1.01	90	92
$S_{14}I_{64}B_{22}^{119}$	1.02	87	92
$S_{14}I_{57}B_{29}^{109}$	1.02	89	92
$S_{34}I_{36}B_{30}^{113}$	1.01	90	92

Sample	M_w/M_n
PS-*b*-PEO	
$S_{53}EO_{47}^{3.6}$	1.09
$S_{12}EO_{88}^{102}$	1.01
PEO-*b*-PEB-*b*-PEO	
$PEO_{36}PEB_{28}PEO_{36}^{13}$	1.13
$PEO_{29}PEB_{42}PEO_{29}^{8.6}$	1.08
$PEO_{27}PEB_{46}PEO_{27}^{8.0}$	1.08
$PEO_{25}PEB_{50}PEO_{25}^{7.1}$	1.09
$PEO_{22}PEB_{56}PEO_{22}^{6.4}$	1.08
$PEO_{18}PEB_{64}PEO_{18}^{5.6}$	1.11
$PEO_{16}PEB_{68}PEO_{16}^{5.2}$	1.12
PE-*b*-PEP-*b*-PEO	
$E_{24}EP_{57}EO_{19}^{69}$	-
$E_{11}EP_{71}EO_{18}^{123}$	-
$E_{18}EP_{57}EO_{25}^{133}$	-
$E_{19}EP_{40}EO_{41}^{138}$	-
PS-*b*-PEP-*b*-PS	
$S_8EP_{71}S_{21}^{121}$	-
$S_{13}EP_{77}S_{10}^{119}$	-
$S_{14}EP_{66}S_{20}^{119}$	-
PS-*b*-PEP-*b*-PE	
$S_8EP_{71}E_{21}^{121}$	-
$S_{13}EP_{76}E_{11}^{121}$	-
$S_{14}EP_{64}E_{22}^{122}$	-
$S_{13}EP_{57}E_{30}^{112}$	-
$S_{33}EP_{37}E_{30}^{115}$	-

List of Synthesized Copoly(ether ester)s

Sample	w (PBT) [%]	M_n(PEO) [g/mol]	x_{HS}[a]	l_{HS}[b]	melt
PBT50-4600	50	4600	0.983	58.3	turbid
PBT50-2510	50	2510	0.975	40.1	turbid
PBT50-2190	50	2190	0.973	37.2	turbid
PBT50-1730	50	1730	0.970	33.0	turbid
PBT40-2510	40	2510	0.963	27.1	slightly turbid
PBT40-2190	40	2190	0.960	25.1	slightly turbid
PBT40-1730	40	1730	0.955	22.4	slightly turbid
PBT40-1380	40	1380	0.951	20.2	clear
PBT30-1380	30	1380	0.925	13.4	clear
PBT20-1380	20	1380	0.878	8.2	clear
PBT45-1000	45	1000	0.954	21.8	clear
PBT40-1000	40	1000	0.944	17.9	clear
PBT35-1000	35	1000	0.932	14.7	clear
PBT30-1000	30	1000	0.916	11.9	clear
PBT25-1000	25	1000	0.894	9.5	clear
PBT20-1000	20	1000	0.864	7.4	clear
PBT10-1000	10	1000	0.739	3.8	clear
PBT40-820	40	820	0.941	16.9	clear
PBT30-820	30	820	0.911	11.2	clear

[a] Mole fraction of hard segment (PBT).
[b] Average hard segment length calculated according to $l_{HS}=1/(1-x_{HS})$.

List of Publications

(1) Schmalz, H.; Abetz, V.; Lange, R.; Soliman, M.; New Thermoplastic Elastomers by Incorporation of Nonpolar Soft Segments in PBT-Based Copolyesters; *Macromolecules* **2001**, *34*, 795.

(2) Schmalz, H.; Böker, A.; Lange, R.; Krausch, G.; Abetz, V.; Synthesis and Properties of ABA and ABC Triblock Copolymers with Glassy (A), Elastomeric (B), and Crystalline (C) Blocks; *Macromolecules* **2001**, *34*, 8720.

(3) Schmalz, H.; Böker, A.; Lange, R.; Abetz, V.; ABC Triblock Copolymers with Crystalline End Blocks and their Use as Thermoplastic Elastomers; *Polym. Mater. Sci. Eng.* **2001**, *85*, 478.

(4) Arnal, M. L.; Balsamo, V.; López-Carrasquero, F.; Contreras, J.; Carrillo, M.; Schmalz, H.; Abetz, V.; Laredo, E.; Müller, A. J.; Synthesis and Characterization of Polystyrene-*b*-poly(ethylene oxide)-*b*-poly(ε-caprolactone) Block Copolymers; *Macromolecules* **2001**, *34*, 7973.

(5) Lanzendörfer, M.; Schmalz, H.; Abetz, V.; Müller, A. H. E.; Application of FT-NIR Spectroscopy for Monitoring the Kinetics of Living Polymerizations; *Polym. Prep. (Am. Chem. Soc., Div. Polym. Chem.)* **2001**, *42*, 329.

(6) Schmalz, H.; van Guldener, V.; Gabriëlse, W.; Lange, R.; Abetz, V.; Morphology, Surface Structure, and Elastic Properties of PBT-Based Copolyesters with PEO-*b*-PEB-*b*-PEO Triblock Copolymer Soft Segments; *Macromolecules* **2002**, *35*, 5491.

(7) Schmalz, H.; Knoll, A.; Müller, A. J.; Abetz, V.; Synthesis and Characterization of ABC Triblock Copolymers with Two Different Crystalline End Blocks: Influence of Confinement on Crystallization Behavior and Morphology; *Macromolecules* **2002**, *35*, 10004.

(8) Schmalz, H.; Abetz, V.; Müller, A. J.; Thermal and Self-Nucleation Behavior of Molecular Complexes Formed by *p*-Nitrophenol and the Poly(ethylene oxide) End Block within an ABC Triblock Copolymer; *Macromol. Symp.* **2002**, *183*, 179.

(9) Schmalz, H.; Knoll, A.; Müller, A. J.; Abetz, V.; Crystallization Behavior of End Blocks in ABC Triblock Copolymers; *Polym. Prep. (Am. Chem. Soc., Div. Polym. Chem.)* **2002**, *43*, 371.

(10) Müller, A. J.; Balsamo, V.; Arnal, M. L.; Jakob, T.; Schmalz, H.; Abetz, V.; Homogeneous Nucleation and Fractionated Crystallization in Block Copolymers; *Macromolecules* **2002**, *35*, 3048.

(11) Gabriëlse, W.; van Guldener, V.; Schmalz, H.; Abetz, V.; Lange, R.; Morphology and Molecular Miscibility of Segmented Copoly(ether ester)s with Improved Elastic Properties as Studied by Solid-State NMR; *Macromolecules* **2002**, *35*, 6946.

(12) Lanzendörfer, M. G.; Schmalz, H.; Abetz, V.; Müller, A. H. E. Application of FT-NIR Spectroscopy for Monitoring the Kinetics of Living Polymerizations. In *In-Situ Spectroscopy of Monomer and Polymer Synthesis*; Puskas, J. E.; Storey, R., Eds.; Kluwer Academic/Plenum: New York/Dordrecht, 2002, pp 67.

(13) Schmalz, H.; Müller, A. J.; Abetz, V.; Crystallization in ABC Triblock Copolymers with Two Different Crystalline End Blocks: Influence of Confinement on Self-Nucleation Behavior; *Macromol. Chem. Phys.* **2003**, accepted.

(14) Schmalz, H.; Abetz, V.; Lange, R.; Thermoplastic Elastomers Based on Semicrystalline Block Copolymers; *Composites Sci. Technol.* **2003**, accepted.

(15) Schmalz, H.; Lanzendörfer, M. G.; Abetz, V.; Müller, A. H. E.; Anionic Polymerization of Ethylene Oxide in the Presence of the Phosphazene Base *t*-BuP_4 – Kinetic Investigations Using In-Situ FT-NIR Spectroscopy and MALDI-ToF MS; *Macromol. Chem. Phys.* **2003**, submitted.

Erklärung

Hiermit erkläre ich, daß ich die Arbeit selbständig verfaßt und keine anderen als die angegebenen Quellen und Hilfsmittel benutzt habe.

Ferner erkläre ich, daß ich anderweitig mit oder ohne Erfolg nicht versucht habe, eine Dissertation einzureichen oder mich einer Doktorprüfung zu unterziehen.

Bayreuth, den 31.07.2002